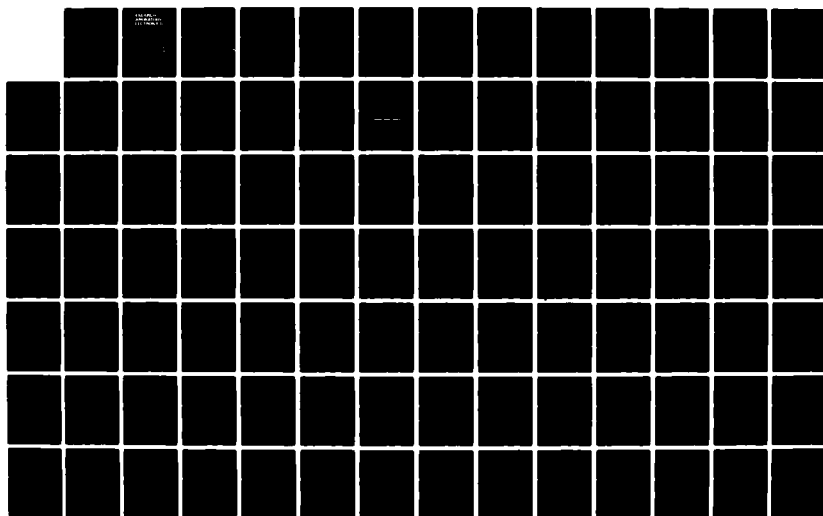AD-A134 812   RLE (RESEARCH LABORATORY OF ELECTRONICS) PROGRESS   1/3
REPORT NUMBER 125(U) MASSACHUSETTS INST OF TECH
CAMBRIDGE RESEARCH, LAB OF ELECTRONICS J ALLEN JAN 83
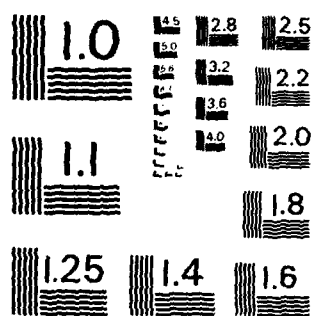UNCLASSIFIED   F/G 5/2   NL

MICROCOPY RESOLUTION TEST CHART

NATIONAL BUREAU OF STANDARDS-1963-A

RESEARCH LABORATORY of ELECTRONICS

No. 125
Jan. 1983

PROGRESS REPORT

AO-A134812

83 11 17 028

Massachusetts Institute of Technology • Cambridge, Massachusetts 02139

Massachusetts Institute of Technology

RESEARCH LABORATORY OF ELECTRONICS

RLE PROGRESS REPORT No. 125

January 1983

DTIC
ELECTE
NOV 1 8 1983

Submitted by: J. Allen

1

A

Research includes:

Table of Contents

---

[26]Trademark of the A.P.   167

List of Figures

/

General Physics

1. Molecule Microscopy

Academic and Research Staff

Prof. J.G. King, Prof. A.P. French, Dr. A. Essig, Dr. J.A. Jarrell, Dr. S.J. Rosenthal

Graduate Students

J.G. Yorker

1.1 Research Objectives

Francis L. Friedman Chair

John G. King, Joseph A. Jarrell

Molecule microscopy depends on the spatial variation of emissions of neutral molecules from the sample in vacuum. It produces images that reveal variations in the number of molecules present on the surface of (or, in some cases, coming through) the sample. These molecules can have been part of the sample, or may have been applied as a stain. There being no useful lens for neutral molecules, spatial resolution must be obtained as follows. An aperture can be scanned above a sample from which molecules are evaporating so that only molecules from one region of the sample can enter a detector, as determined by the geometry of the straight line molecular paths. Or the aperture can be at the end of a micropipette equipped with a permeable plug, useful when the sample is in liquid solution as with surviving tissue. Finally, the sample can be kept at such a temperature that negligible evaporation of molecules occurs except where local stimulation of evaporation by heating, electron stimulated desorption (ESD) or other means takes place in response to a localized scannable pulsed source of energy, such as a focused beam of electrons. We have done some work with all three systems: aperture or "pinhole,"[1] micropipette[2] and scanning desorption.[3,4]

Status

We are not at present continuing work with the aperture or "pinhole" type instrument—it could have been developed beyond the initial stage described in reference 1 where the first pictures ever taken with evaporating water molecules are exhibited, but the other forms appeared to be more useful. Thus the scanning micropipette MM (SMM)[2] is being applied to studies of transport in tissue at M.I.T. (see 1.3 below) at Massachusetts General Hospital and at Boston University School of Medicine. We have worked on various aspects of the scanning desorption molecule microscope (SDMM). Thus, to establish the contrast mechanism for SDMM with thermal desorption as it might be used in biology, we have studied the desorption of water from representative samples of protein, carbohydrate and lipid.[5] As a frozen thin sample is raised from 100 K to 800 K three kinds of peak in the rate of desorption of water are found—peaks around 120 K from the sublimation of ice in zero

order, sample specific BET peaks in the range from 220 K to 500 K and pyrolysis peaks above 500 K[6]. As long as the sample is not pyrolysed it can be restained. We have also investigated the ESD of water and ethanol from the same samples[3] and find cross sections around 10^{-16} cm^2. We have also studied a variety of thermal desorption techniques including heating by localized addressable microheaters, a project in microstructure construction limited at present to micrometer resolution; and heating by focused laser light.[4]

In summary, with our accumulated knowledge, we are now in a position to design an SDMM with either micrometer or nanometer resolution. Yorker[4] exhibits pictures of water desorbed from a stearic acid droplet and from squamous cells with 5 μm resolution and discusses in general how to get micrometer resolution. Such instruments are of interest in physiological studies. but do not help at the more fundamental molecular level where much higher resolution is needed. Recently we have figured out how to design a SDMM with nanometer resolution. Why is it important? Because SDMM with its surface specific and essentially chemical contrast mechanism has many applications in which the localization of small molecules on sample surfaces can be used to give otherwise unobtainable information. Studies of the distribution of water on biological surfaces can give information about the sites where it binds and help elucidate the various specific recognition processes that take place at these surfaces. Water plays a role in corrosion initiation and failure in metallurgy, and in catalytic reactions in chemistry. We expect the SDMM to be useful wherever the irregular nature of samples does not permit diffraction studies of the adsorbate.

1.2 Design of Nanometer SDMM

How big a signal do we have to work with? Consider a monolayer of water adsorbed on a surface— a 2 nm spot will have about 40 molecules and they must provide the signal that eventually generates one element of the picture produced by the SDMM. Initially we plan to have 10^4 elements in the picture each 2 nm by 2 nm with 3 to 5 shades of gray (attainable if the background is less than 3 counts per element) and requiring 10^2 seconds exposure.

Thermal desorption is feasible for 10 nm resolution with thin samples on thin substrates, but because the spread in heat is comparable to the substrate thickness we choose to use ESD to attain 2 nm resolution. The sample will be on a thin (10 nm) substrate to minimize the effects of "bloom." For a desorbing pulse 10^{-6} seconds long and with ESD cross-sections of 10^{-16} cm^2 currents of 10^{-12}A must be delivered to a 2 nm spot, well within the current state of the art. The desorbed neutrals will impinge on and stick to a cold tungsten tip of 1 μm radius. The tip oscillates at 100 Hz (eventually under servo control to ca 0.1 μm) from a position 1 μm above the sample to a position at the entrance of a time of flight (TOF) mass spectrometer. When the tip is above the sample it collects a pulse of desorbed molecules. When it is above the TOF tube a short (10^{-9}sec) positive high voltage (400 kV) pulse is applied to the tip which field desorbs and ionizes the molecules with high efficiency and sends the ions down the TOF tube for detection with appropriate fast electronics.

How low a pressure must be maintained in the vacuum system? If less than 1 molecule is to hit the detector tip during 1 cycle of the desorption–detection process, the pressure should be in the vicinity of 10^{-9} Pa, readily attainable—most easily by cryopumping in this case.

References

1. J.C. Weaver and J.G. King, Proc. Nat. Acad. U.S.A. 70, 2781 (1973).
2. J.A. Jarrell, J.W. Mills , and J.G. King, Science 211, 277 (1981).
3. B.R. Silver, Ph.D. Thesis, Department of Physics, M.I.T., 1976.
4. J.G. Yorker, Ph.D. Thesis, Department of Physics, M.I.T., 1982
5. D.G. Lysy, Ph.D. Thesis, Department of Physics, M.I.T., 1976.
6. J.G. King and D.G. Lysy, ASMS Conference Proceedings, WPA3, 1983.

1.3 Scanning Micropipette Molecule Microscopy (SMMM)

Joseph A. Jarrell, John G. King

The major goal of this research is the study of water transport at the cellular level across hormonally responsive tissues that model the distal tubules of the mammalian kidney, specifically amphibian urinary bladder epithelium.

During the past year we have successfully applied techniques for the microinjection of fluorescent dyes to this epithelium and demonstrated that the cells are coupled together and hence act as a syncytium. Previous attempts by others to demonstrate this coupling using electrophysiological techniques had produced conflicting data.[1,2] Indeed, the validity of using such techniques in this epithelium has been disputed.[3]

These microinjection techniques, in conjunction with the scanning micropipette molecule microscope, will now enable us to examine the role of intercellular communication in the hormonal response (by the microinjection of cAMP) and to begin to elucidate the various intracellular biochemical events that occur between hormone binding on the basolateral cell membrane and the increase in water permeability that occurs at the apical cell membrane, by microinjecting various suspected intermediates such as the catalytic subunit of cAMP–dependent protein kinase.

References

1. W.R. Loewenstein, S.J. Socolar, S. Higashino, Y. Kanno, and N. Davidson, Science 149, 295 (1965).
2. L. Reuss and A. Finn, J. Gen. Physiol. 64, 1 (1974).
3. J.T. Higgins, B. Gebler and E. Frömter, Pflügers Arch. 371, 87 (1977).

Publications

Jarrell, J.A., "Reversible CO_2-Induced Inhibition of Dye–Coupling in Necturus Gallbladder,"

Am. J. Physiol.: *Cell Physiol. (in press)*.

Jarrell, J.A., C.A. Rabito, and J.G. King, "Applications of Intracellular Dye Injection and Mass Spectrometry to the Study of Epithelial Transport," in M.A. Dinno, T. Rozzell, and A. Callahan (Eds.), <u>Physical Methods in the Study of Cellular Biophysics</u> (A.R. Liss, Co.), to be published.

1.4 Electrical Neutrality of Molecules

Francis L. Friedman Chair

Anthony P. French, John G. King

The present experimental *upper limit on any departure from* neutrality of molecules is approximately 10^{-21} of one elementary charge. This can be interpreted as a limit on the proton-electron charge *difference, or on the charge on the neutron, or on some* combination of these. The occurrence of *innumerable transformations involving both leptons and baryons, and our long-standing belief in the conservation of electric charge as a fundamental* law of nature, certainly support the assumption of exact equality of charges of either sign on all elementary particles. Nevertheless, the possibility *that there might be some minute difference* between electron and proton charges is something that cannot be ruled out on *the basis of any existing experimental evidence or theoretical scheme, and its existence would have profound implications.*

The fundamental interest of this question has led to a number of experiments by various investigators. These experiments have involved three different approaches: (1) direct tests for any *net charge in a volume of gas released from a container;* (2) tests for a charge on an isolated body (analogous to the Millikan oil-drop experiment); (3) molecular-beam deflection experiments.

In 1973 King and Dylla[1] pioneered a new technique based on the fact that an electric field, periodic in time, applied to a homogeneous medium will excite acoustic waves at the same frequency if the molecules of the medium are not completely neutral. (This is separable from any induced polarization effects, which will occur at doubled frequency).

Using SF_6 gas in a spherical container, with microphones in the walls to detect acoustic waves set up by an oscillating voltage on a central electrode, King and Dylla were able to match the sensitivity (~ 1 part in 10^{21}) of neutrality determinations by the three previous methods. There is reason to believe that a well-designed experiment using a liquid medium instead of a gas might make it possible to gain as many as six orders of magnitude in sensitivity in such measurements. We have done some preliminary studies of matching of high-Q resonating microphones to cavities containing cryogenic liquids with encouraging results. We also have modest funds to continue the work during 1983.

References

1. H. Dylla and J. King, Phys. Rev. A Z, 1224 (1973).

2. Semiconductor Surface Studies

Academic and Research Staff

Prof. J.D. Joannopoulos, Dr. J. Ihm, D.-H.T. Lee

Graduate Students

Y. Bar-Yam, A.D. Stone

2.1 Excitations at Surfaces and Interfaces of Solids

Understanding the properties of surfaces of solids and the interactions of atoms and molecules with surfaces has been of extreme importance, both from technological and academic points of view. The recent advent of ultrahigh vacuum technology has made microscopic studies of well-characterized surface systems possible. The way the atoms move to reduce the energy of the surface, the number of layers of atoms involved in this reduction, the electronic and vibrational states that result from this movement, and the final symmetry of the surface layer are all of utmost importance in arriving at a fundamental and microscopic understanding of the nature of clean surfaces, chemisorption processes, and the initial stages of interface studies, both from the experimental and theoretical points of view, is simply the determination of the precise positions of the atoms on a surface. Currently, there are many surface geometries, even for elemental surfaces, that remain extremely controversial.

The theoretical problems associated with these systems are quite complex. We are, however, currently in the forefront of being able to solve for the properties of real surface systems (rather than simple mathematical models). In particular, we have recently developed a method of calculating the total ground-state energy of a surface system from "first principles" so that we may be able to provide accurate theoretical predictions of surface geometries. Preliminary results of metal atoms deposited on a semiconductor surface look very promising. The first total energy map for an interacting atom-surface system has been obtained. The map clearly illustrates possible chemisorption sites as well as specific migration or diffusion channels.

3. Atomic Resonance and Scattering

Academic and Research Staff

Prof. D. Kleppner, Prof. D.E. Pritchard, Dr. T. Ducas, Dr. D. Kelleher, Dr. A.M. Lyyra, Dr. K.L. Saenger, Dr. W. Spencer, Dr. G. Vaidyanathan, Dr. X. Zhong

Graduate Students

S. Atlas, L. Brewer, S.L. Dexheimer, C.W. Engelke, T. Gentile, P.L. Gould, B. Hughey, R.G. Hulet, M.M. Kash, P.D. Magill, A.L. Migdall, P.E. Moskowitz, W.P. Moskowitz, T.P. Scott, N. Smith, B.A. Stewart, R.E. Walkup, G.R. Welch

3.1 Rydberg Atoms in a Magnetic Field

Michael M. Kash, Daniel Kleppner, George R. Welch, Zhong Xubin

The general structure of atomic hydrogen in an arbitrarily strong magnetic field remains an unsolved problem of atomic physics. The Hamiltonian for hydrogen in a uniform magnetic field is known; the eigenstates are not. Theoretical research has yet to produce solutions which can elucidate the atom's behavior at all levels of excitation and field strength.

Highly excited, or Rydberg, atoms in laboratory-sized magnetic fields (about 10 Tesla) have strong principal quantum number "mixing". Even numerical solutions fail in this regime. Our studies suggest, however, that there is an approximate dynamical symmetry. In principle, identifying this symmetry provides a complete solution to the problem. The clue to the symmetry's existence is the near crossing of energy levels of different principal quantum numbers for states of the same azimuthal quantum number and parity. The "no-crossing theorem" implies that there must be a constant of motion, or another observable which commutes with the Hamiltonian, at least in an approximate fashion.

Is this suggestion of an approximate dynamical symmetry correct, or are these near crossings of hydrogen's energy levels in a magnetic field merely manifestations of the fundamental inadequacy of the numerical methods? We hope to answer this question by experiment.

The immediate goal of our research is to map out the energy levels of a Rydberg atom in a strong magnetic field in the region of a level crossing. The use of an atomic beam permits the measurement of energy levels without the first-order Doppler shift because the beam moves parallel to the magnetic field so that there is no electric field in the rest frame of the atom, and hence no motional Stark shift. The experiment employs dye lasers provided by the M.I.T. Regional Laser Center. These lasers are

actively stabilized and have a short-term linewidth of about 5 MHz, permitting a relatively high resolution experiment. (Previous experiments had over a 1000 MHz linewidth.)

The excitation scheme for producing lithium Rydberg atoms is 2s→3s via two photons of 735 nm, and 3s→~40p via one photon of ~620 nm. This method produces odd parity Rydberg states. In the presence of a magnetic field, only angular momentum states of the same parity are coupled by the diamagnetic term in the Hamiltonian. The Rydberg states accessed in this experiment cannot contain any zero angular momentum states. Consequently, they have minimum perturbation from the non-hydrogenic core of lithium. (The residual level repulsion from the core penetration of the 40p state is estimated to be 300 MHz.)

Detection of Rydberg atoms is accomplished by field ionization. The excited atoms drift into a region of high electric field and are ionized. The electrons are detected with a surface barrier diode.
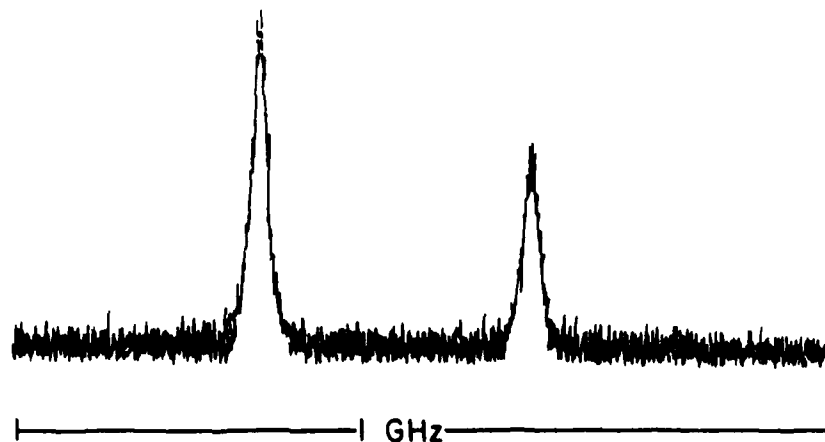
Figure 3-1: Two–Photon Resonance in Lithium

We have observed the initial state of excitation, two–photon 2s→3s transition. Atoms in the 3s state spontaneously decay to the 2p state, emitting 813 nm photons, and then decay to the 2s state, emitting 617 nm photons. The latter signal is collected by an optical fiber, and passed through an interference filter which rejects the 735 nm laser light. The fluorescence is detected with a photomultiplier tube. Results are shown in Fig. 3-1. Both the $2^2S_{1/2}$ and $3^2S_{1/2}$ states possess hyperfine structure. The scan width is 1 GHz. Knowing the ground state hyperfine splitting of ^7Li, 803.5 MHz, yields a result for the $3^2S_{1/2}$ hyperfine splitting of about 170 MHz. Most of the linewidth is from the Doppler shift of the unapertured atomic beam.

Publications

Kleppner, D., M.G. Littman, and M.L. Zimmerman, "Rydberg Atoms in Strong Fields," in R.F. Stebbings and F.B. Dunning (Eds.), Rydberg States of Atoms and Molecules, (Cambridge University Press, 1982).

3.2 Multiphoton Ionization

Lawrence R. Brewer, Fritz Buchinger, Daniel Kelleher, Daniel Kleppner

Multiphoton ionization can occur whenever intense light interacts with matter. The study of multiphoton ionization is an active area of contemporary research in optical physics because of its intrinsic interest and because it often has dramatic experimental consequences. Theoretical interest lies in understanding the breakdown of perturbation theory, the role of coherence in multiphoton processes, and the restructuring of atomic states in intense fields. Experimental interest stems from the rich variety of multiphoton processes that can be observed, and the challenge of executing well characterized experiments which can be compared in detail with theory. A significant theoretical advance is the recent work by Reinhardt and his colleagues who have developed a non–perturbative theory for multiphoton ionization of hydrogen.[1] We have studied resonant four photon ionization of hydrogen near threshold. The resonant process is the three photon excitation of the 1s–2p transition: a fourth photon then ionizes the atom at threshold.

The experiment is carried out in an atomic beam. Hydrogen is provided by a liquid nitrogen cooled rf dissociator. The atoms pass through an accommodator which can be cooled to liquid helium temperature. The system is pumped by a baffled oil diffusion pump.

Photoionization occurs by absorption of four identical photons at a wavelength near 364.6 nm. Our system employs a tunable dye laser–amplifier near 554.6 nm, which is pumped by a Nd:YAG laser. 50 mJ is produced in a 5 nsec pulse at a repetition rate of 10 pps. This pulse is mixed with a 150 mJ pulse at 1060 nm (the Nd:TAG fundamental), providing 15 mJ at 364.6 nm. The dye laser frequency is monitored with an Iodine absorption cell.

The photoions are swept out by a pair of field plates and collected by a linear electron multiplier. The signal is integrated, digitized, and stored in a computer.

Fig. 3–2 shows lineshapes for the process we are studying as calculated by the methods of Ref. 1. Two features are conspicuous: as the laser power increases, the line center shifts to the blue of the threshold frequency for ionization, and the line broadens. We have observed both of the features in our data. We have recently obtained our first results using multimode laser light. Data is shown in Fig. 3–3. The signal to noise ratio is high and the change in shape of the photoionization curve with increasing laser power is marked.

References

1. C.R. Holt, M.G. Raymer, and W.P. Reinhardt, Phys. Rev. A 27, 2971 (1983).
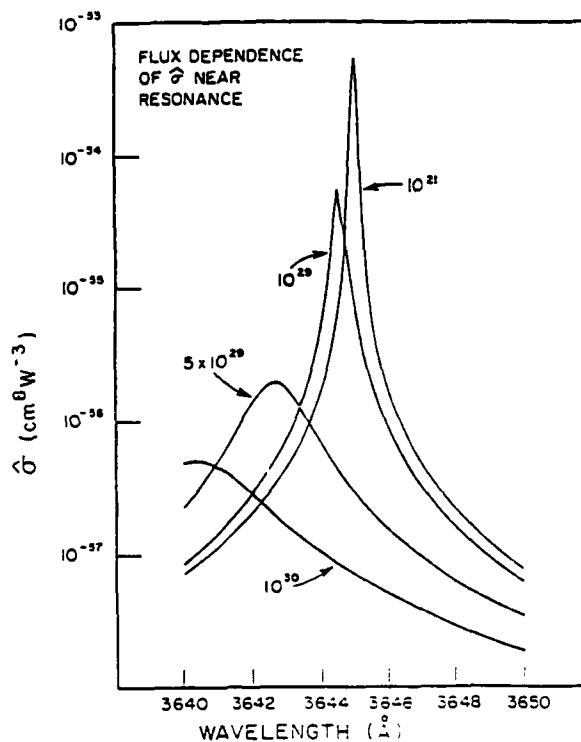
Figure 3-2: The cross section for 4 photon ionization of atomic hydrogen as calculated by Reinhardt for a single frequency laser. To facilitate comparison, the cross section has been divided by I^3. As the intensity increases, the peaks shift to the blue and become broader.

3.3 Atoms in "Circular" States

Randall G. Hulet, Daniel Kleppner

We have produced a population of atoms in Rydberg states with $|m| = n - 1$, where m and n are the magnetic and principal quantum numbers respectively. We refer to these states as "circular" because in the classical limit they describe an electron in a circular orbit. Atoms in circular states possess a number of useful and interesting properties: among all the states with a given principal quantum number, they have the largest magnetic moment, smallest Stark effect and longest radiative lifetime. Their collision cross sections are expected to be highly anisotropic. Only one transition is available for spontaneous emission ($n \rightarrow n - 1$; $|m| \rightarrow |m| - 1$), allowing them to serve as useful
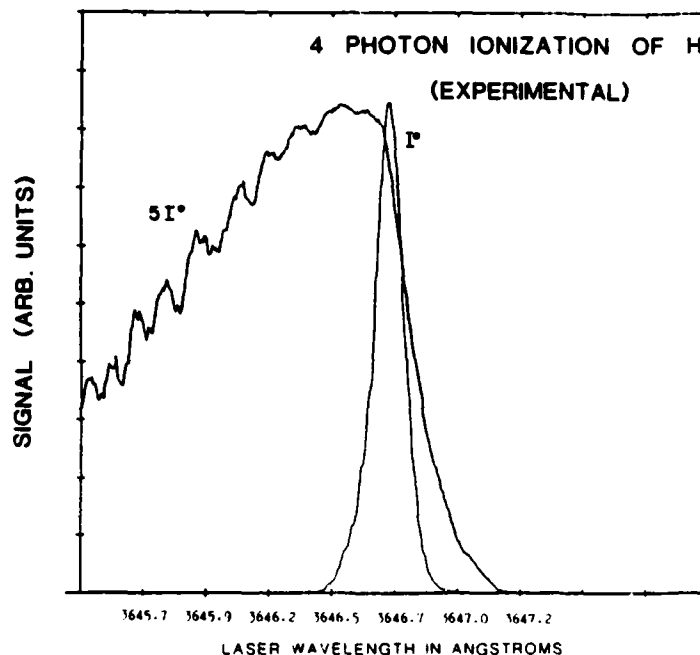
Figure 3-3: Ionization profiles produced by laser intensity I° and at five times that intensity 5I°. As the laser intensity is increased, the ionization profile becomes broad and asymetric and is shifted to the blue of threshold.

approximations to two level systems. For these reasons, and others, the circular states are particularly attractive for high precision Rydberg state spectroscopy.

We have developed a simple method for transferring a population of atoms in a low-m Rydberg state to a circular state, with essentially 100% efficiency. The atoms are transferred by a series of adiabatic rapid passages induced by a microwave field and an electric field which decreases linearly with time. Each adiabatic rapid passage causes $|m|$ to increase by 1; the process terminates when the atom reaches the circular state. We have demonstrated the method with lithium, $n = 19$, but for ease of explanation we shall consider hydrogen, $n = 4$, neglecting electron and nuclear spin.

The energy of hydrogen (in cm^1) in an electric field F is given to first order by $W = -(1/2n^2 - 3nF(n_1 - n_2))R$, where n_1 and n_2 are the parabolic quantum numbers ($n_1 + n_2 + |m| + 1 = n$). R is the Rydberg constant, and F is in atomic units, $5.14 \times 10^9 V/cm$. The energy levels for $n = 4$ are shown in Fig. 3-4a. Initially, the lowest $|m| = 0$ state is populated: $|m| = 0$, $n_1 = 0$. A series of transitions satisfying $\Delta |m| = 1$, $\Delta n_1 = 0$ is induced by adiabatic rapid passages, as indicated by the heavy arrows. Because of the second order Stark effect (not shown in Fig. 3-4a), the transitions occur consecutively in time.

To further illustrate the process, the energy levels for the $n_1 = 0$ states are shown in Fig. 3–4b with the second order Stark effect W_2 included and exaggerated for clarity. The microwave frequency is slightly below the resonance frequency for the initial transition $|m| = 0 \rightarrow 1$. As the field decreases, the transitions are consecutively encountered as shown in Fig. 3–4b.
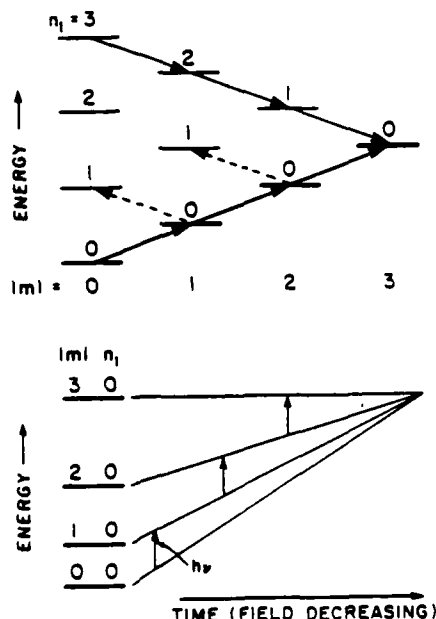
Figure 3-4: Schematic diagram of the excitation process, illustrated with hydrogen, n = 4. a) (above) Energy levels in an electric field, neglecting the second order Stark effect. The bold arrows show the excitation path used to populate the circular state, $|m| = 3$; the light arrows show an alternative excitation route; the dashed arrows show "leakage" transitions which must be avoided. b) (below) The progression of $n_1 = 0$ levels in a decreasing field, with the second order Stark effect exaggerated for clarity. An adiabatic rapid transition can occur whenever the energy level separation passes through resonance with the microwave frequency ν. Because of the second order Stark effect these transitions occur successively, "stepping" the population along the route shown in a), above.

The experiment employed the n = 19 manifold of lithium. An atomic beam was used and the Rydberg state was populated by two–step pulsed excitation: $2^2S_{1/2} \rightarrow 2^2P_{3/2}$ (671 nm) and $2^2P_{3/2} \rightarrow$ Rydberg (~354 nm). An electric field was applied using copper field plates which were carefully spaced 6.9 mm apart. Ions were collected through a grid drilled in the lower plate over a length of 20 mm.

The atoms were excited by 5 ns laser pulses in a field of 830 V/cm. The microwave power was turned on and the field was linearly decreased to 806 V/cm during a 5 μs period. The first transition ($|m| = 2 \rightarrow 3$) occurred at 824 V/cm; the last ($|m| = 17 \rightarrow 18$) occurred at 810 V/cm. The microwave power was turned off and the atomic population analyzed by field ionization. The field was abruptly switched to 4.4 kV/cm and then ramped to 5.9 kV/cm over a 2.5 μs period. During this period $|m|$ states which ionize at progressively higher fields were successively detected and recorded by a transient analyzer.
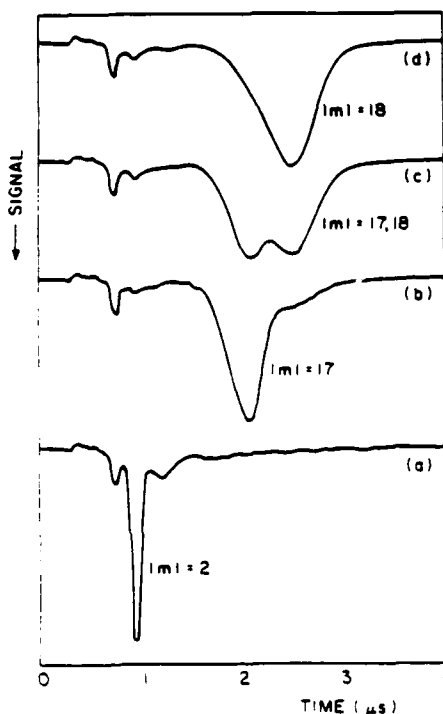
Figure 3-5: Distribution of population in lithium for various values of $|m|$ as revealed by selective field ionization. States are n = 19, n_1 = 0. The ionization field increases with time. The ionization thresholds occur in increasing fields as $|m|$ increases. a) $|m|$ = 2 states initially populated by laser excitation in a field of 830 Vcm^{-1}. The signal is clipped due to saturation of the detector. The small peak to the left is due to $|m|$ = 0 atoms. The small peak to the right is due to $|m|$ = 2 atoms which ionize hydrogenically. The $|m|$ = 2 peak occurs at approximately 4.5kVcm^{-1}. b) Same as a), but with the adiabatic rapid passage field ramp on for a time τ_{rp} = 4μs. The $|m|$ = 2 population has been transferred predominantly to $|m|$ = 17. c) τ_{rp} increased: ionization signals for $|m|$ = 17 and 18 are both visible. d) τ_{rp} > 4.5. μs. The $|m|$ = 18 circular states is populated. No further change in the ionization signal occurs with increasing τ_{rp}. The ionizing field is approximately 5.9 kVcm$_{-1}$.

Experimental results are shown in Fig. 3-5. To demonstrate the progression of the population transfer, the "on" time of the rapid passage field ramp and of the microwave power, was successively increased. In curve a, $\tau < 1$ μs, no transitions have occurred and the initial states, n = 19, |m| = 2, are displayed. Because of the laser linewidth (0.1 cm^{-1}), and power broadening effects, an m = 0 state is also excited; its ionization signal occurs at the lowest field. The |m| = 2 states appear as a well resolved peak shortly thereafter.

As the time τ is increased, the ionization signal moves to longer times, indicating that the atoms are being transferred to higher |m| states as shown in curves b and c. The ionization signal from adjacent |m| states overlap in this region, but as higher values of |m| are reached, the signals start to be resolved. Finally, as shown in curve d, for $\tau > 4.5$ μs, the circular state, |m| = 18, is populated. No further changes occur with increasing τ. The signals are in good agreement with ionization rate calculations.

3.4 Laser Induced Fluorescence Study of NaAr

Walter P. Lapatovich, A. Marjatta Lyyra, Philip E. Moskowitz, Mark D. Havey, David E. Pritchard

Van der Waal molecules are interesting from the standpoint of molecular physics because they are so different from ionic and covalent molecules. Not only are the potentials weaker by a factor of 100–1000 and the interatomic separations correspondingly larger, but the spectra contain information from a wider range of internuclear separations. For instance, levels up to dissociation are often thermally populated.

The study of NaAr represents a situation where most of the observed vibrational levels in the excited states ($A^2\Pi_r$ and $B^2\Sigma^+$ from the Na 3p atomic limit) are $\leq$15% from the dissociation limit. Long range analysis has been utilized extensively to predict unobserved vibrational levels and their deperturbed rotational constants as well as potential parameters for the above mentioned electronic states. Several perturbations close to the $A^2\Pi_{1/2}$ dissociation limit have been observed and analyzed. The observation of highly excited vibrational levels of the $A^2\Pi_r$ state also enabled us to determine the ground state well depth from long range analysis.

The NaAr study together with our earlier work on NaNe[1,2] represent the state of the art in diatomic van der Waals molecular spectroscopy and provide the most accurate determination of the potentials experimentally possible.

References

1. R.A. Gottscho, R. Ahmad–Bitar, W. Lapatovich, I. Renhorn, and D.E. Pritchard, J. Chem. Phys. <u>75</u>, 2546–2559 (1981).
2. W.P. Lapatovich, R. Ahmad–Bitar, P.E. Moskowitz, I. Renhorn, R.A. Gottscho, and D.E. Pritchard, J. Chem. Phys. <u>73</u>, 5419–5431 (1980).

3.5 Vibrationally Inelastic Collisions

Susan L. Dexheimer, Charles W. Engelke, Peter D. Magill, Katherine L. Saenger, Neil Smith, David E. Pritchard

During the past few years we have developed a general picture of Rotationally Inelastic (RI) Collisions involving both theoretical and experimental advances. We have shown that the hundreds of measured rate constants describing these collisions can be reproduced to within 10% by simple analytic expressions containing 3 to 4 fitting parameters and that the qualitative behavior of these rate constants is easily explained in terms of simple dynamical ideas.

The more complete understanding of collision induced energy transfer that we desire, however, requires study of Vibrationally–Rotationally Inelastic (VRI) processes. The increased complexity of VRI collisions (they involve a change in both vibrational and rotational quantum numbers) makes them more interesting to examine but more challenging to explain with the simplicity that worked so well for pure RI collisions. Previous theoretical treatments have been hampered by the lack of high quality experimental data and are inadequate due to their neglect of rotation.

During this past year we have started to measure level to level rate constants $k_{v_i j_i \rightarrow j_f v_f}$ for Li_2^*—rare gas atom systems. Our preliminary results for Xe are shown in Fig. 3–6 where we have plotted $k_{v_i j_i \rightarrow v_f j_f}$ versus j_f for $v_i = 4$, $\Delta V = -3$ and $j_i = 14, 28, 44$. With increasing j– there is both a dramatic increase in the magnitudes of the rate constants and a narrowing of their distribution in j_f. Nothing like this has been observed previously. These are important clues to the significant role of rotation in vibrational energy transfer.

3.6 Diffraction of Sodium Atoms by a Standing Wave Laser Field

Philip E. Moskowitz, Phillip L. Gould, Susan Atlas, David E. Pritchard

Perhaps the most important problem which has arisen in atomic physics as a result of the laser concerns effects of intense optical radiation on simple atomic systems. The momentum transferred to

3×10^{-11}

$Li_2^* - Xe$

$v_i = 4 \quad \Delta v = -1$

$\Delta \quad j_i = 14$

$x \quad j_i = 28$

$o \quad j_i = 44$

$k_{v_i, j_i \to v_f, j_f}$, $cm^3 s^{-1}$

j_f
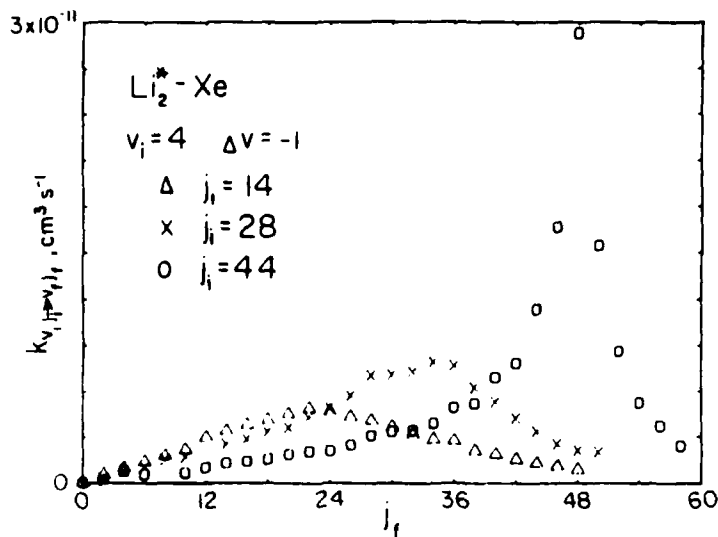
Figure 3-6

atoms by a standing wave optical frequency field is a central question in this arena because the force on the atoms is simply the spatial gradient of the energy of the combined atom-field system—the "dressed" atom. A study of atoms scattered by a perpendicularly oriented standing wave field is a study of the basic induced dipole interaction between atoms and optical frequency fields.

INTENSITY [c/s]

DEFLECTION [ℏk]
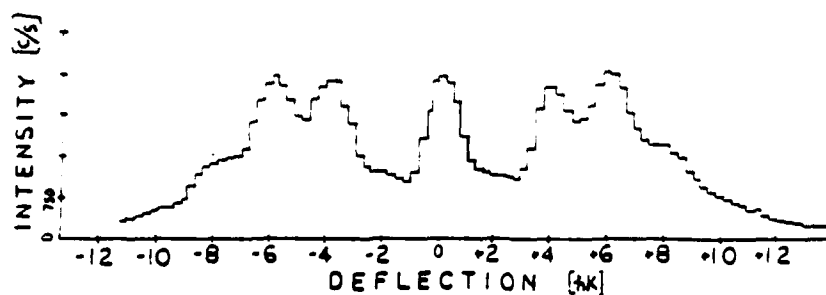
Figure 3-7

In revealing the nature of the interaction of intense radiation fields on atomic systems, our experiment resolves a controversy apparent in the many relevant theoretical publications of the last few years. In contrast to two previous experimental efforts[1,2] which have been inconclusive, we have constructed a supersonic beam machine with the momentum resolution of a single photon ($p_\gamma = hk$), and an atom-field interaction time of the order of the spontaneous lifetime of the sodium $3S_{1/2} \to 3P_{3/2}$ transition. The single frequency dye laser is tuned near resonance with this transition, one of

the so-called sodium "D-lines". This, and a state-of-the-art neutral atom detector, has enabled us to display phenomena previously unobserved: a symmetric splitting of the atomic beam and a periodic modulation of $2\hbar k$ in the momentum distribution (Fig. 3-7).

The observed magnitude of the splitting as a function of the field strength has enabled us to apply certain semiclassical theories[3] to our data with success. We have also explained the periodic modulation as originating from an adiabatic interaction of the atom with the field, and have called this diffraction.[4]

References

1. E. Arimondo, H. Lew, and T. Oka, Phys. Rev. Lett. 43, 753 (1979).
2. V.A. Grinchuk, E.F. Kuzin, M.L. Nagaeva, G.A. Ryabenko, A.P. Kazantsev, G.I. Surdutovich, and V.P. Yakovlev, Phys. Lett. 86A, 136 (1981).
3. A.P. Kazantsev, G.I. Surdutovich, and V.P. Yakovlev, Opt. Comm. 43, 180 (1982).
4. P.E. Moskowitz, P.L. Gould, S. Atlas, and D.E. Pritchard, Phys. Rev. Lett., submitted for publication.

3.7 A Search for Radiative Transitions in Atom-Molecule Systems

Alan L. Migdall, Robert E. Walkup, David E. Pritchard

A new transition mechanism has been proposed[1-3] as a generally useful spectroscopic tool with specific applications to producing population in otherwise optically inaccessible molecular states. The process consists of an atom and a molecule during a collision acting as a quasi-molecule that makes a single photon radiative transition that leaves the atom in a new electronic state while the molecule changes its vibration and/or rotation state.

We have developed guidelines for choosing a system in which to best observe such a transition. Using these guidelines we chose two optimal systems to study. Our experimental measurements on these systems showed that even under these favorable conditions radiative collisions are difficult to observe. This observation, along with our guidelines, leads us to conclude that this type of radiative process will not have the general applicability that has been suggested.

References

1. P. Hering and Y. Rabin, Chem. Phys. Lett. 77, 506 (1981).
2. J. Lukasik and S. Wallace, Phys. Rev. Lett. 47, 240 (1981).
3. J.C. White, Opt. Lett. 5, 199 (1980).

3.8 Rotationally Inelastic Collisions

Timothy A. Brunner, Neil Smith, Thomas P. Scott, David E. Pritchard

We have completed and published a comprehensive review[1] of the theory and application of the several scaling and fitting laws for Rotationally Inelastic (RI) collisions which we developed under AFOSR support. The review will serve as a guide for allowing broader application of this approach by other members in the field.

We have shown[2] that a classical limit impulsive calculation can allow analytic evalution of the RI basis rate constant $k_{\ell \to 0}$ which predicts the power–law dependence $k_{\ell \to 0} \propto [\ell(\ell + 1)]^{-\gamma}$. This provides simple theoretical support for this previously observed empirical observation which has been shown[1] to give good agreement with experimental and theoretical results in a large variety of RI collision systems.

We have completed measurements and preliminary analysis[3] of the relative velocity dependence of RI cross–sections in $Li_2^*(A^1\Sigma) - Xe$. These cross–sections show an unusually strong dependence on velocity. Calculations using classical trajectory methods are presently underway to predict the experimental results, and thus gain information on the previously unknown $Li_2^* - Xe$ interaction potential.

References

1. T.A. Brunner and D.E. Pritchard, in K.P. Lawley (Ed.), <u>Dynamics of the Excited State</u>, (John Wiley and Sons, 1982).
2. T.A. Brunner, T.P. Scott, and D.E. Pritchard, J. Chem. Phys. <u>76</u>, 5641 (1982).
3. N. Smith, T.P. Scott, and D.E. Pritchard, Chem.Phys. Lett. <u>90</u>, 461 (1982).

4. Reaction Dynamics at Semiconductor Surfaces

Academic and Research Staff

Prof. S.T. Ceyer

Graduate Students

J.D. Beckerle, M.B. Lee, M. McGonigal, J. Simonson, S.L. Tang

Sylvia T. Ceyer

The mechanism of the reactions of a gaseous species such as F_2 with a semiconductor surface such as Si is complex. The mechanism may involve several processes, including the adsorption of the molecule on the semiconductor surface, dissociation of the adsorbed molecule, diffusion of the dissociated species to a reactive site, reaction with the surface, and then desorption of the product molecule. The purpose of this research is to study the dynamics of the first two processes, the adsorption and dissociation of a molecule incident on a surface. We would like to understand how a molecule falls apart on a surface. For example, does the molecule first adsorb and then diffuse to a reactive site and then dissociate or are the dissociation and adsorption processes concerted? What feature of the potential energy surface of the molecule–surface interaction dictates which dynamics occur? Variation of the energy of the incident molecule is a convenient probe of these dominant features of the interaction potential because the dynamics and hence the observed dissociation probability depend strongly on the incident energy relative to the interaction potential.

However, studies of the effect of the energy of the incident molecule on the dissociation probability are virtually nonexistent because most surface studies are undertaken after adsorption of ambient molecules. This implies that molecules strike the surface from all directions and with energies characterized by a 300 K Maxwell–Boltzmann distribution. We have just begun to design and build an apparatus to investigate the effect of the incident energy on the probability of dissociative adsorption. This apparatus employs molecular–beam techniques to define and control the energy of the incident molecule (up to 50 kcal/mole and 10 kcal/mole translational and internal excitations, respectively). The presence and amount of dissociation are detected sensitively ($\geq$ 0.1% of a monolayer) by high–resolution electron–energy–loss spectroscopy, a vibrational spectroscopy. These fundamental studies on the effect of a molecule's incident energy on dissociative adsorption are important because of the unknown chemistry these "hot" neutral molecules carry out during the plasma etching of semiconductors, where translationally and internally excited molecules are produced by numerous collisions with fast ions and electrons. The long–range goal of this research is to provide far–reaching correlations between the observed dynamics and the potential energy surfaces on which molecule–surface reactions occur.

1

5. X–Ray Diffuse Scattering

Academic and Research Staff

Prof. R.J. Birgeneau, Prof. J. Akimitsu, Dr. A.R. Kortan, Dr. M. Sutton

Graduate Students

P.A. Heiney, H. Hong, L.J. Martínez-Miranda, S.G.J. Mochrie, B.M. Ocko, E. Specht

Joint Services Electronics Program (Contracts DAAG29-80-C-0104 and DAAG29-81-K-0029)
Robert J. Birgeneau

In this research program, modern x–ray scattering techniques are used to study the structures and phase transitions in novel states of condensed matter. We have two principal experimental facilities. At M.I.T. we have three high–resolution computer controlled x–ray spectrometers using either a conventional or high intensity rotating anode x-ray generator. The angular resolution can be made as fine as 1.8 seconds of arc; this enables one to probe the development of order from distances of the order of the x–ray wavelength, ~ 1 Å, up to 30,000 Å. The sample temperature may be varied between 2 K and 500 K with a relative accuracy of 2×10^{-3}K. We are currently installing a two spectrometer system at the National Synchrotron Light Source at Brookhaven National Laboratory. This makes possible high resolution scattering experiments with a flux more than three orders of magnitude larger than that from a rotating anode x–ray generator. This opens up a new generation of experiments. Synchrotron x–ray scattering experiments are also carried out on a wiggler beam line at the Stanford Synchrotron Radiation Laboratory.

As part of this JSEP program we are designing and building an x–ray compatible high vacuum single crystal surface apparatus. This will enable us to use synchrotron radiation to study the structure and transitions occurring at single surfaces. The possibilities with this seem virtually unlimited. Our current experiments in this program are concentrated in two areas: (i) the growth, structure, and phase transitions of intercalant materials, most especially bromine–intercalated graphite, (ii) the structure and phase transitions of smectic liquid crystals.

5.1 Intercalation Compound Structures and Transitions

Intercalation compounds represent a family of materials in which a foreign species (e.g. Br_2) is inserted between the layers of a lamellar material such as graphite. If the intercalant enters every *n*th layer then the resultant material is referred to as a stage–*n* intercalation compound. We have initiated a program to study "in–situ", using high resolution x–ray scattering techniques, both the intercalation process itself and the structure and transitions of the intercalation compound as a function of

temperature, concentration, and stage index. Our . ~al work has concentrated on the system bromine-intercalated graphite $C_{7n}Br_2$.[1,2]

The intercalate plane is found to have three sublattices and each sublattice has a centered ($\sqrt{3} \times 7$) rectangular structure with four Br_2 molecules per 2D unit cell in the commensurate phase. The coherently ordered in-plane bromine regions exceed 10,000 Å in size. In the stage-4 material a commensurate-incommensurate (CIT) transition is observed at 342.20 ± 0.05°K. In the incommensurate phase, a stripe domain pattern becomes established in a single domain of a sublattice along the 7-fold direction. The incommensurability as a function of reduced temperature exhibits power law behavior with an exponent of 0.50 ± 0.02 confirming existing theories. The relative shifts observed for the various harmonics are accurately predicted by a sharp domain wall with $4\pi/7$ phase shifts. A power-law lineshape reflecting the lack of true long range order is observed for the incommensurate intercalant layer, yielding values for the exponent η consistent with model calculations. The intercalate layer exhibits a continuous melting transition from a two-dimensional solid phase to a smectic liquid crystal phase, occurring at 373.41 ± 0.10°K for a stage-4 compound.

We are continuing these detailed studies for lower stage material; we have also carried out some initial experiments on graphite intercalated with potassium and mercury. This system exhibits superconductivity at 1 K and thus is of particular interest.

5.2 Smectic Liquid Crystals

Liquid crystals are made up of rod-like molecules. In the nematic phase the axes of the molecules align parallel to each other but the centers of mass of the molecules are still randomly distributed so that one has a pure fluid structure factor. In the smectic A and C phases a one-dimensional sinusoidal density wave is set up either along (A) or at an angle (C) to the molecular axis. Thus, these smectics are like solids in one direction and fluids in the other two. These systems exhibit particularly interesting phase transitions which present an important challenge to modern theories of critical phenomena. At lower temperatures many liquid crystal materials exhibit more ordered phases such as smectic B, F, and G. These have well-developed in-plane triangular order. If the order is truly long range then the phase is a plastic crystal. Otherwise, the smectic may be a realization of a novel phase of matter labelled a "stacked hexatic" with long range order in the crystalline axes but only short range order in the positions of the molecules. We have recently studied in some detail the smectic phases and phase transitions in two related materials, heptyloxybenzylidene-heptylaniline (70.7)[3] and butyloxybenzilidene-heptylaniline (40.7).[4]

Our work in 70.7 has concentrated primarily on the B-phase. We have carried out an x-ray diffraction study using both rotating anode and synchrotron sources of structures and restacking transitions within the B phases. The system evolves from a hexagonal close-packed structure, through intermediate orthorhombic and monoclinic phases, to a simple hexagonal structure. The

monoclinic phase has a temperature–dependent shear which transforms the system from orthorhombic to hexagonal. The latter three phrases exhibit a single– $\vec{q}$ sinusoidal modulation of the molecular layers. The sinusoidal modulation is believed to represent a precursor to the tilted (G) phase at lower temperatures. This behavior is much richer than anyone had previously considered possible within the B–phase. The experiments demonstrate most clearly that there is need for a significant development of theories for the structures of quasi-2D molecular solids.

In 40.7 we have carried out an encyclopaedic study of all of the liquid crystal phases and phase transitions. Here we emphasize our results for the smectic A – smectic C transition. This is a second order transition in which the molecular axis spontaneously tilts with respect to the density wave direction. This transition would appear to be the simplest liquid crystal phase change; in spite of that, it has been the subject of considerable controversy in the literature.

In our previous JSEP work we have argued, using a Landau theory and the Ginzburg criterion, that A–C transitions should exhibit mean field behavior over the temperature range accessible by current experimental techniques. However, if interpreted naively, recent measurements in two materials, butyloxybenzylidene–heptylaniline (40.7) and azoxy–4, 4'–di–undecyl–α–methylcinnimate (AMC–11), seem to contradict this prediction. Specifically, over the reduced range 5×10^{-3} to 5×10^{-5} in both cases the tilt follows a power law with $\beta \simeq 0.36$; that is, these materials seem to exhibit helium–like critical behavior. By carrying out order parameter, heat capacity and light scattering measurements we have found that the data are uniquely described by mean field theory with an unusually large sixth order term. The measured β = .36 thus represents a crossover from β = ½ to ¼ regimes demonstrating that the original Ginzburg criterion arguments are correct. We do not, however, have a plausible microscopic explanation for the large sixth order term.

References

1. A.R. Kortan, A. Erbil, R.J. Birgeneau, and M.S. Dresselhaus, Phys. Rev. Lett. <u>49</u>, 1427 (1982).
2. A. Erbil, A.R. Kortan, R.J. Birgeneau, and M.S. Dresselhaus, Phys. Rev., submitted for publication.
3. J. Collett, L.B. Sorensen, P.S. Pershan, J.D. Litster, R.J. Birgeneau, and J. Als–Nielsen, Phys. Rev. Lett. <u>49</u>, 553 (1982).
4. R.J. Birgeneau, C.W. Garland, A.R. Kortan, J.D. Litster, M. Meichle, B.M. Ocko, C. Rosenblatt, L.Y. Yu, and J. Goodby, Phys. Rev. A <u>27</u>, 1251 (1983).

6. Phase Transitions in Chemisorbed Systems

Academic and Research Staff

Prof. A.N. Berker, Dr. D. Blankschtein, Dr. J.S. Walker

Graduate Students

D. Andelman, R.G. Caflisch, M. Kardar, S.R. McKay

Undergraduate Students

R.E. Goldstein, R.J. Lenk

Surfaces and interfaces abound in our physical environment, and as systems which are low dimensional and therefore fluctuation dominated, embody fundamental problems of many–body physics. Our research group is studying a variety of low–dimensional and fluctuation–dominated systems. Such studies start with microscopic descriptions, such as the interactions of an overlayer in the presence of a constraining substrate, or the configuration energies and entropies of a helix–coil polymer immersed in an electrolyte. The eventual outcome is macroscopic, measured or measurable properties. Another important outcome is the understanding of mechanisms generic to many–body physics.

Through the discovery and development of the renormalization–group method, extraordinary advance has been achieved in recent years in phase transitions and critical phenomena. This approach successfully deals with a large number of coupled degrees of freedom in a stepwise manner, by thinning out a fraction of the degrees of freedom, and repeating this operation over and over. Thus, our program utilizes the renormalization–group method, but also any other theoretical tool as may be necessary. Important technical advances have been achieved in this respect.

6.1 Oxygen on Nickel and other Chemisorption Phase Diagrams

Robert G. Caflisch, A. Nihat Berker

Epitaxial adsorption onto a square substrate is studied with a Hamiltonian including nearest–neighbor exclusion, second and third–neighbor pair and trio interactions. The resulting phase diagrams[1] exhibit 2x2, $\sqrt{2} \times \sqrt{2}$, and 2x1 ordered phases and a disordered phase. Thus, all three ordered structures observed with oxygen on nickel (100) are obtained for the first time within the same phase diagram in the coverage and temperature variables. The 2x1 phase has an important entropy content and appears only at intermediate temperatures. Simple ground–state energy analysis

or classical mean–field calculations, therefore, completely miss this phase. Other cross–sections of our global phase diagram should be applicable to chemisorbates such as oxygen, sulfur, selenium, or tellurium, on substrates such as nickel, copper, tungsten, or platinum (100). First– and second–order phase boundaries are evaluated, punctuated by tricritical, critical–end, bicritical, and tetracritical points. Reentrant tricriticality is found, yielding closed–loop coexistence regions. The possibility of two distinct 2x2 phases, with uniaxial order or a novel biaxial order, is raised for the first time. We use a Migdal–Kadanoff approximation on a cell system, with renormalization–group flows in sixteen energy levels.

In a separate work[2] in collaboration with Prof. J.D. Joannopoulos' group, total–energy ground state calculations are combined with renormalization–group analysis to predict the surface reconstruction of Si (100).

6.2 Commensurate–Incommensurate Phase Transitions, Domain Walls, and Helicity in Two–Dimensional Systems

Mehran Kardar, A. Nihat Berker

Upon increased adsorption, registered overlayers become incommensurate with their substrate by forming high–density domain walls, which results in interactions (between domains) of a helical character. For this phenomenon, we introduced the helical Potts model, which successfully reproduced several experimental observations with krypton on graphite, from Prof. Birgeneau's group, and with krypton and deuterium coadsorbed on graphite. A q–state generalization of this model has been studied on the square lattice.[3] At low temperatures, this model can be mapped onto the six–vertex model of Baxter in direct fields. This mapping indicates the presence of a modulated incommensurate phase. This phase exhibits a virtual ordering, in the sense that the correlations over large separations neither go to a non–zero constant, as in a truly ordered phase, nor do they decay exponentially to zero, as in a disordered phase. Instead, a weak algebraic decay of correlations occurs, with a critical exponent $\eta = 2/q^2$ at low temperature. A Lifshitz–like multicritical point is located where the registered, modulated, and disordered phases meet.

6.3 Multicritical Phenomena in Cubic Symmetry Systems

Robert G. Caflisch, Daniel Blankschtein

Phase transitions which are predicted to be first–order by the classical Landau theory can in fact be driven second–order by critical fluctuations. This fluctuation–induced criticality occurs in cubic

systems which are almost tricritical. Application of symmetry–breaking perturbations suppresses fluctuations and may restore first–order behavior via tricritical points. We are currently studying the effect of off–diagonal, quadratic symmetry–breaking perturbations on cubic systems undergoing fluctuation–induced transitions. We expect a wide variety of bicritical and tetracritical–like phase diagrams, also featuring tricritical, critical and critical–end points. Our approach combines mean–field theory, large–anisotropy expansion, and renormalization–group analysis. The relevance of cubic models to oxygen chemisorbed on nickel (111) has been noted by other workers. The cubic phase diagrams may also be realizable experimentally by applying uniaxial stresses or magnetic fields to systems exhibiting structural or magnetic phase transitions, such as $KMnF_3$, $RbCaF_3$, $BaTiO_3$, MnO, TbP, etc.

6.4 Crossover to Equivalent–Neighbor Multicritical Behavior

Joint Services Electronics Program (Contract DAAG29-80-C-0104)
Mehran Kardar, A. Nihat Berker

Exact solutions of models of many–body systems, though difficult to achieve, are of crucial importance to our understanding of physical phase transition phenomena. Our recently introduced central–limit minimization method, based on a new statistical mechanical proof, yields new classes of exactly solvable Hamiltonians. Using this method, systems with both short– and long–range interactions are solved exactly.[4] Such situations could occur, for example, in chemisorption or surface reconstruction systems with short–range covalent bond formation and long–range dipolar couplings. Crossover from fluctuation–dominated to mean–field criticality is described in arbitrary spatial dimension. Phase diagrams are derived, with lines of classical and non–classical second–order transitions and first–order transitions, meeting at multicritical points and exhibiting new types of critical behavior.

6.5 Hydrogen–Bonding and Helix–Coil Transformations

Joint Services Electronics Program (Contract DAAG29-80-C-0104)
Raymond E. Goldstein, A. Nihat Berker

The conformational changes undergone by certain biological macromolecules, such as poly–γ–benzyl–L–glutamate in ethylene dichloride + dichloroacetic acid, are proposed to arise from the same interplay of energy versus entropy that causes lower critical–solution points in liquid mixtures, which have been studied extensively in this group. In these mixtures, hydrogen bonds between unlike molecules are responsible for the reappearance of a miscible (substitionally long–range disordered) phase below a lower critical temperature, but concurrently with increased short–range orientational order, so that entropy is decreased according to the third law. This results

in closed–loop coexistence regions. Note that we have also predicted closed–loop coexistence regions in chemisorbed systems. In certain macromolecular solutions, an ordered helical state evolves into a random–coil state with decreasing temperature. This reversal from the expected ordering trend is explained by associating to the polymer–solvent hydrogen bonds, the role played by unlike–molecule bonds in liquid mixtures. A Potts model is used to carry out the statistical mechanics of these macromolecular solutions. Experiments to clarify the relationship outlined above are proposed.

6.6 Improved Renormalization–Group Transformations

David Andelman, Raymond E. Goldstein, James S. Walker, A. Nihat Berker

In its rapid evolution to an everyday calculational tool, the renormalization–group method incorporates correlated fluctuations, but yet has become more amenable than classical approaches to many problems. This is certainly the case, for example, for the calculation of the multicritical, multistructure phase diagrams of chemisorbed systems described above. One approach which we have introduced is to map, by a so-called prefacing transformation, a system with complicated further–neighbor interactions onto one with complicated local degrees of freedom coupled by nearest–neighbor interactions, and readily renormalizable. This renormalization is most easily done by a Migdal–Kadanoff procedure. We have also investigated replacing the ad hoc bond–moving prescription of this approximation by a systematic procedure. The free energy is required to be preserved by matching perturbative series expansions. The approach is characterized by a small parameter, and can be order-by-order extended. A significant improvement is obtained over the standard Migdal–Kadanoff calculation, with little increased effort. A detailed application to q–state Potts models in two and three dimensions has been presented.[5,6] In a most recent development, the bond–moving procedure is fixed by an exact finite–lattice calculation. The resulting renormalization–group transformation is applied to infinite, thermodynamic systems. This new method is most promising in that it produces quantitative results for three–dimensional systems.

References

1. R.G. Caflisch and A.N. Berker, "Oxygen Chemisorbed on Ni(100): Renormalization–Group Study of the Global Phase Diagram," Phys. Rev. B, submitted for publication.
2. J. Ihm, D.H. Lee, J.D. Joannopoulos, and A.N. Berker, "Structural Phase Diagrams for the Surface of a Solid: A Total Energy/Renormalization–Group Approach," Phys. Rev. Lett., submitted for publication.
3. M. Kardar, "Phase Boundaries of the Isotropic Helical Potts Model on a Square Lattice," Phys. Rev. B 26, 2693 (1982).

4. M. Kardar, "Crossover to Equivalent-Neighbor Multicritical Behavior in Arbitrary Dimensions," Phys. Rev. B 28, 244 (1983).

5. J.S. Walker, "Exact Preservation of the Free Energy in a Modified Migdal-Kadanoff Approximation," Phys. Rev. B 26, 3792 (1982).

6. D. Andelman and J.S. Walker, "Preserving the Free Energy in a Migdal-Kadanoff Approximation for the q-State Potts Model," Phys. Rev. B 27, 241 (1982).

7. Optics and Quantum Electronics

A. Nonlinear Phenomena

Academic and Research Staff

Prof. C.G. Fonstad, Prof. H.A. Haus, Prof. E.P. Ippen, Prof. M.M. Salour, Dr. Y. Yamamoto, F.W. Barrows, E. Wintner

Graduate Students

N. Dagli, J. Fujimoto, C. Gabriel, M.N. Islam, S.H. Kim, M. Kuznetzov, A. Lattes, L. Molter-Orr, M. Stix, N. Whitaker, A.M. Weiner, G.E. Williams, J. Zayhowski

7.1 Picosecond Optical Signal–Sampling Device

The goal of the research is to develop prototype optical waveguide devices that operate at rates of many tens of Gigahertz. Such devices can be driven either electrically, by microwave oscillators, or optically. Examples of the former devices are samplers, multiplexers and demultiplexers. Examples of the latter are optical logic gates described in Section 7.3. In contrast to work done elsewhere with broadband microwave drive circuits,[1-3] we have concentrated on narrowband microwave circuits, because they permit operation with lower drive powers. We have constructed a waveguide Mach Zehnder interferometer in $LiNbO_3$ with Ti indiffused waveguides that functions as a sampler producing samples of 16 ps FWHM of an optical waveform at 20 GHz when driven with a 10 GHz sinewave. Preliminary results pointed toward microwave enhanced photo-refractive effects which led to gradual deterioration of device performance. A new structure with electrodes deposited on top of a SiO_2 layer on top of the $LiNbO_3$ greatly reduced these photorefractive effects. The device performance was verified by measurement of the optical spectrum[4] because direct detection of the samples by second harmonic generation is not possible due to the low optical powers used to avoid photorefractive damage. The next steps to be pursued are:

(a) Construction of symmetric microwave drive structure, to be driven push–pull. Such a structure reduces further the effect of the microwave enhanced photo–refractive effect because it tends to symmetrize the index changes in the Mach Zehnder interferometer. Symmetric index changes do not affect device performance.

(b) Construction of two interferometers in cascade. Two interferometers driven in cascade

produce as their output the product response. A phase shift φ of the microwave drive at frequency ω_m, $\varphi = \omega_m \tau$, in the second interferometer with respect to the first one, traces out the autocorrelation function $T(\tau) T(t \ \tau)$ of the optical intensity response function $T(t)$.

(c) Construction of a (multiplexer) demultiplexer by replacing the (input) (output) Y of the interferometer by a 3 db waveguide coupler.

The fabrication of the interferometers is carried out at the M.I.T. Lincoln Laboratory in collaboration with Dr. F.J. Leonberger.

References

1. K. Kubota, J. Noda, and O. Mikani, "Traveling Wave Optical Modulator Using a Directional Coupler LiNbO$_3$ Waveguide." IEEE J. Quant. Electron. QE–16, 7, 754 (1980).
2. M. Izutsu, Y. Yamane, and T. Sueta. "Broad–Band Traveling–Wave Modulator Using a LiNbO$_3$ Optical Waveguide." IEEE J. Quant. Electron. QE–13, 4, 287 (1977).
3. M. Izutsu, T. Itoh, and T. Sueta. "10 GHz Bandwidth Traveling Wave LiNbO$_3$ Optical Waveguide Modulator," IEEE J. Quant. Electron. QE–14, 6, 394 (1978).
4. L. Molter–Orr and H.A. Haus. "20 GHz Optical Waveguide Sampler," IEEE J. Quant. Electron., accepted for publication.

7.2 Devices for High–Rate Optical Communications

Clifton G. Fonstad, Hermann A. Haus

(a) Monolithic Mode–Locked Lasers

By active mode–locking a diode laser it is possible to produce optical pulses of under 5 picoseconds duration at repetition rates exceeding 10^{10} per second. Such pulse trains used with high frequency guided wave optics components like those discussed in the following section could form the basis of fiber optical communications systems with data rates in excess of 100 G/s. Existing lasers, however, are mode–locked in an external cavity and the associated mirrors, lenses, positioners, and optical bench are far too cumbersome to be useful outside the laboratory. We are consequently studying very long, non–uniformly excited diode lasers which we expect to be able to mode–lock without the use of an external cavity.

Lasers with multiple segment contacts each 600 μm long are being fabricated. A four–segment laser is 2.4 μm long and is expected to mode–lock at approximately 12.5 GHz; a three–segment laser at 17 GHz.

The initial long lasers fabricated were oxide–defined stripe contact (Ga, Al) As/GaAs double heterojunction laser diodes. Measurements on these devices, however, showed that even 600 μm

long diodes were actually only operating as super-radiant diodes and showed no evidence for cavity resonances. Consequently, it was determined that a laser structure having built-in guiding and lower spontaneous emission background would be required.

Such lasers were obtained through A. Ceruzzi of Laser Diode Laboratories in the form of Gaussian channelled-substrate planar (GCSP) wafers. These were fabricated into one, two, three, and four segment devices which have subsequently shown laser operation at all lengths. To our knowledge, the three and four segment lasers are the longest ever produced.

While capable of lasing in lengths up to 2.4 mm, the GCSP lasers still have a significant amount of background amplified spontaneous emission and have not yet been mode-locked. Work is presently concentrating on fully characterizing shorter devices and on mode-locking the three-segment lasers. We are at the same time investigating the possibility of obtaining multi-quantum well (MQW) laser material which has recently been demonstrated (1983 Device Research Conference) to have very low absorption, an important feature for these devices.

(b) Guided Wave Optics in InP

To complement the work on monolithic mode-locked diode lasers described above, we are studying the development of III-V based guided wave optics structures suitable for modulating, multiplexing, and demultiplexing trains of pulses from such lasers. As such, these structures must be efficient, low-loss, and compact, and must be capable of being driven at 100 GHz or more, with modest power requirements. To this end we have, in addition to our own earlier efforts on material preparation and InP guide characterization, continued our research on development of multiguide couplers and switches, and collaboration with Dr. F. Leonberger of Lincoln Laboratories on III-V waveguide design and characterization.

The three-guide coupler, developed earlier in this effort, remains a very exciting development and one we are pursuing aggressively. The concept is simply that bends, which of necessity are long and gradual, i.e., very space-consuming, can be eliminated in optical waveguide circuitry if couplers are made, not by bending two guides so that they come close to each other, but rather by inserting a third guide in between the two guides to be coupled. The coupling length of a three-guide structure is only 1.4 times that of a two-guide coupler, and the overall length including the bend transition regions is much less. We are presently fabricating and studying shallow-rib and metal-gap three-guide couplers in GaAs based planar guide structures. Our next goals are to demonstrate efficient switching in three-guide switch-couplers, and to define the minimum limits on guide spacing and coupling length.

Our measurement system has been extensively restructured to incorporate a scanner mirror to facilitate the display of output guide mode profiles. The sample is now also mounted horizontally, and a base for mounting the probers necessary for the switch studies, has been installed.

Our model for heterostructure rib waveguide analysis developed earlier has also been extended and has recently been successfully applied to fit coupling length data obtained on two- and three-guide passive waveguide couplers. This is an important step because the design of complex switching systems will require the ability to predict, i.e., design, the coupling length prior to fabrication.

(c) Multiple-Waveguide Couplers

The interconnection of optical waveguide devices requires the control of the path(s) of the optical signal. Waveguide Y's and bends with small optical loss are possible only with small deflection angles. It is possible to construct Y's, and produce transfer of optical radiation parallel to itself, by coupling of parallel optical waveguides. In the last report we outlined the applications of three waveguide couplers. In the meantime, we have developed the theory for N parallel waveguides of varied coupling between the guides, so as to fully transfer power from one outermost waveguide to the one on the opposite side.[1]

In a system with an odd number of waveguides it is possible to adjust the coupling between the guides so that all of the power entering the central waveguide is transferred symmetrically to the outermost waveguide, or vice versa.[1] In this way one may construct waveguide Y's without bends. This may have advantages in fabrication of waveguide Mach Zehnder interferometers.

In this connection it is of interest to compare the radiation loss of conventional waveguide Y's with the radiation loss of effective Y's produced by waveguide coupling. We have begun a theoretical study of radiation loss[2] and came to the conclusion that, with proper parameter adjustment, the coupled waveguide version can perform at least as well as the conventional Y for the same effective divergence angle. Further, studies concerning the optimization with regard to radiation loss are in progress.

At Lincoln Laboratory, fabrication and testing of coupled three-waveguide structures has been initiated. The performance of the guides was as predicted, for weak coupling- large guide-separations. With increased coupling, shorter transfer lengths, the transfer from one outermost guide to the other wave not perfect. We are currently engaged in developing a theory for the "proximity effects" so that fabrication can correct for it.

References

1. H.A. Haus and L. Molter-Orr, "Coupled Multiple Waveguide Systems," IEEE J. Quant. Electron. QE-19, 5, 840-844 (1983).
2. M. Kuznetsov and H.A. Haus, "Radiation Loss in Dielectric Waveguide Structures by the Volume Current Method," IEEE J. Quant. Electron., accepted for publication.

(d) Quantum Theory of Laser Oscillator Locking

Semiconductor lasers, by virtue of their small size and short resonator–relaxation–time, exhibit large quantum noise often dominating the classical noise contributions. Phase modulation of semiconductor lasers is being tested in the laboratories[1,2] for possible use in optical communications. No quantum theory of oscillator locking has been published in the literature to our knowledge. We have initiated a theoretical study of quantum noise in a locked oscillator. This study was motivated, apart from its relevance to phase–modulation of semiconductor lasers, by the question whether a locked oscillator output provides an ideal quantum measurement of the phase of the locking signal. Linear laser amplifiers are known to provide an ideal simultaneous quantum measurement of amplitude and phase.[3-6] A locked oscillator sacrifices amplitude information by gain–limiting, but reproduces the phase of the injection signal (except for the phase–noise introduced by the oscillator). We found that a locked oscillator approaches an ideal measurement to not better than 3 db (doubling the fundamental noise imposed by the Heisenberg uncertainty principle).[7]

References

1. Y. Yamamoto and T. Kimura, "Coherent Optical Fiber Transmission System," IEEE J. Quant. Electron. QE-17, 6, 919–935 (1981).
2. G.L. Abbas, V.W.S. Chan, and T.K. Yee, "Local Oscillator Excess Noise Suppression for Homodyne and Heterodyne Detection," Preprint, M.I.T. Lincoln Laboratory, Lexington, Massachusetts.
3. H.A. Haus and J.A. Mullen, "Quantum Noise in Linear Amplifiers," Phys. Rev. 128, 5, 2107–2143 (1962).
4. H.A. Haus and C.H. Townes, "Comments on 'Noise in Photoelectric Mixing'," Proc. IRE 50, 6, 1544–1545 (1962).
5. E. Arthurs and J.L. Kelley, "On the Simultaneous Measurement of a Pair of Conjugate Observables," Bell Systems Tech. Journal 44, 725–729 (1965).
6. C.M. Caves, "Quantum Limits on Noise in Linear Amplifiers," Phys. Rev. D 26, 8, 1817–1839 (1982).
7. H.A. Haus and Y. Yamamoto, "Quantum Noise in Injection Locking of Laser Oscillator," to be submitted for publication.

7.3 Picosecond Optics

Waveguide optics, or the more ambitiously named Integrated Optics, will not compete seriously with integrated electronics in all those functions that can be performed electronically. Optical devices have a more demanding topology (e.g., optical waveguides have transverse dimensions of several optical wavelengths and do not permit sharp bends) and higher power requirements. However, waveguide optics can perform certain signal processing functions at greater speeds than electronic circuits. High speed signal processing is one application in which waveguide optics can seriously

compete with electronics.

We are currently working on the realization of all-optical logic gates. The basic structure is shown in Fig. 7-1. The central guide is pulse excited in one polarization (TM–mode) the outer "control" guides are excited by synchronous pulses in an orthogonal polarization (TE–mode). The cotraveling pulses in orthogonal polarizations change the index as "felt" by their "partner" via the third order nonlinearity $\chi^{(3)}$. Depending upon the applied dc voltage in one arm of the interferometer, and the use of input ports, the device can perform as an XOR gate, AND gate and inverter.
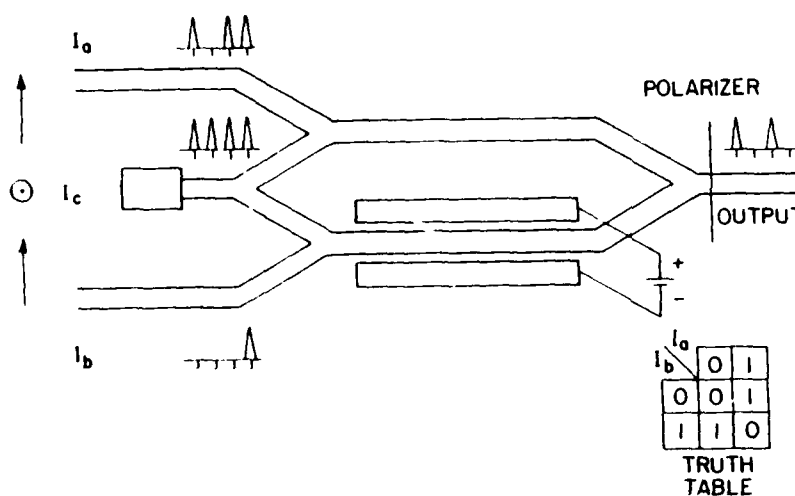
Figure 7-1

We have demonstrated operation of the device fabricated in $LiNbO_3$ as a picosecond waveguide modulator.[1] The testing of the device produced the first measurement of $\chi^{(3)}$, or n_2, in $LiNbO_3$. The value found was: $3 \times 10^{-9} (Mw/cm^2)^{-1}$.

With the available optical powers this value was too small to produce XOR operation, an optically induced phase shift of π in one of the arms. Therefore, picosecond optical-optical modulation was demonstrated on the first device of this kind.[1] The nonlinear coefficient $\chi^{(3)}$ in GaAs is two orders of magnitude higher than the one found for $LiNbO_3$. Waveguide fabrication in GaAs has made progress in the last years so that fabrication in GaAs can be attempted.

Our future work will be aimed at producing a waveguide logic gate in GaAs. We are also investigating nonlinear processes with higher nonlinearities than those attributed to insulating bulk GaAs, e.g., optical hole–electron generation. Such processes have relaxation times of nanoseconds and as such are not usable for picosecond devices. However, there are several possibilities for

increasing the relaxation rates which would then make them applicable to picosecond signal processing at power levels available from semiconductor lasers.

References

1. A. Lattes, H.A. Haus, F.J. Leonberger, and E.P. Ippen, "An Ultrafast All–Optical Gate," IEEE J. Quant. Electron., accepted for publication.

7.4 Ultrashort Pulse Formation

Erich P. Ippen

We have extended and refined our analytical model for pulse shaping and shortening in passively mode–locked dye lasers and semiconductor lasers. Last year this model was developed to include, in mode–locking theory, the effects of coherent pulse coupling in colliding–pulse ring lasers. As a result of numerical studies based on the model, we were able this year to introduce the concept of 'pulse shortening velocity' (PSV) as an accurate and practical measure of mode–locked laser performance. With PSV we have, for the first time, a straightforward prescription for shorter pulses that includes coherent coupling and illuminates the effects of different types of resonator dispersion. A paper on the subject has been accepted for publication in the IEEE Journal of Quantum Electronics.

7.5 Femtosecond Laser System

Erich P. Ippen

For optical studies in the femtosecond time domain, we have constructed during the past year a passively–mode–locked cw ring dye laser that operates in the colliding–pulse (two counterpropagating beams) configuration. This laser oscillator is now a stable, reliable source of pulses as short as 60 fsec at a repetition rate of 88 MHz. The pulses have individual energies of about 10^{-10}J and peak powers on the order 10^3W, sufficient for a variety of pump–probe studies as well as for observation of transient parametric scattering by degenerate 4–wave mixing.

High power amplification of femtosecond pulses from the oscillator has also been accomplished. The pulses are passed through four dye amplifier stages, each transversely pumped with energy from a frequency–doubled Q–switched Nd:YAG laser. Each amplifier stage is isolated optically from the succeeding stages by a free–flowing absorber stream that can be saturated only by the amplified pulse. Proper adjustment of gain and saturable absorption in each of the sections is found to be important to maintaining ultrashort pulse durations. After four stages we have achieved pulse

energies of 400 μJ with pulse durations of 70 fs. More energy can be achieved with longer pulses. This system is now available for application to a wide variety of time–resolved measurements.

7.6 Parametric Scattering with Femtosecond Pulses

We have begun to investigate, theoretically and experimentally, transient parametric scattering (TPS) by degenerate 4–wave mixing with femtosecond pulses. Our initial attention has focused on two potentially important applications: the first is the generation of shorter pulses by the nonlinear scattering process; the second is the direct measurement of femtosecond coherence (dephasing) properties of molecules and solids. Our theoretical work has already clarified the existing analysis of scattered intensity as a function of material response times and has led us to propose a new, three–pulse technique for resolving ambiguities. Experimentally, we have made preliminary observations of femtosecond pulse shortening by TPS in molecular dye solutions. Measurements are in progress to determine the dependence of this shortening on the specific dye molecule, pulse power, and relative delay between two pulses. With optimization, we expect to be able to generate pulses shorter than 40 fsec.

7.7 Near-IR Diagnostics

Work progressed significantly this year in the development of a picosecond dye laser source for the GaA ℓ As bandedge regime. Our dye laser is synchronously–pumped by about 1 watt of 6471 Å power from a mode–locked Kr^+ laser. With specially designed mirrors, birefringent tuning plates, and a new nontoxic solvent, we have extended the tuning range of a single dye (Oxazine 750) to cover completely the wavelength region of interest: 7600 Å - 9000 Å. Over this range we have obtained approximately transform–limited pulses of 4 psec in duration and average powers ranging from several hundred milliwatts at peak to about 25 mW at the long wavelength end. Pulses from this laser have been used, in conjunction with another research program, to demonstrate picosecond optical switching with optical nonlinearities in $LiNbO_3$ waveguides. Our laser is especially suited for these studies because of reduced damage in $LiNbO_3$ at longer wavelengths. By the end of this year application to studies of picosecond saturation in GaA As waveguides will also have begun.

7.8 Quaternary (InGaAsP) Diagnostics

During the past year we have begun studies of carrier dynamics in quaternary semiconductor films of InGaAsP on InP. For fabrication of thin film samples we have established collaboration with colleagues at Bell Telephone Laboratories. Holmdel, New Jersey and RCA Research Laboratories, Princeton, New Jersey. Our first experiments have utilized pulses from a mode–locked cw Nd:YAG laser to excite and probe at $\lambda = 1.06\mu$ changes in interband absorption in thin film samples. Preliminary results very nicely show recombination to be due to a combination of linear and nonlinear (Auger) processes. Further work with different material compositions and different laser wavelengths will now be used to provide a clearer separation of effects. For this purpose, and also for long wavelength waveguide studies, we have spent time this year building a tunable, picosecond F–center (KCℓ:Tℓ) laser for $1.4\mu < \lambda > 1.6\mu$. Crystals have been obtained from L.F. Mollenauer of Bell Laboratories, and laser performance will be characterized in the near future. We have also begun to pursue a novel, and we think very interesting, approach to studies of carrier dynamics: the use of surface–acoustic–wave electrode structures to detect picosecond nonradiative relaxation. The technique utilizes, high repetition rate, picosecond pulse trains to generate a spatially and temporarily periodic carrier density. Nonradiative recombination is resonantly detected by a similarly periodic electrode structure.

B. Grating Structures

Academic and Research Staff

Prof. H.A. Haus, Dr. J. Melngailis, D.-P. Chen

Graduate Students

E.M. Garber, M.N. Islam

7.9 Surface Acoustic Wave Gratings

Several types of surface acoustic-wave (SAW) devices operate on the principle of coherent reflection of the waves from gratings. The gratings used are generally shallow with a depth equal to a few percent, at most, of the grating period. Thus, apart from a small reflection from each groove edge, the SAW, to first order, propagates in the grating undisturbed. Small deviations from this lowest order model, which result in a slowing and attenuation of the wave in a grating, are important in some critical devices. Resonators, in which a surface acoustic wave bounces between two gratings as in a Fabry-Perot cavity, are used as high-Q frequency standards. Here, frequency shifts occur due to the propagation in a finite-depth grating. Reflective-array compressors are used to compress chirped radar waveforms which are often up to 80 μsec in length. The frequency within the waveform varies monotonically over the length of the pulse. The compressor, in effect, adds the signal at the head of the pulse to the signal at the tail with the correct phase and amplitude. Thus, transit time and attenuation within a grating must be accurately controlled.

Our work on surface acoustic-wave grating structures has a dual goal: (a) development of methods of analysis of grating structures that are simpler than those generally employed, and (b) utilization of simple analytical methods in the design of novel structures using surface acoustic waves.

We have applied a variational principle to predict the radiation loss from gratings, a problem of importance in the design of Reflective Array Compressors of small insertion loss. Because of the radiation loss the system is not "self-adjoint". Our work[1] showed how one may adapt the variational principle to treat this case. Experimental results on the insertion loss of ion milled groove-gratings were obtained and compared with theory.[2]

Currently we are extending the variational treatment to metal-strip gratings with a twofold objective: (a) To obtain relatively simple analytic expressions for the reflection of by metal-strips. (b) To understand the spurious response of transducers whose likely cause are the higher order

transverse modes of the transducer acting as a reflection grating. Preliminary studies have shown that the change of propagation velocity caused by metalization of $LiNbO_3$ and quartz can be predicted simply, analytically using the variational principle with a very high degree of accuracy when compared with published computer analyses. This finding gives us confidence that the accuracy of the approximate analytic treatment of metal gratings will be satisfactory.

In another investigation, the optimum design of unidirectional transducers is pursued. Unidirectionality is achieved by combining the reflective properties of a grating interspersed with an interdigital transducer. This work is done in cooperation with Dr. C. Hartmann of RF Monolithics.

Because of our concurrent work in optical waveguide structures it was natural for us to investigate the question whether useful structures may be built combining the surface acoustic wave interactions via the acousto-optic effect, with the guiding properties of optical waveguides. Optical guiding layers made with proton exchange permit adjustment of the difference between the ordinary and extraordinary optical indices.[3] One may construct Y- propagating optical waveguides in X–cut $LiNbO_3$ in which the TE and TM modes are coupled by a SAW of given frequency. This permits the construction, in principle, of an acousto-optic spectrum analyzer with no optical lenses. Preliminary theoretical studies suggest better resolution and greater dynamic range than the one achieved with more conventional designs.[4]

References

1. H.A. Haus and M.N. Islam, "Application of a Variational Principle to Systems with Radiation Loss," IEEE J. Quant. Electron. QE–19, 1, 106–117 (1983).
2. M.N. Islam, H.A. Haus, and J. Melngailis, "Radiation Loss for Normal and Oblique Incidence Gratings," 1982 Ultrasonics Symposium, pp. 92–95.
3. J.L. Jackel, C.E. Rice, and J.J. Veselka, "Proton Exchange for High–Index Waveguides in $LiNbO_3$," Appl. Phys. Lett. 41, 7, 607–608 (1982).
4. H.K. Barnoski, R.V. Chen, T.R. Joseph, J.Y.M. Lee, and V.G. Ramer, "Integrated–Optical Spectrum Analyzer," IEEE Trans. Cir. Systems CAS–26, 12, 1113–1124 (1979).

42

8. Photonics

Academic and Research Staff

Prof. S. Ezekiel, J. Kierstead

Graduate Students

D. DiFillipo, P.R. Hemmer, R.E. Meyer, B.W. Peuse, D.R. Ponikvar, M.G. Prentiss, G.A. Sanders, R.E. Tench

8.1 Ultrahigh-Resolution Spectroscopy and Frequency Standards in the Microwave and MM Wave Regions Using Optical Lasers

Philip R. Hemmer, Shaoul Ezekiel

In this program we are considering an attractive possibility for obtaining ultrahigh resolution in the microwave and mm regions using optically induced Raman transitions in atomic beams. The research is centered around the interaction of two laser fields with a three level system in an atomic beam. Of particular interest is the basic study of coherent two-photon excitations in a folded three level system in which exceedingly narrow resonances can be obtained when the initial and final levels are long lived states. As is well known, the linewidth is determined only by the initial and final level decay rates for a Doppler Free system such as an atomic beam.

In order to achieve such narrow linewidths, laser frequency jitter must be eliminated and the time the atom spends in the excitation field must be made as long as possible to reduce the transit time linewidth. We eliminate laser jitter by correlating the jitter in the two lasers since the transition frequency of interest depends on the difference in the laser frequencies. In summary, we are able to make a transition from the first level to the final level indirectly via the intermediate level and achieve a linewidth equivalent to that obtained by a direct transition from the first to the final level using a microwave or mm wave source.

Our initial experiments have been conducted with an atomic beam of sodium and dye lasers. In this case the difference in the laser frequencies is 1772 MHz. Laser jitter in each beam was correlated by simply deriving one laser frequency from the other by an acousto-optic frequency shifter driven at 1772 MHz. A linewidth of 650 Hz was achieved by using Ramsey's separated oscillator method with a 30 cm separation between the interaction regions. We have also stabilized the 1772 MHz oscillator to

the Ramsey resonance and achieved a stability of 5.6 x 10^{-11} for an averaging time of 100 seconds.

Future work is concerned with the study of level shifts in the resonance Raman scheme which influence the ultimate performance of such a stabilization system. In addition we are considering various techniques for cooling the Na Beam so as to achieve narrower transit time linewidths.

References

1. J.E. Thomas, S. Ezekiel, C.C. Leiby, Jr., R.H. Picard, and C.R. Willis, Opt. Lett. 6, 298 (1981).
2. J.E. Thomas, P.R. Hemmer, S. Ezekiel, C.C. Leiby, Jr., R.H. Picard, and C.R. Willis, "Observation of Ramsey Fringes Using a Stimulated Resonance Raman Transition in a Sodium Atomic Beam," Phys. Rev. Lett. 4, 867 (1982).
3. P.R. Hemmer, S. Ezekiel, and C.C. Leiby, Jr., "Stabilization of a Microwave Oscillation Using a Resonance Raman Transition in a Sodium Beam," in W.D. Phillips (Ed.), Laser-Cooled and Trapped Atoms, Nat. Bur. Stand. (U.S.), Special Publication 653, June 1983, p. 47.
4. P.R. Hemmer, S. Ezekiel, and C.C. Leiby, Jr., "Stabilization of a Microwave Oscillation Using a Resonance Raman Transition in a Sodium Beam," Opt. Lett., August 1983, to be published.

8.2 Resonant Light Diffraction by an Atomic Beam

Bruce W. Peuse, Mara G. Prentiss, Shaoul Ezekiel

We have observed resonant light diffraction by an atomic beam of 2-level sodium atoms. This grew out of an effort to develop new techniques of performing absorption spectroscopy in low density atomic beams, that are capable of achieving quantum noise limited sensitivity. As a result of using such techniques, we found that the absorption lineshape exhibited an asymmetry even for weak fields and the magnitude of this asymmetry depended on the position and size of the detector. In contrast, the lineshape determined by collecting the fluorescence for the same atoms did not exhibit any asymmetry. Moreover, we measure the on-resonance and also the off-resonance absorption as a function of detector position.

We explain the observed distortion in the absorption lineshape and the spatial absorption behavior as a manifestation of the interference between light scattered by the atoms with the excitation beam at a given position of the detection plane. In other words, we have observed a diffraction-like pattern due to the laser beam propagating across a thin atomic beam. The difference between on-resonance and off-resonance behavior is explained by the dependence of the phase of the scattered field on frequency. Our calculations are in good agreement with the experimental data.

The above diffraction phenomena along with the resulting lineshape distortion can be eliminated by placing the detector very close to the interaction region, but this is clearly not feasible. However, it is

possible to achieve the same results by imaging the fields in the interaction region at the detection plane. In our experiment this was accomplished by placing two lenses of equal focal length f in the laser beam after the interaction region. In this way, the fields in the interaction region are faithfully reproduced at the image or detection plane. When the apertured detector is scanned along the image plane while the laser is held on resonance, the spatial pattern that results no longer shows any diffraction behavior. Moreover, the lineshape dictortion was also eliminated by using this imaging technique.

References

1. B.W. Peuse, M.G. Prentiss, and S. Ezekiel, "Distortion in Atomic Beam Absorption Lineshapes," Journal de Physique Colloque C8. Supplement au n°12, Tome 42, C8–53. December 1981.
2. B.W. Peuse. M.G. Prentiss, and S. Ezekiel, "Observation of Resonant Light Diffraction by an Atomic Beam." Phys. Rev. Lett. 49, 269 (1982).
3. B.W. Peuse, M.G. Prentiss, and S. Ezekiel, "Elimination of Lineshape Distortion in Laser Absorption Spectroscopy in Atomic Beams," Opt. Lett. 8, 154 (1983).

8.3 Precision Atomic Beam Studies of Atom–Field Interactions

Bruce W. Peuse, Mara G. Prentiss, Shaoul Ezekiel

The interaction of radiation with two and three level quantum mechanical systems is of much interest because it involves basic processes. So far we have studied the interaction of 2–level and 3–level sodium atoms with one and also with two monochromatic fields provided by stable, single frequency dye lasers. One laser acts as the pump and interacts primarily with two of the levels. The second laser then probes the absorption between either one of these levels to a third level. In this way, we have studied a cascade system, a Vee system and also an inverted Vee system. In the case of a weak pump field, our probe data was in very good agreement with theoretical calculations. However, when the pump was made very intense the probe data could not be explained by the a.c. stark effect alone. Atomic recoil had to be included in the calculations in order to explain the peculiarities observed.

References

1. R.E. Tench, B.W. Peuse, P.R. Hemmer, J.E. Thomas, and S. Ezekiel, "Two Laser Raman Difference Techniques Applied to High Precision Spectroscopy," Journal de Physique, Colloque C8, Supplement au n°12, December 1981.
2. P.R. Hemmer, B.W. Peuse, F.Y. Wu, J.E. Thomas, and S. Ezekiel, "Precision Atomic–Beam Studies of Atom–Field Interactions," Opt. Lett. 6, 531 (1981).
3. B.W. Peuse, R.E. Tench, P.R. Hemmer, J.E. Thomas, and S. Ezekiel, "Precision Studies in 3–Level Systems," in A.R.W. McKellar, T. Oka, and B.P. Stoicheff (Eds.), Laser Spectroscopy V (Springer–Verlag 1981) p. 251.

Photonics

8.4 Measurement of Natural Predissociation Effects in Iodine Molecules

Robert E. Tench, Donald R. Ponikvar, Shaoul Ezekiel

In our continuing study of the interaction of two monochromatic fields with folded 3–level systems in vapors, we have performed extremely high resolution measurements of Doppler free resonances in I_2. With weak copropagating pump and probe fields we have observed linewidths as narrow as 50 kHz, vapors, we have performed extremely high resolution measurements of Doppler free resonances in I_2. With weak copropagating pump and probe fields we have observed linewidths as narrow as 50 kHz, determined, in principle, by the relaxation rates of the first and final levels with a small contribution from the relaxation rate of the intermediate level. For counterpropagating fields we have observed a probe linewidth of about 150 kHz that is determined primarily by twice the relaxation rate of the intermediate level. We are using this doubling of the intermediate level relaxation rate to perform precision measurements of the nature linewidths of the many hyperfine transitions in the P(13) 43–0 and R(15) 43–0, B–X transitions at 5145 Å. Because of natural predissociation effects in the I_2 molecule, the natural width of each hyperfine component will be different. Our precision measurements will therefore enable us to study in more detail such predissociation phenomena.

Since molecular iodine is being considered as a reference molecule in the visible region of the spectrum, precision linewidth and lineshape measurements of individual hyperfine components as well as the spacing between components is of much interest.

References

1. R.E. Tench, B.W. Peuse, P.R. Hemmer, J.E. Thomas, and S. Ezekiel, "Two Laser Raman Difference Techniques Applied to High Precision Spectroscopy," Journal de Physique, Colloque C8, Supplement au n°12, Tome 42, December 1981.
2. R.E. Tench and S. Ezekiel, "Precision Measurements of Hyperfine Predissociation in I_2 Vapor Using a Two–Photon Resonant Scattering Technique," Chem. Phys. Lett., to be published.

8.5 Passive Ring Resonator Method for Sensitive Inertial Rotation Measurements in Geophysics and Relativity

Glen A. Sanders, Raymond E. Meyer, John Kierstead, Shaoul Ezekiel

Precision measurement of inertial rotation is of much interest in a number of areas, such as navigation, geophysics, and relativity. The geophysical applications include the measurement of the

various effects that cause fluctuations in the earth's rotation rate Ω_E, ranging from 10^{-7} to $10^{-9}\Omega_E$, for example, nutation, precession, wobble, and tidal-friction effects. The relativistic effects range in sensitivity from 10^{-9} to $10^{-11}\Omega_E$ and include measurements of the preferred frame and the drag parameters.

The advent of the laser in 1960 rekindled the interest in the use of the Sagnac effect for sensing inertial rotation by optical means. Several approaches to implementing the Sagnac effect have been under investigation. These include active techniques such as the ring laser gyro, and passive techniques employing passive ring resonators or multiturn fiber-optic interferometers. In all these approaches, the measurement sensitivity scales with the area enclosed by the light path. Typically, to reach the sensitivity needed to measure the geophysical and relativistic effects mentioned previously, it is necessary to consider areas between 10^2 and $10^4\,m^2$.

Our research effort centers around the passive resonator technique. Our present setup is a square cavity, 70 cm on a side, mounted on a super invar table. The difference between the resonance frequencies of the cavity for clockwise (cw) and counterclockwise (ccw) propagation induced by inertial rotation is measured by a 1/2-mW He-Ne laser, mounted external to the cavity. We have reduced the short-term random drift to about $3 \times 10^{-4}\Omega_E$ (where Ω_E is earth rotation rate) in an averaging time of 30 seconds which is close to the photon shot noise limit in our setup. The study of long-term drift is in progress.

References

1. G.A. Sanders, M.G. Prentiss. and S. Ezekiel, "Passive Ring Resonator Method for Sensitive Inertial Rotation Measurements in Geophysics and Relativity," Opt. Lett. 6, 569 (1981).
2. R.E. Meyer, G.A. Sanders, and S. Ezekiel, "Observation of Spatial Variations in the Resonance Frequency of an Optical Resonator," J. Opt. Soc. of Am., to be published.

8.6 Closed Loop, Low Noise Fiberoptic Rotation Sensor

David Di Fillipo, Mara G. Prentiss, Shaoul Ezekiel

The fiberoptic gyroscope has been receiving considerable attention for the past several years. A number of different approaches have been studied, and as these studies progress a number of problems were uncovered.

Our present approach employs a 200 m long fiber wound around a 19 cm diameter spool and operated in a closed loop mode. Our measurement approach is based on the use of two acousto-optic frequency shifters placed within the fiber interferometer for providing nonreciprocal

phase modulation as well as nonreciprocal frequency offsets needed in closed loop operation. Short-term random drift is about 0.03°/hr for averaging times of 30 seconds which is close to that predicted by the photon shot noise limit in our setup. The long-term performance departs from the photon noise limit and considerable effort is at present directed into the sources of long-term drift. In this connection, we have predicted and observed an intensity-induced nonreciprocity in the fiberoptic gyro. We found that a nonreciprocal phase shift of 1.4×10^{-6} radians can be generated by a one microwatt power difference between the oppositely propagating light beams. Our fiber is 200 m long with a core diameter of 4.5 microns, and wound on a 19 cm diameter spool. The intensity dependent nonreciprocal phase shift, which is attributed to a four wave mixing process in the quartz medium, is equivalent to a rotation rate of 0.2°/hr in the present geometry, and therefore stresses the need for a strict intensity control in precision fiber rotation sensors.

References

1. J.L. Davis and S. Ezekiel, "Closed Loop, Low Noise Fiberoptic Rotation Sensor," Opt. Lett. 6, 505 (1981).
2. M.G. Prentiss, J.L. Davis, and S. Ezekiel, "Closed Loop, High Sensitivity Fiber Gyroscope," in S. Ezekiel and H.J. Arditty (Eds.), Fiberoptic Rotation Sensors (Springer-Verlag 1982).
3. S. Ezekiel, J.L. Davis, and R.W. Hellwarth, "Observation of Intensity-Induced Nonreciprocity in a Fiberoptic Gyroscope," Opt. Lett. 7, 457 (1982).

8.7 Fiberoptic Ring Resonator Gyroscope

Raymond E. Meyer, John Kierstead, Shaoul Ezekiel

In addition to the fiber interferometer method described in the previous section we are also investigating the use of an all-fiber ring resonator as a sensor of absolute rotation. The principle here is similar to that of the discrete mirror resonator method that has been under development in our laboratory for several years. In brief, the mirror resonator is simply replaced with a single mode fiber resonator and the input-output coupling is accomplished by means of a fused evanescent wave fiber coupler. At present the finesse of the 3 meter fiber resonator is 140. Preliminary data on short-term noise is about 0.5°/hr ($\tau = 1$ second) (rms) which is 10 times greater than the shot noise limit in our present setup.

References

1. R.E. Meyer and S. Ezekiel, "Fiberoptic Resonator Gyroscope," presented at First International Conference on Optical Fiber Sensors, IEE, London, England, April 1983.

9. Optical Spectroscopy of Disordered Materials and X–Ray Scattering from Surfaces

Academic and Research Staff

Prof. J. D. Litster, Dr. L.E. Kupferberg[1]

Graduate Students

B.D. Larson, L.E. Solomon

A. Studies of Micellar Liquid Crystals

Decylammonium chloride in aqueous solution of ammonium chloride forms disk–like micelles about 2 nm thick and 6 nm diameter. These may be completely disordered (isotropic phase), orientationally ordered with no positional order (nematic phase), or be positionally ordered in one direction (the neat soap or smectic A phase). We have been using the dichroism of dye probes to study the anisotropic rotational diffusion of the micelles in each of these three phases. Since we use one dye molecule for every 75 to 100 micelles, there should be little effect on the ordering of the micelles.

Our experiments showed that the interaction between the dye molecules and the micelles can be quantitatively described by an orientational order parameter $S_D = (1/2) \langle 3 \cos^2 \alpha - 1 \rangle$, where α is the angle between the dye transition moment and the micelle symmetry axis. The micelles can, in turn, be described by a similar order parameter $S_M = (1/2) \langle 3 \cos^2 \Theta - 1 \rangle$, where Θ is the angle between the micelle symmetry axis and the optic axis of the liquid crystal. In the isotropic phase $S_M = 0$. The dichroism of the solution is proportional to the product $S_D S_M$. We expect that S_D, which is the average of interactions that involve only one dye molecule and one micelle, will be the same in all phases. From our measurements we deduce $S_D = 0.4$, the discontinuity in S_M at the first order nematic–isotropic transition is 0.4, S_M rises to 0.8 at the nematic–neat soap transition, shows no discontinuity at the transition, and continues to increase slowly as the neat soap phase is cooled.

We observed the rotational diffusion by transient dichroism measurements. Our main goal is to determine if the neat soap phase is being formed of surfactant bilayers (the traditional picture) or micelles whose concentration varies periodically in space in the solution. Our data suggest the latter. However, we found that our laser pulse disturbs both orientational order parameters from the

---

[1]Assistant Professor, Department of Physics, Worcester Polytechnic Institute, Worcester, Massachusetts

equilibrium values. S_D relaxes rapidly and dominates the short time (t < 500 ps) behavior. To answer the question definitively, we are beginning experiments with dyes that have a high singlet to triplet conversion and hence longer excited state lifetimes; these will permit us to observe the much slower (t > 10 ns) motion of the micelles directly.

B. Energy Transfer Studies

Our goal is to use energy transfer between dye molecules to study short range orientational order of molecules in liquid crystal phases and obtain information to complement that which can only be obtained on much greater length scales by light scattering. We have begun experiments with the laser dyes rhodamine 640 (Rh640) and oxazine 725 (Ox725). As the emission spectrum of Rh640 almost perfectly overlaps the absorption spectrum of Ox725, this pair is ideally suited to energy transfer experiments.

Preliminary experiments have been carried out with the dyes dissolved in ethanol. Pure Rh640 has a fluorescence lifetime we measure from time dependent absorption following a bleaching pulse to be 4.0 ns, while that of Ox725 is about 770 ps. When the two dyes are mixed and the Rh640 absorption measured at a wavelength where Ox725 gives no observable signal, the lifetime drops to 2.8 ns indication energy transfer from Rh640 to Ox725 has taken place. The experiments will continue, subject to the constraints of Dr. Kupferberg's teaching duties at Worcester Polytechnic Institute.

Publications

Litster, J.D. and R.J. Birgeneau, "Liquid Crystals: their Phases and Phase Transitions," Physics Today 35, 26 (1982).

Collett, J., L.B. Sorensen, P.S. Pershan, J.D. Litster, R.J. Birgeneau, and J. Als-Nielsen, "Synchrotron X-Ray Study of Novel Crystalline-B Phases in Heptyloxybenzylidene-Heptylaniline (70.7)," Phys. Rev. Lett. 49, 553 (1982).

Rosenblatt, C. and J.D. Litster, "Magnetic Birefringence Determination of the Tilt Susceptibility at the Smectic A – Smectic C Phase Transition in Butoxybenzylidene-Heptylaniline," Phys. Rev. A 26, 1809 (1982).

Litster, J.D., "Scattering Spectroscopy of Liquid Crystals," in H.Z. Cummins and A.P. Levanyuk (Eds.), Light Scattering Near Phase Transitions, (North Holland), in press.

Birgeneau, R.J., C.W. Garland, Jr., A.R. Kortan, J.D. Litster, M.Meichle, B.M. Ocko, C. Rosenblatt, and L-J. Yu, "The Smectic A – Smectic C Transition: Mean Field or Critical?" Phys. Rev. A 27, 1251 (1983).

Safinya, C.R., L.J. Martinez-Miranda, M.Kaplan, J.D. Litster, and R.J. Birgeneau, "High Resolution X-Ray Scattering Study of the Nematic to Smectic-C Transitions in 8S5/7S5 Mixtures," Phys. Rev. Lett. 50, 56 (1983).

Litster, J.D., "Structural Studies of Nematic and Smectic Phases," Phil. Trans. Roy. Soc. A309, 145 (1983).

Garland, C.W., M. Meichle, B.M. Ocko, A.R. Kortan, L.J. Yu, J.D. Litster, and R.J. Birgeneau, "Critical Behavior at the Nematic-Smectic-A Transition in Butyloxybenzylidine Heptylaniline (40.7)," Phys. Rev. A 27, 3234 (1983).

Kumar, S., L.J. Yu, and J.D. Litster, "Orientation Fluctuations of a Lyotropic Nematic Liquid Crystal Measured by Quasielastic Light Scattering," Phys. Rev. Lett. 50, 1672 (1983).

Post, M.V., S.B. Thesis, Department of Electrical Engineering and Computer Science, M.I.T., June 1982.

52

10. Infrared Nonlinear Optics

Academic and Research Staff

Prof. P.A. Wolff, Dr. R.L. Aggarwal, Dr. F. Brown, Dr. C. Jagannath, Dr. L.R. Ram-Mohan, Dr. Y.C.S. Yuen

Graduate Students

E. Gamble, K. Kash, J.B. McManus, J. Warnock, S. Wong, E. Youngdale

10.1 Infrared Nonlinear Processes in Semiconductors

In doped, narrow gap semiconductors there is a sizeable nonlinear (Raman) interaction between two laser beams and plasma waves. This interaction can be used to coherently excite plasmons of well–defined wave vector. An experiment to test this idea was performed[1] in thin n–InSb plates; plasmon excitation was detected via FIR radiation ($\simeq 100\mu$) emitted at the plasma frequency by the thin–film modes. The FIR power observed was lower than anticipated, but in other respects the measurements confirmed theory.

Though acoustic plasma waves were predicted many years ago, they have not been observed in crystals until recently.[2] Light scattering spectra of optically excited electron–hole plasmas in GaAs exhibit a novel, low frequency resonance. The position and carrier–density variation of this line agree with those predicted by RPA theory of the acoustic plasmon. In previous light scattering studies of optically excited electron–hole gases, the acoustic plasmon resonance was not observed, presumably because of plasma inhomogeneity. Uniform plasmas were assured in this work by creating electron–hole pairs in thin ($\simeq 4000$ A) GaAs epilayers, bounded by transparent (Ga,Al)As layers. The investigation was performed in collaboration with Dr. A. Pinczuk and Dr. J. Shah of Bell Laboratories.

Intense, degenerate four wave mixing has been observed[3] at room temperature in p-type (Hg,Cd)Te with a CO_2 laser pump. The experiments yield a nonlinear susceptibility, $\chi^{(3)} = 5 \times 10^{-6}$ esu, with $p = 2.5 \times 10^{17}$ holes/cc. This value exceeds, by several orders of magnitude, any previously observed nonresonant, nonlinear susceptibility. The large $\chi^{(3)}$ is attributed to intervalence band transitions which modulate the plasma contribution to the dielectric function. The nonlinear susceptibility is proportional to the light–to–heavy hole relaxation time, which is estimated to be $(2-4) \times 10^{-12}$ sec.

Theoretical calculations[4] suggest that, in semiconductor crystals with spatially varying effective mass, there is a large enhancement of the free-carrier nonlinear susceptibility. Structures of this type can be grown via MBE techniques. The variable-mass effect is most pronounced when the mass varies rapidly in space, though large amplitude fluctuations are not required. Nonlinear coefficients in the 10^{-4} - 10^{-5} esu range are anticipated at 10.6 μ.

Nonlinear optical studies of donors in Ge and Si are continuing. Four-wave mixing spectroscopy has been used to study[5] the stress dependence of the ground state multiplet of phosphorus donors in Si. This work was made possible through the development of a quantitative stress cryostat. The experiments determine the stress deformation potential, Ξ_a, characterizing the 1s ground state multiplet.

The stress cell has also been coupled to a superconducting magnet to measure the combined stress (F) and magnetic field (B) dependence of the donor levels. With F constant one observes four-wave resonances, as a function of B, for various values of the difference frequency, $\Delta\omega$, between two CO_2 laser beams. Preliminary experiments on As donors in Ge with stress F $\|$ [110] yield a value 0.03 $\mathrm{cm}^{-1}/\mathrm{T}^2$ for the diamagnetic coefficient of the 1s $(A_1) \rightarrow$ 1s(B_1) transition in the high stress limit. This value is in excellent agreement with a theory which takes into account both valley re-population and the change in size of the ground state, 1s(A_1), wave function.

References

1. J.B. McManus, Appl. Phys. Lett. <u>41</u>, 692 (1982).
2. A. Pinczuk, Jagdeep Shah, and P.A. Wolff, Phys. Rev. Lett. <u>47</u>, 1487 (1981).
3. S.Y. Yuen, Appl. Phys. Lett., accepted for publication.
4. S.Y. Yuen, Appl. Phys. Lett., <u>42</u>, 331 (1983).
5. C. Jagannath and D.M. Larsen, Bull. APS <u>28</u>, No. 3, 534 (1983).

Other Publications

Jagannath, C., to be published.

Larsen, D., (private communication).

Kash, K., P.A. Wolff, and W.A. Bonner, "Nonlinear Optical Studies of Picosecond Relaxation Times in n-GaAs and n-GaSb," Appl. Phys. Lett. <u>42</u>, 173 (1983).

Ram-Mohan, L.R. and P.A. Wolff, "Joint-Density of States in Interband Transitions in Semiconductors in a Magnetic Field," Phys. Rev. B <u>26</u>, 6711 (1982).

Kash, K., "Nonlinear Optical Studies of Electron Dynamics in Semiconductors," Ph.D. Thesis, Physics Department, M.I.T., September 1982.

11. Quantum Optics and Electronics

Academic and Research Staff

Prof. M.M. Salour, Dr. G.W. Fehrenbach, Dr. A. Fuchs, Dr. P. Jaanimagi,
Dr. P.H. Kayoun, Dr. P. Kumar, Dr. R. Welte, F.W. Barrows

Graduate Students

N.S. Bergano, R.S. Bondurant, M. Maeda R.S. Putnam, J. Yorsz

11.1 Nonlinear Optical Interactions in Semiconductors

U.S. Air Force – Office of Scientific Research (Contract F49620-79-C-0071)
Michael M. Salour

The aim of this program is to investigate a variety of novel, nonlinear optical interactions that accompany, or immediately follow, the creation of an electron–hole pair in semiconductors. We have previously reported tunable cw laser action with platelet semiconductors in both mode–locked and unmode–locked configuration using CdS, CdSe, and CdSSe. These optically pumped semiconductor platelet lasers do not require complicated heterostructures and thus may be easily changed to different wavelength regimes by varying the sample composition. With a potentially continuous tuning range between 500 nm and 1.5 μm they may become useful tools for spectroscopy in both the time and frequency domains.

More recently we have achieved the first optically pumped, mode–locked semiconductor laser operating at wavelengths longer than 1.0 μm. Laser operation was achieved in two separate compostions of $In_{1x}Ga_xAs_yP_{1y}$ at 1.1 and 1.2 μm with x = .20, y = .4 and x = .24, y = .55, respectively. Pulses as short as 7 ps were obtained with tunability over a range of 26 nm. Cw operation was also achieved with a reduced duty cycle to compensate for the comparatively poor thermal conductivity of the quaternary layer.

In collaboration with Dr. T.C. Harman of Lincoln Laboratory we have also operated the first optically pumped HgCdTe laser in an external cavity. The laser operates in the range of 1.2μ – 2μ with samples prepared by liquid phase epitaxy on CdTeSe substrates. We have achieved a peak output power of 50 watts when mode–locked with an average output power of as much as 5.6 MW. Outputs pulses as short as 5.3 psec were measured with a time–bandwidth product of 0.55. Unmode–locked operation, and operation at temperatures above 10°K were also demonstrated.

During the past year we have also demonstrated platelet semiconductor lasing for the first time in a ring resonator. Low threshold has been achieved with bidirectional operation of the ring but strong

coupling effects have thus far prevented unidirectional operation.

11.2 Picosecond Dye Laser Optics

Michael M. Salour

Our picosecond dye laser system has been extended to high power operation by the addition of four dye amplifier stages. A frequency-doubled, Q-switched Nd:YAG laser pumps the dye amplifiers in synchronism with a pulse from the train of a synchronously-mode-locked dye oscillator. A pulse from the oscillator is then amplified to peak powers of several gigawatts (for pulse duration of several picoseconds at a repetition rate of 10 Hz). An electron-optic streak camera, interfaced to a multichannel analyzer and minicomputer, has been adapted for use at the 10 Hz repetition rate.

For the system's initial demonstration we have performed time resolved laser induced fluorescence spectroscopy of the hydroxyl radical in flame. The results reported extend previous measurements of $OH^2\Pi(v'=0)$ quenching rates in subatmospheric pressure flames to atmospheric pressures. The application of this technique to even higher pressure flames appears feasible. The collisional quenching lifetime following excitation of the $R_2(4)^2\Pi(v'=0) < \cdots ^2\Sigma^+(v''=0)$ transition was measured to be 1.8 ns in the burned gas region of an atmospheric pressure, premixed methane-air flame.

We have also reported the first experimental technique for compensating the pulse broadening in single-mode optical fibers, using the "slow" anomalous pulse propagation in the exciton-polariton resonance in a direct-gap semiconductor. Mode-locked dye laser pulses of 0.7-ps duration at 8180 Å were propagated through a 100-m single-mode optical fiber and emerged with 2.8-ps duration. We have demonstrated the compensation of this pulse broadening in optical fibers by passage through a 6.3 – μm-thick GaAs crystal, taking advantage of the group velocity dispersion around the discrete $n = 1$ exciton-polariton resonance.

11.3 Nonlinear Spectroscopy of Atoms and Molecules

Michael M. Salour

A series of novel experiments has been initiated to study the photon statistics of light produced by degenerate 4-wave mixing (DFWM). The goal of this work is the generation of light in two-photon coherent stages.

Considerable advance has been made in achieving the laser stability required for the observation of non–classical statistics. Output from a frequency–stable ring dye laser is amplified in a 3–stage dye amplifier pumped by a frequency–doubled Q–switched Nd:YAG laser. Use of a novel pulse shaping network has resulted in the generation of nearly transform–limited pulses of 4 nsec duration. DFWM has been observed in Na vapor. So far, photon counting measurements made both on reflected and transmitted probe beams have yielded Poisson statistics. High loss and background fluorescence has restricted these measurements to the regime of classical statistics. Several alternative schemes are being pursued.

58

12. Microwave and Millimeter Wave Techniques

Academic and Research Staff

Prof. B.F. Burke, Prof. R.L. Kyhl, Dr. D.H. Roberts

Graduate Students

B.R. Allen, C.L. Bennett, A.C. Briancon, J.A. Garcia-Barreto, P.E. Greenfield, J.N. Hewitt, V. Dhawan, C.R. Lawrence, J.H. Mahoney

12.1 Cooled FET Amplifiers at 8 and 15 GHz

MESFETS increasingly dominate the microwave amplifier field. The inherently low noise of the field effect is aided by the fact that majority carrier devices can operate at cryogenic temperatures with a 3 to 4 fold reduction in noise.[1-9] The operating frequencies for this study were chosen for their interest to radio astronomy. Specifically, 8.45 GHz is the proposed frequency for space VLBI,[10] and 15 GHz is of importance for background radiation observations.[11]

The astronomical requirements of over 1 GHz bandwidth and under 100° K noise temperature a e challenging design goals in the intermediate step of fabricating a reliable, cryogenically cooled low noise FET amplifier. The amplifier doubles as a test jig in the experimental study of FET gain and noise properties at high frequencies and low temperatures. Design features include easy device replacement and alternate versions for chip and packaged transistors to enable comparative study. For packages, duroid (teflon) substrate and solder connections are employed; the chip version is functionally identical, but eliminates solder joints and uses quartz substrate for the microstrip circuits. Impedances are tunable over a wide range, using broadband open–circuited stub lines. Substrate processing techniques including vacuum evaporation, plating and photolithographic etching were developed to enable rapid realization of any desired microstrip pattern.

The conclusions drawn are as follows: packaged transistors feature easy handling but suffer from parasites and from unpredictable thermal behavior. Solder joints are occasional failure sites when thermally cycled, but special alloy solders can eliminate this problem. Chips have no package parasitics and are in direct thermal contact with the cold stage. However, the necessary bonding procedures are complex and have low yield since bare FETs are easily degraded by mishandling. The peeling of metallization off the bonding pads when thermally cycled (between 300° K and 20° K) seems to be a persistent problem. Accurate characterization of scattering and noise parameters is

difficult on existing equipment. For packaged transistors at 8 – 9 GHz,[13] where network analyzer data is reliable, the results are as follows: T_{min}, the minimum noise temperature, is reduced by a factor of 3 on cooling most FETs from 300° K to 77° K; Z_{opt} ($= R_{opt} + j X_{opt}$), the input impedance for realizing T_{min}, has its real part (R_{opt}) decreased by a factor of 1.5 – 2 and its imaginary part (X_{opt}), approximately unchanged; the noise conductance (g_n) is halved, which reduces the sensitivity of noise temp T to deviations of input impedance Z($= R + j X$) from Z_{opt}, via the equation $T = T_{min} +$

$T_o \frac{gn}{R} |Z - Z_{opt}|^2$ (T_o is the ambient temperature). Similar behavior is found at 15 GHz, but some varieties of device show much less improvement, for reasons as yet uncertain. Extensive study of a variety of transistors including more accurate impedance and noise measurement is needed to separate the contributions and identify the temperature dependances of the various known FET noise mechanisms.

This study involved devices with 1/2 micron gate lengths. New devices with 1/4 micron gates, soon to be available, will be active well beyond 30 GHz. These will require precision circuit techniques and measurements for the full realization of their potential.[14,15]

References

1. R. Pucel, H. Haus, and H. Starz, "Signal and Noise Properties of Gallium Arsenide Microwave Field Effect Transistors," Advances in Electronics and Electron Physics, (Academic Press, New York, 1975).
2. W. Baechtold, "Noise Behavior of Ga–As FETs with Short Gate Lengths," IEEE Trans. Electron Devices ED–19, 5, (1972).
3. H. Fukui, "Optimal Noise Figure of Microwave Ga–As MESFETs," IEEE Trans. Electron Devices MTT–27, 7, (1979).
4. H. Fukui, "Design of Microwave Ga–As MESFETs for Broadband Low–noise Amplifiers," IEEE Trans. Microwave Theory Tech. ED–26, 7, (1979).
5. S. Weinreb, "Low Noise Cooled Ga–As FET Amplifiers," IEEE Trans. Microwave Theory Tech. MTT–28, 10, (1980).
6. C. Liechti and R. Larrick, "Performance of Ga–As MESFETs at Low Temperatures," IEEE Trans. Microwave Theory Tech. MTT–24, 1, (1976).
7. D. Williams, W. Lum, and S. Weinreb, "L–Band Cryogenically Cooled Ga–As FET Amplifiers," Microwave Journal 23, 10, (1980).
8. S. Weinreb, D. Fenstermacher, and R. Harris, "Ultra–Low Noise 1.2 to 1.7 GHz Cooled Ga–As FET Amplifiers," IEEE Trans. Microwave Theory Tech. MTT–30, 6, (1982).
9. G. Tomasetti, S. Weinreb, and K. Wellington, Electronics Division Internal Report No. 222, National Radio Astronomy Observatory, Charlottesville, Virginia.
10. R.A. Preston, et al., "The Future of VLBI Observatories in Space," M.I.T. Radio Astron. Contributions, 1982, No. 5.
11. R. Weiss, "Observations of the Cosmic Microwave Background," Annual Rev. Astron. Astrophys., 1982.
12. C.H. Oxley, et al., "Q–Band Microstrip Techniques," IEEE Colloquium Digest, January 1982.
13. A.C. Briançon, "A 8.45 GHz Ga–As FET Amplifier," S.M. Thesis, Department of Electrical Engineering and Computer Science, M.I.T., May 1983.
14. C.H. Oxley, A. Peake, and R. Bennett, "Q–Band Ga–As FET Single Stage Amplifier," Electron.

14. C.H. Oxley, A. Peake, and R. Bennett, "Q-Band Ga-As FET Single Stage Amplifier," Electron. Lett. 18, 6, (1982).

15. H. Mizuno, "Ga-As FET Mount Structure Design for 30 GHz-Band Low Noise Amplifiers," IEEE Trans. Microwave Theory Tech. MTT-30, 6 (1982).

13. Microwave and Quantum Magnetics

Academic and Research Staff

Prof. F.R. Morgenthaler, Prof. R.L. Kyhl, Dr. T. Bhattacharjee, D.A. Zeskind

Graduate Students

M. Borgeaud, L. Hegi, C.M. Rappaport, N.P. Vlannes

Frederic R. Morgenthaler

Objective

Our objective is to develop an understanding of electromagnetic, magnetostatic, and magnetoelastic wave phenomena and to employ them to create novel device concepts useful for microwave signal–processing applications. We are especially interested in developing novel device concepts for the millimeter wavelength portion of the electromagnetic spectrum.

13.1 Millimeter Wave Magnetics

The Microwave and Quantum Magnetics Group within the M.I.T. Department of Electrical Engineering and Computer Science and the Research Laboratory of Electronics recently began a research program aimed at developing coherent magnetic wave signal processing techniques for microwave energy which may form either the primary signal or else the intermediate frequency (IF) modulation of millimeter wavelength signals.

Emphasis has been placed upon developing advanced types of signal processors that make use of quasi–optical propagation of electromagnetic and magnetostatic waves propagating in high quality single crystal ferrite thin films.

Field displacement nonreciprocity can occur in the case of forward–volume waves that have strong magnetostatic character. For millimeter wave frequencies, that generally require ferrite materials with high magnetostatic anisotropy, we have investigated the nonresonant low bias field limit in which the dominant frequency dependence of the Polder permeability tensor arises from the off–diagonal component. As expected, when the modes have strong electromagnetic– and weak magnetostatic–characters, it is more difficult for bias gradients to induce the desired field

displacement nonreciprocity. Nevertheless, the analysis indicates which factors tend to maximize the effect.

13.2 New Techniques to Guide and Control Magnetostatic Waves

D.D. Stancil and F.R. Morgenthaler reported the propagation characteristics of magnetostatic surface waves in a rectangular yttrium iron garnet film placed between strips of mumetal and in the plane of the strips. The microstrip excitation structure was designed so as to permit the strips to extend along the entire path of propagation, thereby minimizing field nonuniformities in the longitudinal direction. These experiments suggest that nonuniform in-plane fields can be used to alter the dispersion characteristics of the waves. A theoretical argument is also presented describing a possible energy localization mechanism in nonuniform in-plane fields. In addition, experiments are described in which nonuniform fields caused by a slot in a mumetal covering layer are used to guide magnetostatic surface waves through a turn of 160°.

13.3 Optical and Inductive Probing of Magnetostatic Resonances

During the course of his doctoral research, Nickolas Vlannes developed a new induction probe that measures microwave magnetic field patterns of magnetostatic waves in LPE-YIG thin films. The probe's sensing element is either a strand of 25.4 μm diameter gold wire wrapped around a plastic support, or an aluminum rectangular loop photolithographically fabricated on glass. The gold wire method yielded a smallest resolution of 120 μm and the aluminum loops achieved a smallest size of 45 μm. Each sensing element is attached to rotation and tilt stages for proper alignment of the sensing element. This assembly is mounted on a balance arm which is counterbalanced to minimize pressure on the crystal and sensing element. The balanced arm is supported by a vertical translation stage mounted on horizontal X-Y translation stages with 2.5 μm accuracy and total travel of one inch in X and Y.

The probe is designed for studies of amplitude profiles, dispersion relations and phase propagation

direction. Investigations of magnetostatic surface waves (MSSW) under uniform and nonuniform in-plane magnetic field conditions have been done.

13.4 Magnetostatic Wave Dispersion Theory

F.R. Morgenthaler and T. Bhattacharjee analyzed magnetostatic surface wave (MSSW) propagation on one or more co-planar rectangular films of finite width and gave numerical solutions using an integral equation formulation. In the case of uniform in-plane bias, the eigenfrequencies and the associated eigenvectors are obtained by solving the couples equations which determines the frequency dispersion and spatial form of MSSW potentials. In addition to modes having the expected localization of energy on the film surfaces, the results confirm the existence of certain modes having primary energy concentration at the film edges.

The formulation is also specialized to the case of two uniformly magnetized rectangular parallel strips separated by an air gap and coupled via the fringing fields of magnetostatic waves. The results should prove useful in modelling directional couplers for MSSW.

13.5 Magnetoelastic Waves and Devices

The S.M. thesis entitled "Improvements in the Design of Microwave Magnetoelastic Delay Lines," by Alan Keith Wadsworth is completed. The abstract follows:

A linearly dispersive microwave delay line employing a non-linear axial magnetic field profile is described. The delay line operates by utilizing the magnetoelastic interaction between spin waves and elastic waves in a magnetically saturated rod of Yttrium Iron Garnet (YIG). The linear dispersion is varied by magnetically controlling the spin wave dispersion relation.

The theory of operation of the magnetoelastic delay line is reviewed. General equations allowing for the creation of linear dispersion using non-linear axial magnetic field profiles are developed. The issues of wave conversion efficiency and spin wave ray path focusing are examined for non-linear field profiles.

Measurements made on a YIG delay line designed to produce linear dispersion using a non–linear axial magnetic field are reported. The dispersion obtained agrees with theoretical predictions. The insertion loss obtained was improved by 14–17 db over previous attempts using the same thin film antennae. The operating range of the device was 2.1–2.6 GHz.

13.6 Microwave Hyperthermia Group

FreJeric R. Morgenthaler

Objective

Our understanding of both physics and physiology is challenged in trying to optimize techniques for heat production and for the thermometry associated with hyperthermia modalities used in connection with cancer therapy.

Fundamental considerations are based on designing proper microwave applicators which must be able to handle the microwave power required to raise the temperature of the tumor. They must also minimize the amounts of microwave power being delivered to the healthy tissue or being radiated into free space.

13.7 Design of Planar Arrays

Frederic R. Morgenthaler, Carey M. Rappaport, Tushar Battacharjee

One needs to design an optimum antenna for focusing microwave energy at any preselected region (which should be as small as possible). Usually, the points of interest lie in the Fresnel–region but because living tissues appear as lossy dielectrics to electromagnetic waves, the problem is severe. Our program is only a few months old, yet initial progress has been made on the computer modelling of microwave power deposition in biological tissue by radiation from annular ring arrays designed to focus electromagnetic power in a predetermined region. Those factors that limit the degree of focusing from a planar array have been examined in detail. Naturally, the loss of the tissue dominates the design and provides a fundamental barrier. For a given on–axis focal position, increasing the aperture of a Fresnel–like lens beyond a certain value is ineffective, this gives rise to a concept of array synthesis using "zones of influence". This is made clear from the theoretical expression for the complex electric field strength at the on–axis focal position $z = z_o$ produced by a circular–aperture of radius R that employs continuous radial phase correction to produce what is in effect a continuous Fresnel lens plate (which can be approximately realized in terms of step wise phase correction of annular ring sections). If the amplitude of the (linearly–polarized) aperture field is E_o, then

$$\frac{E(z_0)}{E_0} = (j\beta) z_0 \left[E_1(\alpha z_0) - E_1\left(\alpha\sqrt{z_0^2 + R^2}\right)\right]$$

$$+ e^{-z_0} - \frac{z_0}{\sqrt{z_0^2 + R^2}} e^{-\alpha\sqrt{z_0^2 + R^2}} \tag{13.1}$$

where

$$E_1(x) = \int_x^{\infty} \frac{e^{-u} du}{u} \qquad \text{for } x > 0$$

when $R \to \infty$, Eq. (13.1) saturates at a value

$$\frac{E_{max}}{E_0} = \left[(j\frac{\beta}{\alpha}) \alpha z_0 E_1(\alpha z_0) + e^{-\alpha z_0}\right]$$

Since $\alpha z_0 E_1(\alpha z_0) \lesssim e^{-\alpha z_0}$, it follows that the maximum enhancement that can be expected is

$$\lesssim \sqrt{1 + (\frac{\beta}{\alpha})^2} \, e^{-\alpha z_0}$$

the near equality holds for $\alpha z_0 \gg 1$.

14. Radio Astronomy

Academic and Research Staff

Prof. A.H. Barrett, Prof. B.F. Burke, Prof. J.W. Dreher, Prof. R.L. Kyhl, Prof. J.H. Lang, Prof. J.R. Melcher, Prof. P.C. Myers, Prof. D.H. Staelin, Dr. D H. Roberts, Dr. P.W. Rosenkranz, Dr. M. Shao, J.W. Barrett, J.G. Kang, D.C. Papa

Graduate Students

A.D. Ali, B.R. Allen, J.T. Armstrong, C.L. Bennett, P.J. Benson, A.C. Briançon, M.M. Colavitz, V. Dhawan, E.E. Falco, J.A. Garcia-Barreto, P.M. Garnavich, P.E. Greenfield, S.M.A. Harton, J.N. Hewitt, J.M. Jackson, J.-S. Jin, J.J. Komichak, R.H. Lamb, C.R. Lawrence, J.H. Mahoney, D.C. Murphy, K.S. Nathan, S.-M. Shih, J.M. Sulecki, B.I. Szabo, J.V. Vallerga, W. Williams, Y. Yam

14.1 Microwave Spectroscopy of the Interstellar Medium

Alan H. Barrett

During 1982 the following programs of research on the interstellar medium were pursued:

1. A detailed study of the Sgr A molecular cloud, located approximately 5 arc minutes from the galactic center and believed to be closely associated with the center, has been completed in the microwave lines of NH_3, HNCO, and $C^{18}O$. The $\ell - b$ and $\ell - v$ maps in NH_3 and HNCO are very similar, suggesting that both molecules are probes of high–density (10^4 cm^{-3}, and greater) material. The $C^{18}O$ maps suggest a fairly uniform temperature throughout the cloud whereas a $HNCO/C^{18}O$ ratio varies by a factor of ten in the cloud. This variation is believed to be attributed to differences in chemical composition within the cloud.

VLA observations of the NH_3 J,K = 3,3 line reveal condensations within the Sgr A cloud whose angular size is less than 5 arc–seconds, corresponding to a linear dimension of 0.25 pc, with brightness temperatures of the order of 100 K. Only about 15%, or less, of the NH_3 appears to be in identifiable condensations.

2. The NH_3 lines have been regarded as a fairly reliable "thermometer" of the interstellar gas because the intensities of the hyperfine lines could be fit very closely with a single excitation temperature. However, examples have now been found where this is not the case. We have found at least five sources which exhibit hyperfine intensity anomalies. We hope to be able to correlate this effect with other properties of the source, such as an IR source, high–velocity outflow, OH and/or

H_2O masers, etc.

3. The molecular clouds in the Taurus region have been studied in the CO line at 2.6 mm. A large amount of data was acquired, using the 1.2 m telescope of Columbia University and the Goddard Institute of Space Studies, and is not fully reduced. However, one significant conclusion is the detection of a large shell of CO surrounding a group of T–Tauri stars. This shell may have originated from the mass loss of the T–Tauri stars.

4. A deep, continuum study of the Sgr A molecular cloud with the VLA at 6 cm and 2 cm has revealed the presence of both thermal and nonthermal sources in the cloud. These sources were previously undetected but their relationship to the cloud is quite clear since they have a positional coincidence with the NH_3 peaks in the cloud. Further studies are planned.

14.2 Galactic and Extragalactic Radio Astronomy

Bernard F. Burke

Gravitational Lenses

The work of Greenfield, Roberts, and Burke on VLA studies of the double quasar 0957 + 561 is nearing publication. This massive study, which consisted of observing the object at wavelengths of 2, 6, 18, and 21 cm, covered the period June 1979 – December 1980, and included studies of the spectra, polarization properties, and gravitational lens properties of the object, was summarized in the thesis of P.E. Greenfield as follows:

1. The radio map gives more constraints on possible lens models, and the only acceptable models fall within a narrow range of parameters. The original "double ellipsoid" model is unacceptable, but by relocating the mass associated with the foreground cluster and changing its scale length, a satisfactory fit can be found to the data.

2. Time variations seem to have occurred during the early periods of observation that may give an interesting new class of cosmological measurement.

3. The two quasar images are polarized, and exhibit different rotation measures. The rotation measure of the B quasar, which is seen shining through the giant cD galaxy in the foreground, is greate by 100 rad/m^2, implying an average magnetic field of about 1 μG through a 10^{-2} el/cm^3 pathlength of 10^4 pc, which seems remarkably high. We are investigating the anomaly further.

In May 1982, we reobserved the object with the additional collaboration of J.N. Hewitt and A.K. Dupree. The B and G images show irregularities that are consistent with those present in the December 1980 data. Now, with the perfection of self–calibration routines at the VLA; we have been

able to imp'ove the results greatly. Greenfield's model (developed in 1981) predicts the observed anomaly in the B image, and the extended nature of the G source, partly associated with the galaxy, has raised interesting questions about the nature of the third image.

We have also been reexamining the mass models, and continuing our time–variation studies of the quasar images. We believe that the double quasar data now gives the best–defined value of the mass–to–light ratio ever determined for a cluster of galaxies.

14.3 Interacting Galaxies

The pair of galaxies NGC 4038/39 (known as "the antennae") have been observed at 21 cm by the VLA in both the C and D arrays. Theoretical studies are now in progress to use these new data to derive the orbital history of the pair of galaxies, and to see if the combined morphological and velocity field information can also give new data on massive halos associated with the galaxies (a massive halo gives a softening of the galactic gravitational field when test particles travel close enough). So far, we conclude that:

1. The conventional interpretation is not an accurate representation, since one long tidal arm for each galaxy is not consistent with the dynamics that the new data demand (the work of Toomre and Toomre was, after all, only intended to be a first demonstration of the reasonability of forming long tails by tidal interactions).

2. The only long arms probably are connected to only one of the two galaxies.

3. The orbital history of the interacting pair can probably be specified with some precision.

The final purpose, the search for evidence for a massive halo, will require the completion of the orbital analysis before a definitive statement can be made.

14.4 The 6 cm Radio Survey

The next step has been to observe the entire band of sky between – 3° and + 20° with the 300–ft. transit telescope of the NRAO. This survey has now been completed and consists of analysis of the gain of the 300–ft. telescope as a function of position and time, and of the time variability of the 123 calibrator sources.

14.5 Morphology and Optical Identifications

We have been able to derive a list of 1000 sources for detailed study from the MA survey. These were observed with the VLA at 6 cm to get accurate positions, and 992 of the source positions were measured on the Palomar Sky Survey Plates for optical identifications. This work formed the Ph.D. thesis of C.R. Lawrence at M.I.T. A number of interesting conclusions can be drawn from this work, which is the largest single optical identification study yet undertaken:

1. 50% of the sources having flux greater than 150 mJy, and 39% of those fainter than 150 mJy, have visible optical PSS counterparts.

2. 45% of the sources have flat spectra ($|\alpha| < 0.5$). Roughly 2/3 of these have optical PSS counterparts.

3. The steep spectrum sources only have an identification rate of 30%, and the empty field sources tend to have the steepest spectra.

4. Almost half the observed sources are unresolved with the VLA.

5. The easily recognizable class of double radio sources has the lowest PSS identification rate (15%). These exhibit separations ranging from 0.3 to 100 arc-sec. Many of them are undoubtedly distant radio galaxies, some are probably quasars. If the morphology can be better understood, these may prove to be a most interesting cosmological probe.

6. An easily recognizable class of triple sources has been found, and a surprising fraction (80%) have PSS counterparts, setting them aside most clearly from the double class discussed above. Their spectral indices are unusually steep.

7. There is no correlation between radio spectral index and likelihood of identification.

8. Over 25% of all steep spectrum sources are less than 1 arc-second in size. These have a PSS identification rate of 42%, higher than for extended steep-spectrum sources, but much lower than for unresolved flat-spectrum sources.

14.6 Interstellar Masers

The study of the full Stokes parameters for the OH maser W30H has been completed, and is nearly ready for publication. The magnetic field is remarkably uniform for these maser sources; the field for all 6 clear Zeeman pairs is 5 ± 1 gauss, and pointing away from us in all cases. The follow-up experiment, performed February 1982, is still in the reduction process.

14.7 VLBI Studies

A 327 MHz VLBI experiment, in collaboration with R. Simon of NRL and others, is being planned for October 1983, and we will take responsibility for the Haystack electronics and operations.

Polarization studies of continuum sources at milliarcsecond resolution have been carried out in collaboration with D. Roberts of Brandeis. The first experiment was successful, and the data have been reduced at Brandeis. A new experiment, to be carried out in late 1983, is being prepared for.

The 7-mm cooled mixer that was built by B. Allen as part of his Ph.D. thesis in Electrical Engineering at M.I.T. has been operated on the Haystack radio telescope successfully. The first tests were made in the single-dish mode, observing SiO masers as test sources. The total single-sideband system temperature was 350 K, with a device temperature of 250 K. The NRAO maser is less noisy,

but has a far narrower instantaneous bandwidth. New devices now on the bench will undoubtedly replace this mixer eventually, but it is currently the best fully operable 7-mm mixer on any radio telescope. A VLBI experiment at 7-mm is currently being planned jointly with K. Johnston of NRL.

14.8 Planned Program, 1983-84

1. The gravitational lens work will emphasize continued studies of 0957 + 561, plus a new program to look for many more gravitational lens examples. We plan to examine 3000 sources with the VLA, and expect 5 to 10 new examples of gravitational lenses. It turns out that the "snapshot" ability of the VLA makes it far more advantageous to use the VLA to find the candidates, following up later with optical verification, than the other way around.

2. The studies of interacting galaxies will continue. The NGC4038/39 work will now emphasize theoretical studies, while we will be proposing VLA 21-cm line studies of new candidates.

3. The MG survey will be completed. We have proposed a new section of the survey, to cover declinations 20° to 50°, since our extensive software library will allow us to extend the survey with very little expenditure of manpower.

4. Correlations of radio and optical properties of radio sources will continue. Here, the work of Lawrence et al., has generated an exciting new range of projects. The highest priority will be to obtain redshifts of a number of sources (only 21 of the 602 sources studied have measured redshifts). One sharp result of Dr. Lawrence's work is the derivation of the number of measured redshifts needed to distinguish between pairs of models presented by Peacock and Gull (MN <u>195</u>. 611 (1981)). Strong sources (5 GHz S > 1 Jy) cannot do the job, because more sources would be required than exist in the sky; only by going to fluxes in the range 50–150 mJy can there be a reasonable expectation of distinguishing models.

5. Work on VLBI studies of interstellar masers will continue, but the emphasis of the work will shift to H_2O and SiO masers.

6. The continuum VLBI work will consist of 4 parts: collaboration with the Brandeis group on polarization studies will continue, 7-mm VLBI techniques, still in developmental stages, will be pursued, low-frequency VLBI will continue at 327 MHz while we prepare a still longer-wavelength experiment, and the new initiative described under (7) below will require VLBI observations in many cases.

7. The morphological and identification work of Lawrence has generated a new class of radio and optical projects. There are 318 point sources, of which 175 have OSS counterparts. Over half of these are almost certainly quasars, and these constitute the largest radio-selected sample currently available. The taking of spectra of these will require collaborators, who are currently being sought out. The 92 double sources, mostly have no PSS counterpart, will be examined at other frequencies with the VLA, and searches for faint optical counterparts down to m ≈ 24 will be carried out with the MASCOT CCD at the McGraw-Hill Observatory. There are 46 sources in a category

called "core-double". These doubles with an obvious nuclear source near the mid-point (and clearly distinguishable from the "triples"—there are only 15) will receive immediate optical follow-up. Finally, we are planning to use the Arecibo telescope to reobserve all 1000 sources in our VLA sample at 21 cm to obtain a set of uniform spectral indices. The fluxes will be directly comparable with the 300 ft. 6 cm measurements since the beamwidths are about the same size.

14.9 Jovian Decametric Radiation

David H. Staelin, Philip W. Rosenkranz, Peter M. Garnavich

The Planetary Radio Astronomy (PRA) experiment on the Voyager 1 and 2 spacecraft observed Jovian decametric radio emission in 198 channels distributed over the band from 1.2 kHz to 40.5 MHz. "Arcs" in the frequency-time domain have been associated with radio emission near the local electron-cyclotron frequency with a hollow conical emission pattern. Theory suggests that such conical emission might be produced by magnetospheric currents generated by the satellite Io as it traverses the magnetospheric fields. These currents, on the order of 10^6 amps, are believed to propagate in an Alfvén wave that is reflected repeatedly between the northern and southern Jovian ionospheres. These currents traveling along the magnetospheric field lines should be spaced in Jovian longitude by an amount that depends upon the Jovian magnetic field strength and the plasma density in the magnetosphere, which is dominated by the plasma located in the "plasma torus" produced near the orbit of Io by volcanic activity. It would be natural to associate the spacing of the Jovian arcs with the spacing between the separate reflections of the Io-generated currents.

In part to test this hypothesis a catalog of 200 arcs and 200 arc gaps was constructed from the Voyager 1 and Voyager 2 decametric data. Work began on relating these observed arc characteristics to the Alfvén-wave model.

Jovian S-bursts, in contrast to the Jovian arcs, have durations on the order of milliseconds. Certain S-bursts that are V-shaped in the frequency-time domain were studied theoretically and were successfully explained as arising from dense bunches of coherent electrons produced by ~ 10 Hz longitudinal modulation of ~ 1 keV superimposed on outward-moving ~ 2.5 keV electron beams moving in or near the Io magnetospheric flux tube. This ballistic model for S-bursts suggests the degree of coherence in the emitting electrons, a lower boundary for magnetospheric ion densities, and an interpretation for the origin of L-burst emission.

References

1. D.H. Staelin and P.W. Rosenkranz, "Formation of Jovian Decametric S-Bursts by Modulated Electron Streams," J. Geophys. Res. **87**, pp. 10401-10406, Dec. 1, 1982.

14.10 Long–Baseline Astrometric Interferometer

Michael Shao, David H. Staelin, M. Mark Colavita, Peter M. Garnavich

During 1982 the Mark II optical astrometric interferometer was successfully used to track stellar fringes for the first time at Mount Wilson Observatory in California. This instrument has two 10–inch siderostat mirrors 3.4 meters apart in a north–south direction. Within the ~ 2–inch aperture the positions of red and blue fringes are independently estimated every ~ 2–10 ms. thus permitting the state of the atmosphere to be measured and compensated over time intervals sufficiently short that the atmosphere can be considered "frozen".

It was discovered that the instrument was too narrowband to permit the two–color technique to work successfully. This was due to a defective beamsplitter and mirrors that were degraded in the blue portion of the spectrum. It further appeared that the optical dispersion in the two bands of the interferometer were slightly mismatched, which reduced fringe visibility. These deficiencies are now being corrected.

The primary purpose of the Mark II experiment is demonstration and evaluation of the two–color technique for obtaining relative astrometric positions accurate to ~ 10^{-3} arc sec rms for stellar separations $< \sim 1°$. Experiments to demonstrate wide angle ($\gtrsim 10°$) and absolute astrometry are also being planned for the Mark II instrument in collaboration with the Naval Research Laboratory. Future versions of the interferometer are expected to achieve 10^{-4} arc sec relative position accuracy over 1–2° stellar separation, which would be adequate to detect a Jupiter near a one solar mass star at a distance of several parasecs, with a signal–to–noise ratio of ~ 10.

14.11 Tiros–N Satellite Microwave Sounder

Philip W. Rosenkranz, David H. Staelin, Krishna S. Nathan

The National Oceanic and Atmospheric Administration (NOAA) routinely reduces data from one or two operational polar orbiting weather satellites; these now carry infrared spectrometers and a four–channel passive microwave spectrometer (MSU) for the purpose of mapping the three-dimensional temperature field of the atmosphere at six– or twelve–hour intervals. The purpose of this research program is continued improvement in the utilization of the passive microwave data produced by these NOAA satellites.

Work continued on a study of the growth of initial–state errors in numerical weather prediction

models. These experiments used the National Center for Atmospheric Research computer. The method involved the addition of perturbing functions to the initial wind and temperature fields. A class of test functions was found which avoids the generation of gravity waves in the model. On October 1, 1982, support for this work was switched to NASA Grant NAG5-10.

A two-dimensional temperature profile retrieval algorithm was written and tested for MSU data. The two dimensions are vertical and along the satellite track. This algorithm is a minimum-mean square error spatial filter of the type described in Ref. 1. It showed lower temperature errors than a comparable one-dimensional (vertical) retrieval, even when instrument noise was subtracted from the one-dimensional retrieval errors. This improvement was attributed to the additional information introduced by horizontal correlation of atmospheric temperature statistics.

References

1. P.W. Rosenkranz, "Inversion of Data from Diffraction-Limited Multiwavelength Remote Sensors, 1, Linear Case," Radio Sci. <u>13</u>, 1003-1010 (1978).

14.12 Improved Microwave Retrieval Techniques

Philip W. Rosenkranz, David H. Staelin, Krishna S. Nathan

This program is directed toward development of improved techniques for retrieval of atmospheric temperature, wind, and humidity fields from passive microwave measurements of the earth, as obtained from satellites.

Work on a robust scheme for retrieval of water vapor profiles from measurements near 183 GHz was concluded this year. The results were published in Ref. 1.

Studies of the growth of errors in a numerical weather prediction model were shifted from NOAA support to support by this grant during the year. The purpose of this work is to understand how initial errors introduced by remote sensing systems impact forecasts, and the implications for design of global monitoring sytems incorporating satellite sensors. In a preliminary series of numerical experiments run on the National Center for Atmospheric Research computer, we found that the initial wind error was most important in determining the growth of forecast error with time. Temperature forecast errors were largely produced by differential advection of temperature in the perturbed forecast relative to the unperturbed forecast. A second conclusion was that the forecast error can be equated to a superposition of error fields due to components of the initial perturbation field, for a few hours, and for initial wind errors $\leq$ 2 m/s.

References

1. P.W. Rosenkranz, M.J. Komichak, and D.H. Staelin, "A Method for Estimation of Atmospheric

14.13 Scanning Multi-Channel Microwave Radiometer (SMMR)

Philip W. Rosenkranz, David H. Staelin, Xi Ru Xu

On October 24, 1978, the Nimbus-7 satellite was launched into polar orbit carrying the Scanning Multi-Channel Microwave Radiometer (SMMR) and other instruments. SMMR separately measures vertically and horizontally polarized terrestrial thermal radiation at wavelengths of 0.81, 1.4, 1.7, 2.8, and 4.6 cm. The mechanically scanned antenna maps all 10 channels completely over a 780-km wide swath beneath the spacecraft with a ground resolution ranging from ~ 30 km to ~ 150 km, depending on wavelength. During 1982 contributions were made to the retrieval algorithm to be used operationally for estimates of global water vapor abundance over ocean. A method for estimating atmospheric water vapor over the highly reflecting polar icecap and terrestrial ice sheets was also developed. Some evidence was found for the creation of humid air masses over and downwind of major transient polynyas in the north polar icecap. Three of the SMMR frequencies were also used independently to estimate snow accumulation rates in Antarctica, and the resulting maps were found to be in reasonable agreement with each other and with *in situ* observations.

14.14 Video-Bandwidth Compression Techniques

David H. Staelin, Donald E. Troxel, Alan S. Willsky, Ali D.S. Ali, Biswa Ghosh, Katherine H. Lambert, Joan M. Sulecki

During 1982 significant progress was made on the design and fabrication of a video input/output port for the Nova-4 computer. It will be capable of displaying 8-bit monochrome video images as large as 128 x 240 pixels; a 4-bit option permits up to 256 x 240 pixels per frame, and data can then be transferred at twice the normal rate. The normal rate of data transfer between the frame store system and the disk memory is ~ 320 kbps. The input/output devices include a monochrome video camera and a monochrome video monitor.

Two major techniques for image coding are being explored initially. These are adaptive two-band coding and morphological coding. In two-band coding the images are separated into high frequency and low frequency components which are then quantized differently; typically 6-8 bits and 0-2 bits are employed for the low and high frequency components, respectively. Morphologically coded images are decomposed into their major morphological elements which resemble the brush strokes of an artist. This study includes analysis of methods for performing the decomposition and

reconstruction of the images, and of the "ambiguity noise" which results when arbitrary choices must be made between different representations which are similar in appearance.

The primary objective of this work is to develop a better understanding of the intrinsic limits to the coding of full-motion head-and-shoulders monochrome images for videophone applications. Coding techniques appropriate for image transmission in the range 9.6-56 kbps are being developed and studied.

14.15 Communications Satellites

Intelsat (Contract Intel-188)
David H. Staelin, Ali D.S. Ali

During 1982 previously developed cost models for various network elements were explored to improve understanding of minimum cost architectures for large integrated satellite and terrestrial communications networks appropriate for the period 1990-2000. Optimum architectures were determined as a function of system traffic capacity (typically 0.5-30 Gbps), the total area of coverage (typically 1-64 x 10^6 km^2), and other variables. Major parameters of both TDMA and FDMA architectures at 4/6, 12/14, and 20/30 GHz were optimized; these parameters included the number of ground stations, number of satellite beams, number of orbital slots, transmitter power, and others.

References

1. D.H. Staelin and R.L. Harvey, "Future Large Broadband Switched Satellite Communications Networks," final Technical Report on Contract NAS5-25091, Research Laboratory of Electronics, M.I.T., December 1979.
2. D.H. Staelin, et al., "Satellite Network Architecture: Technology Issues," Final Technical Report under Intelsat Contract Intel-188, Research Laboratory of Electronics, M.I.T., July 30, 1982.

14.16 Electrostatically-Figured Membrane Reflector

Joint Services Electronics Program (Contract DAAG29-80-C-0104)
Lockheed Missiles and Space Company (Contract LS90B4860F)
Jeffrey H. Lang, Timothy L. Johnson, David H. Staelin, Yeung Yam, Shih-Ming Shih, William C. Karl

This project is directed toward the theoretical development [1-13] and experimental evaluation[2,3,6,8,10-13] of control systems for large space structures. The theoretical development has concentrated on the design of control systems which can stabilize open-loop-unstable structures[1-3,6,10,11], and can operate successfully in the presence of actuator and sensor spillover.[4,5,7,9,11-13] The experimental evaluation of these control systems has been performed on a laboratory-scale large space structure involving an electrostatically-figured membrane reflector

(EFMR) 2 m in diameter. Concurrently, this project is directed toward the development of the EFMR for use in space–based antennas.[1-3,5-8,11,12]

The EFMR concept utilizes electrostatic force distributions to shape a flexible conducting membrane into a reflector with the desired figure. The EFMR is specifically designed to permit the construction of self–deployable, low–mass antennas with reflector diameters between 30 m and 300 m. A 300 m antenna constructed with an EFMR should have a mass near 3000 kg. Further, based upon models of EFMR electromechanical dynamics, it appears that the EFMR could exhibit a diameter–to–surface–tolerance ratio between 10^5 and 10^6 with a focal–length–to–diameter ratio of unity or less. This surface tolerance results in diffraction–limited antenna beamwidths of 60 arc·s to 6 arc·s, and appears achievable with fewer than 100 electrostatic force actuators and reflector figure sensors.

Due to the flexibility of the reflector, active reflector figure control is necessary. The design of the requisite control system has been the main concern of this project. In particular, two aspects of EFMR figure control have been examined closely: the stabilization of open–loop–unstable EFMR's, and the effects of actuator and sensor spillover on closed–loop EFMR figure control. The generality of this research has been preserved so that it can be applied to other large space structures. The EFMR equilibrium figure is capable of supporting propagating–wave disturbances and Rayleigh–Taylor instabilities. Although the instabilities can be avoided, they are present with the most advantageous EFMR geometries. Consequently, their stabilization is essential. A control system which achieves their stabilization has been successfully designed and experimentally demonstrated. It is also important to suppress EFMR figure disturbances. A control system designed for this task, and that of EFMR stabilization if necessary, is generally based upon a finite–dimensional EFMR model. The actual control system, however, must interact with the neglected EFMR dynamics through actuator and sensor spillover, which may destabilize the closed–loop control system. To contend with this, an analysis of spillover has been performed which has led to control system design constraints which, if applied, generally guarantee the closed–loop stability of the EFMR figure control system. The success of the constraints has been experimentally demonstrated.

References

1. J.H. Lang, J.R. Gersh, and D.H. Staelin, "Electrostatically–Controlled Wire Mesh Antenna," Electron. Lett. 14, 20, 665–666 (1978).
2. J.H. Lang, "Computer Control of Stochastic Distributed Systems with Applications to Very Large Electrostatically Figured Satellite Antennas," Ph.D. Thesis, Department of Electrical Engineering and Computer Science, M.I.T., November 1979.
3. J.H. Lang and D.H. Staelin, "Electrostatically–Controlled Large–Aperture Reflecting Satellite Antennas," Proceedings of the IEEE Conference on Decision and Control, December 1980, pp. 991–993.
4. J.H. Lang, "A Perturbation Analysis of Spillover in Closed–Loop Distributed–Parameter Systems," Proceedings of the IEEE Conference on Decision and Control, December 1980, pp. 750–754.

5. J.H. Lang, D.H. Staelin, T.L. Johnson, Y. Yam, and S. Shih, "Basic Research on Electrostatically-Figured Membrane Reflectors," Progress Report to the Lockheed Missiles and Space Company, December 1980.

6. J.H. Lang, "Experiments on the Electrostatic Control of a Flexible Membrane and Their Relation to Membrane Antenna Figure Control," *Proceedings of the AIAA Guidance and Control Conference*, August 1981, pp. 187-191.

7. J.H. Lang, D.H. Staelin, T.L. Johnson, Y. Yam, and S. Shih, "Basic Research on Electrostatically-Figured Membrane Reflectors," Progress Report to the Lockheed Missiles and Space Company, December 1981.

8. J.H. Lang and D.H. Staelin, "Electrostatically Figured Reflecting Membrane Antennas for Satellites, IEEE Trans. Autom. Control 27, 3, 666-670, June 1982.

9. Y. Yam, J.H. Lang, T.L. Johnson, S. Shih, and D.H. Staelin, "Large Space Structure Model Reduction and Control system Design Based upon Actuator and Sensor Influence Functions," *Proceedings of the NASA Workshop on Applications of Distributed System Theory to the Control of Large Space Structures*, July 1982.

10. J.H. Lang and D.H. Staelin, "The Computer-Controlled Stabilization of a Noisy Two-Dimensional Hyperbolic System," IEEE Trans. Autom. Control 27, 5, 1033-1043, October 1982.

11. J.H. Lang, "Electrostatically-Figured Membrane Reflectors: An Overview," *Proceedings of the NASA Large Space Structure Technology Conference*, December 1982, pp. 575-582.

12. J.H. Lang, D.H. Staelin, T.L. Johnson, Y. Yam, and S. Shih, "Basic Research on Electrostatically-Figured Membrane Reflectors," Progress Report to the Lockheed Missiles and Space Company, December 1982.

13. Y. Yam, "Large Space Structure Model Reduction and Control System Design Based Upon Sensor and Actuator Influence Functions," Ph.D. Thesis, Department of Aeronautics and Astronautics, M.I.T., June 1983.

15. Electromagnetic Wave Theory and Remote Sensing

Academic and Research Staff

Prof. J.A. Kong, Prof. R.L. Kyhl, Dr. W.C. Chew, Dr. R.-S. Chu, Dr. H.K. Liu, Dr. M.A. Zuniga, H.-Z. Wang, X. Xu

Graduate Students

S.-L. Chuang, T.M. Habashy, Y.Q. Jin, J.K. Lee, S.L. Lin, D.W. Park, S.Y. Poh, A. Sezginer, R.T.I. Shin, F.J. Vallese

15.1 Electromagnetic Waves

Joint Services Electronics Program (Contract DAAG29-80-C-0104)
Jin Au Kong, Tarek M. Habashy, Soon Yun Poh

Electromagnetic waves are studied with applications to microstrip antennas,[1,2] microwave integrated circuit problems,[3-5] geophysical subsurface probing,[6,7] and scattering from helical structures.[8-10] Radiation and resonance characteristics of the annular-ring microstrip antennas and two coupled circular microstrip disk antennas are studied rigorously using numerical techniques, matched asympotic analysis, and newly developed Hankel transform analysis. The classical subject of dipole antenna radiation in the presence of stratified earth as applied to geophysical probing is studied. A new double-deformation technique has also been developed to analyze transient electromagnetic phenomena. Electromagnetic wave scattering from helical structures has been studied using physical optics and modal approaches. Also, the Smith-Purcell radiation problem is solved taking into account the penetrable properties of metallic gratings.[11]

15.2 Remote Sensing with Electromagnetic Waves

National Science Foundation (Grants ENG78-23145 and ECS82-03390)
Jin Au Kong

Remote sensing with electromagnetic waves has been studied with the theoretical models of random media, discrete scatterers, and random distribution of discrete scatterers. These models are used to simulate snow-ice fields, forest, vegetation, and atmosphere.[12-16] Scattering and emission of electromagnetic waves by such media bounded by rough interfaces are investigated.[17-22] Multiple scattering effects of electromagnetic waves by a half space of densely distributed discrete scatterers are studied.[23-26] The quasi crystalline approximation is applied to truncate the hierarchy of multiple

scattering equation and the Percus–Yevick result is used to represent the pair distribution function. The strong fluctuation theory is also applied to the study of electromagnatic wave scattering by a layer of random discrete scatterers.[27,28]

15.3 Acoustic Wave Propagation Studies

Schlumberger-Doll Research Center
Jin Au Kong, Shun-Lien Chuang, Soon Yun Poh, Apo Sezginer

Multiple scattering of acoustic waves by random distributions of discrete scatterers has been studied with the use of quasi crystalline–coherent potential approximation and Percus–Yevick equation.[23] The same technique is also used to study electromagnetic wave scattering by unbounded and half–space of densely distributed discrete scatterers.[25,29] In addition, the radiation and resonance of microstrip line structures,[1-3,5] geophysical subsurface probing by dipole antennas,[6,7] and scattering of waves from helical structures[8,10] have been studied.

15.4 Remote Sensing of Vegetation and Soil Moisture

National Aeronautics and Space Administration (Contract NAG 5-141)
Jin Au Kong, Robert T. Shin

In the remote sensing of vegetation and soil moisture, the scattering effects due to volume inhomogeneities and rough surfaces play a dominant role in the determination of radar backscattering coefficients and radiometric brightness temperatures.[15,22,30] The strong fluctuation theory for electromagnetic wave propagation in a random medium with large variance of permittivity function is developed.[27,28] This is particularly pertinent for vegetation canopy since the contrast of permittivity between vegetation, which is essentially water droplets, and air is very large. For row structures in plowed vegetation fields, we have developed a modal theory with the extended boundary condition approach to study electromagnetic wave scattering and emission.[17-20] These theoretical models have been used to interpret the experimental data collected from vegetation fields.[14,31]

15.5 Passive Microwave Snowpack Experiment

National Aeronautics and Space Administration (Contract NAS5-26861)
Jin Au Kong, Robert T. Shin

A multi–frequency microwave radiometer with wavelengths ranging from 8 mm to 4.6 cm was used to study the microwave thermal emission from snowpacks in the Sleepers River Valley of Northeastern

Vermont.[21,32] The radiometer used was an "Engineering Model" of the Scanning Multichannel Microwave Radiometer (SMMR), flown on the Seasat and Nimbus-7 satellites. Due to the weather cycles in the area, there were prominent ice layers embedded in the snowpacks. These ice layers cause the interference effects which modify the emission characteristics of the snowpack. Analysis of the preliminary results indicate that the incidence angle dependence of the brightness temperature of the snowpack containing the ice layers is quite different from that of more homogeneous snowpacks typical of Rocky Mountains.

15.6 Remote Sensing of Earth Terrain

Jin Au Kong, Robert T. Shin

Extensive work has been accomplished in the development of theoretical models that account for absorption, scattering, layering, and rough surface effects of earth terrain.[15,22,30] Electromagnetic wave scattering and emission from periodic surfaces have been solved using a rigorous modal theory.[18,19] The results satisfy the principles of reciprocity and energy conservation and include shadowing and multiple scattering effects. Active and passive remote sensing of atmospheric precipitation is studied with the vector radiative transfer equations.[12,16] Electromagnetic wave scattering from a layer of random discrete scatterers has been studied with the strong fluctuation theory[28] and the quantum mechanical potential approach.[24-26]

References

1. S.M. Ali, W.C. Chew, and J.A. Kong, "Vector Hankel Transform Analysis of Annular-Ring Microstrip Ant nna," IEEE Trans. Antennas Propag. AP-30, 637–644 (1982).
2. T.M. Habashy, S.M. Ali, and J.A. Kong, "Impedance Parameters and Radiation Pattern of Two Coupled Circular Microstrip Disk Antennas," J. Appl. Phys. 54, 493–506 (1983).
3. W.C. Chew and J.A. Kong, "Microstrip Capacitance for a Circular Disk through Matched Asymptotic Expansions," SIAM J. Appl. Math 42, 302–327 (1982).
4. S.M. Ali, T.M. Habashy, and J.A. Kong, "Resonance in Two Coupled Circular Microstrip Disk Resonators," J. Appl. Phys. 53, 6418–6429 (1982).
5. T.M. Habashy and J.A. Kong, "Asymptotic Evaluation of Resonance Frequencies for Two Coupled Circular Microstrip Disk Resonators," IEEE MTT-S International Microwave Symposium, Boston, Massachusetts, May–June 1982.
6. A. Ezzeddine, J.A. Kong, and L. Tsang, "Time Response of a Vertical Electric Dipole over a Two-Layer Medium by the Double Deformation Technique," J. Appl. Phys. 53, 813–822 (1982).
7. W.C. Chew and J.A. Kong, "Asymptotic Approximation of Waves Due to a Dipole on a Two-Layer Medium," Radio Sci. 17, 509–513 (1982).
8. A. Sezginer and J.A. Kong, "Physical Optics Approach for Scattering by Thin Helical Wires," Radio Sci., accepted for publication.
9. A. Sezginer, S.L. Chuang, and J.A. Kong, "Modal Approach to Scattering of Electromagnetic Waves by a Conducting Tape Helix," IEEE Trans. Antennas Prop., accepted for publication.

10. A. Sezginer and J.A. Kong, "Electromagnetic Wave Scattering by Thin Helical Wires," <u>URSI–IEEE/APS Joint Symposium</u>, University of New Mexico, Albuquerque, May 1982.

11. S.L. Chuang and J.A. Kong, "Smith–Purcell Radiation from a Charge Moving Above a Penetrable Grating," <u>IEEE MTT–S International Microwave Symposium</u>, Boston, Massachusetts, May–June 1983.

12. Y.Q. Jin and J.A. Kong, "Passive and Active Remote Sensing of Atmospheric Precipitation," Appl. Opt., accepted for publication.

13. J.A. Kong, "Theoretical Models for Remote Sensing of Snow," <u>First Japan/US Snow and Evapotranspiration Workshop</u>, Tokyo, Japan, March 1982, pp. 6.1–6.10.

14. J.A. Kong, "Active and Passive Remote Sensing of Earth Terrain at Millimeter Wavelengths," <u>NATO Workshop on Target/Background Modelling Techniques at Millimeter Wavelengths</u>, US Army ERADCOM/Harry Diamond Laboratories, Adelphi, Maryland, May 1982.

15. J.A. Kong, S.L. Lin, S.L. Chuang, and R.T. Shin, "Remote Sensing of Soil Moisture and Vegetation," <u>URSI Symposium</u>, Boulder, Colorado, January 1983.

16. Y.Q. Jin and J.A. Kong, "Mie Scattering of Electromagnetic Waves by Precipitation," <u>Optical Society of America Topical Meeting on Optical Techniques for Remote Probing of the Atmosphere</u>, Lake Tahoe, Nevada, January 1983.

17. S.L. Chuang and J.A. Kong, "Wave Scattering from a Periodic Dielectric Surface for a General Angle of Incidence," Radio Sci. <u>17</u>, 545–557 (1982).

18. S.L. Chuang and J.A. Kong, "Wave Scattering and Guidance by Dielectric Waveguides with Periodic Surface," J. Opt. Soc. Am., accepted for publication.

19. J.A. Kong, S.L. Lin, and S.L. Chuang, "Microwave Thermal Emission of Periodic Surface," accepted for publication.

20. S.L. Chuang and J.A. Kong, "Extended Boundary Condition Approach to Wave Scattering by Periodic Structures," <u>Benjamin Franklin Symposium on Advances on Antenna Propagation and Microwave Techn</u>   ., Philadelphia, Pennsylvania, May 1982.

21. R.T. Shin, J.C. Shiue, and J.A. Kong, "Rough Surface Effects on the Passive Remote Sensing of Snow," <u>Snow Symposium II</u>, CRREL, Hanover, New Hampshire, August 1982.

22. R.T. Shin and J.A. Kong, "Thermal Microwave Emission from a Scattering Medium with Rough Surfaces," <u>URSI Symposium</u>, Boulder, Colorado, January 1983.

23. L. Tsang, J.A. Kong, and T. Habashy, "Multiple Scattering of Acoustic Waves by Random Distribution of Discrete Spherical Scatterers with the Quasicrystalline and Percus–Yevick Approximation," J. Acoust. Soc. Am. <u>71</u>, 552–558 (1982).

24. L. Tsang and J.A. Kong, "Scattering of Electromagnetic Waves from a Half–Space of Densely Distributed Dielectric Scatterers," accepted for publication.

25. L. Tsang and J.A. Kong, "Scattering of Electromagnetic Waves from a Half–Space of Densely Distributed Dielectric Scatterers," <u>IEEE/APS Symposium</u> and <u>URSI Meeting</u>, Houston, Texas, May 1983.

26. L. Tsang and J.A. Kong, "Theory of Microwave Remote Sensing of Dense Medium," <u>URSI Symposium</u>, San Francisco, California, 1983.

27. L. Tsang, J.A. Kong, and R.W. Newton, "Application of Strong Fluctuation Random Medium Theory to Scattering of Electromagnetic Waves from a Half–Space of Dielectric Mixture," IEEE Trans. Antennas and Prop. <u>AP–30</u>, 292–302 (1982).

28. Y.Q. Jin and J.A. Kong, "Strong Fluctuation Theory for Electromagnetic Wave Scattering by a Layer of Random Discrete Scatterers," accepted for publication.

29. L. Tsang and J.A. Kong, "Effective Propagation Constants for Coherent Electromagnetic Wave Propagation in Media Embedded with Dielectric Scatterers," J. Appl. Phys. <u>53</u>, 7162–7173 (1982).

30. J.A. Kong, "Theoretical Models for Microwave Remote Sensing of Vegetation and Soil Moisture," <u>AgRISTARS Symposium</u>, Houston, Texas, December 1982.

31. J.A. Kong, "Remote Sensing of Soil Moisture and Vegetation," <u>PRISM and AgRISTARS Soil Moisture Research Review</u>, U.S. Department of Agriculture, Beltsville, Maryland, March–April 1982.

32. J.C. Shiue, R. Shin. B. Hartline, J.A. Kong, and A.T.C. Chang, "Microwave Radiometric Observations of Snow and Ice in Northeastern U.S.," <u>Snow Symposium II</u>, CRREL, Hanover, New Hampshire, August 1982.

MICROCOPY RESOLUTION TEST CHART

NATIONAL BUREAU OF STANDARDS-1963-A

86
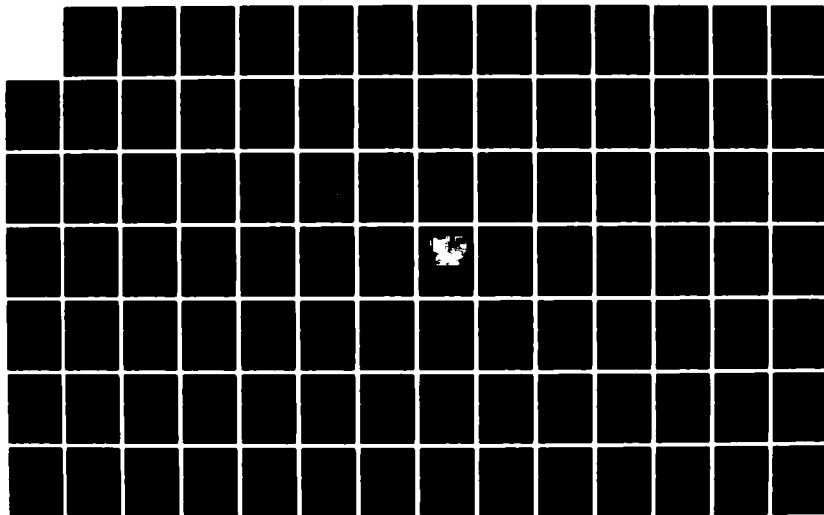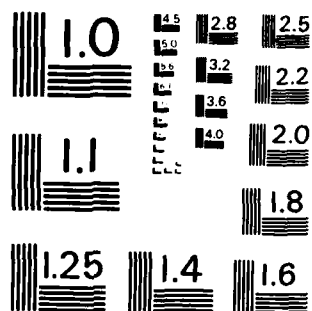
16. Electronic Properties of Amorphous Silicon Dioxide

Academic and Research Staff

Prof. M.A. Kastner, S. Oda

Graduate Students

J.H. Stathis

The objective of this program is to study the electronic properties of amorphous SiO_2 (a–SiO_2) using pulsed laser excitation. There is a great deal of evidence that many of the optical and transport properties of this technologically important material are dominated by defects. Electron spin resonance experiments have identified a number of radiation–induced defects and certain types of defects present in unirradiated bulk a–SiO_2 and films of a–SiO_2 thermally grown on Si. Our work over the past several years has identified a number of photoluminescence (PL) bands which probably originate at intrinsic defects. The PL may be a more sensitive probe of the defects than other techniques.

One major goal of our current research is to determine which of the several PL bands we observe arises at the same, and which at different, PL centers. To do this we are carrying out time–resolved PL measurements at a variety of temperatures for a–SiO_2 prepared in a number of different ways. The time–resolved spectroscopy allows us to unambiguously identify PL bands by their different decay rates. The temperature dependence of the PL decay is important because it can provide information about whether two different PL bands can originate at the same defect. The excitation–energy dependence of the intensity of the various PL bands will also help to differentiate among PL centers.

The preparation of the glass, however, is the most direct probe of which bands arise at different centers. Neutron irradiation, for example, increases the intensity of some PL bands but not others. During the past year we discovered that our molecular flourine laser causes photo–induced optical absorption (PA) in a–SiO_2 and simultaneously enhances some of the PL bands. This may provide another means of correlating the various bands. We are also preparing to measure the time dependence of PA. Such measurements have proved very important in the study of the narrower band–gap chalcogenide glasses.

We have also begun studies on thermally grown oxide films. We have made a preliminary observation of PL from a 1 μm thick film of a–SiO_2 grown on single crystal Si at Lincoln Laboratory

Transient photoconductivity experiments on a–SiO_2 using the same films as well as bulk samples are beginning. Theoretical work on the interpretation of such photoconductivity experiments has led to interesting predictions for the experiments.

Publications

Kastner, M.A., "Dielectric Relaxation and Delayed–Collection Field Experiments in Amorphous Semiconductors," Solid State Comm. 45, 191 (1983).

17. Photon Correlation Spectroscopy and Applications

Academic and Research Staff

Prof. S.-H. Chen

Graduate Students

M. Kotlarchyk, Y.S. Chao, C. Mizumoto, E. Sheu

17.1 Research Program

A high-resolution spectroscopic technique based on scattered light intensity fluctuation measurement has been in use for some time. Our method is a variation of the digital time-domain pulse correlation technique using a 256-channel clipped correlator developed in the laboratory. The correlator-multichannel memory system is controlled by a PDP 11/MINC computer system which is capable of high-speed data acquisition and analysis necessary for the study of time-varying phenomena.

We have developed theoretical methods to calculate quasi-elastic light-scattering spectra from cells undergoing Brownian motions or self-propelled motions in liquid media. The methods have been successfully tested with a model bacterium Escherichia coli, and applicability of the model calculation to cells of dimensions of the order of a micron has been ascertained. The photon correlation technique is further developed to incorporate a flow method which permits us to study time-dependent phenomena with a temporal resolution greater than the time taken for the accumulation of the correlation function. The combined theoretical and experimental progress now enables us to perform the following three categories of experiments:

1. Motility characteristics of bacteria in response to external stimuli such as light and chemical

2. Study of traveling-band formation of bacteria as a result of chemotaxis

3. Study of conformational change and denaturation of globular protein induced by amphiphillic molecules

4. Study of Brown Dynamics in strongly interacting colloids

Recently another powerful technique has been brought into our study of macromolecular solutions.

Small angle neutron scattering has been demonstrated by us to be an exceptionally versatile tool for studies of structure and interactions of strongly interacting colloids. Active experimental program is being pursued at small angle scattering centers at Oak Ridge and Brookhaven National Laboratories.

Publications

Chen, S.-H. and F.R. Hallett, "Determination of Molide Behavior of Prokaryotic and Eukaryotic Cells by Quasi–elastic Light Scattering," Quarterly Rev. Biophys. 15, 1 (1982).

Tanner, R.E., B. Herpigny, S.-H. Chen, and C. Rha, "Conformational Change of Protein/SDS Complexes in Solution — A Study by Dynamic Light Scattering," J. Chem. Ph . 76, 3866 (1982).

Bendedouch, D., S.-H. Chen, W.C. Kochler, and J.S. Lin, "A Method for Determination of Intra- and Inter–Particle Structure Factors of Macroions in Solution from Small Angle Neutron Scattering," J. Chem. Phys. 76, 5022 (1982).

Kotlarchyk, M., S.-H. Chen, and J.S. Huang, "Temperature Dependence of Size and Polydispersity in a Three Component Microemulsion by Small Angle Neutron Scattering," J. Phys. Chem. 86, 3273 (1982).

Bendedouch, D., S.-H. Chen, and W.C. Koehler, "Structure of Ionic Micelles From Small Angle Neutron Scattering," J. Phys. Chem. 87, 153 (1983).

Bendedouch, D., S.-H. Chen, and W.C. Koehler, "Determination of Interparticle Structure Factors in Ionic Micellar Solutions by Small Angle Neutron Scattering," J. Phys. Chem. 87, 2621 (1983).

Bendedouch, D. and S.-H. Chen, "Study of Intermicellar Interaction and Structure by Small Angle Neutron Scattering," J. Phys. Chem. 87, 1653 (1983).

Bendedouch, D. and S.-H. Chen, "Structure and Interparticle Interactions of Bovine Serum Albumin in Solution Studied by Small Angle Neutron Scattering," J. Phys. Chem. 87, 1473 (1983).

Kotlarchyk, M., S.-H. Chen, and J.S. Huang, "Critical Behavior of a Microemulsion Studied by Small–Angle Neutron Scattering," Phys. Rev. A 28, 508 (1983).

Chen, S.-H., C.C. Lai, J. Rouch, and P. Tartaglia, "Critical Phenomena in a Binary Mixture of n–hexane and nitrobenzene: Analysis of Viscosity and Light Scattering Data," Phys. Rev. A 27, 1086 (1983).

18. Submicron Structures Fabrication and Research

Academic and Research Staff

Prof. H.I. Smith, Dr. A.M. Hawryluk, Dr. J. Melngailis, Dr. C.V. Thompson, D.P. Chen, T. Yonahara

Graduate Students

E.H. Anderson, H.A. Atwater, S.Y. Chou, S.S. Dana, C.J. Keavney, R.F. Kwasnick, H. Lezec, M. Schattenburg, J.A. Stein, A.C. Warren

18.1 Submicron Structures Lab

The Submicron Structures Laboratory at M.I.T. is developing techniques for fabricating surface structures of nanometer to micrometer linewidths and using these structures in a variety of research projects. This laboratory contributes to an expansion of microsystems research at M.I.T. Submicron structures fabrication has become a distinct discipline with a world-wide and growing community of practitioners. Fabrication techniques include various forms of lithography (optical, electron beam, x-ray, ion beam), etching (aqueous, reactive plasma, sputtering), growth (oxidation, plating, epitaxy), and deposition (evaporation, chemical deposition, sputtering). With these techniques it is possible to fabricate experimental structures with minimum feature sizes smaller than certain characteristic distances important in a variety of scientific fields (e.g., coherence length, mean-free-path, wavelength, grain size, domain size, living-cell diameter). For example, metal wires with widths below 10 nm can be fabricated, and electrical conduction in such structures studied. New insights are needed to understand the behavior of matter at such small dimensions.

Although the scientific applications at small dimensions have motivated some of the research on submicron structures fabrication, the main driving force has come from the integrated circuits industry. Much activity is aimed at developing the technology and the scientific understanding that will bring integrated electronic devices into the submicron domain. The hope is that this will lead to systems of higher performance.

The main research projects of the Submicron Structures Laboratory, fall into four categories: submicron structures fabrication (nos. 2 to 3), electrical properties of submicron structures (nos. 4 to 5), device films on insulating substrates (nos. 6 to 8), and periodic structures and applications (nos. 9 to 12).

18.2 Microstructure Fabrication at Linewidths of 0.1 mm and Below

Erik H. Anderson, Andrew M. Hawryluk, Robert F. Kwasnick, Alan C. Warren, John Melngailis, Henry I. Smith

A variety of techniques for fabricating structures with linewidths of 0.1 μm and below are under development. These include: holographic lithography, x–ray lithography using crystallographic–template masks, spatial–period–division and reactive–ion etching. A variety of holographic techniques have been developed which permit exposure of large–area (~5 cm diameter) patterns with improved control of line/space ratio and resist profile. In x–ray lithography with C_K sources the intrinsic resolution is ~100 Å. Hence, resolution depends almost exclusively on mask fabrication techniques. Crystallographic templates of triangular and square–wave cross section are etched into Si substrates using anisotropic chemical means. Following techniques developed by Flanders at M.I.T. Lincoln Laboratory, these are replicated into polyimide, which is then shadowed with W to produce the x–ray mask. Linewidth of 30 nm with minimum edge ripple have been obtained. Research on spatial–period–division has shifted from an x–ray to a deep UV approach using a combination of diffraction gratings and multilayer mirrors on SiO_2 and LiF masks. With this technique, and in collaboration with D. Ehrlich of M.I.T. Lincoln Laboratory and R. Osgood of Columbia University, we expect to expose large–area grating patterns having 400 Å linewidths. Reactive–ion etching of structures with linewidths ~0.1 μm and below is investigated to improve control of cross–sectional profile and determine contamination effects. This research employs new techniques we developed for preparing samples for TEM analysis.

18.3 Reactive Sputter Etching Studies

Christopher M. Horwitz

Extensive reactive sputter etching studies have been carried out. As a result, a more complete understanding of electrical properties of the plasma has been achieved, a new type of etching configuration has been discovered, and a new etch for Al and Al–Cu alloys has been demonstrated.

By careful measurements of the peak–to–peak rf voltage and the induced DC voltage on the target electrode, the ion energies at both the target and the chamber walls can be deduced. The effects of

various geometries on the ratio of these two ion energies was investigated.

The power dissipated in the rf discharge has been measured by separating out the power dissipated in the matching network. Thus, for the first time, data on power dissipation in the plasma was determined as a function of peak-to-peak rf voltage, pressure, and system geometry.

The etch rate of SiO_2 in CHF_3 was studied in order to achieve reproducibility. The dependence on gas pressure, flow rate and voltage were measured. Increasing the effective capacitance between rates.

A target configuration with two facing electrodes both at the same target potential (also called a hollow cathode), was investigated. The plasma between these two electrodes is seen to be much more intense than in the normal chamber. At a pressure of 0.3 Pa the etch rate of SiO_2 in CF_4 was found to be 60 times higher than on a conventional open target.

With SiF_4/O_2 gas mixtures, aluminum, Al_2O_3, and Al-Cu-Si alloys were etched while the horizontal faces of other materials, such as AZ photoresist, were covered with SiO_x. This is potentially an important etch for Al since the gas contains no chlorine and thus problems of corrosion and undercut are avoided.

18.4 Electronic Conduction in Ultra-Narrow Silicon Inversion Layers

Robert F. Kwasnick, Marc A. Kastner, John Melngailis

Silicon n-channel field-effect transistors have been fabricated with a gate cross-section of 50 nm x 50 nm and gate lengths of 10 μm or 125 μm. The narrow-gate was fabricated by evaporating aluminum at a glancing angle against a step in the gate oxide. The narrow-gate devices exhibit oscillations in their conductance as a function of gate voltage near gate-voltage threshold, at temperatures $\leq$10K. Wide-gate devices identically fabricated on the same (100) silicon wafer exhibit no such oscillations. Detailed experiments are underway to explore the dependence of these oscillations on temperature, drain voltage, substrate bias, and magnetic field. There is evidence that ionic motion on the surface changes the detailed structure of the oscillations. This suggests that the oscillations are associated with strong disorder in the potential experienced by the quasi-one-dimensional electron gas contained in the inversion layer.

18.5 Corrugated–Gate MOS Structures

Alan C. Warren, Dimitri A. Antoniadis, John Melngailis, Henry I. Smith

The principal aim of this work is to demonstrate and understand the effects of a periodic potential variation upon conduction electrons in Si inversion layers. MOS transistors have been fabricated with 300 nm period gratings etched in the gate insulator. Initial testing indicates a successful fusion of standard planar technology with the required submicron structures processing, yielding high–quality, well–behaved devices at room temperature. The immediate goal is to test the devices at very low temperatures (~1–3°K) and attempt to demonstrate the quantum effects due to a quasi–one–dimensional density of states (conduction parallel to grating) and due to superlattice dispersion (conduction perpendicular to grating). In the future, we anticipate using the facilities of the National Magnet Laboratory to test the devices. Characterization of the grating with regard to uniformity, line/space ratio and sidewall angle is also being initiated.

18.6 Graphoepitaxy of Si and Model Materials

Stephane S. Dana, Erik H. Anderson, Carl V. Thompson, Henry I. Smith

Graphoepitaxy, in which an overlayer film is crystallographically oriented with respect to an artificial surface pattern, has been demonstrated. However, to achieve single–crystal films on a variety of substrates, for electronic and optical devices, the mechanisms of nucleation, growth, coalescence and reorientation need to be understood so that orientation–spread and defects can be eliminated. We conduct basic studies of graphoepitaxial mechanisms in silicon, and model materials (i.e., materials that exhibit large interfacial anisotropies and easy reorientation). This research is aimed at developing means of producing crystalline films of semiconductors and optically active materials on insulating substrates. Two low–temperature approaches to silicon graphoepitaxy are pursued: SiI_4 chemical vapor deposition (CVD) and solid–state surface–energy driven secondary recrystallization. The SiI_4 CVD is carried out in closed tubes, both single and two–zone, generally with temperature oscillation to produce alternating deposition and etch–back. In the experiments on solid–state recrystallization, very thin silicon films are used in order to favor surface energy driven grain growth. Similar approaches are used with the model materials.

18.7 Zone Melting Recrystallization of Si for Solar Cells

Harry A. Atwater, Henry I. Smith

Zone–melting recrystallization of Si on SiO_2 has produced high–quality crystalline films with (100) texture, suitable for MOSFET devices. We are investigating the feasibility of using this technique to produce low–cost solar cells. A planar constriction technique was developed that allows us to select a single in–plane orientation. Also, subboundaries were shown to terminate when solidification passed through channels about 20 μm wide. A (100) texture was achieved in Si films up to 50 μm thick.

18.8 Zone Melting Recrystallization of InSb and InP

Christopher J. Keavney, Henry I. Smith, Clifton G. Fonstad

The success of Si zone–melting–recrystallization in producing device–quality films has prompted us to investigate if similar results can be achieved with the III-V materials. These materials present special problems of adhesion and stoichiometry control. Films are prepared by ion beam sputtering and flash evaporation. Natural oxides, Si_3N_4 and SiO_2 are used as encapsulants, and zone melting is done with a heated W wire in vacuum or an Ar atmosphere. A (111) texture predominates in zone recrystallized films of InSb. Planar constriction techniques may permit single–crystal films to be produced.

18.9 Submicrometer–Period Gold Transmission Gratings and Zone Plates for X–Ray Spectroscopy and Microscopy

Andrew M. Hawryluk, Mark L. Schattenburg[2], Henry I. Smith, Natale M. Ceglio[3]

Gold transmission gratings with periods of 0.2 and 0.3 μm and thicknesses ranging from 0.5 to 1 μm are fabricated using a combination of holographic lithography, x–ray lithography, and electroplating. These gratings are either supported on polyimide membranes or are made self–supporting by the

---

[2]M.I.T. Center for Space Research

[3]Lawrence Livermore Laboratory

addition of crossing struts. They are used to analyze the x–ray emission from plasmas produced by high–power lasers. Fresnel zone plate patterns are created on x–ray masks by electron beam lithography in collaboration with I.B.M. T.J. Watson Research Laboratory and Cornell University. These are then used to x–ray expose patterns in thick resists. After electroplating, the finished structures are used in soft x–ray imaging experiments at the Stanford Synchrotron Laboratory.

18.10 High Dispersion, High Efficiency Transmission Gratings for Astrophysical X–Ray Spectroscopy

Lawrence Livermore Laboratory (Contract 2069209)
Mark L. Schattenburg[4], C.R. Canizares[4], Andrew M. Hawryluk

Gold gratings with spatial periods of 0.1 – 10 μm make excellent dispersers for high resolution x–ray spectroscopy of astrophysical sources in the 100 eV to 10 KeV band. These grating' planned for use in the Advanced X–ray Astrophysics Facility (AXAF) which will be launched in th 1980's. In the region above 3 KeV, the requirements of high dispersion and high efficiency dictat use of the finest period gratings with aspect ratios approaching 10:1. We have developed a vari techniques for high–aspect–ratio fabrication and can now produce gratings of 7:1 aspect ratic the region below 3 KeV the gratings must be made free–standing. The effort here is to decreas loss in efficiency due to absorption in the support structure without sacrificing grating strength.

18.11 Switchable Zero–Order Diffraction Gratings as Light Valves

U.S. Navy - Office of Naval Research (Contract N00014-79-C-0908)
Josephine A. Stein, John Melngailis, Henry I. Smith, J.A. Rajchman[5], Henry M. Paynter[6]

The aim of this research is to produce a simple, inexpensive, compact light valve which could serve as an element in a matrix–addressable array. The proposed light valve consists of two facing, aligned phase gratings (of period, say 1.5 to 5 μm) in transparent media. Displacing one grating 1/2 of a period with respect to the other switches the device from a transmitting to a blocking state. In the blocking state a periodic π phase shift grating is produced in the wave front of the light, thus cancelling the zero order. In the transmitting state a uniform $\pi/2$ shift occurs instead, and no

---

[4]M.I.T. Center for Space Research

[5]Private Consultant

[6]Mechanical Engineering Department

cancellation occurs. The micromotion needed can be achieved by making the gratings out of polyvinylidene fluoride (PVF_2), a transparent, strong piezoelectric. Electrodes have been evaporated on sheets of PVF_2, lateral motion has been observed, and the appropriate piezoelectric coefficient d_{31} has been measured. A technique for embossing gratings in PVF_2 using a press has been developed. All of the fabrication steps needed are consistent with low cost.

18.12 Filters Based on Conversion of Surface Acoustic Waves to Bulk Plate Modes in Gratings

Dong-Pei Chen, John Melngailis, Hermann A. Haus

The almost–100%–efficient, narrow–band conversion of surface acoustic waves to bulk plate modes in normal incidence gratings was previously reported. Based on this phenomenon a novel filter, which promises to be low–loss and compact has been demonstrated. Two gratings of different periods are used in which k–vector–matching conditions must be precisely satisfied. Because not all parameters are well enough known for precise design, one of the gratings was chirped about 3% in order to satisfy the matching. With this structure, filters have been built on YZ $LiNbO_3$ and a few on ST quartz. Center frequencies of the filters were between 160 and 185 MHz and bandwidths between 0.13 and 0.36 MHz. The loss due to the two conversions in the gratings has been at best –5 dB. Only –1 to –2 dB of loss was expected. The observed loss appears to correlate with the lack of parallelism of the two crystal faces. The lowest loss was on crystals which were specially polished to have the two faces parallel to better than 0.006 degrees.

18.13 Collaborative Projects

The unique equipment and expertise of the Submicron Structures Laboratory has served as a resource for numerous researchers from other laboratories. Some examples are the following:

a) The directional and selective reactive ion etching based on $SiCl_4$ gas was used by S. Cabral and D. Rathman of Lincoln Laboratory to etch 0.3 μm period gratings in silicon for the permeable–base transistor.

b) S.W. Pang of Lincoln Laboratory and C.M. Horwitz have studied damage in silicon MOS devices produced by reactive ion etching. Instead of the expected damage due to ion bombardment or irradiation, the degradation of the silicon was found to be due to contamination by impurities sputtered from the chamber walls.

c) H. Bickford of I.B.M., Essex Junction, visited M.I.T. and, together with C.M. Horwitz, studied the undercutting of silicon masked with photoresist during reactive ion etching.

Publications

Ceglio, N.M., G.F. Stone, and A.M. Hawryluk, "Microstructures for High Energy X-Ray and Particle Imaging Applications," J. Vac. Sci. Tech. 19, 886 (1981).

Horwitz, C.M. and J. Melngailis, "Reactive Sputter Etching of Si, SiO_2, Cr and Other Materials with Gas Mixtures Based on CF_4 and Cl_2," J. Vac. Sci. Tech. 19, 1408 (1981).

Hawryluk, A.M., N.M. Ceglio, R.H. Price, J. Melngailis, and H.I. Smith, "Gold Transmission Gratings with Submicrometer Periods and Thicknesses >0.5 μm," J. Vac. Sci. Tech. 19, 897 (1981).

Tsumita, N., J. Melngailis, A.M. Hawryluk, and H.I. Smith, "Fabrication of X-Ray Masks Using Anisotropic Etching of (110) Si and Shadowing Techniques," J. Vac. Sci. Tech. 19, 1211 (1981).

Efremow, N., N.P. Economou, K. Bezjian, S.S. Dana, and H.I. Smith, "A Simple Technique for Modifying the Profile of Resist Exposed by Holographic Lithography," J. Vac. Sci. Tech. 19, 1234 (1981).

von Känel, H. and J.D. Litster, "Light Scattering Studies on Single-Layer Smectic p-Butoxybensilidene p-Octylaniline," Phys. Rev. B 23, 3251 (1981).

Liao, P.F., J.G. Bergman, D.S. Chemla, A. Wokaun, J. Melngailis, A.M. Hawryluk, and N.P. Economou, "Surface Enhanced Raman Scattering from Microlithographic Silver Particle Surfaces," Chem. Phys. Lett. 882(2), 355 (1981).

von Känel, H., J.D. Litster, J. Melngailis, and H.I. Smith, "Alignment of Nematic Butoxybensilidene Octylaniline by Surface Relief Gratings," Phys. Rev. A 24, 2713 (1981).

Geis, M.W., H.I. Smith, B.Y. Tsaur, J.C.C. Fan, E.W. Maby, and D.A. Antoniadis, "Zone-Melting Recrystallization of Encapsulated Silicon Films on SiO_2 - Morphology and Crystallography," Appl. Phys. Lett. 40, 158 (1982).

Horwitz, C.M., "Reactive Sputter Etching of Silicon with Very Low Mask-Material Etch Rates," IEEE Trans. Elect. Devices, ED28, 1320 (1981).

Hawryluk, R.J., A.M. Hawryluk, and H.I. Smith, "Addendum: New Model of Electron Free Path in Multiple Layers for Monte Carlo Simulation," J. Appl. Phys. 53, 5985 (1982).

Bezjian, K.A., H.I. Smith, J.M. Carter, and M.W. Geis, "An Etch Pit Technique for Analyzing Crystallographic Orientation in Si Films," J. Electrochem. Soc. 129, 1848 (1982).

Hawryluk, A.M., H.I. Smith, R.M. Osgood, and D.J. Ehrlich, "Deep UV Spatial Period Division Using an Excimer Laser," Optics Letters 7, 402 (1982).

Geis, M.W., H.I. Smith, B.Y. Tsaur, J.C.C. Fan, D.J. Silversmith, and R.W. Mountain, "Zone Melting Recrystallization of Si Films with a Moveable-Strip-Heater Oven," J. Electrochem. Soc. 129, 2812 (1982).

Atwater, H.A., H.I. Smith, and M.W. Geis, "Orientation Selection by Zone Melting Silicon Films Through Planar Constrictions," Appl. Phys. Lett. 41, 747 (1982).

Horwitz, C.M., "Rf Sputtering - Voltage Division Between Two Electrodes," J. Vac. Sci. Technol. (Jan. 1983), to be published.

Geis, M.W., H.I. Smith, J.C.C. Fan, B.Y. Tsaur, and J.P. Salerno, "Preparation of Oriented Silicon Films on Insulating Amorphous Substrates," Fifth International Conference on Vapor Growth and Epitaxy/Fifth American Conference on Crystal Growth, Coronado, CA, July 19-24, 1981.

Dana, S.S. and H.I. Smith, "Studies of Graphoepitaxy by CVD and Solution Growth," Fifth International Conference of Vapor Growth and Epitaxy/Fifth American Conference on Crystal Growth, Coronado, CA, July 19-24, 1981.

Tatchyn, R., I. Lindau, M. Hecht, E. Kallne, E. Spiller, R. Bartlett, J. Kallne, J.H. Dijkstra, A.M. Hawryluk, and R.Z. Bachrach, "The First Use of Transmission Gratings for Measurements of Optical Constants in the Soft X-ray Range," presented at Cornell Synchrotron Meeting, July 1981, to be published in Nuclear Instruments and Methods.

Ceglio, N.M., A.M. Hawryluk, and R.H. Price, "Space & Time Resolved Soft X-ray Spectra Using X-ray Transmission Gratings," <u>Brookhaven Conference on High Resolution Soft X-ray Optics</u>, SPIE, November 16-20, 1981.

Smith, H.I., "New Approaches to Single-Crystal Thin Films for Devices and Systems Using Surface Patterns," NATO Advanced Research ؛ ـtute, Microelectronics, Les Deux Alps, France, March 14-20, 1982.

Smith, H.I., H.A. Atwater, and M.W. Geis, "Orientation Selection by Zone Melting Silicon Films Through Planar Constrictions," Extended Abstract, <u>161st Meeting, Electrochemical Society</u>, Montreal, Canada, May 9-14, 1982.

Smith, H.I. and M.W. Geis, "The Mechanism of Orientation in Si Graphoepitaxy Using a Strip-Heater Oven," Extended Abstract, <u>161st Meeting, Electrochemical Society</u>, Montreal, Canada, May 9-14, 1982.

Islam, M., H.A. Haus, and J. Melngailis, "Radiation Loss for Normal and Oblique Incidence Gratings," <u>Proceedings of the 1982 IEEE Sonics and Ultrasonics Symposium</u>, p. 92.

Chen, Dong-Pei, J. Melngailis, and H.A. Haus, "Filters Based on the Conversion of Surface Acoustic Waves to Bulk Plate Modes in Gratings," <u>Proceedings of the 1982 IEEE Sonics and Ultrasonics Symposium</u>, p. 67.

Plasma Dynamics

19. Plasma Dynamics

Academic and Research Staff

Prof. T.M. Antonsen, Jr., Prof. G. Bekefi, Prof. A. Bers, Prof. B. Coppi, Prof. T.H. Dupree, Prof. L.M. Lidsky, Prof. J.E. McCune, Prof. M. Porkolab, Prof. L.D. Smullin, Dr. S. Atzeni, Dr. R.H. Berman, Dr. G. Bertin, Dr. G.A. Bonizzoni, Dr. P.T. Bonoli, Dr. T. Boutros-Ghali, Dr. C.M. Celata, Dr. K-I, Chen, Dr. V. Colomer, Dr. R.C. Englade, Dr. M. Gerver, Dr. K. Hizanidis, Dr. J.H. Irby, Dr. R.E. Klinkowstein, Dr. V.B. Krapchev, Dr. J.S. Levine, Dr. S.C. Luckhardt, Dr. A. Palesky, Dr. F. Pegoraro, Dr. P.A. Politzer, Dr. A.K. Ram, Dr. J. Ramos, Dr. M.E. Read, Dr. B. Richards, Dr. G. Rubinacci, Dr. N.N. Sharky, Dr. R.E. Shefer, Dr. V. Stefan[7], Dr. L.E. Sugiyama, Dr. D.J. Tetreault, E.W. Fitzgerald, I. Mastovsky, Y.Z. Yin, M.-L. Xue

Graduate Students

J.G. Aspinall, A.A. Awwad, M. Baghaii Anaraki, P.E. Cavoulacos, B. Chike-Obi, D.E. Coate, K.D. Cogswell, G.B. Crew, A.K. Ezzedine, J. Fajans, A. Ferreira, A.S. Fisher, M.E. Foord, G. Francis, R.C. Garner, T.R. Gentile, P.J. Gierszewski, K.E. Hackett, L.P. Harten, D. Hinshelwood, R.S.-C. Hu, D.K. Ingram, N.A. Ismail, K.D. Jacobs, J.L. Jones, D.A. Kirkpatrick, S.E. Kissel, S.F. Knowlton, G.D. Krc, B.L. LaBombard, B. Lane, A.S. Leveckis, W.P. Marable, M.E. Mauel, M.J. Mayberry, F.S. McDermott, A. Pachtman, S.J. Piet, R.E. Potok, C.M. Rappaport, P.B. Roemer, R.R. Rohatgi, S.E. Rowley, S.R. Shanfield, M.D. Stiefel, G.M. Svolos, D.R. Thayer, C.E. Thomas, T. Uchikawa, S.H. Voldman

19.1 Relativistic Electron Beams and Generation of Coherent Electromagnetic Radiation

This group is concerned with the generation of intense, coherent electromagnetic radiation in the centimeter and millimeter wavelegth range. The primary radiation mechanism which is being studied at the present time is the free electron laser instability which is excited when an electron beam passes through a spatially periodic, transverse magnetic field (wiggler field). This instability is characterized

---

[7]Visiting Scientist from Boris Kidric Institute, Belgrade, Yugoslavia

by axial electron bunching and has emission wavelengths associated with the Doppler upshifted wiggler periodicity.

The experimental facilities include three pulsed high voltage accelerators capable of delivering up to 100 kA of current at 0.5 to 1.5 MV. Their characteristics are summarized below:

Pulserad 110 A

Voltage	1.5 MV
Current	20 kA
Pulse Length	30 ns

Pulserad 615 MR

Voltage	0.5 MV
Current	4 kA
Pulse Length	1 μs

Nereus

Voltage	0.6 MV
Current	100 kA
Pulse Length	30 ns

Intense coherent sources of centimeter and millimeter wavelength radiation find applications in many diverse fields of research and technology including heating and diagnostics of thermonuclear fusion plasmas, photochemistry, solid state physics, and biophysics. One advantage of free electron systems such as the free electron laser are the very high predicted efficiencies which may be attained. Another important advantage is frequency tunability which results from the fact that the radiation frequency is not locked to an atomic or molecular transition or to an electromagnetic mode of a resonant structure but is instead determined by the velocity of the beam electrons.

The research being carried out by this group focuses on some of the basic issues in the development of free electron sources: the interaction of electron beams with different wiggler field geometries, resonant efficiency enhancement in the presence of a uniform guiding magnetic field, effects of beam emittance and velocity spread on the interaction, and the development of cross-field free electron lasers. In addition, the physics of high current field emission diodes which are commonly used as electron sources for intense beams is being studied. Recent work in these areas is summarized in the following sections.

a. The Rippled Field Magnetron (Cross-Field Free Electron Laser)

To achieve efficient conversion of energy from a stream of free electrons to electromagnetic radiation, near synchronism must be attained between the velocity of the electrons and the phase velocity of the wave. In cross-field devices, of which the magnetron is a typical example, this synchronism occurs between electrons undergoing a $v = E_o \times B_o$ drift in orthogonal electric and

magnetic fields, and an electromagnetic wave whose velocity is reduced by a slow-wave structure comprised of a periodic assembly of resonant cavities. The complex system of closely spaced resonators embedded in the anode block limits the conventional magnetron to wavelengths in the centimeter range. Moreover, at high voltages typical of relativistic magnetrons, RF or dc breakdown in the electron beam interaction space, and at the sharp resonator edges poses serious problems.

The rippled-field magnetron is a novel source of coherent radiation devoid of physical slow-wave structures and capable of radiating at much higher frequencies than a conventional magnetron. The configuration of the anode and cathode is similar to the so-called "smooth-bore" magnetron, but it differs from the latter in that the electrons are subjected to an additional field, an azimuthally periodic (wiggler) magnetic field B_ω oriented transversely to the flow velocity v. The resulting $-ev \times B_\omega$ force gives the electrons an undulatory motion which effectively increases their velocity, and allows them to become synchronous with one of the fast TE or TM electromagnetic modes (phase velocity > c) characteristic of the smooth-bore magnetron.

We note that this interaction is the basis of free-electron lasers (FEL). This device differs from the conventional FEL in that the electron source (the cathode) and the acceleration region (the anode-cathode gap) are integral parts of the RF interaction space. This makes for high space-charge densities and for large growth rates of the FEL instability.

The magnetron configuration is cylindrical rather than linear as in conventional FEL's, and the system is therefore very compact. The cylindrical geometry also allows for a continuous circulation of the growing electromagnetic wave, and because of this internal feedback, the rippled-field magnetron is basically an oscillator rather than an amplifier as is the case of the FEL.

We have obtained measurements of millimeter-wave emission from the rippled field magnetron. In these experiments the magnetic wiggler field is produced by a periodic assembly of samarium-cobalt bar magnets positioned behind the smooth, stainless steel electrodes. Maximum radiated power in the 26.5-60 GHz frequency band is obtained with a wiggler periodicity of 2.53 cm and a wiggler field amplitude of 1.96 kG. Under these conditions a narrow band spectral line is observed with a line width at the half power points of less than 2.2 GHz. The center frequency of this line can be varied from 32 GHz to 46 GHz by varying B_z between 5.8 kG and 9 kG. No deterioration in line profile is observed over this range. The total radiated power above 26.5 GHz measured with this wiggler is 300 kW; which is more than a factor of thirty above the broad-band noise observed with no wiggler.

b. Low Voltage Free Electron Laser

Many theoretical studies have been devoted to free electron lasers comprised of an electron stream traversing a periodic, circularly polarized magnetic (wiggler) field, as can be generated with bifilar, helical, current-carrying wires. The electron dynamics in these systems exhibit simple properties that have considerable theoretical appeal. However, from the experimental point of view large amplitude,

circularly polarized wiggler fields are difficult to attain because of the large currents that are required *in their windings; and for long pulse or steady-state operation,* bifilar conductors may be entirely out of the question. In view of the above, studies of free electron lasers have begun in which the electron beam is subjected to a periodic, <u>linearly polarized</u> transverse magnetic field such as can be produced, for example, by an assembly of permanent magnets. Indeed, the use of samarium-cobalt as the magnet material has led to a new generation of magnetic wiggler systems.

Our experimental and theoretical studies are concerned with a low voltage free electron laser in which the electron beam is guided by an axial magnetic field and is perturbed by a linearly polarized samarium-cobalt wiggler field. Typical parameters which we hope to attain are given in Table 1 below:

Table 1. Summary of FEL parameters

Beam voltage (kV)	30
Beam current density (Acm^{-2})	22.3
Axial magnetic field (kG)	1.0
Wiggler field (kG)	0.20
Period of wiggler (cm)	2.0
Radiation wavelength (cm)	5.17
Spatial growth rate of TE mode (dB/M)	20.0
Spatial growth rate of TEM mode(dB/M)	12.2
Efficiency TE mode (%)	63
Efficiency TEM mode (%)	63

This experiment is now in the final stages of assembly. The electron beam is produced by a commercially available electron gun, with slight modifications. The beam has a diameter of 2 mm, and a current of 0.7A when operated at its rated 30 kV. Although the gun is capable of being run continuously, it is currently operated in pulsed mode. The pulse width is variable from 1–5 μsec, with a 0.001 duty cycle.

An axial magnetic field, generated by a series of 15 water-cooled electromagnetic coils guides the electron beam down a 1.5 m long conducting pipe. This uniform field can be varied from 0 to greater than 3 kG.

The linear wiggler magnetic field is produced by 480 SmCo$_5$ permanent magnets. The wiggler has been designed with a great deal of flexibility. It's overall length is 1.2 m, with the 10 cm at each end having an adjustable gap in order to taper the strength of the wiggler as desired. The design

periodicity is 2.0 cm, but the permanent magnets can be rearranged to give shorter and longer periodicities. With a 2.0 cm period, the wiggler field amplitude can be varied from 50 G to 1 kG.

A great deal of attention has been given to the uniformity of the wiggler. Detailed measurements of the individual $SmCo_5$ magnets, and of the assembled wiggler, have led to a thorough understanding of the wiggler. Upon completion, the wiggler field amplitude should be uniform to within 1% at the peaks of all the periods.

When the free electron laser is fully operational, microwave radiation at a frequency of approximately 6 GHz will be measured using crystal detectors. Power and frequency measurements will be made with heterodyning techniques.

The motion of the electrons themselves will be monitored with a Faraday cup. At these low beam voltages, it is possible to use a repelling grid in the cup. This will allow for measurement of the axial velocities of the electrons, and thus a determination of the electron distribution function.

Measurements of the microwave radiation and the electron ballistics will be made simultaneously, enabling correlations between the two to be accurately investigated. All measurements will be carried out for a variety of experimental parameters, including wiggler strength, radiation polarization, and proximity to resonance. When this resonance condition is satisfied, the cyclotron wavelength of an electron in the uniform guiding magnetic field equals the wiggler periodicity. Enhanced growth of the radiation field is predicted as this condition is approached.

c. Velocity Diagnostics of Mildly Relativistic, High Current Electron Beams

The past ten years have seen a great deal of interest in the production of high power millimeter and submillimeter wavelength radiation with free electron devices such as the gyrotron and the free electron laser. In contrast with conventional microwave tubes which typically use 1-10 keV, milliampere beams, these devices employ 50 keV-2 MeV electron beams with current densities of up to tens of kiloamperes per square centimeter. In addition, their operating efficiency is extremely sensitive to the electron velocity components in the beam. We have investigated two velocity diagnostic techniques which may be used with high energy, high current density beams. Both diagnostics have been successfully tested on an electron beam with an energy of 400-1200 keV carrying a current of 1-2 kA.

The first technique involves a simultaneous measurement of the beam current and radial electrostatic potential. The beam current is measured with a Rogowski coil or a current viewing resistor, and the potential is determined from the voltage across a cylindrical capacitor coaxial with the beam. These measurements allow one to determine the time resolved, spatially averaged axial streaming velocity v_z in the beam.

The second diagnostic measures the electron cyclotron wavelength in a beam propagating in a uniform guiding magnetic field. This is accomplished by placing a small pinhole aperture in the path of the beam, and a moveable collector of comparable diameter downstream of the pinhole. The observed spatial periodicity of the collected current allows one to calculate the product $\gamma v_{..}$ in the beam. Here $\gamma = [1 - v_{..}^2/c^2 - v_{\perp}^2/c^2]^{-\frac{1}{2}}$ and $v_{\perp}$ is the transverse velocity component.

We note that the capacitive velocity probe yields information about $v_{..}$ alone, whereas the cyclotron wavelength probe measures a combination of $v_{..}$ and $v_{\perp}$. By combining the two diagnostics, a full description of the electron beam may be obtained. This has been the major aim of our experiments.

d. Cathode Plasma Properties

The properties of the plasma layer formed on the cathodes of pulsed vacuum diodes determine many aspects of the behavior of these devices. Electron flow may be affected by plasma nonuniformity or by plasma instabilities, and the diode pulse length is often limited by gap closure due to expansion of the cathode plasma. The electron flow and gap closure in turn affect the performance of intense ion beam diodes, magnetically insulated transmission lines and intense electron beam driven microwave devices. To control these effects it becomes necessary to control the uniformity, composition, density and temperature of the cathode plasma.

A relevant question concerns the importance of surface contaminants such as the thin layers of pump oils which will exist in most practical vacuum systems. If these impurities dominate cathode plasma formation then variations in cathode material and surface preparation will have little effect on the cathode plasma properties.

We are studying the influence of diode current density, cathode material, cathode surface preparation and diode vacuum condition on the properties of the cathode plasma in a pulsed electron beam diode energized by a Nereus accelerator. The cathode plasma density has been observed to be dependent on the cathode material and to increase with increasing current density. Plasma formation has been observed to occur during the entire diode power pulse. Both electrode materials and constituents of surface contaminants are observed in the cathode plasma. Fast ions have also been observed, moving within the cathode plasma from the cathode toward the anode with kinetic energies far exceeding that which would be expected from a thermal expansion of the cathode plasma.

19.2 Nonlinear Wave Interactions—RF Heating and Current Generation in Plasmas

Abraham Bers, Vladimir Fuchs[8], Dennis Hewett[9], Kyriakos Hizanidis, Vladimir Krapchev, Abhay Ram, V. Stefan[10], Gregory Francis, Leo Harten

The past year has witnessed a major breakthrough in experiments on current drive in tokamak plasmas with externally excited lower–hybrid waves. The two outstanding results were from the Princeton PLT group (400 kWatt of rf power generating 165 kA of plasma current for 3.5 sec, and 420 kAmp for 0.3 sec; plasma density 10^{13}/cm^3, plasma major radius 1.32 m) and from the M.I.T. Alcator C group (1 MWatt giving 200 kAmp for 0.2 sec in a plasma of density 10^{14}/cm^3 and major radius 0.64 m. In both experiments the currents are carried by very energetic electrons (100–500 keV)—a hundred times, or more, the bulk plasma temperature. In addition, both experiments show that the current carrying electrons have a large spread in their energies perpendicular to the magnetic field, i.e., effective perpendicular temperatures that are 50–100 times the bulk plasma temperature. Both of these features were not foreseen, and cannot be adequately described by presently available theoretical models. We have initiated theoretical work and computations aimed at a proper two–dimensional (velocity–space) description of RF current drive including relativistic dynamics of the current–carrying electrons. Our results to date are given in subsections (a) and (b).

A basic problem in either energy deposition (i.e., heating) or momentum deposition (i.e., current drive) by RF in ⊾ plasma concerns the calculation of an effective particle diffusion coefficient induced by the RF fields. In the past year we have initiated a numerical study of a simple model for electrons interacting with a wavepacket. The results indicate that with increasing RF field amplitude a transition occurs from a quasilinear to a new nonlinear regime in which the diffusion is much reduced and perhaps not even well–defined. The results are described in subsection (c).

During the past year we have also formulated a relativistic generalization of the criteria that distinguish absolute from convective evolutions of instabilities. This opens up a way of studying electromagnetic instabilities in relativistic plasmas, and is summarized in subsection (d).

Finally, in subsection (e) we report on the completion of our analytical and computational work related to RF coupling for ion–cyclotron heating of plasmas.

---

[8]Visiting Scientist from IREQ - Hydroquebec, Monreal, Canada

[9]Plasma Fusion Center, M.I.T.

[10]Visiting Scientist, Boris Kidric Institute, Belgrade, Yugoslavia

a. Steady State Solution of the Two–Dimensional Fokker–Planck Equation with RF Diffusion

We have studied analytically and numerically the 2D Fokker–Planck equation with an RF diffusion. The results are directly applicable to the problem of lower–hybrid current drive in a tokamak. Previously reported[1] numerical results fail to exhibit important differences between the one–dimensional and two–dimensional theories. Our 2D study shows that there is a significant broadening of the distribution function in the perpendicular direction. The perpendicular temperature ($T_\perp$) in the resonant domain is much greater, often by an order of magnitude, compared with the bulk electron temperature T_B}.[2,3] As a result both current (J) and power dissipated (P) are enhanced in 2D theory, compared to the 1D result by the factor:

$$J_{2D} \approx J_{1D}\, T_\perp / T_B\,, \quad P_{2D} \approx P_{1D}\, T_\perp / T_B \tag{19.1}$$

where $J_{2D}(J_{1D})$ is the current in 2D(1D) theory and $P_{2D}(P_{1D})$ is the power dissipated in 2D(1D) theory. We note that the figure of merit J/P is unchanged from the one previously reported.[1] The importance of our results lies in the fact that it allows us to explain the observed current with significantly smaller change in the position of the power spectrum launched by the waveguide array.

b. The Relativistic Generalization of the Two–Dimensional Fokker–Planck Equation with RF Diffusion

The relativistic generalization of the quasilinear theory of current drive[1] is motivated by the fact that the RF spectra in Alcator C, PLT (and certainly in future reactor scale devices) have phase velocities that extend into regions where relativistic effects must be taken into account. In Alcator C and PLT the accessibility wave number of the excited spectrum implies a phase velocity resonant with particles of 170 and 500 keV respectively, while the corresponding lowest resonant energies (highest wave numbers) are about 30 keV. However, inside the plasma it is necessary that the spectrum extend below 30 keV and eventually connect to the thermal bulk (of 1 keV) at energies near 5 keV. Several mechanisms have been proposed to account for the existence of rf fields at phase velocities in this gap between 30 keV and 5 keV. We have been mainly concerned with a proper treatment of the more energetic electrons that carry the major part of the current.

The current generated by the applied rf field is mainly carried by energetic electrons in the tail of the distribution function since these are the particles which resonate with the applied field while the thermal bulk remains more or less unaffected (Maxwellian). The energetic particles experience collisions with the thermal electrons and ions as well as quasilinear diffusion (QD) due to the RF spectrum. The relativistic Fokker–Planck (FP) operator which describes the thermalization of highly energetic electrons generated by the RF is formulated on the basis of the relativistic Balescu–Lenard collision operator[4] taken in the Landau limit. The Landau operator, which acts in momentum–space, has further been expanded keeping terms of order up to $(p_{thermal}/p_{tail\ electrons})^2$. We thus obtain a Fokker–Planck operator which in the limit of a cold background plasma is reduced to that of Mosher.[5]

The energy, momentum and velocity moments of the relativistic Fokker–Planck operator provide the relaxation rates of the average energy, average momentum and current respectively, carried by the energetic tail electron. In a steady state operation one requires all these three relaxation mechanisms to balance the RF power and momentum being fed to the electron. For the nonrelativistic limit, the momentum and velocity relaxation are identical. By solving the related three balance equations one obtains the RF power and the current generated as function of the average kinetic energy of the tail electrons as well as the figure of merit, namely, the ratio of the current generated to the power dissipated. We thus find:

$$\left(\frac{I}{P_D}\right)_{Amp/Watt} \cong \frac{31.2 \quad f(\epsilon)}{\ln\Lambda_t \quad R_m n_{20}} \tag{19.2}$$

where $\ln\Lambda_t$ is the Coulomb logarithm for the tail electrons, R_m is the major radius of the plasma in meters, n_{20} is the plasma density in units of $10^{20}/m^3$; the function $f(\epsilon)$, of the particles' energy, is

$$f(\epsilon) \cong \frac{(\epsilon + 1)^2 - 1}{(\epsilon + 1)^{3/2}(\epsilon + 2 + Z_i)^{1/2}} \tag{19.3}$$

where $\epsilon = (\mathcal{E}_0/mc^2)$ is the effective energy $\mathcal{E}_0$ of the current carrying electrons normalized to the rest energy, and Z_i is charge number of the ions in the bulk plasma.

We have also solved the combined Fokker–Planck and quasilinear diffusion equation modeling the distribution function by $f_{||}(p_{||},p_\perp) = \exp[-p_\perp^2/2m_e T_\perp(p_{||})] F(p_{||})/2\pi m_e T_\perp(p_{||})$ where $p_{||}$, $p_\perp$ and $T_\perp(p_{||})$ are the parallel, perpendicular to the magnetic field momenta and perpendicular temperature, respectively. In this ansatz we then allow a $p_{||}$–dependence of $T_\perp$. In fact, this is borne out by recent experiments on PLT which indicate perpendicular temperatures of the current carrying tail electrons considerably higher than the temperature at the thermal bulk.[6] Integrating the Fokker–Planck equation over $p_\perp$ we obtain an equation for $F(p_{||})$ which generalizes the one–dimensional nonrelativistic results. Combining the general solution for $F(p_{||})$ with the perpendicular energy moment of the FP + QL equation we obtain an equation for $T_\perp(p_{||})$ which is then solved numerically. Our model predicts a considerable perpendicular temperature in the region where the RF spectrum applies, the maximum of which depends very sensitively on the width of the spectrum. For example, for an average diffusion coefficient $D_0 = 10$ (normalized to the bulk collisional diffusion) referred to a spectrum centered at $p_0 = 10$ and having a width $\Delta p = 10$ (both normalized to the thermal momentum) we predict a temperature profile with a maximum $T_\perp$ about 7.5 T_{BULK}, while for $p_0 = 15$, $D_0 = 5$ and $\Delta p = 20$ the maximum $T_\perp$ is about 28 T_{BULK}.

c. Diffusion and Current Generation by Coherent Wavepackets

The momentum transfer and diffusion of electrons periodically interacting with a coherent longitudinal wavepacket is considered.[8,9] Applying the resonance overlap criterion, we establish the

stochastic threshold and the stochastic region Δ_{stoch} in velocity space.[10] Discrete mapping and direct numerical integration of the single-particle dynamics is used to corroborate the resonance overlap results and to find the momentum transfer to, and diffusion of, electrons in the field. Above a certain threshold, which depends on field strength, spectrum width and electron cycling length, the interaction is non-adiabatic and particle motion is stochastic within a bounded, not necessarily simply-connected, region of velocity-space. The nature of the interaction, and also the source of stochasticity, depends on the ratio of two basic time scales in the problem: the particle transit time through the wavepacket which is also the autocorrelation time τ_{ac}, and the particle bounce time τ_b in the wavepacket.

When $\tau_{ac} \ll \tau_b$, the particle-velocity scattering is everywhere local in velocity-space and the diffusion approximation holds. An increase in $\langle v \rangle$ and $\langle \delta v^2 \rangle$ is positively correlated with the onset of stochasticity. We find a net induced current $j \sim \Delta v_{stoch}$ and in the weak-field regime an initial rate of change of the variance $\langle \delta v^2 \rangle / 2t$ equal to the quasilinear-theory diffusion coefficient.[11] In the strong-field regime momentum transfer and stochasticity persist owing to nonadiabatic transitions between trapped and untrapped states as the electron traverses the wavepacket. The diffusion coefficient substantially deviates from the quasilinear value, scaling approximately as the square root of the field strength. In general, however, the scattering in v-space tends to lose its local, diffusive character.

d. Pulse Shapes of Absolute and Convective Instabilities for Relativistic Observers

The problem of describing the propagation of an instability in a plasma and, in particular, of deciding between convective and absolute instabilities has been of considerable interest.[12] The qualitative aspects of determining linear instabilities and distinguishing between the absolute and convective instabilities by using the pinch-point analysis has already been developed.[13] The space-time asymptotic pulse shape for these instabilities has been obtained for non-relativistic observer velocities.[14] Such an analysis is strictly applicable to electrostatic instabilities involving non-relativistic dynamics of the plasma particles. We have developed the generalization to the relativistic theory for the asymptotic pulse evolution which is applicable to electromagnetic instabilities in plasmas involving relativistic dynamics.[15,16] The theory has been applied to the studies of instabilities in an infinite plasma immersed in a static uniform magnetic field ($\vec{B}_0$) with stationary ions and highly anisotropic electron distribution functions. We have looked at instabilities that propagate parallel to $\vec{B}_0$ and perpendicular to $\vec{B}_0$ and evaluated their corresponding pulse shapes. The dispersion relation for these waves is derived from the complete set of Maxwell's equations and the relativistic Vlasov equation. The electromagnetic instabilities of the type considered are of interest in the studies of: the generation of electromagnetic energy by relativistic electron beams; instabilities due to ECRH heated energetic electrons in the end-plugs of tandem mirror plasmas; and unstable radiations in space plasmas.

e. Antenna–Plasma Coupling Theory for ICRF Heating

We have completed our analysis to determine the coupling characteristics of an external antenna structure (consisting of a current-carrying sheet protected from the plasma by an idealized Faraday Shield) to a plasma for the purposes of exciting the fast component of waves in the ion-cyclotron range of frequencies.[17,18] The analysis is carried out in the slab geometry with a current sheet of finite extent in the poloidal (y) and toroidal (z) directions while the shield and the plasma are assumed to be infinite in y and z. The plasma is described by its cold dielectric tensor with density ($n(x)$) and magnetic field ($B_0(x)$) inhomogeneities in the radial (x) direction. The major conclusions of our three-dimensional analysis are the following:

(A) The radiation impedance of the antenna

· is significantly modified by including the finite poloidal extent of the antenna

· decreases with increasing $\nabla n(x)$ at the shield

· is an increasing function of the external rf source frequency (for a fixed $n(x)$ and electrical length of the current sheet)

(B) The plasma impedance is highly asymmetric with respect to the poloidal wave number. This implies that an appropriately phased set of poloidal antennas would allow more power to be coupled to the plasma.

(C) The excited electric and magnetic fields inside the plasma do not disperse significantly beyond the antenna dimensions.

References

1. C.F.F. Karney and N.J. Fisch, Phys. Fluids 22, 1817 (1979).
2. V. Krapchev, K. Hizanidis, A. Bers, and M. Shoucri, "Current Drive by LH Waves in the Presence of a DC Electric Field," Bull. Am. Phys. Soc. 27, 1006, (1982).
3. D. H. Hewett, V. Krapchev, J. P. Friedberg, and A. Bers, "Fokker–Planck Investigations of RF Current Drive," paper 1P10 Proc. 1983 Sherwood Theory Meeting, Arlington, Virginia.
4. K. Hizanidis, K. Molvig, and K. Swartz, M.I.T. Plasma Fusion Center Report PFC/JA–81–21 (1981) accepted for publication in J. Plasma Phys.
5. D. Mosher, Phys. Fluids 18, 846 (1975).
6. S. von Goeler, et al., Bull. Am. Phys. Soc. 27, 1069 (1982).
7. K. Hizanidis, V. B. Krapchev, and A. Bers, "Current Drive by Lower–Hybrid Waves Acting on Runaway Electron Tail," Bull. Am. Phys. Soc. 27, 1006, (1982).
8. K. Matsuda, in Proceedings of the Fourth Topical Conference of Radio–Frequency Heating in Plasmas. Austin, Texas, 1981, paper B10; also "Stochastic Current Drive by Plasma Waves, General Atomic Co. Report GA–A16303, July 1981.
9. T. H. Stix, in F. Sindoni (Ed.) Proceedings of the Third Symposium on Plasma Heating in Toroidal Devices, by (Editrice Compositori, Bologna, 1976), p. 159.
10. B. V. Chirikov, Phys. Reports 52, 263 (1979).
11. V. Fuchs, G. Thibaudeau, V. Krapchev, A. Ram, and A. Bers, "Diffusion and Momentum Transfer for Particles Interacting with Coherent Wavepackets," Bull. Am. Phys. Soc. 27, 957 (1982).

12. A. Bers, "Space–Time Evolution of Plasma Instabilities— Absolute and Convective," in Handbook of Plasma Physics, Vol. 1, Chapter 32, (North Holland Publishing Company) to be published 1983.
13. R. J. Briggs, Electron Stream Interaction with Plasmas, (M.I.T. Press, 1964).
14. L. S. Hall and W. Heckrotte, Phys. Rev. 166, 120 (1968).
15. A. Bers and A. K. Ram, "Relativistic Pulse Shapes of Absolute and Convective Instabilities," Bull. Am. Phys. Soc. 27, 919 (1982).
16. A. Ram and A. Bers, "Relativistic Evolution of Electromagnetic Instabilities," paper 2Q24, 1983 Sherwood Theory Meeting, Arlington, Virginia.
17. A. Ram and A. Bers, "Antenna–Plasma Coupling Theory for ICRF Heating of Large Tokamaks," Proceedings of Third Joint Varenna-Grenoble International Symposium on Heating in Toroidal Plasmas, Grenoble, France, March 22–27, 1982.
18. A. Ram, A. Bers, M.I.T. Plasma Fusion Center Report PFC/CP–82–2 (1982).

19.3 Tokamak Research: RF Heating and Current Drive

George Bekefi, Miklos Porkolab, Stanley C. Luckhardt

The Versator II program consists of a number of diverse experiments on the interaction of externally excited lower–hybrid waves with a tokamak plasma. The lower–hybrid wave has a frequency between the electron and ion cyclotron frequencies and is introduced into the plasma with an antenna consisting of a phased array of waveguides. By adjustment of the relative phase between adjacent waveguides, $\Delta\Phi$, the spectrum of waves in $k_\parallel$, where $k_\parallel$ is the wave number parallel to the magnetic field, can be controlled.

The lower–hybrid wave can interact with either plasma electrons or ions depending on the wave phase velocity and the particle velocity. Wave–electron interaction occurs for electrons with parallel velocity, $v_\parallel \simeq \omega/k_\parallel$, in resonance with the wave phase velocity. This interaction allows lower–hybrid wave power to be deposited into plasma electrons which can heat the plasma. The wave interaction also increases the parallel momentum of the electrons and reduces their collisionality; and these effects allow the wave to drive a net electron current. The lower–hybrid wave electron interaction is seen to have two applications to tokamak fusion research. The RF current drive effect may allow a tokamak fusion reactor to operate in steady state with the needed plasma current driven by waves instead of inductively driven by a transformer, and wave power deposited in the electrons can heat the plasma supplying some of the temperature increase needed to reach fusion conditions, $T \simeq 10$ KeV.

The lower–hybrid wave can also interact with the ion population if the plasma density and magnetic field are sufficiently high. The lower–hybrid wave obeys the dispersion

$$\omega^2 = \omega_{LH}^2 \left(1 + \frac{Mi}{Me} \frac{k_\parallel^2}{K^2} \right) \tag{19.4}$$

where ω_{LH} is the lower hybrid resonance frequency,

$$\omega_{LH}^2 = \frac{\omega_{pi}^2}{1 + \omega_{pe}^2/\omega_{ce}^2} \tag{19.5}$$

Ion interaction occurs for ions with velocity $V_i = \omega/k_\perp$, the wave can interact with ions having much lower velocity than electrons since the $k_\perp$ of the wave reaches very large values, $k_\perp \gg k_\parallel$, when $\omega \sim \omega_{LH}$. Thermal effects also modify the dispersion relation when $\omega \sim \omega_{LH}$ leading to possible conversion of the lower–hybrid wave into a "hot plasma" wave, this wave also interacts with the ion component. The lower–hybrid wave–ion interaction, in principle, could also be useful for heating a plasma toward fusion temperatures; though, so far, lower–hybrid ion heating has not been reliably demonstrated in experiments.

Versator II is a medium sized research tokamak with the following parameters: major radius R_o = 40.5 cm, limiter radius a = 13 cm, toroidal field = 15 kGauss, plasma current = 30–60 kA.

The lower–hybrid RF system used in the current experiments consists of a 150 kW, 800 MHz klystron, and a waveguide power splitter with four output channels. The phase of each output can be continuously adjusted (0°–360°) with mechanical phase shifters. Such phase control allows traveling wave spectra to be launched either parallel or anti-parallel to the direction of the electron ohmic drift, $\Delta\Phi = \pm 90°$, or a standing wave spectrum can be excited with $\Delta\Phi = 180°$.

The results of earlier experiments can be summarized as follows: in the Versator experiments a significant fraction of the ohmic heating current was replaced by RF generated current in a regime of low density. Above $\bar{n}_{crit} = 6 - 7 \times 10^{12} cm^{-3}$ a significant decrease in current drive efficiency was observed.[1] During LHCD (lower–hybrid current drive) in the low density regime, the Parail–Pogutse tail anisotropy instability[2] was observed and was found to cause periodic losses of a significant fraction of the tail current.[3] In combined LHCD and electron cyclotron heating experiments on Versator II, it was found that the tail mode could be stabilized by addition of electron cyclotron heating, $P_{ECH} \gtrsim 20$ kW, and the periodic current losses were eliminated.[3] In recent experiments, a novel antenna arrangement was used to launch waves from the top of the torus.

19.3.1 Top Launching Experiments

Ray tracing theory[4,5,6] has shown that traveling waves launched from the top of the torus in the direction:

$$\vec{s} = \vec{B} \ I_p/|B| |I_p| \tag{19.6}$$

experience an upshift in their $N_\parallel = ck_\parallel/\omega$ due to toroidal effects. Generally, as a wave launched in this way propagates toward the center of the plasma it slows down along field lines, and is often absorbed in the first poloidal transit through the center of the plasma. Waves launched from the top

in the $-\vec{s}$ direction suffer a large downshift of $N_{\parallel}$. Similarly, waves launched from the outer midplane of the torus suffer an initial $N_{\parallel}$ downshift, making first pass absorption less likely in present day tokamaks due to the difficulty in satisfying the Landau damping resonance condition. In typical cases, side launched waves make many poloidal passes before they are completely absorbed; in general, some RF power may be lost (e.g. due to collisional absorption at the plasma edge). Thus, top launching is expected to give an improved power absorption efficiency and an interaction with lower energy electrons, when compared with side launching.

The $N_{\parallel}$ upshift, however, is expected to result in reduced current drive efficiency, as indicated by the simple quasi–linear theory result[7] (in practical units)

$$\frac{I_{RF}}{P_D} = \frac{17g}{N_{\parallel f}^2 R_o n_{15}} \frac{kA}{kW} \tag{19.7}$$

where I_{RF} is the RF generated current, P_D is the power dissipated, $N_{\parallel f}$ is the mean $N_{\parallel}$ value of the absorbed power spectrum, R_o is the major radius in cm, n_{15} is the density in units $10^{15} cm^{-3}$, and g is a factor usually of order unity depending on the width of the absorbed wave spectrum. Thus, to maximize the RF generated current, absorption of lower $N_{\parallel}$ components is desirable. It appears from the above considerations that the top launched traveling waves may be an efficient means of heating electrons; however, owing to their upshift in $N_{\parallel}$ the current drive efficiency may be reduced when compared to the side launched waves. Measurement of this difference in current drive efficiency is then expected to be a first sensitive test of the prediction of the ray tracing theory.

The top launch coupler consists of a stainless steel four–waveguide array inserted into a top rectangular port of the Versator vacuum chamber. The waveguide gap size is 1 cm and the waveguide width is 21 cm. With 90° relative phasing between adjacent waveguides, a traveling wave spectrum with peak at $N_{\parallel o} \simeq 8$ is launched. Due to space limitation in the port, a reduced width waveguide was used, leading to higher RF electric fields than in the previously used side coupler, which had a width of 24.5 cm. These higher RF electric fields initially caused a waveguide breakdown problem. A solid titanium waveguide array was installed, but the breakdown power level did not improve. Best results were obtained after a carbon coating was applied to the waveguide surfaces.[8] With this arrangement more than 100 kW of power, corresponding to a power density of 1.3 kW/cm^2, has been coupled into plasma without evidence of waveguide plasma formation or arcing. We find that the power handling capability of the antenna is seriously degraded by discharge cleaning of the tokamak vacuum chamber. However, when impurity control is provided by titanium deposition on the chamber walls and discharge cleaning is eliminated, this high power operation becomes possible.

In preliminary experiments with the top launch coupler, current drive measurements have been made in the low density regime, $n_e < 10^{13} cm^{-3}$. Monitored signals show the usual characteristics of

RF generated currents. Loop voltage and plasma current measurements indicate voltage drops and plasma current increases during the RF pulse when traveling waves are launched in the electron drift direction. When waves are launched in the opposite direction little or no voltage drop is observed.

In Table I, a comparison of current drive obtained with the top launch and side launch couplers is presented. Both side and top launch grills are phased at 90° giving a peak in the launched $N_{\parallel}$ spectrum at $N_{\parallel o} = 8$. Comparison is made in terms of the scaling parameter S defined as

$$S = \frac{I_{RF}}{P_{NET}} \hat{n}_{15} R_o (cm) \tag{19.8}$$

in units of $kA/(kW \cdot cm^2) \times 10^{15}$ where I_{RF} is the RF generated current, P_{NET} is the net power coupled into the plasma, $\hat{n}_{15}$ is the average density in units of $10^{15} cm^{-3}$ and R_o is the major radius in cm. The theoretically predicted value for S then depends only on the characteristics of the absorbed power spectrum and absorption efficiency, from Eq. (19.4):

$$S = 17 \, g \, \eta / N_{\parallel}{}^2_f \tag{19.9}$$

where η is the power absorption efficiency, $P_{dissipated} = \eta P_{net}$, g is a dimensionless spectral shape factor usually of order unity, and $N_{\parallel f}$ is the peak of the absorbed power spectrum taking all toroidal shifts into account. The observed values of S for the top launching experiment are significantly smaller than observed with the side coupler. In typical cases $S_{side}/S_{top} \sim 6 - 8$. This decrease in S appears to be consistent with a toroidal upshift in $N_{\parallel}$.

Table 1

	Top Launch Grill	Side Launch Grill
$\Delta\varphi$	90°	90°
$N_{\parallel o}$	8	8
$\hat{n}$	$6 \times 10^{12} cm^{-3}$	$4 \times 10^{12} cm^{-3}$
I_p	40 kA	32 kA
$\Delta V/V_L$	0.18	0.5
q(a)	5.8	7.2
$I_{RF} \simeq \Delta V/V \, I_p$	7.3 kA	16 kA
P_{NET}	45 kW	8 kW
$S = \hat{n}_{15} \dfrac{R_o I_{RF}}{P_N}$	0.039	0.32

Soft x-ray spectroscopic measurements of the intermediate energy range 1 keV $<\epsilon_\gamma<$ 25 keV indicate the formation of an electron tail during RF injection. In Fig. 19-1 the soft x-ray spectrum of an ohmic discharge shows a thermal feature, $\epsilon_\gamma \lesssim$ 3 kV, evidence of a small runaway component, $\epsilon_\gamma >$ 5 kV, and some metallic impurity line radiation. During RF injection an electron tail is formed as indicated by the factor of 5 - 10 enhancement in the x-ray spectrum in the energy range 5 - 15 keV. There is also a large enhancement in line radiation 4 keV $<\epsilon_\gamma<$ 8 keV, indicating a possible build-up of metallic impurities during the RF pulse; however, this increase does not significantly change the Z_{eff} of the discharge. Similar soft x-ray behavior is observed for both $\pm$ 90° phase RF injection. Tail formation in the energy range 3-15 keV is consistent with the expected upshift of the antenna $N_\parallel$ spectrum, for $\Delta\Phi$ = +90°; however, the similarity of the soft x-ray spectra for $\pm$90° does not appear to fit the simple ray tracing picture. Further experiments are needed to clarify this observation.
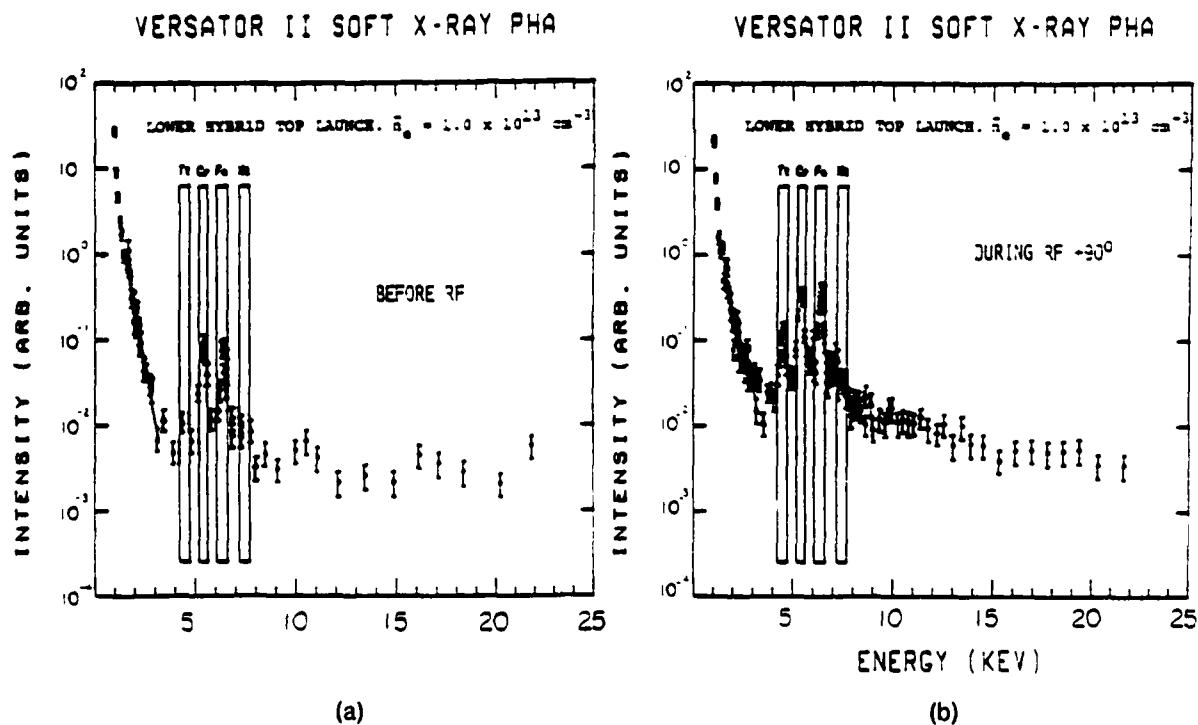
Figure 19-1: Soft x-ray spectra of
(a) ohmic discharge before RF pulse
(b) during injection of 45 kW of lower-hybrid power

19.3.2 Particle Confinement

Density increases have consistently been observed during lower–hybrid current drive (LHCD), e.g. Ref. 14. There are three apparent causes which could account for this density increase. They are: (1) increased recycling of hydrogen neutrals neai ·e edge of the plasma (2) increased impurity influx and (3) improvement of particle confinement.
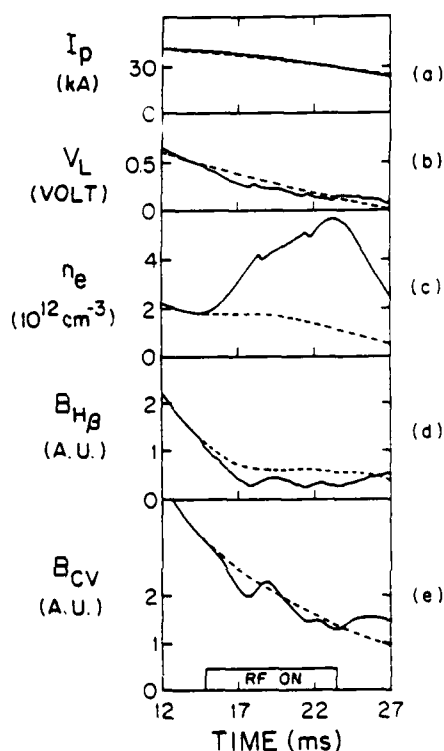
Figure 19-2: Temporal evolution of signals during the LHCD density increase:

(a) plasma current, (b) loop voltage, (c) density, (d) central chord brightness of H_β4661A, (e) central chord brightness of CV 2271A P_{RF} = 10 kω, $\Delta\varphi$ = +60°

The temporal evolution of plasma parameters and signals of relevant diagnostics are shown in Figs. 19-2 and 19-3. A 1/2 m Jarrel–Ash monochromator has been used to monitor neutral hydrogen emissions. Most measurements have been made with H_β(4861Å) line emission; however, both $H\alpha$(6563Å) and H_β have the same temporal dependences. During the RF pulse the density increases by ~ 100%in this case. Nevertheless, the H_β emission decreases by ~ 30 - 60% compared to ohmically heated discharges and then shows periodic small fluctuations. These variations on the H_β signal are correlated with loop voltage spikes and $2\omega_{ce}$ emission caused by the tail instability loss of electrons to the limiter and chamber walls. The decrease of H_β emission is consistent with the edge density decrease measured by a Langmuir probe (Fig. 19-3). The density increase during the RF has been simulated with gas puffing through a port located 158° toroidally away from the visible

<center>117</center>

monochromator port. The H_β emission increases in this case. Thus, if there is an extra neutral hydrogen flux introduced by the RF, the H_β emission should show a similar increase. The observed decrease of H_β emission and edge density during LHCD indicate the ionization rate at the plasma edge is decreasing even though the bulk density is increasing. Thus, the density build-up cannot be explained as an increase in gas flux or recycling.
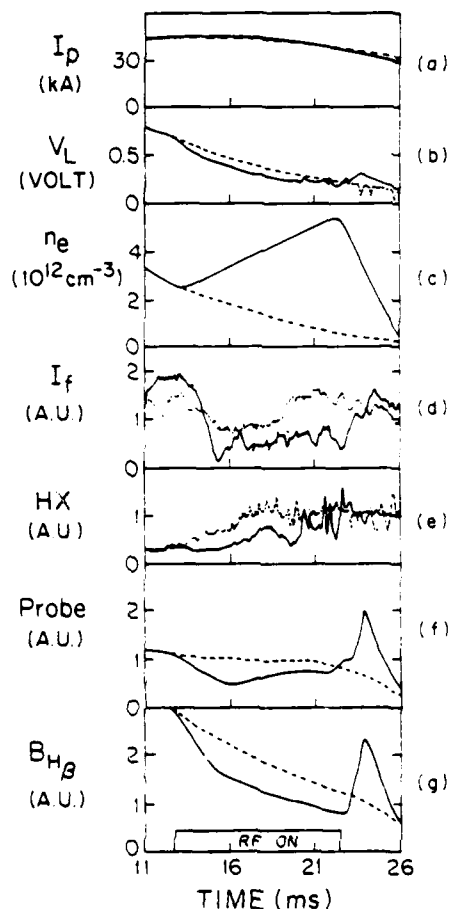
Figure 19-3: Temporal evolution of signals during LHCD density increase
(a) plasma current, (b) loop voltage, (c) density, (d) density fluctuation level from 2 mm microwave scattering, fo = 325 kHz, (e) hard x-ray signal, (f) edge density from Langmuir probe, (g) central chord brightness of H_β

The behavior of light impurities has been monitored using the CV, OV, and CIII lines. CV emission has shown some slight decrease which might be related to a small decrease in electron temperature during the RF pulse, Ref. 1, or a reduced recycling rate for these impurities. Since impurity influx has to pass the plasma edge to reach the center, we would expect to observe an increase of all the edge lines if there is an increase in impurity flux. These measurements indicate that there is no increase in

light impurity influx during the RF. The remaining possible explanation of the observed density increase is an improvement in particle confinement. In the typical example shown in Fig. 19–3, the density increases by a factor of two and H_β emission decreases consistent with a factor of 2 – 4 increase in τ_p during LHCD. The "drift–wave" frequency range fluctuations are also observed to decrease during current drive. Fig. 19–3 shows fluctuation signals at 325 kHz averaged over a few shots with and without RF, respectively as obtained from 2 mm microwave scattering. The drop in fluctuation is conservatively estimated to be 5 dB.

In summary, the observed increase in plasma density cannot be fully explained as an increase in recycling or ionization; rather a decrease is observed. Neither is there any appreciable increase of light impurity influx. There is an accumulation of evidence consistent with a significant increase of particle confinement during LHCD.

19.3.3 Versator Upgrade

The successful production of an RF driven plasma current in Versator II gives rise to the possibility of tokamak operation sustained solely with RF power. At present a major construction project is underway on Versator II upgrading the magnetic field systems to allow a fully RF driven tokamak plasma to be produced.

The RF driven state will be reached by the following method: the tokamak discharge will be initiated with the ohmic heating transformer, producing an inductively driven plasma current; then after a 10–15 msec start–up phase, RF power will be injected into this target plasma to build up an RF driven component of the total current. During the build–up of the RF current, the current in the transformer primary will be brought to zero and the transformer will be open circuited. At this point maintenance of the plasma current is provided by RF current drive only. To insure that all inductively driven currents are eliminated, the total plasma current will be sustained with dI/dt = 0 for approximately two "L/R" times.

To make the transition from the inductively–driven discharge to the RF driven regime, the Versator II magnetic field systems and the RF power system will be upgraded to allow plasma equilibrium to be maintained for up to 60 msec; this will allow a 15 msec transition phase, and a 35 msec RF driven phase, limited only by the pulse duration of the toroidal field power supply.

19.3.4 S–Band Current Drive Experiment

Currently under construction for Versator II is a 2.45 GHz high frequency lower–hybrid current drive experiment. The purpose of this experiment is to determine whether the 800 MHz current drive density limit of $\bar{n}_e \lesssim 6 \times 10^{12} \mathrm{cm}^{-3}$ first found on Versator II can be improved by raising the RF source frequency.

The 2.45 GHz RF system will consist of two 50 kW Varian 5K70SH–2 klystrons, along with a power

splitting and phase shifting network which will feed a 4-waveguide array. Present designs call for vacuum waveguide dimensions of .8 cm x 8.64 cm, which corresponds to a maximum injected power density of 3.6 kW/cm^2. The maximum pulse length will be 40 ms.

At the present time, fabrication of the high power RF system is under way, along with the design and procurement of the power monitoring and phase detection circuitry. Initial klystron testing and lower power coupling experiments are scheduled for the end of 1983, with high power current drive experiments commencing in 1984.

The new 2.45 GHz RF system will be capable of operating simultaneously with the present 800 MHz system to allow a detailed comparison of lower-hybrid current drive near the density limit at each frequency.

19.3.5 Tail Mode Instability

The Parail-Pogutse tail anisotropy instability is normally present during lower-hybrid current drive on Versator. In earlier experiments[3] it was shown that relaxation oscillations present on the loop voltage, second harmonic cyclotron emission, and other diagnostics were also accompanied by sudden losses of a significant fraction of the tail current during LHCD. It was also found that the addition of more than 20 kW of electron cyclotron heating power could stabilize the relaxation oscillations by increasing the tail $T_\perp$. These relaxation oscillations are also accompanied by intense RF bursts, measurable by an RF probe, occurring simultaneously with the sudden increases in $2\omega_{ce}$ emission and loop voltage. In present experiments the frequency spectrum of these RF bursts has been measured with an RF probe in the limiter shadow. The bursting is found to exist over a wide frequency range. In Fig. 19-4 the intensity of the RF bursts detected by the RF probe is plotted as a function of their frequency in a low density ohmic discharge, and during the LH power pulse with 10 kW of coupled power at $\Delta\Phi = 60°$. The frequency spectrum of the tail mode bursts appears to broaden from 9 GHz in the ohmic case to 12 GHz during LHCD. The spatial distribution of the high energy electron tail has been obtained with a scanning hard x-ray spectrometer. Massive lead collimators and vertical viewing into a recessed port area insures that x-ray emission from the plasma, as opposed to the wall or limiter, is detected. Emission measurements are shown in Fig. 19-4 for ohmic discharges, and during RF injection at $\bar{n} = 3 \times 10^{12}$ cm^{-3} and $P_{RF} = 20$ kW. The initial ohmic discharge contained a significant runaway tail component and RF injection at this power level did not significantly change the high energy, $\varepsilon_\gamma > 30$ keV, x-ray emission or its spatial profile. The hard x-ray emission is found to be strongly peaked in the center of the plasma with a width of approximately 5 cm, although the actual distribution may be even narrower in view of the spatial resolution of the collimator, 3 cm. It is interesting that the quasilinear theory[2] predicts that instability of a narrow beam should result in a broad spectrum fpi < f < fpe of RF bursts in agreement with experiment.

FREQUENCY SPECTRUM OF RF BURSTS

OHMIC PLASMA   LHCD
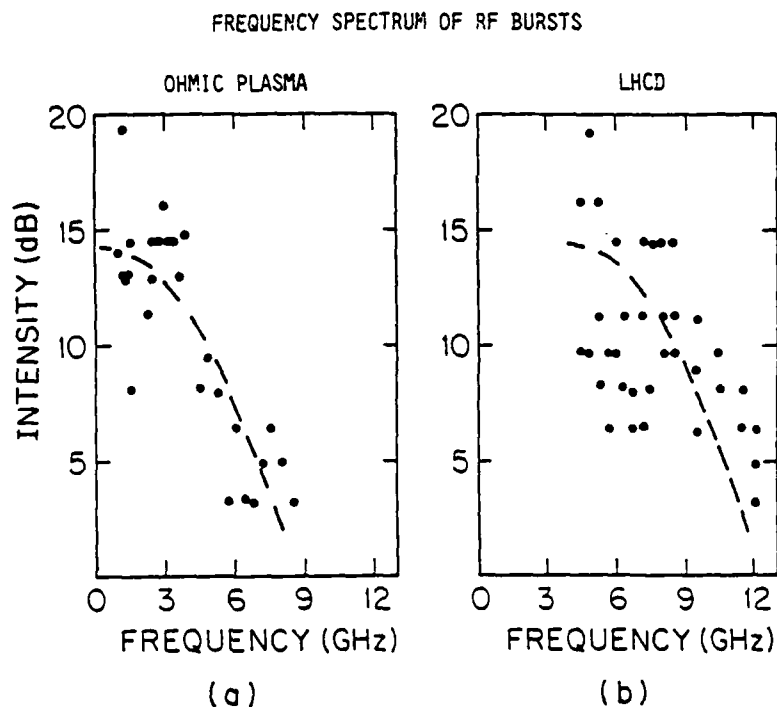
Figure 19-4: Frequncy spectrum of RF bursts with/without LHCD from RF probe in limiter shadow

19.3.6 Ion Heating

Ion heating experiments employing a waveguide grill antenna located at the conventional side position on the midplane of Versator have been completed. At a toroidal field of $B_0 = 1.4T$ and density $\bar{n}_e = 1.3 - 3 \times 10^{13} cm^{-3}$, a poorly confined perpendicular tail in the ion distribution is formed during RF injection. In the density range $2.4 - 2.8 \times 10^{13} cm^{-3}$, heating of the ion bulk distribution is occasionally observed; a maximum ion temperature rise of 50 eV for 50 kW transmitted RF power has been recorded. Although ion heating in Versator can be expected to be inefficient on theoretical grounds, the cause of the irreproducibility of the heating results is not well understood.

Recently, initial ion heating investigations have been performed using a grill which launches lower hybrid waves from the top of the Versator plasma. Though this antenna is designed for use in lower–hybrid current–drive experiments, the radial propagation characteristics allowed by this grill are predicted to be beneficial for ion heating as well as current drive, although the launched spectrum of the grill is not optimal for the former. Results to date indicate that, as for the previous grill position, an ion tail with a short confinement time ($< 150 \mu s$) is created over roughly the same density range as for the side launching experiments. No bulk heating is measured for transmitted powers of up to 100 kW. Compared to the case with the previous antenna, the ion tails seen in these recent studies are of

lower temperature (0.2 keV versus 1.0 keV) and extend to lower energies (0.4 keV versus 1.2 keV). Contrary to what is qualitatively expected from toroidal ray tracing theory, no significant asymmetry in the fast ion effects with respect to the grill phasing relative to the plasma current is observed.

19.3.7 Diagnostic Experiments

The Versator II tokamak experiments are supported by a complete range of plasma diagnostic experiments. The progress on some of these experiments is summarized as follows:

19.3.8 UV and Visible Diagnostics

Vacuum Ultraviolet (UV) spectroscopy has been used as a routine diagnostic to yield ion temperature during the lower–hybrid ion heating (LHH) experiments. The ion temperature has been obtained by measuring Doppler widths of various impurity line emissions in the UV region (e.g. OVII 1623Å, CV 2271Å, OV 2781Å and CIII 2297Å). Preliminary results from the LHH experiment launching the wave from a top port were not positive. Doppler measurements from UV did not show any significant bulk temperature increase during the RF compared to Ohmic cases; nevertheless, the perpendicular charge–exchange diagnostics showed a tail formation ($\bar{n}_e \sim 2.5 \times 10^{13} cm^{-3}$, $B_T \sim 13$ kg, $I_p \sim (50\text{--}60)$ kA, $P_{RF} \sim 100$ kW).

The UV, visible and a H_α photodiode (filter halfwidth 10Å) have been incorporated with lower–hybrid current drive (LHCD) experiments. The UV diagnostics have been used to monitor impurity influxes during the RF. There is no appreciable change of impurity influxes during the RF. The visible monochromator and photo diode detector have been used to measure H_α emissions at various toroidal positions (e.g. the limiter, the gas port, the RF port, etc.). The results show a slight decrease of the 20–40% during the RF; this implies that the volume ionization rate of hydrogen neutrals has also been decreased. Typically, a density increase is observed during LHCD, and since the extra influxes of either neutral hydrogen or impurities decreases or does not change, it is concluded that the particle confinement during current drive probably has increased.

In summary, UV and visible diagnostics have been used in studies of heating efficiency and particle confinement during lower hybrid heating and current drive experiments.

19.3.9 Thomson Scattering

Tokamaks commonly use Thomson scattering to measure profiles of electron temperature, $T_e(r)$, across the minor radius of the plasma. The scattered laser light has a Doppler–broadened spectrum, with a width related to the electron velocity distribution (and hence to T_e) and an intensity proportional to n_e at the laser's focus.

For the past two years, Thomson scattering has been a valuable plasma diagnostic in Versator's various RF (microwave) heating and current drive experiments. The measurements are summarized

below:

In electron cyclotron heating experiments up to 100 kW at 35 GHz, in a mixture of ordinary and extraordinary modes, was injected from the high–field side of the plasma at varying angles to the toroidal field. The consequence was a large ($\leq$ 70%) but irreproducible increase in the bulk electron temperature with the consistent production of a superthermal electron tail. The results were largely independent of wave polarization or the angle of injection.

In lower hybrid ion heating experiments a phased array of waveguides, mounted on the outside wall of the torus, has injected up to 100 kW at 800 MHz. For ion heating, a suitable waveguide spacing and phasing was selected to launch lower hybrid waves with $n_{\parallel} \sim 5.5$ into a high–density ($\bar{n}_e \sim 2.5 \times 10^{13}$ cm^{-3}) plasma. Thomson scattering measurements of electron temperature and density profiles were unchanged by RF in the ion heating density regime. Measurements are planned at lower density during RF current drive.

19.3.10 X–Ray Measurements

In early 1983, a NaI hard x–ray detector, pulse height analysis system was constructed for Versator II. The purpose of this diagnostic is to measure the bremsstrahlung radiation spectrum from the high energy (20 keV – 1 MeV) superthermal electrons present in low density ($\bar{n}_e \leq 1 \times 10^{13}$ cm^{-3}) ohmic and RF current driven discharges.
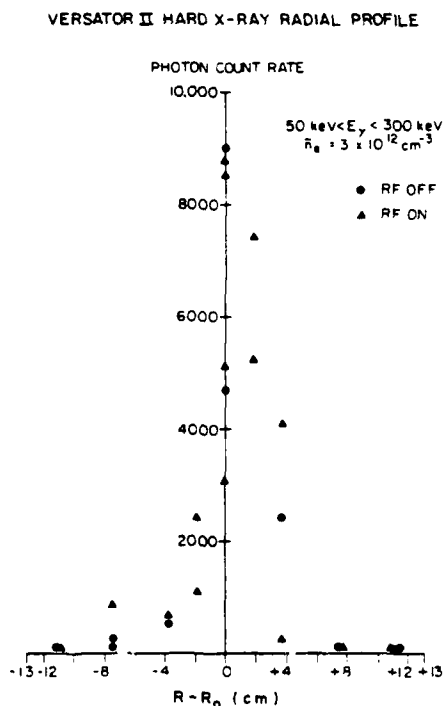
Figure 19-5: Hard x–ray profiles from scanning hard x–ray spectrometer

Typical hard x-ray spectra in the current drive regime ($\hat{n}_e \leq 6 \times 10^{12}$) have slopes of 30–50 keV and maximum detected photon energies of 500–800 keV. The NaI radial profile, scanned from below the torus for $E_\gamma = 50 - 300$ keV, is strongly peaked on the major radius (FWHM $\simeq 5$ cm) for both RF and ohmic plasmas (Fig. 19–5). Time resolved NaI measurements have revealed that this x-ray emission can be dominated by periodic bursts which correlate with the runaway tail anisotropy instability previously observed in Versator LHCD experiments.[3] Using a Si(Li) soft x-ray detector, which scans the plasma cross section from the side, it has been found that the bursting x-ray emission comes primarily from the upper half of the torus. Measurements with the Si(Li) detector PHA system have also been made during lower hybrid electron heating experiments in the density range $\hat{n}_e = 1 - 2 \times 10^{13}$. Although no measurable electron bulk heating has been found with soft x-rays, consistent enhancements of the electron tail (E $>$ 5 keV) are observed (Fig. 19–1). The RF tail intensity profile is peaked on the horizontal midplane (FWHM $\simeq 10$ cm), but is up/down asymmetric, with the greatest RF enhancement occurring in the upper half of the torus. Presently, x-ray studies are concentrating on the LH current drive density limit by measuring the effect of RF injection on the electron distribution function near the critical density.

References

1. S.C. Luckhardt, M. Porkolab, S. Knowlton, K.-I. Chen, A. Fisher, and F. McDermot, Phys. Rev. Lett. 48, 152 (1982).
2. V.V. Parail and O.P. Pogutse. Nuclear Fusion 18, 3, 303 (1978).
3. S.C. Luckhardt, et al., "Heating of Toroidal Plasmas," 3rd Joint Varenna—Grenoble International Symposium, CEN–Grenoble, France, 2, 529 (1982).
4. P.T. Bonoli and E. Ott, Phys. Fluids 25, 2, 359 (1982).
5. D.W. Ignat, Phys. Fluids 25, 2, 359 (1982).
6. Y. Baranov and V.I. Fedorov, Nuclear Fusion 20, 9, 1111 (1980).
7. N.J. Fisch, Phys. Rev. Lett. 41, 873 (1978).
8. J. Timberlake, et al., J. Vac. Sci. Technology 20, 4, 1309 (1982).

19.4 Physics of Thermonuclear Plasmas

Bruno Coppi

The theme of our research program is the combined experimental and theoretical investigation of plasmas in which fusion reactions have a significant influence on their thermal energy balance and physical properties.

Our characteristic line of interest involves plasmas with relatively high densities, in the range 10^{14} to 10^{15} particles/cm^3, in view of their attractive confinement properties, and magnetic confinement configurations that are suitable to contain the high energy (in the MeV range) charge particles that are produced by fusion reactions. The line of experimental devices that we have developed for this is represented by its prototype, the Alcator A machine, and is characterized by toroidal plasma columns

that can sustain both high currents and current densities. This requirement, leading to adoption of toroidal magnet configurations of compact size and relatively high fields, has made it possible to achieve and maintain the record values for the combined confinement parameters "$nT\tau$", the product of the peak particle pressure nT and the energy replacement time τ, and "$n\tau$". In addition, a sequence of plasma regimes of basic physical interest, in terms of the different characteristics of the particle distributions in velocity space that can be generated and of the collective modes that are excited, has been produced. The conditions where nearly impurity-free plasmas can be obtained have been realized at the same time.

By combining these experimental results with the theoretical analysis of the global transport properties in the plasma regimes that have been attained so far and the known physics of deuterium – tritium fusing plasmas, it has been possible to formulate a research program directed toward studying thermonuclear ignition by a series of compact devices that are called Ignitors.

The conceptual design of one of these devices has been completed in 1982 and has been successfully reviewed by an international panel convened by the C.E.C. (Euratom). This was chaired by Sr. John Adams (CERN), and the other members were R. Bickerton (JET), P. Reardon (Princeton), P. Rebut (JET), and M.N. Rosenbluth (U. Texas).

An independent program involving a compact device that has about the same philosophy and dimensions as Ignitor but gives a more enhanced role to heating by adiabatic compression is already underway in the Soviet Union. In fact the subject of compact ignition experiments has been the theme of an official U.S.-U.S.S.R. exchange held in July 1982 at Moscow and Leningrad with the participation of two of us (B. Coppi and R. Parker).

In 1980 we pointed out the feasibility of experimental fusion reactors that do not utilize tritium as a primary fuel, but are based on reactions such as D-He^3 that do not produce neutrons. These ideas have generated widespread interest and this has been enhanced in 1982 by the beginning of a serious[2,3] effort to investigate whether plasmas with spin polarized nuclei can be used as fuels in order to decrease further the already low fraction of energy produced in the form of neutrons in D-He^3 reactors. In fact the results of our studies indicate that an experimental program for an analysis of the "burn" conditions for these so-called advanced fuels can be undertaken with present day technologies and on the basis of existing knowledge of the physics of magnetically confined plasmas.[1]

One of the necessary conditions for (the feasibility of) these experiments is to produce plasmas in which the peak plasma pressure is a finite fraction of the magnetic pressure without exciting macroscopic instabilities. In early 1978 we took a first step in this direction when we demonstrated the existence of a "second stability" region that is relevant to these experiments, regarding the onset of a set of modes, so-called "ballooning".[4,5] These had been thought previously to severely limit the value of the plasma pressure relative to that of the confining magnetic field. Following a similar line of

thinking, in 1981 we reported that another important class of modes, the so-called "internal kinks" also tend to become stable[6] in a second-stability region. This region of stability overlaps the corresponding one of "ballooning" modes. Therefore, now we can invision a sequence of plasma equilibria[7] that involve increasing values of the plasma temperature and remain macroscopically stable while the desired thermonuclear burn conditions are achieved.

At relatively low plasma densities, lower than 10^{13} particles/cm, where the plasma current induced by the applied d.c. electric field is carried by superthermal electrons, a regime labelled the "slide-away", was first identified[8] by a series of experiments carried out in 1974 and 1975 on the Alcator A machine. Recently, a similar regime has been observed to be induced by the appropriate injection of microwaves at the so-called lower hybrid frequency. A series of successful experiments that have produced this form of "current drive" have been carried out both on the Versator II and the Alcator C devices. In fact, current drive has been observed for record high densities with the latter experimental device while appropriate analytical and numerical models for the physical processes involved have been formulated.

As is traditional with our mode of operation, during 1982 we have maintained an effective system of close collaborations with national and overseas institutions for both our theoretical and experimental program. Our contributions have been presented at major national and international meetings.

References

1. B. Coppi. M.I.T./R.L.E. Report PRR–80/24 (1980).
2. R.M. Kulsrud, H.P. Furth, E.J. Valeo, and M. Goldhaber, "Fusion Reactor Plasmas with Polarized Nuclei." Phys. Rev. Lett. 49, 1248 (1982).
3. B. Coppi, F. Pegoraro, and J. Ramos. "Instability of Fusing Plasmas and Relevant Depolarization Process," paper submitted for the 1983 Sherwood Theory Meeting, Washington, D.C., March 1983.
4. B. Coppi and M.N. Rosenbluth, in Plasma Physics and Controlled Nuclear Fusion Research (1965), Vol. 1 (International Atomic Energy Agency, Vienna, 1966) p. 617.
5. B. Coppi, G.B. Crew, and J.J. Ramos. Comments Pl. Phys. Contr. Fus. Res. 6, 109 (1981).
6. G.B. Crew and J.J. Ramos, Phys. Rev. A 426, 1149 (1982).
7. B. Coppi, G. Crew, and J. Ramos, M.I.T./R.L.E. Report PTP–82/6 (1982) to be published in Comments Pl. Phys. Cont. Fus. Res.
8. B. Coppi, A. Oomens, R. Parker, L. Pieroni, F. Schuller, S. Segre, and R. Taylor, M.I.T./R.L.E. Report PRR–74/18 (1974).

Communication Sciences and Engineering

20. Optical Propagation and Communication

Academic and Research Staff

Prof. R.S. Kennedy, Prof. J.H. Shapiro, Dr. R.H. Rediker, Dr. P. Kumar

Graduate Students

P.L. Bogler, R.S. Bondurant, J.J. Fratamico, F. Hakimi, S.T. Lau, M. Maeda, P.L. Mesite, T.T. Nguyen, J. Ocenasek, D.M. Papurt, J.J. Prisco, R.P. Schloss, P.D. Shapiro, S.S. Wagner, A.K. Wong

The central theme of our programs has been to advance the understanding of optical and quasi-optical communication and radar systems. Broadly speaking, this has entailed: developing system-analytic models for important optical channels; using these models to derive the fundamental limits on system performance; and identifying, and establishing the feasibility of, techniques and devices which can be used to approach these performance limits.

20.1 Atmospheric Optical Communication Systems for Network Environments

Jeffrey H. Shapiro, Trung T. Nguyen, Albert K. Wong

A local computer network is prototypically a high-bandwidth (1-10 Mb/s) geographically compact (0.1-10 km diameter) packet-switched network that employs coaxial cable or fiber optics as its transmission medium. Atmospheric optical communication links are a natural choice for certain high-bandwidth short-haul terrestrial transmission applications in which cable rights-of-way are unobtainable, or frequent link and network reconfiguration is necessary. Such links are therefore attractive candidates for local network applications including bridges between buildings containing cable subnetworks, and temporary quick-connects for new outlying users for which cable runs are unavailable. This program addresses the problem of how best to employ atmospheric optical communication links, which experience occasional outages due to local adverse weather conditions, in a local computer network, whose high-level protocols are designed to provide 100% end-to-end message reliability.

The principal task for the past year has been the design and construction of a pair of 10 Mb/s atmospheric optical communication transceivers to be used, in succeeding years, in local network experiments on the M.I.T. campus. Each transceiver will use a 2 mW semiconductor laser collimator pen module in the transmitter, and an avalanche photodiode/preamplifier module in the receiver. In

addition to the optical transceiver work, we have begun analysis on how atmospheric optical links can best be employed in various key network roles.

20.2 Atmospheric Propagation Effects on Infrared Radars

Jeffrey H. Shapiro, David M. Papurt, Sun T. Lau, Paula L. Mesite

Compact coherent laser radars have the potential for greatly improved angle, range, and velocity resolution relative to their microwave–radar counterparts. This program is aimed at obtaining a quantitative understanding of target-reflection and atmospheric-propagation effects on the performance of compact coherent laser radars through a combination of theory and experiments. Under a collaboration arrangement with the Optics Division of the M.I.T. Lincoln Laboratory, the experimental portions of the research are being carried out on the compact CO_2–laser radars under development there.

During the past year we have completed examination of the combined effects of turbulence and target speckle/glint on the performance of a 2–D pulsed–imager radar.[1-4] The principal conclusions drawn from this work are as follows. First, the compact radar system model must include beam jitter. Second, jitter-corrected glint target returns do show turbulence–induced lognormal scintillation. Third, turbulence–induced beam jitter is the cause for staring–mode speckle target decorrelation.

The focus of our work has now shifted to moving-target indication (MTI) systems. In particular, we have begun to study many of the same turbulence and speckle issues as they impact the Lincoln Laboratory continuous–wave CO_2 laser heterodyne–reception Doppler radar.[5]

References

1. J.H. Shapiro and S.T. Lau, "Turbulence Effects on Coherent Laser Radar Target Statistics," Appl. Opt. 21, 2395–2398 (1982).
2. D.M. Papurt, "Atmospheric Effects on Heterodyne–Reception Optical Radars," Ph.D. Thesis, Department of Electrical Engineering and Computer Science, M.I.T., May 1982.
3. S.T. Lau, "Decorrelation Time of Speckle Targets Observed with a Heterodyne–Reception Optical Radar," S.M. Thesis, Department of Electrical Engineering and Computer Science, M.I.T., June 1982.
4. D.M. Papurt, J.H. Shapiro, and S.T. Lau, "Measured Turbulence and Speckle Effects in Laser Radar Target Returns," Proc. SPIE 415, (1983).
5. D.G. Biron and B.E. Edwards, "Moving Target Imaging Radar Utilizing Both Intensity and Velocity Information," CLEO 1982 Technical Digest, (Opt. Soc. of Am., Pheonix, Arizona, 1982) pp. 128–129.

20.3 Improved Millimeter–Wave Communication Through Rain

Jeffrey H. Shapiro, John J. Fratamico, Philip L. Bogler

The increased path loss due to rain has long been recognized as a key factor limiting the extension of microwave satellite communications into the millimeter–wave spectral band. This program is aimed at understanding the extent to which millimeter–wave communication performance under severe rain conditions can be improved through exploitation of multiply–scattered radiation. Toward this end we have developed efficient numerical procedures for solving the scalar transport equation for the total transmission, angular spread, multipath spread, and Doppler spread of the multiply–scattered radiation.[1] Evaluation of these parameters has been performed for propagation at 35, 44, 95, 130, 210, and 300 GHz in various rain rates.[1]

We have combined the preceding propagation work with the appropriate communication analysis[2,3] for the millimeter–wave channel and reached the following conclusions. In a heavy rainstorm a satellite–to–ground link at 95 GHz or above which has suf‛:cient power for multi–Mb/s communication in clear weather may have sufficient power for multi–Kb/s communication if adaptive angle diversity reception of the scattered radiation is employed. Direct–beam reception will not function at these data rates, nor will nonadaptive angle diversity reception. The array needed for the adaptive combiner is far beyond the current state of the art, but may evolve out of the need for phased arrays to be used in millimeter–wave radars.

References

1. J.J. Fratamico, "Millimeter–Wave Propagation through a Turbid Atmosphere," Ph.D. Thesis, Department of Electrical Engineering and Computer Science, M.I.T., November 1982.
2. J.J. Fratamico, P.L. Bogler, and J.H. Shapiro, "Adaptive Diversity–Combining for Improved Millimeter–Wave Communication through Rain," IEEE J. Sel. Areas in Commun. SAC-1, (1983).
3. P.L. Bogler, "Electromagnetic Wave Propagation in Multiple–Scattering Atmospheres with Applications to Adaptive Communication," Ph.D. Thesis Proposal, Department of Electrical Engineering and Computer Science, M.I.T., January 1983.

20.4 Two–Photon Coherent State Light

Jeffrey H. Shapiro, Prem Kumar, Roy S. Bondurant, Mari Maeda, Stuart S. Wagner

Recent theory has shown that the generation of light beams with quantum states of superior fluctuation behavior may be possible. These states, called two–photon coherent states (TCS), are minimum uncertainty states of the electromagnetic field processing an asymmetric noise division

between the quadratures. The purpose of this research is to generate TCS light via degenerate four-wave mixing in sodium vapor, and to verify some of the predicted TCS fluctuation characteristics via photon counting measurements.

During the past year we have: set up the mixer and verified conjugate-wave generation; developed a photon counting scheme for making accurate statistical measurements on nanosecond duration optical pulses;[1] and devised a pulse-conditioning technique to minimize excess noise in the four-wave mixer output beams.[2] Work is now proceeding on quantum-noise measurements.

In addition to the main experimental effort we have begun analysis of the use of TCS light in phase-sensing interferometers[3] and of fundamental limits in phase/amplitude heterodyne measurements.[4]

References

1. R.S. Bondurant, P. Kumar, J.H. Shapiro, and M.M. Salour, "Photon-Counting Statistics of Pulsed Light Sources," Opt. Lett. 7, 529-531 (1982).
2. P. Kumar and R.S. Bondurant, "Improving the Pulse Shape in Dye Laser Amplifiers: A New Technique," Appl. Opt. 22, 1284-1287 (1983).
3. R.S. Bondurant, "Theoretical and Experimental Aspects of Quantum Noise Reduction and Precision Measurement," Ph.D. Thesis Proposal, Department of Electrical Engineering and Computer Science, M.I.T., November 1982.
4. S.S. Wagner, "An Investigation of the Uncertainties in Signal Energy and Phase in Optical Detection," S.M. Thesis, Department of Electrical Engineering and Computer Science, M.I.T., September 1982.

20.5 Fiber-Coupled External-Cavity Semiconductor High-Power Laser

Robert H. Rediker, Robert P. Schloss, Farhad Hakimi

During the past year an external cavity to contain five semiconductor gain elements operating in parallel has been designed and built. A photograph of this cavity is shown in Fig. 19-1. Starting from left to right the first plate attached to the four Super-Invar rods holds the micromanipulators and piezo-electric elements which will be used to properly position the gain elements. In back of this plate are the thermoelectric elements which are used to control individually the temperature of each elemen* The thermoelectric elements are connected to the gain elements by a flexible copper strap. The next plate will contain a lens which focuses all the collimated radiation from the gain elements on the spatial filter to be held by the third plate from the left. The spatial filter which contains thirteen 3 μm slits on 10.5 μm centers is the Fraunhoffer diffraction pattern of the gain elements' radiation if these elements are emitting in coherence. Filters have been built for us of blackened Si_2N_3 by integrated circuit techniques. The single pass transmission of the filter for coherent radiation input

from the five elements is ~3 times that if the radiation is incoherent. The next plate will contain a lens to recollimate the radiation; the last plate will contain a partially reflecting mirror
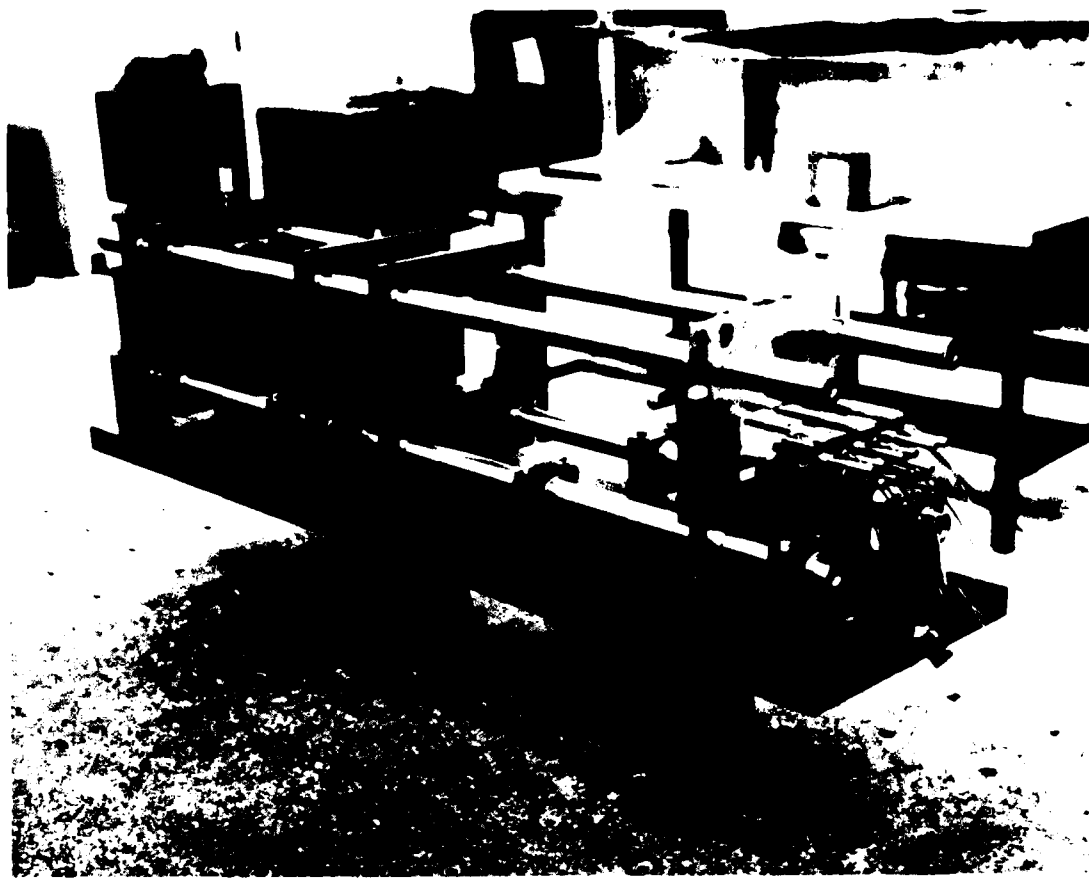
Figure 20-1: Photograph of External Cavity

Thermoelectric control circuits with sensors have also been built to control the temperature of each semiconductor gain element to 0.5×10^{-3}°C. (This temperature control is equivalent to controlling the 820-nm wavelength of the gain element radiation to 3×10^{-5} nm.) This sophisticated control will enable us to tune and detune the output wavelength of each element if the element were operating by itself. We will thus be able to quantify the tolerance for "locking into coherence" to wavelength variations. The sophisticated positioning controls in the cavity shown in Fig. 20-1 will enable us to also quantify the mechanical tolerances for "locking into coherence". These tolerances will give an indication of the ease with which this "high-power-laser" concept can be taken from laboratory to general use.

21. Digital Signal Processing Group

Academic and Research Staff

Prof. A.V. Oppenheim, Prof. A.B. Baggeroer, Prof. J.S. Lim, Prof. J.H. McClellan, Prof. B.R. Musicus

Graduate Students

A.J. Barabell, T.E. Bordley, P. Chan, S.R. Curtis, W.P. Dove, F.U. Dowla, G.L. Duckworth, C. Esmersoy, M.J. Glaser, D.W. Griffin, W.A. Harrison, D. Izraelevitz, T.H. Joo, A.L. Kurkjian, D.M. Martinez, E.E. Milios, D.R. Mook, C. Myers, S.H. Nawab, T.N. Pappas, M.D. Richard, J.-P. Schott, H. Sekiguchi, R. Sundaram, P.L. VanHove, D.L. Wang, M.S. Wengrovitz

21.1 Introduction

The Digital Signal Processing Group is carrying out research in the general area of digital signal processing. While a major part of our activities focus on the development of new algorithms, there is a strong conviction that theoretical developments must be closely tied to applications and to issues of implementation. The application areas which we deal with principally are speech, image and geophysical data processing. In addition to specific projects being carried out on campus, there is close interaction with Lincoln Laboratory and with the Woods Hole Oceanographic Institution.

In the area of speech processing, we have over the past several years worked on the development of systems for bandwidth compression of speech, parametric modeling of speech using pole–zero models, time–scale modification of speech, and enhancement of degraded speech. Recently we have obtained some important new results on time–scale modification of speech, growing out of a more general set of issues involving the estimation of a signal after its short–time Fourier transform has been modified. We are also exploring new techniques for speech enhancement using adaptive noise cancelling when multiple microphones are available.

There are also a number of projects related to image processing that we are currently pursuing. One project is restoration of images degraded by additive noise, multiplicative noise, and convolutional noise. Out of this project, we have developed a new image restoration system which is applicable to restoring images degraded by various different types of degradation. Our current work in this project involves development of new image restoration systems by exploiting additional available information such as the range map in infrared radar images. Another project is development of new image coding techniques by reducing quantization noise in PCM image coding or by reducing blocking effect in cosine transform image coding. Our approach to first decorrelate the quantization

noise, and then reduce the quantization noise by a noise reduction system, led to a noticeable improvement in the performance of a simple PCM image coding system. We are currently working on the extension of these results to a more complex PCM image coding system. To reduce the blocking effect in cosine transform image coding, we have studied two approaches. In one approach, the coder is modified to account for the blocking effect and in the second approach, the coded image with blocking effect is processed to reduce the blocking effect. In both approaches, we have developed specific algorithms that significantly reduce the blocking effect in cosine transform coding. Another project that we are currently exploring is the development of a very low bit rate (below 50 kbits/sec) video–conferencing system. The specific approach we are currently studying is to model a human face, which is a regular feature in typical video–conferencing applications, with a set of parameters and then synthesize the image at the receiver from the coded parameters. This approach is analogous to modeling human speech for speech coding, which led to significant bit rate reduction without seriously degrading the speech intelligibility.

In the area of geophysical data processing, there are a variety of ongoing and new projects. During March–May 1980, we led a large acoustics and geophysics experiment, FRAM II, in the eastern Arctic. This was followed by an even more extensive program in March–May 1982, FRAM IV. Both of these experiments implemented an array of hydrophones and geophones with multichannel digital data recording. Work has been carried out on applying adaptive array processing to the measurement of the reverberation associated with the resulting acoustic signals, as well as the phase and group velocities of the seismic paths within the seabed and water column for refraction and bottom interaction studies. Work is also currently under way to examine the properties of several velocity function inversion techniques for multi–channel seismic ocean–bottom interaction data. The array data at FRAM II and FRAM IV are also being used to measure the scattering function of the channel at low frequencies and the directional spectra of the ambient noise in the Arctic. Associated with the acoustics experiment is a project aimed at extending the parabolic wave equation approximation for modeling underwater acoustics. The summers of 1983 and 1984 mark the beginning of a series of geophysical and acoustic experiments in the marginal ice zone of the Arctic. In these MIZEX experiments, large multichannel telemetered arrays will be used to receive acoustic signals propagated across ocean and crustal paths marking the transition between the open waters of the Atlantic, and the ice covered regions of the Arctic Ocean. The goals are to study the acoustic transmission properties of the laterally inhomogeneous and time varing water column, and to characterize the crustal velocity–depth function in this region.

Two additional projects related to geophysical signal processing in the context of ocean acoustics are the development of an algorithm for data processing to measure the acoustic reflection coefficient from the ocean bottom both for the deep water and shallow water cases. Out of this work has come a Hankel transform algorithm as well as a new method for generating synthetic data.

In both the context of image processing and geophysical data processing we have obtained some

significant results in the multi–dimensional high resolution spectral estimation problem. Specifically, we have developed new algorithms for maximum entropy power spectrum estimation which are computationally simple relative to previous approaches and applicable to both equally spaced and non–equally spaced data for both one–dimensional and two–dimensional signals. This algorithm has been applied to investigate the characteristics of multi–dimensional maximum entropy spectral estimates. In addition, we are investigating several approaches to improve the performance of the maximum likelihood method for spectral estimation.

Recently, we have proposed a new approach to the problem of estimating multiple signal and/or parameter unknowns using incomplete and noisy data. Our Minimum Cross–Entropy Method applies an information theoretic criterion to optimally estimate a separable probability density for the signal model. Not only does this new approach include all the various Maximum Likelihood and Maximum *A Posteriori* methods as degenerate cases, but it also directly leads to a simple iterative method of solution in which we alternate between estimating the various unknowns, one at a time. We are now exploring applications to statistical problems, iterative signal reconstruction, short–time analysis/synthesis, and noisy pole/zero estimation.

Another interesting area of research is the connection between signal processing algorithms and computer architectures. The "speed" of an algorithm depends not only on how many operations it requires, but also on how suitable it is for the computer architecture it runs on. With the advent of VLSI technology, it is now possible to build customized computer systems of astonishing complexity for very low cost. Exploiting this capability, however, requires designing algorithms which not only use few operations, but also have a high degree of regularity and parallelism, or can be easily pipelined. Directions we are exploring include systematic methods for designing multi–processor arrays for signal processing, isolating signal processing primitives for hardware implementation, and searching for algorithms for multi–dimensional processing which exhibit a high degree of parallelism.

There also are a number of projects directed at the development of new algorithms with broad potential applications. For some time we have had considerable interest in the broad question of signal reconstruction from partial information such as Fourier transform phase or magnitude. We have shown theoretically how under very mild conditions signals can be reconstructed from Fourier transform phase information alone. We have also developed a variety of theories and algorithms relating to signal reconstruction from Fourier transform magnitude and from partial short–time Fourier transform information. We are also exploring the application of some of these theoretical results to problems such as speech and image coding.

A recent and growing emphasis in our group is the combination of signal processing and artificial intelligence techniques. There are a variety of problems in signal analysis that can be approached either from the analytical viewpoint characteristic of signal processing or the symbolic viewpoint characteristic of knowledge–based systems and artificial intelligence. We believe there is

considerable potential for combining these two viewpoints into what we refer to as knowledge-based signal processing. There are currently two projects under way directed at developing this approach in the context of specific signal processing problems. One attempts to exploit artificial intelligence concepts to develop a knowledge based pitch detector and the second, to explore knowledge-based signal processing in the context of signal enhancement. We also expect to couple our work on knowledge-based signal processing into a project at Lincoln Laboratory on distributed sensor nets.

21.2 Parabolic Wave Equation Modeling for Underwater Acoustics

Arthur B. Baggeroer, Thomas E. Bordley

In underwater acoustics, the parabolic (Schroedinger) wave equation is often used as an approximation to the hyperbolic wave equation when solutions are sought in regions with slowly varying inhomogeneities. Such inhomogeneities prevent separation-of-variables or other simple solution techniques from being employed. The rationale behind the parabolic approximation is that if the inhomogeneities are weak, then the component of the field which is due to reflections ought to be small. Thus, it should be legitimate to split the wave equation into a pair of coupled equations in the "transmitted" and "reflected" fields and then solve for the transmitted field with the reflected field set to zero.

This approximation has two significant effects. First, since the equation is reduced to first order in the direction of propagation or range, the original problem is reduced to a comparatively simple initial value problem for which the necessary initial conditions can be readily found. Second, the split fields are decoupled approximants to the true transmitted and reflected fields, possessing a parabolic rather than a circular dispersion relation. Therefore, both the shape and scaling of waves emanating from the source at large angles with respect to the nominal direction of propagation are wrong.

Such errors are of negligible importance in many marine problems. Inhomogeneities in the water column normally are significant only when large distances are involved. Over such ranges, the heavy attenuation in the bottom allows only those waves which possess a small grazing angle with respect to the bottom, or equivalently, which emanate at an angle close to horizontal with respect to the source, from contributing substantially to the solution. Ordinarily then, a good estimate of the field can be obtained, because those waves which contribute the most to the final solution are represented well while only those which contribute little are represented poorly.

When the signals propagating through the bottom are not small or are of interest in themselves, this approach is less satisfactory. Local variations in the acoustic field with range can be rapid due to the presence of distinct material layers in the earth. Thus, the approximation can be poor. In this

research, our concern is to extend the parabolic approximation so that the fields in both the earth and the sea are modelled well.

21.3 Adaptive Image Restoration

Jae S. Lim, Philip Chan

There have been many image restoration techniques developed with the assumptions of global statistical stationarity and an additive signal independent noise model. These assumptions are usually not valid for many applications. The aim of this thesis research is to develop an adaptive algorithm for restoring images corrupted by noise. Without the usual assumption of global stationarity, the algorithm adapts itself to the local statistics of the processed picture elements. The result is the simultaneous reduction of noise and preservation of edges.

The adaptive algorithm will first be developed for an additive noise model. The ultimate aim will be to develop an algorithm for the restoration of infrared radar images corrupted by speckle noise which is signal dependent and non–additive.

21.4 Signal Reconstruction from Partial Fourier Domain Information

Alan V. Oppenheim, Jae S. Lim, Susan R. Curtis

In a variety of practical problems, only the magnitude or the phase of the Fourier Transform (FT) of a signal is available, and it is desired either to reconstruct the signal exactly or to synthesize a signal which retains many of the important characteristics of the original signal. Our work in this area involves two distinct problems. One problem is to identify those portions of the FT which contain most of the "intelligibility" information; the other is to develop conditions under which a signal can be exactly reconstructed from various portions of the FT.

On the intelligibility problem, past work has shown that a signal synthesized with the correct phase and unity or average magnitude maintains many of the important characteristics of the original signal, whereas a signal synthesized from the correct magnitude and zero or random phase does not. In addition, a signal synthesized from the "signed–magnitude" (magnitude and one bit of phase) is

intelligible. Recently, we have found that a signal synthesized from one bit of phase alone is also intelligible. This one bit of phase is contained in both the signed-magnitude and the phase, and thus this result helps to explain the earlier results.

On the exact reconstruction problem, past work has shown that, under mild restrictions, a finite length signal can be exactly reconstructed from its FT phase (to within a scale factor) or from its signed-FT magnitude. In addition, almost all multi-dimensional signals with finite support are uniquely specified by their FT magnitude, although this is not true in the one-dimensional case. Recently, we have developed some new interpretations of these results and removed the finite-length restriction from the signed-magnitude result. Currently, we are developing conditions under which a signal can be exactly reconstructed from one bit of its FT phase.

Despite the potential applicability of these results to a wide range of problems, so far they have been mostly of theoretical value. In addition to solving some remaining theoretical questions, we plan to explore applications of these results.

21.5 Knowledge-Based Pitch Detection

Alan V. Oppenheim, Randall Davis, Webster P. Dove

Knowledge-based signal processing is an effort to design signal processing programs that go beyond purely numerical processing of the data and try to symbolically reason about the problem in order to better solve it. Problems appropriate for this area those whose model is either too complex to be solved directly with a numerical algorithm, and those for which the model is not well understood.

Pitch detection falls into this category both because the speech signal model is not well specified, and because the model for the generation of pitch is not fully understood.

The aim of this project is to develop a program called the **Pitch Detector's Assistant (PDA)** which will both serve to reduce the effort involved in generating hand edited pitch and provide a laboratory for studying and programming the knowledge that makes humans better pitch trackers than existing automatic algorithms.

Existing methods of semi-automatic pitch detection[1] require the user to make a voicing decision and select a pitch individually for every frame. The PDA program is intended to analyze as much of the utterance as it is sure of and then help the user with the remaining difficult portions. Thus we expect a dramatic reduction in the time from the current 30 minutes per second of speech analyzed.

Although there have been projects which combine signal processing and AI technology for particular problems such as speech understanding[2,3] and underwater acoustic signal recognition,[4] the actual signal processing present in these systems has only been used as a means for generating symbolic objects. These objects are then manipulated by the AI portions of the program until an interpretation of the data is complete. The symbols do not provide information to assist subsequent numerical processing, and thus the information flows one way from numeric to symbolic form. The pitch detection problem choice is motivated by the observation that these other problems are ones of recognition (i.e. signals in, symbols out) and naturally lead to solutions which process numerically first and symbolically later.

By choosing a problem which involves signal output we assure the use of numerical processing in later portions of the program. The creation and study of programs which emphasize the interaction between symbolic and numerical processing is the primary purpose of the knowledge-based signal processing effort at M.I.T.

References

1. C.A. McGonegal, L.R. Rabiner, and A.E. Rosenberg, "A Semiautomatic Pitch Detector (SAPD)," IEEE Trans. ASSP 23, 570-574 (December 1975).
2. L. Erman, R. Hayes-Roth, V.R. Lesser, and D.R. Reddy, "The Hearsay-II Speech Understanding System: Integrating Knowledge to Resolve Uncertainty," Computing Surveys 12, 213-254 (June 1980).
3. B. Lowerre and R. Reddy, "The HARPY Speech Understanding System," in W. Lea (Ed.), Trends in Speech Recognition (Prentice-Hall, 1980) pp. 340-360.
4. H.P. Nii, E.A. Feigenbaum, J.J. Anton, and A.J. Rockmore, "Signal-to-Symbol Transformation: HASP/SIAP Case Study," AI Magazine 3, 23-35 (Spring 1982).

21.6 Multi-Dimensional High-Resolution Spectral Analysis and Improved Maximum Likelihood Method

Jae S. Lim, Farid U. Dowla

Although MEM, MLM, and AR-modeling spectral estimation are high resolution spectral estimation algorithms, in multidimensional situations there are problems with each of these methods. The MEM algorithms are iterative and their applications to real world problems is prohibitive from numerical viewpoints. MLM does not quite achieve the resolution which one would like it to have. The AR-modeling has problems as the shape of the spectrum is distorted when the filter mask does not conform to certain symmetry.

We are developing a closed-form high resolution spectral estimation algorithm based on the

concepts of MLM, MEM, and AR spectral estimation. We have found a useful relationship between the MLM and AR signal modeling in multidimensions. By exploiting this relationship and by studying the problem of array design in multidimensions for these algorithms, we propose to present an algorithm with computational properties like the MLM but whose resolution property is better than the MLM.

The performance of the algorithm is being evaluted on synthetic data and on real data in a multichannel radar tracking problem.

21.7 Processing and Inversion of Arctic Refraction Data

Arthur B. Baggeroer, Gregory L. Duckworth

Several seismic refraction and long-range propagation experiments were carried out during the *Fram 2* experiment in the Pole Abyssal Plain of the Eastern Arctic Ocean (May 1980). This work concerns the digital signal processing and inversion methods used to analyze and interpret these multichannel array data for crustal and oceanic velocity structure, and the results of these analyses. Examined are: i) methods for obtaining the partial plane wave decomposition of the data subject to the experimental limitations imposed by the Arctic environment, ii) methods for inverting these decompositions for oceanic and crustal structure, and iii) synthetic seismogram techniques using normal mode and WKBJ theory for use in inversion, algorithm testing, and model verification.

For the plane wave decomposition, conventional time and frequency domain array processing techniques for velocity analysis and slant stacking are contrasted to an optimal adaptive technique. In this method, the time varying statistics of the data are estimated and used to design the optimal time varying frequency-wavenumber filters used to filter the data to obtain the power or slant stack output. The criteria of phase velocity, group velocity (time of arrival), and amplitude estimator bias and stability are discussed. It is shown that the different methods often have complimentary advantages and disadvantages.

To recover the structure, several inversion methods for estimation of the ocean/crust velocity structure from the velocity analyzed refraction data are examined. In this work, an emphasis is placed on techniques which fully utilize the data obtained in this experiment. The incorporation of the directly estimated delay time, $\tau(p)$, and offset, $X(p)$, data as a function of horizontal slowness, p, is carried out. The judicious use of offset data in a velocity/depth migration inversion procedure constrains the resulting models more tightly, especially in the case of sparse offset sampling necessitated by the Arctic environment. The use of the WKBJ approximation in this inversion method allows more complete utilization of the data through inclusion of non-geometric arrivals and amplitude constraints. An iterative algorithm based around velocity-depth migration which checks

for consistency between the τ and offset data using the WKBJ approximation is developed for both types of arrivals. In regions where the lateral homogeneity is not adequate for the migration technique, an approximate linear least-squares inversion procedure is used. This method utilizes all primary and multiple $\tau(p)$ and $X(p)$ information simultaneously in a tomographic technique to invert for laterally varying structures under the assumption that lateral variations are not excessive.

In addition to the refraction experiments, long-range (100–500 km) propagation data are used for the determination of water column and near-bottom sediment velocity structure. The use of the velocity spectral estimation techniques and sonogram analysis on the long range propagation data allows estimation of the modal dispersion curves and travel time structure of the arrivals. These dispersion curves can be inverted for water column sound speed structure, and the travel time data used for ocean bottom velocity structure determination. The use of both normal mode and WKBJ theory tightly constrains the velocity structure using single-shot data as long as the lateral homogeneity of the structure to be examined is sufficient.

The WKBJ synthetic seismogram technique, normal mode analysis and synthesis, and an approximate normal mode analysis/synthesis technique using WKBJ method to approximate the dispersion characteristics of an acoustic model have been examined. Their properties and utility in the inversion techniques are studied, and the results are used as test data for the velocity analysis/slant stack methods.

21.8 Signal Estimation from Modified Short-Time Fourier Transform

Jae S. Lim, Daniel W. Griffin

In several applications, including time-scale modification of speech and speech enhancement by spectral subtraction, the Short-Time Fourier Transform (STFT) of a signal is modified so that it no longer corresponds to the STFT of any sequence. In these cases, we would like to find a time domain sequence that has a STFT closest to the desired STFT. Several methods are being investigated for estimating a sequence whose STFT is closest to a given modified STFT or modified STFT magnitude. One of the methods developed for estimating a signal from modified STFT magnitude has produced excellent results when applied to time-scale modification of speech. Informal listening tests have judged the results of this method superior to Portnoff's time-scale modification method based on the phase vocoder.

21.9 Speech Enhancement Using Adaptive Noise Cancelling Algorithms

Jae S. Lim, William A. Harrison

This research is directed towards evaluating the performance of some general adaptive noise cancelling algorithms in a distributed noise environment. General adaptive noise cancelling algorithms utilize one or more reference microphones that record a correlated version of noise that is additively corrupting a desired signal in the primary microphone. In practice, the desired signal is often recorded by the reference microphones. Under these conditions, the algorithm will attempt to cancel part or all of the desired signal. Under certain conditions, modifications in an adaptive noise cancelling algorithm such as the Widrow–Hoff least mean square algorithm, allows one to still reduce the background noise without severely distorting the desired signal. One application of this work is in reducing the background noise in a jet fighter pilot's speech. Test cases conducted with simulated data have shown some promise that the ANC algorithm can be used to improve the SNR of the pilot's speech.

21.10 Overspecified Normal Equations for Autoregressive Spectral Estimation

Jae S. Lim, David Izraelevitz

There is a one–to–one relationship between a set of P normalized positive definite correlation estimates and the P predictor coefficients derived using autoregressive modeling. Several researchers have proposed the use of M > P correlation estimates to provide a better Pth order model. Specifically, the normal equations are augmented to provide M linear equations between the correlation estimates and the predictor coefficients. Since the system of equations is now overspecified, a least squares solution is required.

In this work a study is presented of some of the properties of the method of overspecified normal equations as applied to the problem of spectral estimation. The main contribution of this research is the derivation of the relationships between the number of correlations used, the model order and the signal–to–noise ratio of the signal, to the characteristics of the resulting spectral estimate. The characteristics studied are the spectral height, bandwidth and area. The method is shown to be a spectral density estimator like the ME method, where spectral *areas* rather than spectral values

for consistency between the τ and offset data using the WKBJ approximation is developed for both types of arrivals. In regions where the lateral homogeneity is not adequate for the migration technique, an approximate linear least–squares inversion procedure is used. This method utilizes all primary and multiple $\tau(p)$ and $X(p)$ information simultaneously in a tomographic technique to invert for laterally varying structures under the assumption that lateral variations are not excessive.

In addition to the refraction experiments, long–range (100–500 km) propagation data are used for the determination of water column and near–bottom sediment velocity structure. The use of the velocity spectral estimation techniques and sonogram analysis on the long range propagation data allows estimation of the modal dispersion curves and travel time structure of the arrivals. These dispersion curves can be inverted for water column sound speed structure, and the travel time data used for ocean bottom velocity structure determination. The use of both normal mode and WKBJ theory tightly constrains the velocity structure using single–shot data as long as the lateral homogeneity of the structure to be examined is sufficient.

The WKBJ synthetic seismogram technique, normal mode analysis and synthesis, and an approximate normal mode analysis/synthesis technique using WKBJ method to approximate the dispersion characteristics of an acoustic model have been examined. Their properties and utility in the inversion techniques are studied, and the results are used as test data for the velocity analysis/slant stack methods.

21.8 Signal Estimation from Modified Short–Time Fourier Transform

Jae S. Lim, Daniel W. Griffin

In several applications, including time–scale modification of speech and speech enhancement by spectral subtraction, the Short–Time Fourier Transform (STFT) of a signal is modified so that it no longer corresponds to the STFT of any sequence. In these cases, we would like to find a time domain sequence that has a STFT closest to the desired STFT. Several methods are being investigated for estimating a sequence whose STFT is closest to a given modified STFT or modified STFT magnitude. One of the methods developed for estimating a signal from modified STFT magnitude has produced excellent results when applied to time–scale modification of speech. Informal listening tests have judged the results of this method superior to Portnoff's time–scale modification method based on the phase vocoder.

21.9 Speech Enhancement Using Adaptive Noise Cancelling Algorithms

Jae S. Lim, William A. Harrison

This research is directed towards evaluating the performance of some general adaptive noise cancelling algorithms in a distributed noise environment. General adaptive noise cancelling algorithms utilize one or more reference microphones that record a correlated version of noise that is additively corrupting a desired signal in the primary microphone. In practice, the desired signal is often recorded by the reference microphones. Under these conditions, the algorithm will attempt to cancel part or all of the desired signal. Under certain conditions, modifications in an adaptive noise cancelling algorithm such as the Widrow–Hoff least mean square algorithm, allows one to still reduce the background noise without severely distorting the desired signal. One application of this work is in reducing the background noise in a jet fighter pilot's speech. Test cases conducted with simulated data have shown some promise that the ANC algorithm can be used to improve the SNR of the pilot's speech.

21.10 Overspecified Normal Equations for Autoregressive Spectral Estimation

Jae S. Lim, David Izraelevitz

There is a one–to–one relationship between a set of P normalized positive definite correlation estimates and the P predictor coefficients derived using autoregressive modeling. Several researchers have proposed the use of M > P correlation estimates to provide a better Pth order model. Specifically, the normal equations are augmented to provide M linear equations between the correlation estimates and the predictor coefficients. Since the system of equations is now overspecified, a least squares solution is required.

In this work a study is presented of some of the properties of the method of overspecified normal equations as applied to the problem of spectral estimation. The main contribution of this research is the derivation of the relationships between the number of correlations used, the model order and the signal–to–noise ratio of the signal, to the characteristics of the resulting spectral estimate. The characteristics studied are the spectral height, bandwidth and area. The method is shown to be a spectral density estimator like the ME method, where spectral *areas* rather than spectral *values*

should be interpreted as estimates of power.

The relationships derived point to the number of correlations used over the minimum, i.e. model order, as a signal–to–noise enhancer. The resulting spectrum is equivalent to the ME spectrum under higher signal–to–noise conditions. Another result is the requirement of a proportionality constant dependent on the number of correlations and the model order which is necessary for unbiased signal–to–noise measurements. This constant is not required however, for measurements of relative power within the same spectral estimate, as in the power ratio of two sinusoids in noise.

The second part of the research presents some empirical studies using computer simulations which verify the theoretical predictions and provide the region of validity of the analysis. Further experiments study the interfering effect of several closely spaced sinusoids. The method of overspecified normal equations is shown to be much more sensitive to this interference than the ME method. Finally, some further empirical studies are made of the resolution capabilities of the method. Using the data derived, an empirical model is derived which seems to agree to some extent with the data.

21.11 Spectral Analysis Methods for Non–Stationary Time Series

Jae S. Lim, Dennis M. Martinez

Spectral analysis methods play an important role in the study of signals and systems. Using spectral techniques, a very broad class of signals (time series) can be described in a manner which provides insight into the signal properties. Furthermore, for a very important class of systems (linear time–invariant), the effect of the system on the signal is easily determined. Consequently in engineering practice, spectral methods are fundamental to most signal analysis methods and system design procedures.

Most of the currently used spectral representations in continuous time map a time series defined over the infinite time interval $-\infty \leq t \leq \infty$, into a functional defined over a particular contour in the complex plane $(\sigma, j\omega)$. For example, the Fourier transform maps the signal x(t) defined for $-\infty \leq t \leq \infty$ into the functional $X(j\omega)$ defined for $-\infty \leq \omega \leq \infty$. Similar mappings are in wide–spread use in discrete time. While such representations provide insight about the global properties of a time series, they do not provide insight into its local properties.

In describing stationary time series, global properties are often sufficient, but this is not the case for non–stationary time series such as are encountered in speech analysis. Consequently a variety of

spectral representations for non-stationary time series have been developed in the past. In speech analysis, the most common non-stationary spectral representation in use is the short-time Fourier transform. Time dependent spectral representations such as the short-time Fourier transform often provide considerably more insight into the properties of non-stationary time series than the Fourier transform itself.

The purpose of the research being conducted is twofold; (1) to review and compare presently defined non-stationary spectral representation methods; and (2) to investigate new techniques for spectral analysis of non-stationary time series.

21.12 Speech Coding Using the Phase of the Long-Time LPC Residual Signal

Alan V. Oppenheim, Evangelos E. Milios

The potential of using the long-time phase of the Fourier transform of the LPC residual signal in speech synthesis has been investigated. The modified residual obtained by using the correct phase and constant magnitude leads to speech that is close to the original, but slightly hoarse. However, if the correct magnitude over a low-frequency band of width about a fifth of the total spectrum and smoothed magnitude in the rest of the spectrum is used, and combined with the correct phase, the hoarseness disappears. Because the phase has a uniform distribution of values between $-\pi$ and π, uniform quantization and binary encoding of the values is appropriate. The low-frequency magnitude has a bell-shaped distribution of values; thus, Huffman coding can be used to advantage. The possibility of using the previous scheme in coding as well as the perceptual importance of the various parts of the long-time Fourier transform of speech and the LPC residual are topics of further research.

21.13 The Numerical Synthesis and Inversion of Acoustic Fields Using the Hankel Transform with Application to the Estimation of the Plane Wave Reflection Coefficient of the Ocean Bottom

Alan V. Oppenheim, George V. Frisk,[11] Douglas R. Mook

[11] Woods Hole Oceanographic Institution

The plane wave reflection coefficient is an important geometry independent means of specifying the acoustic response of a horizontally stratified ocean bottom. Its determination is an integral step in the inversion of acoustic field measurements to obtain the parameters of the bottom and it is used to characterize an environment for purposes of acoustic imaging. This research, completed this year, studied both the generation of synthetic pressure fields to estimate the plane wave reflection coefficient and the inversion of measured pressure fields to estimate the plane wave reflection coefficient. These are related through the Sommerfeld integral, which has the form of a Hankel transform. The Hankel transform was extensively studied in this work and both its theoretical properties and numerical implementation were considered. A fast, NlogN, numerical algorithm was developed for both the Hankel and Abel transforms. The results of the theoretical and numerical studies on the Hankel transform have broad application beyond ocean acoustics. When these results were applied to the generation of synthetic data, the result was hybrid numerical–analytical algorithms which generate extremely accurate synthetic fields without sacrificing computation speed. These algorithms are capable of accurately incorporating the effects of trapped modes guided by slow speed layers in the bottom. The general results for the Hankel transform were also applied to study the inversion of measured pressure field data for the plane wave reflection coefficient. Practical issues associated with the inversion procedure were addressed, including the removal of the source field, sampling the effect of field measurements over a finite range, and uncontrolled variations in source–height. A phase unwrapping and associated interpolation scheme was developed to handle improperly spaced data.

A preliminary inversion of real pressure field data was performed. In parallel, an inversion of a synthetically generated field for similar bottom parameters was also performed and the results of processing the real and synthetic data compared. The estimate for the depth–dependent Green's function obtained from the real data was found to share many features with the depth–dependent Green's function estimated from the synthetic data, suggesting that the total inversion to obtain the plane wave reflection coefficient will soon be possible. Errors in the present estimate of the plane wave reflection coefficient were associated with uncontrolled variations.

21.14 Optimal Signal Reconstruction and ARMA Model Identification Given Noisy and Incomplete Observation Data

Jae S. Lim, Bruce R. Musicus

There are a large number of signal processing applications in which signals and/or model parameters must be estimated from noisy or incomplete observation data. For example, we may need

to reconstruct a finite length signal from noisy measurements of its phase of magnitude. We may want to filter, interpolate and/or extrapolate a finite interval of stationary data, and possibly fit a pole/zero model to the data at the same time. We may be given grouped, truncated, censored, or heavily quantized data and need to estimate the parameters of the probability distribution from which they were drawn. Conventional Bayesian estimation methods, when applied to these problems, would typically require a numerically unpleasant multi-dimensional optimization of a multi-dimensional integral. We have developed a new approach to the problem of estimating multiple unknowns given noisy and incomplete data, however, which leads to a particularly simple and elegant estimation algorithm. We start with a probabilistic model describing the signals and parameters, together with a set of constraints which the signals and parameters are known to satisfy. We then optimally fit a separable probability density to this given model by minimizing a cross–entropy criterion. Surprisingly, all Maximum Likelihood and Maximum *A Posteriori* algorithms for this problem can be treated as degenerate cases of this single approach. Furthermore, it is easy to derive a simple iterative algorithm for calculating the optimal estimates. Each step of this algorithm treats each unknown one at a time, iterating between well–known filtering, interpolation, and/or extrapolation steps to estimate each signal, followed by well–known parameter estimation steps for each parameter. Convergence is guaranteed under mild conditions. Furthermore, this approach has been shown to work well in a variety of problems ranging from statistics to pole/zero estimation.

Another major focus of our research is the development of new algorithms for solving almost–oeplitz sets of linear equations. Equations of this type arise quite commonly in the filtering and signal reconstruction problems we have been investigating, and efficient solution methods are especially critical because the problems must be solved repetitively as the algorithms iterate. Levinson–style recursions have been most commonly discussed in the literature. Fast Choleski methods for solving the same problems can be derived as "mirror images" of the Levinson–style recursion. Using both forward and backward recursions to minimize storage, these fast Choleski methods are particularly valuable for solving the band diagonal, almost–Toeplitz problems that arise when filtering noisy ARMA signal data. These algorithms also strongly resemble "inside out" Euclidian polynomial algorithms, an observation which directly leads to new "doubling algorithms" for solving almost–Toeplitz problems in only $O(N\log^2 N)$ operations. Connections between Euclidian polynomial algorithms and Levinson recursion algorithms are also being explored in other contexts as well; in particular, we have developed a new Euclidian algorithm with "partial pivoting" for evaluating inverse z–transforms and inverse Laplace transforms of rational polynomials.

21.15 The Use of Speech Knowledge in Speech Enhancement

Alan V. Oppenheim, Cory Myers

The problem of speech enhancement from speech corrupted by noise is one which has been of great interest in the signal processing community. Techniques based on estimation theory and based on speech analysis and resynthesis models have been used to differing degrees of success. Such techniques generally make use of only a small amount of the knowledge that is available about the speech process. We propose to build a system for the enhancement of noisy speech which will be able to use more and different types of speech knowledge. This system will attempt to mix various processing tools for signal enhancement with several artificial intelligence tools for symbolic reasoning. Through close cooperation among these tools it is hoped that a speech enhancement system which utilizes large amounts of speech knowledge can be realized.

The major issues being studied in this project are the representation and use of signal processing knowledge. Current work involves the acquisition and representation of acoustic–phonetic knowledge that can be used for speech enhancement. Future work will involve acquisition and representation of knowledge about perception of noisy speech and the behavior of various signal processing algorithms. Mechanisms for reasoning about the choice of signal processing algorithms in different contexts will also be developed. Emphasis will be paid to those situations in which outside symbolic information, e.g., speaker sex, phonetic transcription, etc., is available.

This work is part of a more general project in knowledge–based signal processing, i.e., the attempt to combine techniques from both signal processing and artificial intelligence in a close, cooperative manner.

21.16 Estimation of the Degree of Coronary Stenosis Using Digital Image Processing Techniques

Jae S. Lim, Thrasyvoulos N. Pappas

The aim of this research is the development of an algorithm for evaluating the degree of coronary artery stenosis from coronary cine–angiograms. A cine–angiogram is a sequence of x–ray pictures of the coronary arteries in which a contrast agent has been injected via a catheter. The precise measurement of the stenosis of the coronary arteries is important in the treatment of patients with ischemic heart disease.

The first step will be the determination of the percentage diameter reduction from a single frame of the cine–angiogram. This will require the detection of the boundaries of the coronary arteries and the analysis of the variation of their diameter. Preprocessing of the image for noise reduction will

hopefully lead to improved boundary detection.

Subsequent steps will involve the analysis of multiple frames of the cine–films, and the investigation of densitometric procedures, which use the brightness information within the artery to obtain estimates of the cross–sectional percentage area reduction.

21.17 Automatic Target Detection in Aerial Reconnaissance Photographs

Jae S. Lim, Michael D. Richard

The detecting of small anomalous regions in images has aroused much interest in such areas as optical aerial reconnaissance, radar analysis, terrain classification, and medical diagnosis through imagery. A recently developed algorithm[1] has proven highly successful in detecting small objects or targets in natural terrain such as trees, grass, and fields of aerial photographs. The algorithm uses a significance test to distinguish each image pixel as either background or non–background (i.e., target). Specifically, the background is assumed to be characterized by a nonstationary Gaussian random process. The algorithm further represents the background by a two dimensional (2-D) autoregressive model. *The resulting significance test* is expressed as the error residuals of 2–D linear prediction.

This research will explore several new areas to either develop a superior detection algorithm or to significantly improve the existing one. First, the issue of target modelling will be explored. The current algorithm models only the background and treats targets simply as anomalies in the background. The question arises as to how a suitable model for targets can be incorporated in a detection algorithm. Second, methods to detect and to fully determine the boundaries of larger objects will be considered. The present algorithm can detect only small point objects representing statistical irregularities in the background random process. The issue of detecting larger targets poses significant questions regarding object detection, image segmentation, and boundary extraction. Additional research in these two areas should improve the somewhat favorable results obtained by using linear predictive techniques to detect anomalous regions in images.

Reference

1. T.F. Quatieri, "Object Detection by Two–Dimensional Linear Prediction," M.I.T. Lincoln Laboratory Technical Report 632, January 1983.

21.18 Enhancement of Helium–Degraded Speech

Jae S. Lim, Hiroshi Sekiguchi

Considerable progress in the theory of signal processing by using the Short–Time Fourier Transform (STFT) has been made in the last several years. Particularly, new algorithms have been developed to reconstruct a signal from its modified STFT or from its modified STFT magnitude.

Among various applications of these algorithms, the enhancement of helium–degraded speech is fairly interesting. The problem of helium–degraded speech lies in the poor intelligibility of the speech uttered in high–pressured helium–oxygen atmosphere by deep sea divers. This speech is heavily distorted in the frequency domain primarily due to differences of acoustic properties in the high–pressured helium–oxygen gas. Moreover, it is considerably degraded by additional noise from life–support systems.

Some work has been done to improve the quality of helium speech. However, satisfactory results have not been achieved so far, partially because powerful methods like STFT have not been applied to accomplish a non–linear modification in the frequency domain.

This research intends to propose a new algorithm for enhancement of helium speech by using STFT techniques. The application of STFT on the problem is primarily motivated by intention to easily modify distorted frequency spectrum of helium speech in a non–linear way so that the modified version is closer to the frequency spectrum of the non–degraded original speech. Furthermore the STFT technique provides the possibility of a noise cancellation method with high performance.

21.19 Facial Parameterization for Low Bit Rate Video Conferencing

Jae S. Lim, Ramakrishnan Sundaram

The idea of developing an algorithm for the construction and reconstruction of a human image based on edge information for purposes of video conferencing is being studied. The ultimate goal is to achieve a drastic reduction in the amount of picture information required to be sent over a channel, thus reducing bandwidth without much loss in quality. The algorithm will exploit the connectivity of

the subimages of the human face, thus isolating each for independent edge detection.

Different edge detection schemes like the discrete Laplacian, Roberts' cross gradient, and transform methods are being studied and employed to get most effective detectors. Currently, work is being done on a continuous tone–gray level vertical face without glasses, beard, and moustaches. Those cases are likely to be looked into later.

21.20 Bottom Profile Determination in a Shallow Ocean

Alan V. Oppenheim, George V. Frisk,[12] Michael Wengrovitz

The problem of inverting reflected pressure field data from an acoustic point source in a shallow ocean to determine information about the bottom is being studied. Although there has been recent progress in this area, only the case of a deep ocean has been considered. The deep water case assumes that the reflected field consists only of components which are reflected from the bottom. In the shallow water case, it is necessary to consider the multiple reflections which occur from both the ocean bottom and the ocean surface. This requires the use of algorithms which dereverberate the reflected field data prior to use in an inversion scheme.

There are similarities between this problem and three other problems which have been studied. Iterative maximum likelihood dereverberation schemes have been proposed for use in the study of acoustic well–logging data from a borehole. It is hoped that some of these algorithms may be applicable to dereverberating reflected plane wave data as well as to the originally proposed cylindrical wave data. Also, in a separate study, a very fast algorithm to perform the Hankel transform was proposed. The Hankel transform relates the pressure field to the bottom reflection coefficient function in a deep ocean. This algorithm and other results which deal with removing singularities from the reflection coefficient function may also be applicable. Finally, there is a close relationship between principles involved in acoustic tomography and this problem. Recent progress in the development of inverse scattering algorithms for use in medical tomography may also be applicable to determining ocean bottom profile data from dereverberated scattered field data. This research will explore these and other new methods of inverting shallow ocean data to determine the characteristics of the underlying bottom.

---

[12]Woods Hole Oceanographic Institution

22. Speech Communication

Academic and Research Staff

Prof. K.N. Stevens, Prof. J. Allen, Prof. G. Fant,[13] Prof. M. Halle, Prof. S.J. Keyser, Prof. V.W. Zue, Dr. W. Cooper,[14] Dr. F. Grosjean,[15] Dr. S. Hawkins,[16] Dr. R.E. Hillman,[17] Dr. A.W.F. Huggins,[18] Dr. J. Jakimik, Dr. D.H. Klatt, Dr. L.S. Larkey, Dr. B. Lyberg,[19] Dr. J.I. Makhoul,[18] Dr. E. Maxwell, Dr. L. Menn,[20] Dr. P. Menyuk,[21] Dr. J.L. Miller,[22] Dr. J.S. Perkell, Dr. P.J. Price, Dr. S. Shattuck-Hufnagel, M. Hamada,[19] E.B. Holmberg,[23] S.-Q. Wang [19]

Graduate Students

C. Bickley, F. Chen, K. Church, S. Cyphers, C. Espy, R. Goldhor, D. Huttenlocher, L. Lamel, H. Leung, M. Randolph, C. Shadle, S. Steneff

---

[13] Visiting Professor

[14] Associate Professor, Department of Psychology & Social Relations, Harvard University

[15] Associate Professor, Department of Psychology, Northeastern University

[16] Assistant Professor of Communicative Disorders, Emerson College

[17] Assistant Professor, Department of Speech Disorders, Boston University

[18] Staff Member, Bolt, Beranek and Newman, Inc.

[19] Visiting Scientist

[20] Aphasia Research Center, Boston University

[21] Professor of Special Education, Boston University

[22] Assistant Professor, Department of Psychology, Northeastern University

[23] Department of Speech Disorders, Boston University

22.1 Speech Recognition

The overall objectives of our research in machine recognition of speech are (1) to develop techniques for incorporating acoustic–phonetic knowledge and knowledge of lexical constraints into speech recognition systems; (2) to carry out research aimed at collecting, quantifying, and organizing this knowledge; and (3) to develop prototype systems based on these principles. During the past year progress has been made on several projects related to those broad objectives.

22.1.1 Phonological Properties of Large Lexicons

A given language is constrained in terms of the possible ways that speech sounds or segments can be combined to form meaningful words. Knowledge about such constraints is implicitly possessed by native speakers of a given language. For example, a native English speaker knows that "vnuk" is not an English word. He/she also knows that if an English word starts with three consonants, then the first consonant must be an /s/, and the second consonant must be either /p/, /t/, or /k/. Such knowledge is presumably utilized by speakers of a given language in the process of speech perception, particularly when the acoustic cues of a speech sound are missing or distorted, and it would clearly be advantageous to incorporate knowledge of this kind into a speech recognition system.

We recently conducted a study of the phonotactic constraints of American English by examining the phonemic distributions in the 20,000–word Merriam Webster's Pocket Dictionary. In one part of this study we mapped the phonemes of each word into one of six broad phonemic categories: vowels, stops, nasals, liquids, and glides, strong fricatives, and weak fricatives. (For example, the world "speak", with a phonemic string given by /spik/, is represented as the pattern: [strong fricative] [stop] [vowel] [stop].) We found that, even at this broad phonetic level, approximately one–third of the words in a 20,000–word lexicon can be uniquely specified. If we define the "cohort" of a particular pattern as the set of words having that pattern, then the size of the cohort is the number of words having that pattern. (For example, the words "speak" and "steep" belong to the same cohort.) The average cohort size for the 20,000–woru lexicon was found to be approximately 2, and the maximum cohort size was approximately 200. In other words, in the worst case, a broad phonetic representation of the words in a large lexicon can reduce the possible word candidates to around 1% of the lexicon. Furthermore, over half of the lexical items belong to cohorts of size 5 or less. These results demonstrate that speech recognition systems can use broad acoustic–phonetic classifications of words to reduce the number of possible word candidates to a very small set. Such broad classifications can be performed more reliably than detailed phonetic recognition.

Phonetic variability is not evenly distributed across words and sentences. Certain segments of a word are relatively phonetically invariant, while others are highly variable. For example, the /n/'s in "international" cannot be deleted, while the /t/ and the reduced vowels can be. A set of experiments we are running indicate that the phonetically variable segments of a word provide much less lexical

constraint than phonetically invariant segments. That is, the phonetically variable parts of a word do not aid in differentiating it from other words in the lexicon. In one experiment we used a 6-class broad phonetic representation like the one in our original study. However, in this case, segments in unstressed syllables were ignored unless they were nasals, glides or strong fricatives. So, for instance, "international" would be classified as [vowel] [nasal] [nasal] [vowel] [fricative] [nasal] [glide], which does not depend on phonetically variable parts of the word. This classification scheme partitions the 20,000 word lexicon such that 47% of the words were in cohorts of size 5 or less, which compares favorably with the 54% obtained in the experiment described above. This result demonstrates that speech recognition systems can use broad phonetic classifications to find a small set of possible matching words, even in light of the high phonetic variability in natural speech.

22.1.2 Lexical Access

It is well-known that phonemes have different acoustic realizations depending on the context. Thus, for example, the phoneme /t/ is typically realized with a heavily aspirated strong burst at the beginning of a syllable as in the word "Tom", but without a burst at the end of a syllable in a word like "cat". Variations such as these are often considered to be problematic for speech recognition since they can be viewed as a kind of 'noise' that makes it more difficult to hypothesize lexical candidates given an input phonetic transcription.

In our view, the speech utterance is modeled in terms of two types of acoustic/phonetic cues: those that vary a great deal with context (e.g., aspiration, flapping) and those that are relatively invariant to context (e.g., place, manner, voicing). We have designed a recognizer to exploit variant cues by parsing the input utterance into syllables and other suprasegmental constituents using phrase-structure parsing techniques. Invariant constraints are applied in the usual way to match portions of the utterance with entries from the lexicon.

Only part of the proposed recognizer has been implemented. We have written a program to parse lattices of segments into lattices of syllables and other phonological constituents. Phonological constraints are expressed in terms of phrase-structure rules. For example, we could restrict aspiration to syllable initial position (a reasonable first approximation) with a set of rules of the form:

1. utterance --> syllable

2. syllable --> onset rhyme

3. onset --> aspirated-t | aspirated-k | aspirated-p | ...

4. rhyme --> peak coda

5. coda --> unreleased-t | unreleased-k | unreleased-p | ...

This sort of context–free phrase–structure grammar can be processed with well–known parsers like Earley's Algorithm. Thus, if we completed this grammar in a pure context–free formalism, we could employ a straightforward Earley parser to find syllables, onset, rhymes and so forth. However, it has been our experience that the context–free formalism is not exactly what we want ·· · this task. To serve this purpose, we have implemented a simple language of matrix (lattice) operations. This implementation appears to be easier to work with than many others.

22.1.3 Acoustic Cues for Word Boundaries

Words in continuous speech are rarely delineated by pauses. There are, however, acoustic cues indicating word and syllable boundaries, and knowledge of these cues often helps a listener or a speech recognizer to segment an utterance into words and syllables. For example. the /tr/ sequence in word pairs such as grey train and great rain have very different acoustic realizations although their phonemic transcriptions are essentially the same.

As a pilot study, we have investigated acoustic cues for word boundaries at labial stop–sonorant clusters, similar to the example given above. In this study minimal pair phrases were embedded in carrier sentences in order to enhance any differences between the members of the pairs. The phrases were constrained to provide identical surrounding context for the stop and sonorant under investigation. The format of the phrases was given by:

$$V(\#)\text{labial stop}(\#)\text{sonorant V},$$

where V represents a vowel and (#) an optional word boundary. In total there were 15 minimal pair phrases representing the clusters /bl/, /br/, /pr/, and /pl/, such as sheep raid versus she prayed and bay block versus Babe lock. Three male speakers recorded the minimal pairs in the carrier phrase was "I said – – – – not – – – – ." Each member of the minimal pair occurred in both the sentence medial and sentence final positions of the carrier phrase. The study indicated that:

—The sonorant is devoiced when in a cluster with an unvoiced consonant.

—The onset of a word–initial /r/ is more gradual than when the /r/ is in a cluster.

—Good measures to differentiate the minimal pairs include: voice–onset time, stop–gap duration, sonorant duration, and formant frequency measurements such as F_2 and $(F_2 - F_1)$ for / / and F_2 and F_3 for /r/.

A more extensive study of the acoustic cues for word boundaries is now being conducted. We will be concentrating on the thirty–odd allowable word–initial clusters in English and how the acoustic cues differ when a word boundary divides that cluster.

A supporting study is examining the statistics of allowable consonant clusters in word–initial,

word-final, and word-internal positions in words. These data will make it possible to determine the probability that syllable or word boundary occurs when a particular consonant sequence is detected.

22.1.4 Speaker-Independent, Continuous Digit Recognition

An acoustic-phonetically based continuous digit recognizer is being developed to study the utility of phonetic knowledge in a recognition system. The system is also intended to demonstrate a modular design, so that it can be expanded by modification of knowledge sources. The digit vocabulary was chosen because it forms a constrained task under which many coarticulation and prosody effects occur. This allows one to develop a system, in a constrained environment, which can handle many of the effects occurring in continuous speech. The recognizer will embody concepts found to be important when reading spectrograms. These concepts include using robust information, considering context, using multiple cues and checking for consistency, using acoustic knowledge for initial recognition and then using higher level knowledge to constrain the possibilities, and initially listing of all possibilities and then ruling some out based upon acoustic evidence. These ideas will be incorporated by structuring the system to combine robust, bottom-up information with syntactic and lexical top-down constraints.

The system is to be composed of modular components containing various types of knowledge. The types of knowledge may be acoustic, phonetic, phonological, and lexical. Each component is to be a separate unit which may be modified independently. This modularity will enable one to expand the system to larger vocabularies. The modular system under development is to serve as the framework upon which extensions to larger vocabularies can be made.

22.1.5 LAFS Recognition Model

A LAFS (Lexical Access From Spectra) network has been generated for the task of recognizing connected digits. It is hoped that this representation will be appropriate for speaker-independent connected digit recognition, but preliminary experiments indicate that the spectral distance metric initially proposed for LAFS (a weighted slope metric in the critical-band spectral domain) is not good enough for the task. Current research is directed at the discovery of better metrics.

22.1.6 Interactive Speech Research Facilities

As we mentioned earlier, part of our research goal is to describe and quantify the acoustic characteristics of speech sounds in various phonetic environments. Since such studies often involve the examination of a large body of data, it is essential that we provide a graceful, interactive environment for speech research.

Our research effort in speech recognition makes extensive use of an interactive research facility called SPIRE, developed at M.I.T. specifically for acoustic phonetic research. The SPIRE system draws heavily on the capabilities of a unique personal computer, called the Lisp machine, developed

at M.I.T.'s Artificial Intelligence Laboratory. The SPIRE system allows users to record, transcribe, store, and retrieve spoken utterances. Users are able to configure the high–resolution display to include spectrograms, spectral slices, transcriptions, LPC parameters, energy measures, and other parameters computed from speech. This is accomplished interactively with a pointer, which can also be used to allow a user to listen to sections of the speech, edit waveforms, examine data values, alter display options, and perform other functions.

In addition to SPIRE, an acoustic phonetic experimental facility is also being implemented. This facility, called SPIREX, provides an environment for speech researchers to formulate and execute complicated acoustic phonetic experiments. With the help of SPIREX, statistically meaningful results can be obtained in a convenient manner.

22.2 Auditory Models and Analysis Techniques

Our research on speech recognition and on perceptual correlates of phonetic features has led us to ask whether the relevant acoustic properties associated with phonetic categories might be represented in a more prominent fashion if the speech signal were first processed by a model of the peripheral auditory system. We are developing two such models that are designed to represent different temporal and spectral attributes of speech sounds. Both models process the speech through a set of bandpass filters with critical bandwidths. In one model, special attention is given to the response of the auditory system to signals exhibiting rapid frequency and amplitude changes. In the other model, the processing takes advantage of synchrony in simulations of nerve firing patterns to enhance formant peaks and to extract fundamental frequency.

An invited paper has been written reviewing the status of work on auditory modeling as it relates to models of speech perception. Conclusions were that critical–band filtering, or filtering with wider bandwidth low–frequency filters was a very good idea, but that the field is unsettled in that we do not know the importance of the time–locked aspect of neural encoding. This paper was presented at a conference in Stockholm.

22.3 Speech Synthesis

The formant synthesizer that is used for stimulus preparation in a number of perceptual studies has been rewritten in the language C in anticipation that the PDP-9 computer will be replaced by a newer machine. The synthesizer voicing source has been improved in flexibility by adding control parameters that govern the ratio of the open phase to the total period, the degree of rounding of the waveform corner at glottal closure, the amount of breathiness, and the amount of alternating jitter.

A 20,000–word phonemic dictionary has been hand–edited and converted to speech using a synthesis–by–rule program in order to verify the correctness of the pronunciations. Then an automatic pattern discovery program was used to try to find letter–to–phoneme rules in English.

Results suggest that simple pattern discovery procedures are not sufficiently powerful, and syllable parsing strategies are needed to discover appropriate rules for vowels.

Student projects have begun in the use of a text–to–speech system in a text editor for the blind and on synthesis of Japanese segments by rule.

22.4 Physiology of Speech Production

An overall aim of our work on the physiology of speech production is to develop models for the control of the various articulatory structures as they are manipulated to achieve a desired sequence of acoustic properties for an utterance. In the course of this research we are developing new techniques for the measurement of articulatory movements and for the analysis and processing of multi–channel articulatory data.

During the past year we have completed a cross–language pilot study of sources of variation in strategies for anticipatory coarticulation of lip rounding. A motivation for this work is to determine the extent to which different speakers use different strategies for producing anticipatory movement patterns for lip rounding depending on the language. Results of an experiment on lip retraction for "neutral" consonants occurring between rounded vowels show that variation in anticipatory movement patterns may be related to language–specific patterns of vowel diphthongization.

In collaboration with Dr. Winston Nelson of Bell Laboratories and Dr. John Westbury of the University of North Carolina we have completed a study on three subjects of repetitive jaw movements for speechlike and non–speech movement tasks. Results vary widely across subjects. One subject has movement patterns which appear to be governed by physical constraints at high repetition rates and factors related to speech–motor control skill (such as the possible use of auditory feedback) at lower rates. For this subject there appears to be a region in which both types of influences could be interacting with one another, at about 4 Hz. Movement patterns for the other two subjects suggested that they were less capable of approaching these boundary conditions, perhaps because they were less "skilled" at performing the rather unusual task. Techniques are being developed to explore these findings further.

In collaboration with Dr. Robert Hillman and Ms. Eva Holmberg at Boston University, we have begun work on a project on the use of non–invasive aerodynamic and acoustic measures to study hyperfunctional and other types of voice disorders. Techniques have been worked out to record intra–oral air pressure, oral air flow and the acoustic signal in a way which enables us to derive a number of indirect measures of vocal function. Data processing algorithms have been developed for determining glottal resistance to air flow, vocal efficiency, and parameters derived from the glottal air flow waveform (with the use of inverse filtering). Initial results on normal subjects show substantial agreement with the work of others and with aerodynamically and acoustically based theory. Manipulation of pitch is reflected in changes in parameters describing the shape of glottal air flow

waveforms, and manipulation of loudness is reflected in parameters related to pulmonic driving forces and *force of vocal-fold adduction. There were also results that were inconsistent with previous work,* and these will be explored further.

In a related study, an inverse filtering technique has been used to observe differences in glottal waveforms of normal, creaky, and breathy vowels as spoken at different pitches by two female and two male talkers.

Progress has been made in the development of an alternating magnetic field transducer system for simultaneous tracking of movements of several midsagittal-plane points inside and outside the vocal tract. A new, considerably smaller (4 mm x 5 mm x 2 mm) biaxial, tilt-compensating transducer-receiver has been designed and built and is being tested. The design of high-quality transmitter and receiver electronics has been worked out and a full prototype is under construction.

Physiological data processing software has been enhanced considerably. The functionality of blocked-data type of processing has been increased to include ensemble averaging, sequence plotting and interactive extraction of time and frequency-domain data. Increased programmability now makes the blocked-data signal processor an extremely flexible and useful tool for data processing and extraction. Software for the processing of simultaneous acoustic and palatographic data has been developed and is near completion.

22.5 Acoustics of Speech Production

Acoustical theories of speech production are generally based on a source-filter model. In the simplest version of the theory the source is either the quasi-periodic glottal air flow or is an aperiodic source resulting from turbulence in the flow in the vicinity of a constriction or obstacle. Recent theoretical and experimental studies have been leading to a more adequate description of these sources and of the interaction between the sources and the acoustics of the vocal tract. As a part of his activities during his visit to M.I.T., Gunnar Fant carried out detailed theoretical studies of the glottal waveform, its interaction with the supraglottal tract, and its variation with frequency. This theoretical work was based in part on experimental data collected at Dr. Fant's laboratory in Sweden.

Studies of the characteristics of turbulence noise sources in speech production have been initiated with a series of measurements of the spectrum of sound that is generated when air is passed through mechanical models containing constrictions. The measured sound spectrum is compared with the spectrum that is calculated for an ideal model with an idealized pressure or velocity source located at various points in the vicinity of the constriction. The aim of these studies is to determine how to represent the source characteristics for turbulence noise in speech, including the distribution of the sources in the vocal tract, the spectrum of the sources as a function of position, and the interaction between the sources and vocal-tract acoustics.

22.6 Speech Production Planning

We continued to test a speech production planning model against predicted patterns in both spontaneous and experimentally-elicited speech errors, asking two questions:

1. What are the planning units (as reflected in error units) and how are they represented (as reflected in consistent similarity constraints linking target elements with the intrusions that replace them)?

2. Are there several separate steps in the planning process (as reflected in differences in the constraints governing the interaction of two elements)?

Observations so far suggest the following points:

1. At least one serial-ordering mechanism operates over individual phonemic elements; errors like "lip yoke" -> "yip loke," involving single phonemic segments, are substantially more common than errors involving individual features or syllabic components like – VC or CC – .

2. Phonemically similar elements (like p/f) are more likely to interact than are phonemically dissimilar ones (like g/m), suggesting that the planning representation captures those facts at the point where segmental errors occur.

3. While one planning process is sensitive to errors at all word locations, a second process is apparently protected against errors in word-final position. This second mechanism comes into play when well-formed phrases (rather than lists) are planned. Thus, errors like "leap note -> [nip lot] and -> [lit nop] are both common, but when these words are embedded in phrases ("From the leap of the note"), word-final errors are rare.

4. The segment-serial-ordering mechanism is significantly more likely to confuse two word-initial segments (as in "July dog") than two stressed-syllable-initial segments (as in "largesse dog"). Moreover, these two similarity factors do not interact, again suggesting two separate error-prone mechanisms.

Ongoing experiments and analyses are addressed to three further questions: (1) Does the similarity of adjacent contextual elements affect the likelihood that two segments will interact in an error, e.g. will there be more f/p interactions in "fad pan" than in "fad pin"? (2) Do different error types, like exchanges and substitutions, occur under different similarity constraints, suggesting that they reflect two separate planning mechanisms? (3) Do function words (prepositions, pronouns, wh-words, etc.) participate in segmental errors with content words, or are they processed separately?

In addition, a range of error elicitation methods have been developed, from sentence generation based on triplets of specified words, through recitation of nonsense syllable strings from memory.

The trade-off between (a) experimental control of the phonemic shape of an utterance, and (b) elicitation of normal speech planning, will permit more fine-grained analysis of the differences among error types and thus presumably among separate processing mechanisms.

22.7 Studies of Acoustics and Perception of Speech Sounds

One aspect of our research is concerned with the study of the acoustic and perceptual correlates of various phonetic features. We are interested in delineating the acoustic properties used by listeners in identifying various classes of speech events, and in determining the extent to which these properties are influenced by phonetic context. During the past year we have been examining several of these features.

In one study we have been measuring the acoustic properties of [ℓ] and [r] (in English) in various phonetic contexts, including prestressed, poststressed, and intervocalic, and the influence of these consonants on adjacent vowels. The acoustic properties that we have examined include the formant frequencies during the vowel or consonant and measures of the abruptness of onset at the release of the consonant (greater for [ℓ] than for [r]). Another continuing project has been concerned with the acoustic and perceptual correlates of the feature nasal for vowels, and with the development of procedures for acoustic analysis of nasal vowels. Nonnasal-nasal continua for several vowels have been synthesized by inserting a pole-zero pair in the vicinity of the first formant, and listener judgements of these stimuli (using listeners from several language backgrounds) have helped to establish the acoustic property that distinguishes between nasal and nonnasal vowels. A study of the perception of synthetic syllables arranged along a continuum from [ba] to [wa] has supported previous results that the listener identification of these syllables is influenced by vowel duration as well as by acoustic characteristics at syllabic onset. An acoustic investigation of the fundamental frequency (F_0) changes in the vowel immediately following the release of voiced and voiceless stop consonants in Japanese has shown that the influence of the voicing characteristics of the consonant in F_0 of the vowel is similar to that observed in English and some other languages. A report on a study of the effect of burst amplitude on the perception of place articulation for stop consonants has been completed and submitted for publication.

Our continuing research on the acoustic and perceptual correlates of distinctive features is leading us to revision of our theoretical views concerning the question of invariant acoustic properties associated with distinctive features. We are recognizing the importance of redundant features and the role they play in enhancing the acoustic properties that signal the distinctive feature. During the past year we have been attempting to elaborate a theory that incorporates this concept of distinctive features being associated with redundant or enhancing features. This work has involved collecting examples of the operation of these enhancement features in a variety of languages.

Our investigations of speech acoustics and perception have included studies of prosody as well as segmental factors. An investigation of the influence of fundamental frequency on the comprehension

of sentences is being carried out using a technique in which the F_0 contour of a sentence is manipulated without modifying the segmental aspects of the sentence. Results show that a "normal" F_0 contour leads to a faster comprehension of the sentence than a flat, monotone contour. Current research is aimed at identifying what aspects of the F_0 contour are most salient for the listener.

Another study of perception has been concerned with the formulation of procedures for determining perceived phonetic distance between speech sounds. A Bachelor's thesis has been completed on the perceived phonetic distance between vowel–like synthetic stimuli similar to [i]. Stimuli varied in formant frequency locations, formant bandwidths, spectral tilt, and degree of nasalization or addition of an extra formant peak between F_1 and F_2. Results are consistent with previous research in showing that formant frequency motions are more important in determining perceived phonetic distance than are other stimulus changes. In addition, the splitting of the first formant into two peaks was phonetically quite salient.

22.8 Speech Processing in Children and Older Subjects

Our studies of normal speech production and perception in adults have led us to examine certain aspects of the development of these capabilities in children, and to examine possible changes in these capabilities in the normal course of aging. One project has been initiated to investigate the speech production and speech perception of normally–developing and speech–delayed children, ages 4–6 years. For the speech–delayed children, the study will integrate phonetic and phonological data with data on the perception of misarticulated sounds, while the normal children will be used as control subjects. Another project, being carried out in collaboration with the Communications Biophysics group and with Children's Hospital in Boston, is using acoustic data on the formant frequencies for vowels to examine the development of vowel categories in the production of children. The children are in an age range where they are developing their first few words, and the data show that for most children the open–close distinction is achieved before the front–back distinction. Another study, in collaboration with H.J. Simon at the V.A. Medical Center in Martinez, California, showed that aging has significant influence on the processing of temporal cues in speech.

23. Linguistics

Academic and Research Staff

Prof. A.N. Chomsky, Prof. J.A. Fodor, Prof. M.F. Garrett, Prof. K.L. Hale, Prof. M. Halle, Prof. J.W. Harris, Prof. S.J. Keyser, Prof. R.P.V. Kiparsky, Prof. J.R. Ross

Graduate Students

D. Archangeli, M. Baker, A. Barss, M. Browning, N. Fabb, E. Falk, N. Fukui, I. Haik, K. Johnson, M.-Y. Kang, J. Kisala, J. Levin, L. Levin, M. Magnus, R. Manzini, D. Massam, M. Montalbetti, W. Poser, P. Pranka, D. Pulleyblank, T. Rapoport, M. Rappaport, A. Rochette, S. Rothstein, M. Saito, J. Simpson, M. Speas, R. Sproat, L. Travis, E. Walli, J. Wager

Morris Halle

The ultimate objective of our research is to gain a better understanding of man's mental capacities by studying the ways in which these capacities manifest themselves in language. Language is a particularly promising avenue because, on the one hand, it is an intellectual achievement that is accessible to all normal humans and, on the other hand, we have more detailed knowledge about language than about any other human activity involving man's mental capacities.

Scientific descriptions of language have for a very long time followed a standard format. A number of topics are almost invariably discussed; for example, pronunciation, the inflection of words, word formation, the expression of syntactic relations, work order, and so forth. Moreover, the manner in which these have been treated has also been quite standard. While traditional grammars have many shortcomings, their great practical utility is beyond question; generations of students have acquired adequate command of innumerable languages with the help of grammars of the standard type. A plausible inference that might be drawn from this fact is that languages are somehow not very different from one another and that the traditional standard format has succeeded in capturing essential aspects of what all languages share in common. Accordingly, much of the research of the group has been devoted to studying the common framework that underlies different languages, the general principles that are exemplified in the grammar of different languages. Results strongly indicate that this assumption is indeed correct as far as the linguistic evidence is concerned.

The preceding discussion leads quite naturally to the question, "What evidence from outside of linguistics might one adduce in favor of the hypothesis that all languages are constructed in accordance with a single plan, a single framework?" It seems to us that the most striking evidence in favor of the hypothesis is, on the one hand, the rapidity with which children master their mother

tongue, and, on the other hand, the fact that even a young child's command of his mother tongue encompasses not only phrases and utterances he has heard but also an unlimited number of phrases and utterances he has not previously encountered. To account for these two sets of facts, we must assume that in learning a language a child makes correct inferences about the structural principles that govern his language on the basis of very limited exposure to the actual sentences and utterances. In other words, we must assume that with regard to matters of language a child is uniquely capable of jumping to the correct conclusions in the overwhelming majority of instances, and it is the task of the student of language to explain how this might be possible.

A possible explanation might run as follows. Assume that the human organism is constructed so that man is capable of discovering only selected facts about language and, moreover, that he is constrained to represent his discoveries in a very specific fashion from which certain fairly far-reaching inferences about the organization of other parts of the language would follow automatically. If this assumption is accepted, the next task is to advance specific proposals concerning the devices that might be actually at play. The obvious candidate is the theoretical framework of linguistics for, while it is logically conceivable that the structure of language might be quite distinct from that of the organism that is known to possess the ability to speak, it is much more plausible that this is not the case, that the structures that appear to underlie all languages reflect quite directly features of the human mind. To the extent that this hypothesis is correct – and there is considerable empirical evidence in its favor – the study of language is rightly regarded as an effort at mapping the mysteries of the human mind.

Additional detailed information on various projects connected with this research is available through inquiry to the department head, Dr. Samuel J. Keyser, Room 20D-105, Ext. 4141.

24. Cognitive Information Processing

Academic and Research Staff

Prof. W.F. Schreiber, Prof. D.E. Troxel, Dr. C.W. Lynn, G. Chambers, C. Konrad, M. McIlrath, Dr. K.P. Wacks, R.H. Walker

Graduate Students

R.P. Bishop, R.R. Buckley, G.J. Bunza, Y-M. Chao, R.S. Damon, A. Garcia, P-Q. Hoang, W. Hofmann, M. Isnardi, M.M.A. Khan, E.A. Lee, D.S. Levinstone, J. Lofton, E. Peynard, L. Picard, J. Sara, J-P. Schott, G. Vachon, R.E. Velez

24.1 Picture Coding

Donald E. Troxel, William F. Schreiber

a. Sampling and Reconstruction

Most present–day picture coding is digital; virtually all input and output images are analog. Thus, the conversion from one form to the other is everpresent and important to the quality and efficiency of the overall process. To elucidate the phenomena involved, a systematic study was carried out of a wide variety of pre–sampling and interpolation filters. It was found that, as suspected, the "ideal" low–pass filter was far from best, subjectively, since the least rms error criterion is invalid for human observers. Aliasing resulting from "violation" of the sampling theorem is visually traded off against sharpness and visibility of the sampling structure which occurs with other filters. Several filters studied performed substantially better that the ILPF. The best combination of performance and computational simplicity was found in the "sharpened Gaussian" filter, which has an impulse response not unlike that of human vision.[1]

b. Differential Pulse Code Modulation

This most common of image data compression systems has been widely studied. Its performance depends in marked degree on the characteristics of the signal source, since the presence of very sharp transitions requires an unfavorable trade–off between slope overload and the granular noise which occurs in blank areas. Nevertheless, when this factor is carefully taken into account, we have gotten good results with a form of DPCM in which the companding characteristic is adaptively adjusted to local image properties. In speech coding effective adaptation is possible based only on the coded signal. Because of the isotropic character of vision and images, this is not possible – extra data must be transmitted. Even including this extra data, we have obtained nearly "original" quality at 2.2 bits/pel, non–statistical, and 1.5 bits/pel statistical.[2]

c. Two–channel Coding System

For a number of years we have studied a picture transmission system in which the signal is divided into two channels, a two–dimensional low–pass signal ("lows") which is coarsely sampled and finely quantized, plus the remainder ("highs") which is finely sampled and coarsely quantized with the aid of a tapered randomized quanitizer.[3] While this can be thought of as a crude form of transform coding, the two– or three–channel approach permits tailoring the separate channel coding parameters to well–known human visual properties. While the performance of the non–adaptive version of this system is not as good as the adaptive DPCM system mentioned above, it does feature rather simple implementation and excellent (PCM–like) performance in the presence of channel errors. Under a grant from the Sony Corporation, a real–time hardware system was implemented.[4]

d. Adaptive Two–channel Color Coding System

The above–mentioned system can be substantially improved by adapting the highs quantization to the local signal properties. Blank–area signal–to–noise ratio of 50 db at about 3 bits/pel is possible in most cases. The system is extended to color coding by transmitting a three–color lows signal plus an adaptively–companded achromatic highs signal. The color lows signal is further compressed by mapping to a perceptually uniform color space, akin to the Munsell system of subjective color notation. Excellent quality full color images are possible at four bits/pel, compared with 24 for the uncoded signal. Further compression is possible by statistical (entropy) coding of the two–channel coder output.[5]

e. Randomized DPCM

We have also studied the application of pseudorandom (PRN) noise to the DPCM quantizer. Unlike previous efforts to apply PRN to DPCM, we chose to apply the noise directly to the quantizer inside the feedback loop. The application of PRN greatly reduces the most prominent artifacts of DPCM and allows greater freedom in the choice on the nonlinear quantizer so that slope overload can be reduced.[6]

References

1. J.N. Ratzel, "The Discrete Representation of Spatially Continuous Images," Ph.D. Thesis, Department of Electrical Engineering and Computer Science, M.I.T., August 1980.
2. A. Zarembowitch, S.M. Thesis, Department of Electrical Engineering and Computer Science, M.I.T., 1981.
3. D.E. Troxel et al., "Bandwidth Compression of High Quality Images," presented at the International Conference on Communication, 31.9.1–31.9.5, June 1980.
4 D.E. Troxel et al., "A Two–Channel Picture Coding System: I – Real Time Implementation," IEEE Trans. on Comm. COM–29, 12, 1841–1848 (1981).
5. W.F. Schreiber and R.R. Buckley, "A Two–Channel Picture Coding System: II – Adaptive Companding and Color Coding," IEEE Trans. on Comm. COM–9, 12, 1849–1858 (1981).

6. D.E. Troxel, "Application of Pseudorandom Noise to DPCM," IEEE Trans. on Comm. COM-29, 12, 1763-1767 (1981).

24.2 Digital Wirephoto[24] System

Associated Press (Grant)

Donald E. Troxel, William F. Schreiber

In previous reports, we have discussed the system we developed for the Associated Press for transmitting pictures to newspapers. This comprises cost–effective Laserphoto[23] facsimile transmitters and receivers and a computer-based image processing system (Electronic Darkroom) which permits automatic transmission and reception of pictures over many different channels, conversion between different Wirephoto scanning standards, and simultaneous editing (enlargement, reduction, cropping, combining, filtering, tone scale transformation, caption writing, etc.) of stored images. In this last year of the project, we have continued to improve the system reliability and performance. The major project was the development of a device which automatically overprints the computer file name onto facsimile pictures as they are simultaneously received by the computer and a local facsimile receiver. This greatly reduces the load on the computer system by eliminating the need to automatically retransmit ID or identification copies to enable the photographic editors to easily associate pictures with their computer file names.[1]

References

1. R.S. Damon, "An Automatic Name Generator for Laserphoto Machines," S.M. Thesis, Department of Electrical Engineering and Computer Science, M.I.T., August 1982.

24.3 Graphic Arts Applications

William F. Schreiber, Donald E. Troxel

The vast majority of pictures produced every day are made on printing presses. The printing industry is one of the largest in the country – five times as large as radio and TV broadcasting, and three times as large as the semiconductor industry. This industry is undergoing a true revolution in technology based on electronics and computers. For this and other reasons, our activities in recent years have been focussed on understanding and improving the complicated chain of processes used to translate images of natural scenes, or man–made graphics, into printed pages. This orientation affects our activities in a number of ways:

---

[24]Trademark of the A.P.

1. Our sponsors generally plan to use the products of our research and development in daily production. Thus, the systems must be practical, reliable, and cost-effective.

2. Graphic arts images are of very high quality compared to those usually used by computer image processors. This requires careful attention to certain factors, such as tone reproduction, not always considered of great importance. High quality also implies very large amounts of data to be processed.

3. The images we deal with are intended for human viewing, and the systems we design are always operated by people. Human perceptual and operational capabilities are central to our work.

The principal operations which must be performed are the scanning and editing of individual page components, the selection and arrangement of elements on the page (composition, often erroneously called pagination), the arrangement of pages on the sheet (imposition), and the control of machines which make printing plates for letterpress, offset, and gravure printing.

24.4 Automated Engraving of Gravure Printing

Providence Gravure, Inc. (Grant)
William F. Schreiber, Donald E. Troxel

Gravure printing is characterized by high platemaking costs but inexpensive and very stable operation of the printing press. Thus it is suited primarily to long runs, particularly of color work, of both high and low quality. Substantial economic benefit would accrue from reducing the cost and time required to prepare printing cylinders, perhaps even making it practical to extend gravure printing to certain very significant applications such as daily newspapers.

In the system under development, all photographic steps between the original copy and the cylinder are eliminated by scanning into a computer system. Pictures are interactively edited, and then all components for each page are assembled into a single disk file. Cylinders are engraved directly from computer storage. (In other forms of printing, four color separation films would be made for each page instead.) Imposition and correction for ink and paper are performed in "real" time simultaneously with engraving.

The differences between this system and other existing pre-press systems include substantially reduced storage requirements due to data compression, high cost-effectiveness, the elimination of the need for the operators to have long experience in color printing, a high-speed page composition system, and the ability to perform multiple tasks at the same time. A significant project completed this year was the development of an interactive silhouetting system.[1] Considerable improvement in the representation of line art has been made.[2] The monochrome version of the system is in regular daily production, while the color system is under development.[3]

References

1. L. Picard, "Interactive Picture Segmentation," Ph.D. Thesis, Department of Electrical Engineering and Computer Science, M.I.T., June 1982.
2. J. Sara, "Low Resolution Multi-Level Representation of Bilevel Images," S.M. Thesis, Department of Electrical Engineering and Computer Science, M.I.T., April 1982.
3. D.E. Troxel et al., "Automated Engraving of Gravure Cylinders," IEEE Trans. on Systems, Man and Cybernetics SMC-11, 9, 585-596 (1981).

25. Custom Integrated Circuits

Academic and Research Staff

Prof. J. Allen, Prof. L.A. Glasser, Prof. P. Penfield, Prof. R.L. Rivest, Prof. G.J. Sussman, Dr. H. Shrobe, Jr.

Graduate Students

R. Armstrong, I. Bain, Y. Brown, W.H. Evans, L.P.J. Hoyte, A. Fujimura, M.D. Matson, S.P. McCormick, J.J. Paulos, J. Pineda, L.D. Seiler, J. Siskind, B.C. Williams, J.T. Wroclawski

25.1 Conversion of Algorithms to Custom Integrated Circuits

Jonathan Allen, Paul Penfield, Jr., Ronald Rivest, Gerald Sussman, Howard Shrobe

The design of custom integrated circuits is an instance of the more general problem of the design of complex systems. Certainly if circuits are to be designed that contain between half a million and a million transistors, then techniques for the design of complex systems must be introduced that will assure quick, correct, and economical construction of the fabricated circuits. The established means of dealing with this complexity is to break up the problem into a number of subproblems, each of which can be tackled relatively easily. We also look for regularity in each of these components, so that basic circuits can be repeated many times in a regular array in order to achieve the desired functionality either in terms of arithmetic and logic function or memory. This breaking up of the overall task corresponds to the introduction of structural hierarchy, and visual inspection of contemporary large integrated circuits readily reveals the constituent blocks of this hierarchy. Use of regular structures such as memory, programmed logic arrays, register files, and iterative multiplier arrays makes the number of distinct circuits present in the overall circuit small enough so that substantial design effort can be devoted to each such circuit. There is an additional hierarchy, however, that is orthogonal to the structural hierarchy. This second hierarchy deals with the various qualitatively distinct kinds of representation that must be maintained over all levels of the design. Thus the design representations must range from a functional specification, through architectural representation to logic, circuits, devices, and a detailed geometrical layout specification which is suitable for mask making. It is striking that these different levels of representation are qualitatively different, and yet they must all be aligned to the same basic circuit since they describe in each case some limited aspect of the same overall design. The designer's job is complicated by the need to fully specify all these different levels of description, and yet keep them consistent with each other. For this reason, much of our emphasis in this project is focussed on careful choice of representations at all

these different levels together with the algorithmic means to transform between them.

At the functional level, much of our effort has been devoted to a variety of ad hoc languages for various applications. Thus we have devised high level languages for microprocessor type architectures, as well as languages intended to capture the semantic content of digital signal processing algorithms. As yet, little effort has been expended on a more generalized language, but as the other design tools under investigation become more mature, we are abstracting on the individual languages to design a powerful high level functional specification language. A major emphasis of our research is to introduce within such high level languages the means to perform architectural exploration. We have known for some time the formal requirements necessary to perform space/time trade-offs in a way that preserves the original functional specification. We are now exploring means to introduce into high level languages the linguistic means to perform these trade-offs. In the literature, despite the presence of several high level languages, no such means is currently available, yet the means to increase or decrease the amount of parallelism in a design is clearly an important degree of freedom present to the designer of custom integrated circuits. There exist many different algorithms, especially in the signal processing field, where the amount of parallelism available in the algorithm has not been completely exploited in hardware at this time, so we expect that this capability will be very useful in many applications.

The design of specific circuits has given rise to a number of regular designs such as programmed logic arrays, multipliers, and register arrays. We have devised a number of techniques for abstracting on this experience in order to lessen the overall design burden of optimized circuits. Many approaches to silicon compilation have focussed on general techniques to cover a broad class of architectures. It has become clear to us, however, that there is a strong need for specialized compilers that can provide a degree of efficiency in space, time and power that is simply not attainable in the general case. One example of a specialized compiler is a PLA generator, and several of these have been developed by numerous investigators. Nevertheless, most of these PLA generators have only been able to deal with one particular technology in a particular set of design rules. We have implemented a new style of PLA generator which is capable of learning from example in terms of different technologies, circuit styles, and design rules. In order to use such a technique, the designer uses an interactive graphic system to specify a two-input, two-product term, and two-output programmed logic array which serves as an exemplar for all other possible programmed logic arrays corresponding to this style. Thus the designer may wish to specify NMOS or CMOS technology, two-phase or three-phase clocking, input encoding, output multiplexing, precharging, and other aspects of the design. This is easily accomplished by specifying these features in the exemplar design. These designs are built up readily from a number of cells contained in a library, although additional cells can easily be added to this library at any time. The designer then instructs the system to create a compiler for this style of programmed logic array, and this is quickly accomplished by the computer system. From then on, the designer may specify the logic for any size PLA in the style of the exemplar and this will be appropriately created. It will, of course, enjoy the

efficient design provided by the individual cells, and lead to a highly packed dense design. It is interesting that the technique just described amounts to the development of a compiler compiler, and we believe that such techniques are exceedingly powerful because they provide both highly efficient designs but also a great deal of flexibility from the point of view of the designer. We are currently working on the introduction of more flexible control structures within these compiling strategies that will provide even further increases in flexibility while preserving the optimal properties of these circuits.

Another example of our development of specialized compilers is in the area of multipliers. As the result of a substantial effort in the design of a custom integrated circuit for signal processing, a large parallel multiplier using modified Booth's recoding was designed. This was a highly regular design, and suitable for composition from a small number of distinct cells except for the final carry propagation stage which must be generated procedurally. Once again we have developed a compiler for this style of circuit. The designer merely specifies the size of the multiplier and multiplicand, and the overall layout is immediately generated. In this way a huge amount of circuit design time is saved, and yet the design is very compact and fast. This illustrates the fact that specialized compilers can yield designs that are far more efficient than those which would be generated by any more general capability. Under development is a third type of compiler that would provide for the generation of arbitrary size floating point units. The designer will be able to specify both the kinds of floating point functions that are required as well as the field sizes for both the exponent and mantissa of the floating point representation. Additionally, this design will utilize asynchronous timing techniques so that the completion time of the arithmetic operation can be readily detected. We view these techniques as exceedingly valuable, since they also provide the designer with the means to explore space/time trade-offs in terms of complexity of the arithmetic logic unit vs. the amount of memory needed on chip. When one compares fixed point representations with floating point representations, it is readily apparent that while fixed point arithmetic is relatively simple, the amount of memory needed to store such numbers is greater than for floating point numbers for the same signal to noise ratio, although the latter must utilize more complicated arithmetic units.

We have continued to develop a highly accurate circuit extraction scheme which operates on layout parameters and provides the input specification for circuit simulation. The circuit extraction techniques used contemplate modern high density designs, in that they allow for internodal capacitances as well as capacitances to the substrate. Also resistances of any shape can be readily extracted, and no less than three different techniques are employed for computing the resistances of varying size conductors. The program that accomplishes this task is written in a way that is technology independent, and a default mode readily obtains the topology of the circuit in a form that is useful for unit delay logic simulation. When complete circuit simulation is not possible, then it is appropriate to try to bound the delay through various parts of the circuit through a variety of modeling techniques. We have explored the use of fundamental characterization of nonlinear circuits for this purpose, and have already obtained very tight bounds for the propagation time through tree-like

interconnect networks. Current modeling activities are being applied to circuits involving active devices.

For some years now, a major emphasis of our work has been the development of a general capability for placement and routing of arbitrarily sized rectangular components with interconnect on all four sides. General routing strategies have been developed using a two-pass process. In the first pass, the global routing strategy is developed without concern for track utilization within a particular channel. This design is largely topological in nature, but in the second pass the detailed way in which the wiring nets are assigned to channel tracks is determined in optimal fashion. These techniques have been developed to a very high degree, and high performance channel routers have been one of the by-products of this research. Current emphasis is focussed on the development of placement strategies, although there is a great deal of understanding of this problem from our previous theoretical investigations. This approach to the placement and routing of rectangular components is completely algorithmic in nature, and does not require interaction on the part of the designer. We recognize, however, that in many cases it may be appropriate to use specialized routing procedures, just as specialized compilers are used for the layout of the individual cells. For example, a specialized river router can be rather easily constructed which can be used interactively by the designer to produce highly efficient layouts. A variety of these routers are under construction and are utilized in a way that is complementary to the overall placement and routing strategy.

While the integrated circuits under design are in themselves highly complex, another aspect of *complexity in integrated circuit* design is the nature of the tools and algorithms themselves. Thus, almost all of the artwork analysis tools that are used have performances dependent on the number of rectangles that must be manipulated, and in a large design several million rectangles would have to be contemplated. Thus it is important to be able to focus effectively on techniques for dealing with this amount of data, and two techniques have emerged. On the one hand, it has been possible to improve the algorithms themselves by decomposition techniques into modular cells which can be composed later to form the overall design. We have also been interested in the introduction of special purpose hardware for integrated circuit design. Our first example of these procedures has been the design of special purpose hardware for design rule checking. A single printed circuit board has been designed which utilizes a conventional microprocessor together with four distinct custom integrated circuits for performing course grid type design rule checking of rectangular and 45 degree oriented line designs. This special hardware provides a speed-up of over two orders of magnitude, and is the first such design to be demonstrated in the field. It can be plugged into a work station and thus provide very aggressive performance for interactive use by a designer, particularly on very large designs. We intend to extend our study of the use of special purpose hardware, particularly for such applications as the operations of linear algebra, which are of use both for signal processing and for circuit simulation. We believe that circuit simulation is an exceedingly useful capability, but it is often not used because it is so expensive computationally. Thus the introduction of special purpose hardware would provide this highly useful capability in a much more attractive form.

It is clear from the above discussion that we have attacked a number of the constituent problems of the overall integrated circuit design problem. We are also concerned with the integration of these techniques into a cohesive framework. New work focuses on the utilization of the aforementioned special purpose compilers in a format that maintains technological independence but also the capability for constraining designs to given levels of electrical circuit performance. Optimal design is certainly the result of simultaneous satisfaction of a number of different constraints at all the qualitatively distinct levels of the design hierarchy. The control structures under which this can be accomplished are currently under investigation in the context of high level hardware design languages. We feel that we have benefited a great deal from the implementation of a variety of special purpose solutions to these problems and are now ready to incorporate them in a more general structure.

Publications

Rivest, R.L., "Benchmark Channel-Routing Problems," M.I.T. VLSI memo No. 82-77, February 1982.

Rivest, R.L. and C.M. Fiduccia, "A 'Greedy' Channel Router," Proceedings 1982 Design Automation Conference, June 1982.

Rivest, R.L., "The 'PI' (Placement and Interconnect) System," Proceedings 1982 Design Automation Conference, June 1982.

Evans. W. H. and J. Allen, "MOS Implementations of TTL Architectures: A Case Study," Proceedings IEEE International Conference on Acoustics, Speech, and Signal Processing, May 1982.

Seiler, L., "A Hardware Assisted Design Rule Check Architecture," Proceedings 1982 Design Automation Conference, June 1982.

25.2 A Circuit Theory for Digital VLSI Systems

Lance A. Glasser, Paul Penfield, Jr., Isaac Bain, Charles Zukowski

VLSI circuits are complex nonlinear dynamical systems which seem beyond the domain of most classical network theories. The basic laws of electrostatics – Kirchov's voltage and current laws – hold, but many of the more powerful tools available for linear networks, such as LaPlace transforms, do not. The thrust of our effort is the development of new theories specialized to the realm of VLSI circuits.

The explosive growth in the number of devices in a VLSI circuit and the increased complexity of device models have combined to make the simulation of very large scale circuits extremely costly and, in many cases, almost impossible. We have introduced a technique, called waveform bounding, which addresses this problem. The key observation is that it is sometimes adequate to obtain approximate rather than exact results, provided one understands the magnitude of the uncertainty. Often this can allow one to answer exactly the sort of questions one regularly asks of a circuit simulator, such as, "is this critical path fast enough?" Thus, if the bounds on the delay through a

network are such that if the delay is greater than 55 ns and less than 65 ns, then we can say with certainty that, if the path meets a 70 ns specification and fails a 50 ns specification, more accurate and costly simulation techniques must be used.

Such a technique is only worthwhile if the computer time needed to simulate a VLSI system can be reduced. Preliminary results show that several important circuit simulation problems can be vastly simplified given the freedom to obtain approximate rather than exact answers. These problems include linear RC trees, an interconnect circuit commonly found on MOS VLSI chips; and nonlinear MOS logic gates.

Work in this area now has two thrusts. One is to find new and more general classes of networks to which we can apply our theories; and the second is to improve and tighten the bounds on the networks we can solve. When combined with other circuit simulation techniques being developed in the community, this work may one day form the basis for a powerful new generation of circuit simulation programs.

While a VLSI system might contain millions of transistors, these devices are not, and cannot, be put together in an *ad hoc* manner. Design methodologies, which are self imposed restrictions on the design techniques one will use, limit the number of archetypical circuit forms in a VLSI system. One can conceptualize these circuit forms as being the language in which the design is composed. Like any language it has its correct forms of usage and its incorrect forms. We have research efforts in two aspects of this problem. The first is developing a circuit design language suited to MOS VLSI design which captures the designer's intent. The second is a set of tools for checking the syntactic correctness of designs composed in this language. One problem is that there are many different dialects of the language which one would like to use, depending on the capabilities of the technology and the performance objects of the design. Thus, we are developing a set of computer programs to check a circuit, as it is being composed, for the design methodology under use. Part of the task is to include an easy way to spe   this design methodology. A methodology checker which was specifically designed for a single specific design methodology was written by Clark Baker. Our objective is to generalize this concept so the methodology checker can continue to be used as technology and circuit techniques mature.

25.3 Very Large Scale Integrated Circuit Research

Lance A. Glasser, Mark Matson

A VLSI system can be optimized in many different domains of abstraction including the domains of machine organization, logic design, circuit design, and layout. This project is specialized to various aspects of optimization in the circuit domain. Two important types of optimization, are considered. In

the first we are interested only in raw speed, without regard to power or area resources. The problem here is to design a circuit which runs as quickly as possible. While this capability is often useful, a more common constraint in nMOS circuit design is to meet a delay specification while using the minimum resources. The mathematical tool used for both of these problems is the LaGrange multiplier.

Preliminary results from this investigation have produced inequality theorems about how the delays of the various stages in an optimized design behave. A program has also been developed, based on simple logic gate models, to optimally size transistors in the critical path of an MOS digital circuit. This work is now being generalized to multiple paths and incorporating more accurate models. Results of modern optimization theory are being used in conjunction with special properties of the domain of MOS logic gates to make the program computationally efficient.

Eventually this work will be incorporated into silicon compiler and polycell systems at M.I.T. in order to test how much improvement these specialized optimization programs will produce compared to present techniques.
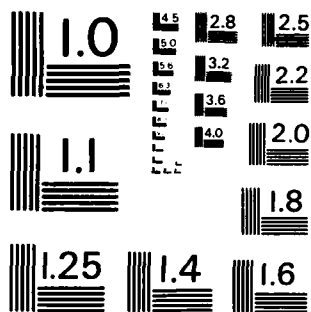
3/3

END
DATE
FILMED
12
DTIC

MICROCOPY RESOLUTION TEST CHART
NATIONAL BUREAU OF STANDARDS-1963-A

26. Communications Biophysics

A. Signal Transmission in The Auditory System

Academic and Research Staff

Prof. W.T. Peake, Prof. W.M. Siebert, Prof. T.F. Weiss, Dr. J.J. Guinan, Jr., Dr. E.M. Keithley, Dr. N.Y.S. Kiang, Dr. W.M. Rabinowitz, Dr. J.J. Rosowski, J.W. Larrabee, F.J. Stefanov-Wagner, D.A. Steffens

Graduate Students

M.L. Gifford, A.D. Krystal, M.P. McCue, C. Rose

26.1 Basic and Clinical Studies of the Auditory System

Nelson Y.S. Kiang, William T. Peake, William M. Siebert, Thomas F. Weiss

Our studies of the auditory system have continued in cooperation with the Eaton–Peabody Laboratory at the Massachusetts Eye and Ear Infirmary. We report projects that were completed during 1982.

Measurements of the input impedance of the cat cochlea are part of our program to evaluate signal transmission through middle–ears and to relate middle–ear function to structural features.[1] We now have rather extensive measurements in one mammalian species (cat) and one reptile (alligator lizard). We plan to extend these techniques to a broader range of vertebrate species to determine the effects of gross structural differences.

Investigations of mechanoelectric transduction in the inner ear continue to be focused on the alligator lizard ear because of its technical and conceptual simplicity.[2,3] These studies have led to a novel hypothesis about the frequency selective mechanisms of the ear in which the receptor cells act not only as mechanoelectric, but also as electromechanical transducers.[4]

Our knowledge of the innervation of mammalian inner–ear receptor cells by cochlear neurons has been unclear, partly because individual neurons could not be conveniently traced over their entire extent. The application of techniques that stain a few cells completely has clearly shown that cochlear neurons are segregated into two classes: the large majority of these neurons have large cell bodies and processes and innervate inner hair cells discretely, i.e., each neuron innervates one or

two inner hair cells; a small fraction of the neurons have smaller cell bodies and processes and innervate outer hair cells diffusely, i.e., each neuron innervates many outer hair cells.[5] Presumably, all of the recordings of fiber activity of the cochlear nerve have been obtained from the larger group; the function of the smaller neurons in the cochlea is unknown.

References

1. T.J. Lynch, III, V. Nedzelnitsky, and W.T. Peake, "Input Impedance of the Cochlea in Cat," J. Acoust. Soc. Am. 72, 108–130 (1982).
2. K. Baden–Kristensen and T.F. Weiss, "Supporting–Cell and Extracellular Responses to Acoustic Clicks in the Free–Standing Region of the Alligator Lizard Cochlea," Hear. Res. 8, 295–315 (1982).
3. K. Baden–Kristensen and T.F. Weiss, "Receptor Potentials of Lizard Hair Cells with Free-Standing Stereocilia: Responses to Acoustic Clicks," J. Physiol. 335, 699–721 (1983).
4. T.F. Weiss, "Bidirectional Transduction in Vertebrate Hair Cells: A Mechanism for Coupling Mechanical and Electrical Processes," Hear. Res. 7, 353–360 (1982).
5. N.Y.S. Kiang, J.M. Rho, C.C. Northrop, M.C. Liberman, and D.K. Ryugo, "Hair–Cell Innervation by Spiral Ganglion Cells in Adult Cats," Science 217, 175–177 (1982).

B. Auditory Psychophysics and Aids for the Deaf

Academic and Research Staff

L.D. Braida, R. Boduch, H.S. Colburn, J. Coker, L.A. Delhorne, L.C. Dowdy, N.I. Durlach, C.L. Farrar, S.G. Feldman, L.J. Ferrier, M.S. Florentine, D.M. Freeman, M. Furst, A.J.M. Houtsma, N. MacMillan, A.W. Mills, P. Milner, W.M. Rabinowitz, C.M. Reed, R.P. Russell, B. Scharf, M.C. Schultz, C.L. Searle, W.M. Siebert, G.P. Widin, P.M. Zurek

Graduate Students

T.T. Allard, C.A. Bickley, N. Bristol, Jr., D.K. Bustamante, S.V. DeGennaro, M.A. Epstein, K.K. Foss, K.J. Gabriel, M. Hagemeister, E.M. Hildebrandt, D.M. Horowitz, Y. Ito, A.L. Laves, J.R. Moser, D. Opalsky, R.C. Pearsall II, J.C. Pemberton, P.M. Peterson, S. Raman, R.J. Rohlicek, G.M. Skarda, R.M. Uchanski, R.S. Waissman, B.A. Yates

26.2 Intensity Perception and Loudness

Louis D. Braida, Nathaniel I. Durlach, Neil MacMillan, William M. Rabinowitz

This research is concerned with the development of a unified, quantitative theory of intensity perception and loudness, and involves the construction and integration of models of sensory processes, short-term memory, perceptual-context effects, and decision making, as well as psychophysical experimentation. During this period, our work has focused on a new model for context coding based on the use of perceptual anchors.

The new model for context coding accounts for the increased sensitivity observed near the extremes of the range when unidimensional stimuli are identified (the resolution edge effect) by assuming that sensations are estimated relative to noisy perceptual anchors with a stochastic ruler. In previous work we have derived the predictions of the model computationally because we have not been able to determine analytic expressions for the conditional densities of the decision variable. According to these computations, the predicted ROC's are closely approximated by straight lines of unit slope on normal coordinates even though the decision densities are not Gaussian. Thus it should be possible to derive a nonlinear but monotonic transformation of the decision variable such that the conditional probability densities of the transformed variable are (at least) approximately Gaussian. Since these densities must have equal variance if the corresponding ROC's are to have unit slope, the required transformation is simply that which equalizes the variances of the conditional densities of the

decision variable. Moreover, since we have been able to compute moments of the decision variable and thus show that the variance of the decision variable increases parabolically from the edge to the middle of the range, the required transformation is simply the arcsin function used to equate variances in statistics. In further analysis we have shown that the transformed densities have nonzero skewness and consequently can only be approximately Gaussian.

Based on the properties of the transformed variable, we have been able to derive analytic approximations for the sensitivities to be expected in identification experiments which illustrate the dependence of sensitivity on model parameters. According to these predictions, 1) there is an upper bound (determined by the average number of ruler steps) to the total sensitivity which can be achieved by increasing the stimulus range, 2) resolution edge effects (whose magnitude is dependent on anchor position and average number of ruler steps) are to be expected in large–range experiments but not in small–range experiments, 3) for a given stimulus range resolution is independent of the *number of stimuli in the set, and 4) when the stimulus range is small, the variance of the decision* variable in the context coding mode is the sum of sensation noise and anchor noise, and thus may exceed trace mode variance in fixed–level two–interval discrimination experiments.

We are currently utilizing these analytic predictions to obtain refined estimates of the parameters of the new context–coding model. A manuscript on this model is being prepared for publication.

26.3 Hearing Aid Research

Louis D. Braida, Norman Bristol, Jr., Diane K. Bustamante, Nathaniel I. Durlach, Kristin K. Foss, Dennis M. Freeman, Eric M. Hildebrandt, Paul Milner, Patrick M. Peterson, Miles P. Posen, Charlotte M. Reed, Roy P. Russell, Rosalie M. Uchanski, Edgar Villchur, Victor W. Zue, Patrick M. Zurek

This research is directed toward improving hearing aids for persons with sensorineural hearing impairments. We intend both to develop improved aids and to obtain fundamental understanding of the limitations on such aids. The work includes study of i) Amplitude Compression, ii) Frequency Lowering, and iii) Clear Speech.

i) Research on amplitude compression, directed towards listeners with reduced dynamic range, involves the study of a multiband compression system based on infinite peak clipping, the development of a principal components compression system, and preliminary study of a multiband automatic volume control system.

A syllabic compression system based on infinite peak clipping has been designed, constructed, and preliminarily evaluated psychoacoustically (Hildebrandt, 1982). The device filters the input into three bands each of which encompasses one of the first three formants of speech. Amplitude

compression is accomplished on a band by band basis via infinite peak clipping within each band and refiltering the clipped signals to their original ranges. The three resulting signals are summed to form the output. Tests with listeners with hearing loss simulated by additive noise achieved large intelligibility differences favoring compressed speech over linearly amplified speech that had been frequency equalized. For phonetically–balanced monosyllables scores averaged 4% and 36%, and for words in sentences 17% and 98%, for unprocessed and processed speech, respectively. However, a simple (wide–band) clipper system also showed good performance. These preliminary experiments suggest that peak clipping may have considerable potential as a means of amplitude compression for the severely hearing–impaired. In future work we will attempt to understand the spectral effects of clipping. We will also conduct further intelligibility studies to determine the nature of the perceptual distortions introduced by the processing. Ultimately, we will determine the benefits of clipping schemes for presenting speech to impaired listeners who have very small dynamic ranges.

We have developed a software signal processing system capable of determining and compressing the principal components of the short term speech spectrum. This includes a 16 channel 1/3 octave digital filter bank and a multichannel digital amplitude compression system. The system is also capable of analyzing the long–term characteristics of processed and unprocessed speech. Principal component compression will be first evaluated in terms of its effect on spectral shapes of speech and its effect on speech intelligibility for normal hearing listeners with hearing losses simulated by noise. To gain insight into this novel form of signal processing, a catalog of how the shapes of sample spectra are affected by compression of each of the principal components singly (and of the lower order principal components, in pairs) will be assembled. These data will be used to specify the characteristics of the principal component compression systems for the intelligibility studies on listeners with normal hearing. The results of these experiments will provide a basis for designing of a principal component compression system for hearing impaired listeners.

Automatic volume control (AVC) is a type of nonlinear signal processing that keeps the long–term output level constant over a wide range of input levels. Although widely suggested for use in hearing aids, this application has not been studied rigorously. One limitation on its use is associated with increases in the background noise level when speech components are weak or absent. We have implemented two AVC algorithms on a 16 channel computer controlled amplitude compression system (Coln, 1978). In one, each channel's level is measured and controlled independently. In the other, all channel levels are controlled on the basis of the overall input level. To reduce noise effects, both techniques incorporated a multichannel noise suppression algorithm (McAuley and Malpass, 1980). Both algorithms were found to be capable of reducing the range of speech level variations, and the relative level of noise to speech was decreased as more noise suppression was applied. However, preliminary tests on a listener with normal hearing indicate that both AVC algorithms degraded speech intelligibility in noise. The degradation was exacerbated by the noise suppression algorithm. We intend to continue to study the function of this AVC system and to attempt to remedy its deficiencies. Preliminary analysis suggests that the techniques used to estimate the short term

spectra of speech and noise may be inaccurate and this may be responsible for some of the intelligibility degradations. It also appears that AVC operation may be improved by use of asymmetric attack and decay dynamics. Use of a faster microcomputer to increase responsiveness is also likely to enhance system performance.

ii) Research on frequency lowering, directed towards listeners with poor hearing at high frequencies, has focused on the perception of low-frequency representations of speech achieved by means of synthetic codes.

Further work has been conducted on artificial coding of consonants and vowels with a 500 Hz bandwidth. Modifications of the original consonant code were introduced in an attempt to reduce confusability of particular pairs of sounds (e.g., /m–n/ and /r–w/) and training on identification was conducted with a second subject. After practicing on various subsets of the consonants, her identification score reached 88% on the full set of 24 coded sounds, a result similar to that obtained on the subject tested previously. A set of coded vowels was created using 10-tone complexes of harmonically spaced pure-tone frequencies from 50 to 500 Hz. The relative amplitudes of the components were patterned after those measured for real speech (lowpass filtered to 2500 Hz and linearly compressed by a factor of 5). Amplitude and duration cues were also coded in the vowel set by varying overall amplitude (such that the overall level of half the vowels was roughly 5 dB higher than for the remaining vowels) and duration (such that six of the vowels were 220 msec and four were 150 msec). Identification scores for one subject ranged between 84–88% following a short amount of practice.

Identification performance on the set of 24 coded consonants constructed with a 500 Hz bandwidth limitation is being compared to performance on naturally produced speech lowpass filtered to 500 Hz. A complete set of results is being obtained on three subjects. In conjunction with this project we are investigating the effect of varying the number of natural speech tokens representing each consonant under lowpass filtering.

Future work with these codes will: 1) explore identification of CV, VC, and CVC syllables drawn at random from the set of 24 consonants and 10 vowels that have been constructed so far; 2) examine the effect of bandwidth in constructing artificial low-frequency codes; and 3) explore further alterations of lowpass filtered speech (not necessarily in real time) to enhance intelligibility.

We have also begun to implement a low-frequency coding scheme that is based on modifying lowpass filtered speech and is capable of operation in real time. The first such code we are exploring is one which Lippmann (1980) found to have a ten percentage-point advantage over ordinary lowpass filtering. This scheme involves using the outputs of four high-frequency analysis filters to control the levels of low-frequency noise bands which are added to the original speech signal (lowpass filtered to 800 Hz). We will compare this scheme to lowpass filtered speech in multiple-token identification tests.

iii) Research on clear speech is concerned with the creation of speech materials that are highly intelligible to impaired listeners through the use of techniques that focus on the speech source rather than on signal processing, and with the determination of the acoustical properties of these materials that are responsible for the high intelligibility.

Work on this project has focused on further analysis of the speech materials and intelligibility results obtained by Chen (1980). Naturally produced clear and conversational CV tokens (6 stop consonants and 3 vowels) were analyzed to determine the VOT and the silence duration between the consonant burst and the start of voicing. Analysis of the acoustic timing measurements showed the following significant effects, speaking mode (15% total variance), voicing (48%), and mode x voicing (13%). No significant effects were found for the silent gap (Laves, 1982).

Our attempts to relate acoustic measurements with the intelligibility results have thus far been inconclusive. In one analysis, we attempted to relate listeners' ability to make voiced/unvoiced decisions to known limitations on duration discrimination for tones masked by noise. Although the dependence of the speech results on S/N was roughly correct, analysis of the voicing scores for different speaker tokens with the same VOT revealed that tokens with the same VOT are perceived quite differently. We plan to analyze the spectral characteristics of the stop burst to gain insight into this problem. After we have obtained a complete set of spectral and timing measurements on these materials, we will prepare synthetic CV tokens in which spectral and temporal differences are varied independently, and we will repeat the Chen intelligibility study with these materials.

References

1. N. Bristol, Jr., "Automatic Volume Control and Noise Suppression for Hearing Aids," S.M. Thesis, Department of Electrical Engineering and Computer Science, M.I.T., 1983.
2. F.R. Chen, "Acoustic Characteristics and Intelligibility of Clear and Conversational Speech at the Segmental Level," S.B. Thesis, Department of Electrical Engineering and Computer Science, M.I.T., 1980.
3. M.C.W. Coln, "A Computer Controlled Multiband Amplitude Compression System," S.M. Thesis, Department of Electrical Engineering and Computer Science, M.I.T., 1979.
4. E.M. Hildebrandt, "An Electronic Device to Reduce the Dynamic Range of Speech," S.B. Thesis, Department of Electrical Engineering and Computer Science, M.I.T., 1982.
5. A.L. Laves, "Consonant Intelligibility and Acoustic Analysis in Clear and Conversational Speech," S.B. Thesis, Department of Electrical Engineering and Computer Science, M.I.T., 1982.
6. R.P. Lippmann, "Perception of Frequency Lowered Consonants," J. Acoust. Soc. Am. 67, Suppl. 1, S78 (1980).
7. R.J. McAuley and M.L. Malpass, "Speech Enhancement Using a Soft Decision Noise Suppression Filter," IEEE Trans. Acoust., Speech, Signal Processing, ASSP-28, 137–145 (1980).
8. C.M. Reed, B.L. Hicks, L.D. Braida, and N.I. Durlach, "Discrimination of Speech Processed by Lowpass Filtering and Pitch-Invariant Frequency Lowering," J. Acoust. Soc. Am., in press.

26.4 Tactile Perception of Speech

Nathaniel I. Durlach, Raymond Boduch, Louis D. Braida, Jackie Coker, Lorraine A. Delhorne, Leonard C. Dowdy, William M. Rabinowitz, Charlotte M. Reed, Robin Rohlicek, Martin C. Schultz, Gregory M. Skarda

The ultimate goal of our research program is to develop tactile aids for the deaf and deaf-blind that will enable the tactile sense to serve as a substitute for hearing. Among the various components of our research in this area are (a) study of tactile communication methods employed by the deaf-blind, (b) development of an augmented Tadoma system, (c) development of a synthetic Tadoma system, and (d) design and evaluation of a wearable, portable aid.

a) We have obtained a substantial set of results on the Tadoma method of communication (in which the deaf-blind person receives speech by placing his hand on the face and neck of the talker and monitoring the various actions associated with the speech-production process). We have recently begun a study of other methods of communication that have evolved within the deaf-blind community itself, including tactile fingerspelling and tactile signing. We are studying these methods to demonstrate that it is possible to communicate language at reasonable rates through the tactile sense and to gain insight into the design of artificial systems.

Our initial goal in the study of tactile fingerspelling and tactile signing is to examine sentence reception as a function of presentation rate and to compare performance of experienced tactile fingerspellers and signers to that measured previously in experienced Tadoma users. Translations of sentence materials used in the study of Tadoma have been made into American Sign Language (ASL) and videotaped by a native deaf signer (who will also administer the tests). Fingerspelled and signed sentence materials will be presented to deaf-blind subjects at various rates of production and subjects will be asked to repeat the sentences either verbally (in the case of fingerspelling) or in sign (for ASL presentation).

b) Based both on direct observation of the Tadoma method and on detailed analysis of the phonemic errors that are made by Tadoma users, we believe that significantly improved results can be achieved by supplementing the information obtained through Tadoma with information on the tongue position of the talker. In order to explore this question empirically, we have developed a system in which information on tongue position is obtained through an electropalatograph (which senses the pattern of contact between the tongue and the roof of the mouth) and presented to the "listener" on a supplementary tactile display derived from the Optacon transducer system.

Experiments are planned with both normal subjects and experienced deaf-blind Tadoma users to determine the extent to which Tadoma performance can be improved by additional information on tongue position, both for segmental and connected speech utterances.

c) To better understand the success of the Tadoma method and to explore transformations of the method that cannot be achieved directly, we are developing a synthetic Tadoma system in which an artificial talking face is driven by signals recorded from the facial actions of a real talking face. During the past year work has continued on acquiring a library of multichannel recordings of facial actions during speech production. Currently, the library includes two repetitions from a single male speaker of a variety of phonemes, words, and sentences drawn from materials used in the testing of Tadoma users. The recordings, originally made on FM analog tape, have been converted (digitized and edited) to computer files appropriate for driving the artificial face.

On the artificial face, a lip-movement system has been integrated into the skull-jaw assembly. The lower lip can move up and down and in and out relative to the jaw, which in turn rotates about an axis through the skull. The upper lip can move in and out relative to the skull. In addition to lip and jaw movements, the face will also be equipped with mechanisms for producing air-flow at the lips and vibration on the neck. When the face is completed, perceptual experiments will be initiated with deaf-blind subjects to determine the adequacy of the system for speech transmission.

d) We are currently designing a wearable, portable aid in which short-term spectral information will be displayed to the abdomen by means of a linear array of vibrators. This system will be field-tested for substantial periods of time by both deaf-blind subjects and sighted deaf subjects. Such long-term field evaluations with wearable aids are essential not only because they constitute the ultimate test of usefulness in "real-world" environments, but also because they provide the only opportunity for serious learning of the new "code".

26.5 Discrimination of Spectral Shape by Impaired Listeners

Charlotte M. Reed, Louis D. Braida, Lorraine A. Delhorne, Nathaniel I. Durlach, Catherine L. Farrar, Mary S. Florentine, Yoshiko Ito, Patrick M. Zurek

The overall long-term goal of this research is to develop an analytic understanding of auditory perception and speech reception in impaired listeners and to develop improved diagnostic procedures and prosthetic devices for such listeners. The specific goals of the initial phase of this research are to (1) measure the ability of listeners with peripheral auditory loss, as well as listeners with normal hearing and with simulated loss, to discriminate stimuli with speech-like spectra on the basis of spectral shape alone and (2) relate these measurements to underlying auditory abilities by means of psychoacoustic experiments on the same subjects and through the development of

quantitative, theoretical models.

Our interest in the perception of spectral shape is motivated by a number of factors. First, spectral shape constitutes a significant cue in the perception of many speech elements. Second, it plays an important role in the acquisition of environmental information and in the perception of music. Finally, study of spectral-shape perception should prove useful in the attempt to understand auditory perception in general. The degree of complexity inherent in the study of spectral shape provides a useful interpolation between highly simplified, artificial situations usually studied in psychoacoustics and the highly complex, natural situations ordinarily encountered by listeners in everyday life.

Our research focuses on the underline discrimination of spectral shape in order to confine our attention initially to performance deficits that are likely to be explainable primarily in terms of periph al auditory deficits. The basic stimuli for these experiments are synthetic versions of steady- e unvoiced fricatives and synthetic versions of the burst portion of unvoiced plosives. These stimi addition to being sufficiently simple to permit interpretation of discrimination deficits in tern underlying psychoacoustic abilities, also focus on one of the primary speech-perception prob encountered by the hearing-impaired (i.e., the discrimination of consonant place-of-articulat The discrimination experiments are structured in such a way that the only perceptual cues available to the listener are those related to spectral shape (i.e., timbre). In particular, subjective duration cues are eliminated by equating the physical durations of stimuli and loudness cues are eliminated by randomly varying the intensity of the stimuli to be discriminated.

The experimental work can be divided into three stages, each of which is designed to contribute additional information concerning the abilities underlying spectral-shape discrimination. To the extent possible, the same subjects (both normal and impaired) will participate in all three stages of experimentation. Stage One is concerned with measuring discrimination performance for pairs of synthetic speech spectra as a function of signal duration and signal-to-noise ratio using a roving-level discrimination paradigm. Stage Two experiments are designed to evaluate the listener's ability to discriminate incremental changes in the spectral shape of the synthetic stimuli in various frequency regions. The basic experiment of this stage can be described as a roving-level detection experiment in which the target is a tone and the masker is a synthetic speech-like stimulus. Stage Three is concerned with the interpretation of the results in terms of more basic psychoacoustic factors. Experiments in Stage Three include fixed-level detection of pure tones in the background of a synthetic speech-like stimulus under both wideband and high- and low-pass filtering conditions, in addition to pure-tone frequency and intensity discrimination experiments.

Our initial theoretical work is directed towards a specification of the peripheral-processor component of the model in sufficient detail to allow us, along with our assumption of an ideal central processor, to derive detailed quantitative predictions for the planned experiments. Our general conceptual framework for spectral-shape discrimination assumes that the incoming signal is

analyzed into a number of frequency channels, the level of activity in each channel is estimated, these estimates are normalized relative to each other (to focus on spectral shape rather than overall level or level within a given channel), and this normalized pattern is then used as the internal datum corresponding to the input signal in the decision process. A model will first be constructed to predict results obtained for normal-hearing listeners and then various modifications will be made to allow predictions of reduced performance obtained for hearing-impaired listeners. The following types of difficulties might be expected in cases of peripheral auditory impairment: auditory frequency analysis may be different from normal, estimation of the level of activity within channels may be deficient, or ability to factor out differences in overall level may be reduced.

Experimental work is currently underway on the three stages of experimentation described above with both normal and impaired listeners. A quantitative theoretical model is also being developed to predict results of Stage One experiments for normal subjects.

C. Transduction Mechanisms in Hair Cell Organs

Academic and Research Staff

Prof. L.S. Frishkopf, Prof. T.F. Weiss, Dr. D.J. De Rosier[25], Dr. C.M. Oman

The overall objective of this project is to study the sequence of steps by which mechanical stimuli excite receptor organs in the phylogenetically related auditory, vestibular, and lateral-line organs. The receptor cells in these organs are ciliated hair cells. Specific goals include the characterization of the motion of the structures involved, particularly the hair cell stereocilia; study of the nature and origin of the electrical responses to mechanical stimuli in hair cells; and investigation of the role of these responses in synaptic and neural excitation.

26.6 Evidence of Length–Dependent Mechanical Tuning of Hair Cell Stereociliary Bundles in the Alligator Lizard Cochlea: Relation to Frequency Analysis

Lawrence S. Frishkopf, David J. De Rosier

We have been studying the mechanical responses to sound in a relatively simple auditory organ, the basilar papilla of the alligator lizard.[1,2] Recently the motion of hair cell stereociliary bundles with respect to the underlying basilar papilla has been measured[3,4] as a function of stimulus frequency, hair cell location, and bundle length. Our purpose has been to determine whether such motion provides a basis for frequency selectivity and tonotopic organization observed in nerve fibers to the organ.

The basilar papilla in the alligator lizard is an elongated auditory receptor organ containing hair cells; it is attached to the basilar membrane which vibrates in response to sound. The axis of symmetry of the stereociliary bundle of each hair cell – presumed to be the sensitive direction for displacement[5] – is perpendicular to the long axis of the papilla.

Characteristic frequencies (CF's) of nerve fibers are between 0.2 and 4 kHz and vary systematically with location in the nerve.[6] Yet velocity measurements along the basilar membrane suggest that its frequency response does not change significantly from one region to another and thus does not provide a basis for the observed variation of nerve fiber CF.[7]

Where then does frequency analysis take place? One possibility is that, within the basilar papilla,

---

[25]Professor, Department of Biology, Brandeis University

modes of motion may occur which are not evident in the measurements of basilar membrane motion. It has also been suggested that the gradual variation in maximum length of the free-standing stereocilia in the posterior two thirds of the organ, from 30 μm in the 1 kHz region to 12 μm in the 4 kHz region, may provide a micromechanical basis for frequency analysis over this range of CF.[6]

To address these issues, motion of the basilar papilla and of the free-standing hair cell stereocilia that results from acoustic stimulation has been observed under a microscope. The cochlear duct was excised and the basilar papilla with its supporting limbus was mounted in a drop of lizard Ringer's solution across an opening in an air filled chamber; the organ was stimulated with tones (0.2 – 5 kHz; 110 – 140 dB SPL) and viewed stroboscopically at 400 – 800X.

We have previously shown[1,2] that (1) the papilla rocks about an axis parallel to its length in the direction of symmetry of the stereociliary bundles, i.e., in the direction of morphologically-predicted sensitivity of the hair cells; (2) the papilla moves in phase along its entire length; (3) above 3 kHz, the displacement of the high-CF region exceeds that of the rest of the papilla, perhaps providing a partial basis for frequency analysis.

Recent observations[3] show that on stimulation stereociliary bundles are displaced relative to the underlying cuticular surface in the direction of presumed hair cell sensitivity, and that the difference in phase between bundle and cuticular displacements is a function of stimulus frequency and of hair cell position along the basilar papilla. Phase vs. frequency data suggest (1) that stereociliary bundles behave like damped mechanical resonators; (2) that resonant frequency varies inversely with the square of bundle length; and (3) that bundle resonant frequency and neural CF are close in value in corresponding regions of the papilla and nerve. These findings are consistent with an explanation of frequency analysis in the papilla based on length-dependent mechanical tuning of stereociliary bundles.

References

1. L.S. Frishkopf, "Mechanical Response Properties of the Basilar Papilla in Alligator Lizard: Failure to Find a Basis for Tonotopic Organization," M.I.T. Research Laboratory of Electronics Progress Report No. 123, pp. 206–207 (1981).
2. L.S. Frishkopf, "Investigation of the Mechanical Basis of Frequency Selectivity and Tonotopic Organization in the Cochlea of the Alligator Lizard," M.I.T. Research Laboratory of Electronics Progress Report No. 124, pp. 205–207 (1982).
3. L.S. Frishkopf, D.J. De Rosier, and E.H. Egelman, "Motion of Basilar Papilla and Hair Cell Stereocilia in the Excised Cochlea of the Alligator Lizard: Relation to Frequency Analysis," Soc. Neurosci. Abs. 8, 40 (1982).
4. T. Holton and A.J. Hudspeth, "Motion of Hair-Cell Stereocilia in the Auditory Receptor Organ of the Alligator Lizard," Soc. Neurosci. Abs. 8, 40 (1982).
5. S.L. Shotwell, R. Jacobs, and A.J. Hudspeth, "Directional Sensitivity of Individual Vertebrate Hair Cells to Controlled Deflection of their Hair Bundles," Ann. N.Y. Acad. Sci. 374, 1–10 (1981).

6. T.F. Weiss, W.T. Peake, A. Ling, Jr., and T. Holton, "Which Structures Determine Frequency Selectivity and Tonotopic Organization of Vertebrate Cochlear Nerve Fibers? Evidence from the Alligator Lizard," in R.F. Naunton and C. Fernandez (Eds.), <u>Evoked Electrical Activity in the Auditory Nervous System</u>, (Academic Press, New York, 1978), pp. 91–112.

7. W.T. Peake and A. Ling, Jr., "Basilar–Membrane Motion in the Alligator Lizard: Its Relation to Tonotopic Organization and Frequency Selectivity," J. Acoust. Soc. Am. <u>67</u>, 1736–1745 (1980).

27. Physiology

Academic and Research Staff

Prof. J.Y. Lettvin, Dr. J. Gardner, G. Geiger, Dr. S. Jhaveri, Dr. L.A. Kamentsky, Dr. L.A. Kamentsky, Dr. D. Perlman, Dr. G.M. Plotkin, Dr. S.A. Raymond, Dr. S. Wiesner

Graduate Students

L.R. Carley, B. Howland, K.J. McLeod, A. Medina, G. Pratt

In the year of 1981–82 our work was as usual divided among a variety of subjects.

J.Y. Lettvin and G.M. Plotkin, collaborating with Prof. Rose of Materials Science, brought out a new version of the origins of Caisson disease (compression sickness) with a list of nucleating events in the human body that generate bubbles in solutions that are supersaturated with gas.

E.R. Gruberg and J.Y. Lettvin successfully showed that the records of primary optic nerve fibers taken from frog tectum were not due to the terminals of the fibers but rather to non-linear responses of subjacent dendrite patches.

J.Y. Lettvin developed a new metal micro–electrode for which a tip of only 3 microns diameter exhibited a real component of its impedance < 20 K Ω at 2 KHz. This is better by an order of magnitude or more than the best metal electrodes to date. It allows for recording in the nervous system with very low noise.

G.M. Plotkin investigated mechanical shear of cancer cells as compared with normal cells and filed a patent on therapeutic applications of his results on two–port organs.

B. Howland and A. Medina developed a new eye chart to replace that of Snellen (that commonly used). Making use of spatial frequencies of black–and–white to be resolved against a gray background, they made a chart such that either the letters or figures could be read or they didn't appear at all. Thus, there was no guessing, as with Snellen charts and the measurement of visual performance is extremely crisp. A patent was filed.

B. Howland invented a simple and reliable way of controlling large three–phase motors by adjustment of frequency. The resulting saving of power can be considerable, and several were installed by the Physical Plant at M.I.T. The design won a prize. A patent has been filed.

L. Linden and J.Y. Lettvin finished a paper on a model for object color constancy in animal vision.

28. Publications and Reports

28.1 Meeting Papers Presented

Topical Meeting on Integrated and Guided-Wave Optics, Asilomar Conference Center, Pacific Grove, California
January 6-8, 1982

Papers in <u>Technical Digest</u>

> H. A. Haus, Picosecond Sampling in Optical Waveguides (paper WA1-1 - WA1-4)

> A. Lattes, C. Gabriel, and H. A. Haus, Double Degenerate Four-Wave Mixing in Optical Waveguides (paper ThA4-1 - ThA4-3)

> R. H. Rediker, R. P. Schloss, A. Mooradian, and D. Welford. External Cavity Controlled Operation of a Semiconductor Diode Gain Element in a Series with an Optical Fiber (paper ThB2-1 - ThB2-4)

159th Meeting, American Astronomical Society, Boulder, Colorado
January 10-13, 1982

Abstracts in Bull. Am. Astron. Soc. <u>13</u>:4 (1981)

> J. T. Armstrong and A. H. Barrett, Observations of HNCO in the SgrA Molecular Clouds (p. 853)

> C. L. Bennett, C. R. Lawrence, J. Hewitt, and B. F. Burke, VLA Source Counts at 6 cm and 2 cm (p. 807)

> P. T. P. Ho, S. Vogel, J. T. Armstrong, and A. H. Barrett, Observations of NH_3 Toward the SgrA Molecular Clouds (p. 853)

> C. R. Lawrence, C. L. Bennett, J. Hewitt, and B. F. Burke, Observations at 6 cm of the 611 MHz Arecibo Source Sample (p. 807)

> P. C. Myers, Low Mass Star Formation in the Dense Interior of Barnard 18 (p. 864)

> E. L. Wright, M. Halpern, and R. Weiss, Sub-Millimeter Measurements of the Anysotropic of the Cosmic Microwave Background

Engineering Foundation Conference on Modeling and Neuromuscular Systems, Santa Barbara, California
January 17-22, 1982

> J. S. Perkell, Mathematical Models and the Physiology of Speech Production

SPIE Technical Symposium and Exhibit, Los Angeles, California
January 25-29, 1982

Papers in Proceedings Vol. 322

J. G. Fujimoto and M. M. Salour, Ultrafast Picosecond Chronography (pp. 137-165)

C. B. Roxlo, R. S. Putnam, and M. M. Salour, Optically Pumped Semiconductor Platelet Lasers (pp. 31-36)

1982 March Meeting, American Physical Society, Dallas, Texas
March 8-12, 1982

Abstracts in Bull. Am. Phys. Soc. 27:3 (1982)

A. N. Berker, Commensurate-Incommensurate Phase Diagrams from the Helical Potts Model (invited paper)

R. M. Bilotta, D. E. Pritchard, and J. A. Serri, Two-Dimensional Model for Rotationally-Vibrational Diatom Inelastic-Scattering (p. 387)

C. Jagannath, E. R. Youngdale, D. M. Larsen, R. L. Aggarwal, and P. A. Wolff, Four-Wave Magnetospectroscopy of the Ground-State of Donors in Germanium (p. 174)

K. Kash, P. A. Wolff, S. Y. Yuen, C. Jagannath, and W. A. Bonner, Free-Carrier-Induced Four-Wave Mixing in GaAs and GaSb (p. 175)

A. R. Kortan, High Resolution X-ray Study of Reentrant Nematic 60 CB-80 CB Mixtures (p. 366)

R. F. Kwasnick, M. A. Kastner, and J. Melngailis, Electronic Conduction in Ultra-Narrow Silicon Inversion Layers

J. B. McManus, P. A. Wolff, and R. L. Aggarwal, Difference Frequency Generation Using Thin Film Plasmons (p. 369)

L. R. Ram Mohan and P. A. Wolff, The Joint Density of States in Interband Transitions in Semiconductors in a Magnetic Field (p. 144)

S. Y. Yuen and P. A. Wolff, Difference-Frequency Variation of the Free Carrier-Induced, Third Order Nonlinear Susceptibility of n-InSb (p.175)

NATO Advanced Research Institute, Microelectronics, Les des Alpes, France
March 15-19, 1982

H. I. Smith, New Approaches to Single-Crystal Thin Films for Devices and Systems Using Surface Patterns

First Japan/US Snow and Evapotranspiration Workshop, Tokyo, Japan
March 16-21, 1982

J. A. Kong, *Theoretical Models for Remote Sensing of Snow*

Third Joint Varenna-Grenoble International Symposium on Heating in Toroidal Plasmas, Grenoble, France
March 22-27, 1982

S. F. Knowlton, M. Porkolab, and S. C. Luckhardt, Suppression of Plasma Formation in Waveguide Antennas for Low-Hybrid Heating

S. C. Luckhardt, P. T. Bonoli, K-I. Chen, B. Coppi, R. C. Englade, A. S. Fisher, S. F. Knowlton, M. J. Mayberry, and M. Porkolab, Lower-Hybrid RF Current Drive Experiments on the Versator II Tokamak

S. C. Luckhardt, G. Bekefi, P. T. Bonoli, K-I. Chen, B. Coppi, R. C. Englade, A. S. Fisher, K. E. Hackett, S. F. Knowlton, M. J. Mayberry, F. S. McDermott, M. Porkolab, J. S. Levine, M. E. Read, and V. L. Granatstein, Lower-Hybrid RF Current Drive and Electron Cyclotron Heating on the Versator II Tokamak

A. Ram and A. Bers, Antenna-Plasma Coupling Theory for ICRF Heating of Large Tokamaks

Fifth Topical Meeting on Optical Fiber Communication and 1982 Conference on Lasers and Electro Optics, Phoenix, Arizona
April 13-16, 1982

H. A. Haus, High Speed Optical Waveguide Switching

A. M. Hawryluk, H. I. Smith, R. M. Osgood, and D. J. Ehrlich, Spatial-Period-Division Using an ArF Laser

M. M. Salour, In GaAsP Optically Pumped Semiconductor Platelet Lasers

M. M. Salour, Light-Induced Unidirectional Light Switching

International Cochlear Implant Conference, New York Academy of Sciences, New York, New York
April 14-16, 1982

K. N. Stevens, Acoustic Properties Used for Identification of Speech Sounds

Catgut Society Meeting, Dekalb, Illinois
April 23-26, 1982

C. J. Chiang and A. J. M. Houtsma, A Comparison Between Expensive and Inexpensive Violin Strings

Workshop on Symbolic Computing in Plasma Physics, Los Angeles, California
April 23-30, 1982

R. Berman, Symbolic Computing, Introduction, Comparison of Different Systems, and Computational Physics Examples

1982 Sherwood Meeting, Santa Fe, New Mexico
April 25-28, 1982

P. T. Bonoli, R. Englade, and B. Coppi, Electron Thermal Transport in Plasmas with Auxiliary Heating

G. B. Crew and J. J. Ramos, High Beta Stability of Ideal MHD Fixed Boundary Modes

R. Englade and P. T. Bonoli, A Computational Model for Lower Hybrid Heating and Current Drive in Tokamaks

V. Krapchev, Current Drive by LH Waves in the Presence of DC Electric Field

F. Pegoraro and L. Sugiyama, Diffusion of Fusion-Produced Particles Due to Shear Alfven Fluctuations

A. Ram and A. Bers, Antenna-Plasma Coupling Theory for ICRF Heating

J. J. Ramos and G. B. Crew, Stabilization of the Internal Kink Mode in Finite Beta Toroidal Plasmas

N. N. Sharky, Simulation of Electron Temperature Profiles for Different Values of 9

N. N. Sharky and B. Coppi, Electron Energy Confinement Time in Ohmically Heated Experiments

V. Stefan and A. Bers, Parametric Phenomena at Electron Cyclotron Resonance Heating of Tokamak Plasmas

L. Sugiyama and R. Englade, Energy Redistribution in Igniting Plasmas

103rd Meeting, Acoustical Society of America, Chicago, Illinois
April 27-30, 1982

Abstracts in J. Acoust. Soc. Am., Vol. 71, Suppl. No. 1, Spring 1982

C. Bickley, Acoustical Analysis and Perception of Breathy Vowels

M. A. Clements, L. D. Braida, and N. I. Durlach, Comparison of Two Tactile Speech Codes (p. S59)

S. DeGennaro, L. D. Braida, and N. I. Durlach, Multiband Syllabic Compression for Severely Impaired Listeners (p. S59)

A. J. M. Houtsma, Inharmonicity of Wound Guitar Strings (p. S9)

A. J. M. Houtsma and E. M. Burns, Temporal and Spectral Characteristics of Tambura Tones (p. S83)

D. H. Klatt, Speech Processing and Phonetic Recognition Strategies: What Can Be Learned from Auditory Physiology and Psychophysics? (p. S111)

L. S. Larkey, Another Look at Reiterant Speech in Prosody Research (p. S113)

P. Lieberman, K. Landhal, and J. H. Ryalls, Sentence Intonation in British and American English (p. S112)

J. S. Perkell, Advances in the Use of Alternating Magnetic Fields to Track Articulatory Movements (p. S32)

P. J. Price and A. G. Levitt, Prosody and the /š/-/č/ Distinction (p. S113)

D. W. Shipman, Development of Speech Research Software on the MIT Lisp Machine (p. S103)

K. N. Stevens and S. Hawkins, Acoustic and Perceptual Correlates of Nasal Vowels (p. S76)

V. W. Zue and D. W. Shipman, Properties of Large Lexicons: Implications for Advanced Isolated-Word Recognition Systems (p. S7)

P. M. Zurek, A Predictive Model for Binaural Advantages in Speech Intelligibility (p. S87)

"Spectral Analysis and Its Use in Underwater Acoustics", Underwater Group Conference, Imperial College, London, England
April 29-30, 1982

Papers in <u>Proceedings</u>

N. A. Malik and J. S. Lim, Implementation of a New Algorithm for Two-Dimensional Maximum Entropy Spectral Estimation (pp. 11.1 - 11.6)

J. H. McClellan and S. W. Lang, Multi-Dimensional MEM Spectral Estimation (pp. 10.1 - 10.8)

1982 IEEE International Conference on Acoustics, Speech and Signal Processing, Palais des Congres, Paris, France
May 3-5, 1982

Papers in <u>Proceedings</u> ICASSP '82

> C. Espy and J. S. Lim, Effects on Noise on Signal Reconstruction from Fourier Transform Phase (pp. 1833-1836)

> W. H. Evans and J. Allen, MOS Implementations of TTL Architectures: A Case Study (pp. 703-706)

> D. H. Klatt, Prediction of Perceived Phonetic Distance from Critical-Band Spectra: A First Step (pp. 1278-1281)

> A. L. Kurkjian, Maximum Likelihood Dereverberation with Applications in Sonic Well Logging (pp. 1862-1865)

> L. F. Lamel and V. W. Zue, Performance Improvement in a Dynamic-Programming-Based Isolated Word Recognition System for Alpha-Digit Task (pp. 558-561)

> S. W. Lang annd J. H. McClellan, The Extension of Pisarenko's Method to Multiple Dimensions (pp. 125-128)

> N. A. Malik, J. S. Lim, and M. J. Glaser, Properties of Two Dimensional Maximum Entrophy Power Spectrum Estimates (pp. 129-132)

> B. R. Musicus, An Iterative Algorithm for Finding Stable Solutions to the Covariance or Modified Covariance Autoregressive Modeling Methods (pp. 244-247)

> H. Nawab, T. F. Quatieri, and J. S. Lim, Signal Reconstruction from the Short-Time Fourier Transform Magnitude (pp. 1046-1048)

> D. W. Shipman and V. W. Zue, Properties of Large Lexicons: Implications for Advanced Isolated Word Recognition Systems (pp. 546-549)

161st Meeting of the Electrochemical Society, Montreal, Canada
May 9-14, 1982

Papers in <u>Proceedings</u>

> H. I. Smith, H. A. Atwater, and M. W. Geis, Orientation Selection by Zone Melting Silicon Films Through Planar Constrictions

> H. I. Smith and M. W. Geis, The Mechanism of Orientation in Si Graphoepitaxy Using a Strip-Heater Oven

NATO Workshop on Target Background Modelling Techniques at Millimeter Wavelengths, Harry Diamond Laboratories, Adelphi, Maryland
May 11-12, 1982

> J. A. Kong, Active and Passive Remote Sensing of Earth Terrain at Millimeter Wavelengths

47th Statistical Mechanics Meeting, Rutgers University, New Brunswick, New Jersey
May 13-14, 1982

M. Kardar, Phase Boundaries of the Isotropic Helical Potts Model on the Square Lattice

Benjamin Franklin Symposium on Advances on Antenna Propagation and Microwave Technology, Philadelphia, Pennsylvania
May 15, 1982

S. L. Chuang and J. A. Kong, Extended Boundary Condition Approach to Wave Scattering by Periodic Structures

1982 IEEE International Conference on Plasma Sciences, Ottawa, Canada
May 17-19, 1982

J. Fajans, G. Bekefi, and B. Lax, Insertion of Electrons into a FEL with Near Resonant Wiggler and Axial Magnetic Fields

V. Fuchs, M. Shoucri, L. Harten, and A. Bers, Steady High-Q Operation of Tokamak Reactors

D. D. Hinshelwood, The Effects of Current Flow on Cathode Plasma Formation on REB Diodes

R. E. Shefer, G. Bekefi, and D. A. Kirkpatrick, A Velocity Diagnostic for a High Current Lowbitron Beam

U.R.S.I. National Radio Science Meeting, University of New Mexico, Albuquerque, New Mexico
May 24-28, 1982

Abstracts in <u>Proceedings</u>

A. Sezginer and J. A. Kong, Electromagnetic Wave Scattering by Thin Helical Wires (p. 60)

NSF Grantee-User Meeting on Optical Communication Systems, University of California, Berkeley, California
June 2-4, 1982

C. Fonstad, III-V Heterostructure Devices for High Speed Fiber Communications

H. Haus, Optical-Waveguide Devices for Picosecond Signal Processing

J. H. Shapiro and D. J. Epstein, Atmospheric Optical Communications

160th Meeting, American Astronomical Society, Troy, New York

June 6-9, 1982

    P. C. Myers and P. J. Benson, Cold Cloud Cores: NH_3 Observations

    M. Shao, M. M. Colavita, P. M. Garnavich, and D. H. Staelin, The MIT-NRL Two-Color Dual Astrometric Stellar Interferometer

1982 International Conference on Plasma Physics, Göteborg, Sweden
June 7-15, 1982

    P. T. Bonoli, B. Coppi, G. B. Crew, R. Englade, F. Pegoraro, J. J. Ramos, N. Sharky, and L. Sugiyama, Finite-β Regimes and Transport Processes in Thermonuclear Plasmas

The Second Telecommunications and Data Acquisition (TDA) Future Space Communications Technology Workshop, California Institute of Technology, Pasadena, California
June 8, 1982

    J. H. Lang and D. H. Staelin, Electrostatically-Figured Membrane Reflectors: Present and Future Technologies

IEEE Conference on Pattern Recognition and Image Processing, Las Vegas, Nevada
June 13-17, 1983

    S. M. Goldwasser and D. E. Troxel, Page Composition of Continuous Tone Imagery (pp. 411-419)

Nineteenth Design Automation Conference, Las Vegas, Nevada
June 14-16, 1982

Papers in <u>Proceedings</u>

    L. Seiler, A Hardware Assisted Design Rule Check Architecture (pp. 232-237)

Kickoff Meeting, Fundamental Research Program, Goddard Space Flight Center, Greenbelt, Maryland
June 15, 1982

    J. A. Kong, Theoretical Models for Remote Sensing of Earth Terrain

XII International Quantum Electronics Conference, Münich, Germany
June 22-25, 1982

    G. Bekefi, Rippled-Field Magnetron

G. Bekefi, W. A. McMullin, and R. E. Shefer, Lowbitron

H. A. Haus, A. Lattes, E. P. Ippen, and F. J. Leonberger, Optical Exclusive OR Gate

H. A. Haus, A. Lattes, C. Gabriel, E. P. Ippen, and F. J. Leonberger, Doubly Degenerate Four-Wave Mixing in $LiNbO_3$ Waveguides

Twentieth ISMM International Symposium, MIMI '82, on Minicomputers and Their Applications, Cambridge, Massachusetts
July 7-9, 1982

D. E. Troxel, Spatial Coordinate Transformations

"Clinical Implications of Research in Child Phonology", La Verne University, La Verne, California
July 8-9, 1982

E. M. Maxwell, Recent Trends in Acoustic Analysis in Child Phonoly

6th International Conference on Spectral Line Shape, Boulder, Colorado
July 12-17, 1982

D. E. Pritchard and R. E. Walkup, Transition Regions in Line Broadening

NASA Workshop on Application of Distributed System Theory to the Control of Large Space Structures, Pasadena, California
July 14-16, 1982

Y. Yam, J. H. Lang, T. L. Johnson, S. Shih, and D. H. Staelin, Large Space Structure Model Reduction and Control System Design Based Upon Actuator and Sensor Influence Functions

2nd Trieste International Symposium on Statistical Mechanics of Adsorption Trieste, Italy
July 26-29, 1982

A. N. Berker, Commensurate-Incommensurate Phase Diagrams from the Helical Potts Mode (invited paper)

Snow Symposium II, U.S. Army Cold Region Research and Engineering Laboratory, Hanover, New Hampshire
August 10-12, 1982

R. T. Shin, J. C. Shiue, and J. A. Kong, Rough Surface Effects on the Passive Remote Sensing of Snow

J. C. Shiue, R. Shin, B. Hartline, J. Fuchs, J. A. Kong, and T. C. Chang, Microwave Radiometric Observations of Snowpack and Ice in North-Eastern U.S.

SPIE 26th Annual International Technical Symposium, San Diego, California
August 22-27, 1982

Papers in SPIE Vol.

P. van Hove, J. S. Lim, and A. V. Oppenheim, Signal Reconstruction from Fourier Transform Amplitude

Ninth International Conference on Plasma Physics and Controlled Nuclear Fusion Research, Baltimore, Maryland
September 1-8, 1982

P. T. Bonoli, B. Coppi, G. B. Crew, R. Englade, F. Pegoraro, J. J. Ramos, N. Sharky, and L. Sugiyama, Finite-β Regimes, Transport Processes and Heating of Thermonuclear Plasmas

L. P. Harten, A. Bers, V. Fuchs, M. Shoucri, and G. Thibaudeau, Thermally Stable High-Q Reactor with Controlled Heating Power

M. Porkolab, J. J. Schuss, Y. Takase, S. Texter, C. Fiore, T. Gentile, R. Gandy, A. Gondhalekar, M. Greenwald, D. Gwinn, S. Kissel B. Lipschultz, E. Marmar, D. Pappas, R. Parker, M. Pickrell, P. Pribyl, J. Rice, J. Terry, R. Watterson, S. Wolfe, S. F. Knowlton, S. C. Luckhardt, G. Bekefi, K. I. Chen, A. Fisher, K. Hackett, M. J. Mayberry, F. S. McDermott, A. Bers, P. T.Bonoli, B. Coppi, R. Englade, V. Krapchev, A. Ram, R. E. Slusher, C. M. Surko, J. S. Levine, M. E. Read, and V. L. Granatstein, Lower Hybrid Heating and Current Drive Experiments on the Alcator C and Versator II Tokamak

A. Ram, L. P. Harten, and A. Bers, Antenna-Plasma Coupling Theory for ICRF Heating of Large Tokamaks

IEEE Solid State Circuits and Technology 1982 Fall Workshop, Village at Smuggler's Notch, Jeffersonville, Vermont
September 8-10, 1982

J. Allen, A Vocal Tract Model IC

American Chemical Society Meeting, Kansas City, Missouri
September 15, 1982

D. H. Klatt, Text to Speech

35th Annual Conference on Engineering in Medicine and Biology, Philadelphia, Pennsylvania

September 22-24, 1982

Abstracts in <u>Proceedings</u>

> H. S. Colburn, Communication-Theory Models of Binaural Interaction (p. 96)

Tri-Service Workshop on Fiber Optic Sensors and Guided Wave Technology, U.S. Army Transportation Center, Ft. Eustis, Virginia
October 5-8, 1982

> S. Ezekiel, Overview of Fiber Optic Gyroscopes (invited paper)

Large Scale Systems Symposium, Virginia Beach, Virginia
October 11-13, 1982

> L. A. Glasser and P. Penfield, Jr., VLSI Circuit Theory

X International Symposium on Discharges and Electrical Insulation in Vacuum, Columbia, South Carolina
October 25-28, 1982

> D. D. Hinshelwood, The Role of Surface Contaminants in Cathode Plasma Formation

IEEE 1982 Ultrasonics Symposium, San Diego, California
October 27-29, 1982

Papers in <u>Proceedings</u>

> D-P. Chen, J. Melngailis, and H. A. Haus, Filters Based on Conversion of Surface Acoustic Waves to Bulk Plate Modes in Gratings (pp. 67-71)

> M. N. Islam, H. A. Haus, and J. Melngailis, Radiation Loss for Normal and Oblique Incidence Gratings (pp. 92-95)

12th Annual Meeting, Society for Neuroscience, Minneapolis, Minnesota
October 31 - November 5, 1982

Abstracts in <u>Proceedings</u>

> L. S. Frishkopf, D. J. DeRosier, and E. H. Egelman, Motion of Basilar Papilla and Hair Cell Stereocilia in the Excised Cochlea of the Alligator Lizard: Relation to Frequency Analysis (paper 16:8, p. 40)

Annual Meeting, Materials Research Society, Boston, Massachusetts

November 1-4, 1982

A. N. Berker, Global Phase Diagrams with Order-Disorder and Structural Transitions: Renormalization-Group Approach (invited paper)

24th Annual Meeting of the Division of Plasma Physics, American Physical Society, New Orleans, Louisiana
November 1-5, 1982

Abstracts in Bull. Am. Phys. Soc. <u>27</u>:8 (1982)

G. Bekefi, R. E. Shefer, and D. D. Nevins, The Rippled Field Magnetron (p. 1063)

R. Berman, D. Tetreault, and T. Dupree, Simulation of a Nonlinear Instability (p. 1105)

A. Bers and A. K. Ram, Relativistic Pulse Shapes of Absolute and Convective Instabilities (p. 919)

P. T. Bonoli, B. Coppi, and R. Englade, Electron Thermal Transport in Plasmas with "Injected" Heating (p. 963)

P. T. Bonoli, B. Coppi, and R. Englade, Analysis of Electron Thermal Transport in Plasmas with Auxiliary Heating (p. 963)

T. Chang, B. Coppi, and J. R. Jasperse, Monte Carlo Simulation of Ion Conic Formation by Lower Hybrid Modes in the Suprauroral Region (p. 1024)

K. I. Chen and M. E. Huber, Observation of Poloidally Asymmetric Line Emissions on the Versator II Tokamak (p. 1060)

B. Coppi, Physics of Neutronless Fusion Reactors (p. 1043)

B. Coppi, Magnetic Reconnection Driven by Velocity Space Instabilities (p. 1071)

G. B. Crew, B. Coppi, and J. J. Ramos, Internal Kink Modes in High Temperature Collisionless Regimes (p. 914)

T. H. Dupree, Simulation and Theory of Holes and Clumps (p. 1038)

R. Englade, P. T. Bonoli, and M. Porkolab, Numerical Simulations of Lower Hybrid Current Drive Experiments (p. 1069)

V. Fuchs, G. Thibaudeau, V. Krapchev, A. Ram, and A. Bers, Diffusion and Momentum Transfer for Particles Interacting with Coherent Wavepackets (p. 957)

R. F. Gandy, M. Porkolab, and J. J. Schuss, Cyclotron Emission During RF Current Drive on Alcator C (p. 937)

K. E. Hackett, A. S. Fisher, M. J. Mayberry, F. S. McDermott, G. Bekefi, J. S. Levine, M. E.

Read, and V. L. Granatstein, Results from the Electron Cyclotron Heating Experiment on the Versator II Tokamak (p. 1081)

A. Hamza, N. Sharky, and B. Coppi, Analysis of Electron Power Balance in Ohmically Heated Discharges (p. 1126)

D. D. Hinshelwood, The Role of Surface Contaminants in Cathode Plasma Formation (p. 1030)

K. Hizanidis, V. B. Krapchev, and A. Bers, Current Drive by Lower-Hybrid Waves Acting on Runaway Electron Tail (p. 1006)

D. Humphreys, R. Englade, and L. Sugiyama, Transport in the Presence of "Sawtooth" Oscillations from Thermonuclear Plasmas (p. 1127)

K. D. Jacobs and G. Bekefi, Electron Motion in a Free Electron Laser (p. 1010)

J. Kesner and B. Lane, Effects of Collisional Dissipation on Tandem Mirrors Trapped Particle Modes (p. 914)

R. E. Klinkowstein, J. Kesner, B. D. McVey, R. S. Post, D. K. Smith, and T. F. Yang, The TARA Tandem Mirror Experiment (p. 967)

S. F. Knowlton, K. I. Chen, S. C. Luckhardt, M. J. Mayberry, and M. Porkolab, Ion Heating by Lower-Hybrid Waves in the Versator II Tokamak (p. 1005)

V. B. Krapchev, K. Hizanidis, and A. Bers, Current Drive by LH Waves in the Presence of a DC Electric Field (p. 1006)

R. M. Kulsrud, Fusion with Polarized Ions (invited paper) (p. 1038)

B. Lane and H. L. Berk, Effect of Ion Landau Bounce Resonance on Tandem Mirror Trapped Particle Modes (p. 910)

S. C. Luckhardt, M. Porkolab, S. F. Knowlton, K. I. Chen, M. J. Mayberry, F. S. McDermott, and J. S. Levine, RF Current Drive Experiments on Versator II (p. 1005)

F. S. McDermott, G. Bekefi, A. S. Fisher, K. E. Hackett, S. F. Knowlton, S. C. Luckhardt, M. J. Mayberry. M. Porkolab, R. Rohatgi, and J. S. Levine, Runaway-Driven Instabilities During RF Heating and Current Drive Experiments on the Versator II Tokamak (p. 1104)

M. Porkolab, J. J. Schuss, Y. Takase, S. Texter, J. Machuzak, P. Bonoli, C. Fiore, R. Gandy, R. Granetz, M. Greenwald, D. Gwinn, B. Lipschultz, E. Marmar, S. McCool, D. Pappas, R. Parker, P. Pribyl, J. Rice, J. Terry, R. Watterson, and S. Wolf, Lower Hybrid Current Drive on the Alcator C Tokamak (p. 1103)

J. J. Ramos and G. B. Crew, Asymptotic Theory of the Internal Kink Mode in Finite Beta Tokamaks (p. 1094)

N. Sharky, Characteristics of Inward Particle Flux Inferred from Experimental Measurements (p. 1001)

N. Sharky and B. Coppi, Electron Energy Confinement Time in Ohmically Heated Experiments (p 1125)

N. Sharky, R. Englade, and B. Coppi, Simulation of Electron Temperature Profiles in Various Experiments (p. 1001)

R. E. Shefer, D. A. Kirkpatrick, and G. Bekefi, A Velocity Diagnostic for Relativistic Electron Beams (p. 1061)

L. Sugiyama, Effect of an $m° = 1$ Magnetic Island on Energy Deposition in Igniting Plasmas (p. 1130)

Y. Takase, M. Porkolab, and J. J. Schuss, Convective Effects on Parametric Excitation of Ion-Sound Quasi-Modes During LHRF Heating of Tokamak Plasmas (p. 1103)

D. Tetreault, Growth Rate of the Clump Instabilities (p. 1105)

G. Vlad and B. Coppi, Bremsstrahlung Cooled "couche" of Tritiumless Plasmas (p. 1043)

S. M. Wolfe, B. Blackwell, C. L. Fiore, W. Fisher, R. Gandy, R. S. Granetz, M. Greenwald, D. Gwinn, S. Kissel, B. Labombard, M. Porkolab, P. Pribyl, and Y. Takase, Scaling of Energy Confinement with Limiter Geometry in Alcator C (p. 936)

104th Meeting, Acoustical Society of America, Orlando, Florida
November 9-12, 1982

Abstracts in J. Acoust. Soc. Am. Vol. 72, Suppl. No. 1, Fall 1982

M. Florentine and A. J. Houtsma, Tuning Curves and Pitch Matches in Unilateral Low-Frequency Hearing Loss: A Case Study (p. S67)

G. V. Frisk, D. R.Mook, J. A. Doutt, E. E. Hays, and A. V. Oppenheim, The Application to Real Data of a Technique for Measuring the Planewave Reflection Coefficient of the Ocean Bottom (p. S97)

M. Hamada, Nasal Vowel Identification Using LPC-Based Formant Analysis (p. S30)

D. H. Klatt and D. W. Shipman, Letter-to-Phoneme Rules. A Semi-Automatic Discovery Procedure (p. S48)

G. E. Kopec, M. A. Bush, and V. W. Zue, Toward an Expert System for Automatic Stop Consonant Identification (p. S48)

M. A. Randolph and V. W. Zue, Synthesis of Continuous Speech by Concatenation of Isolated Words (p. S79)

S. Shattuck-Hufnagel, Position Constraints on Interacting Segments in Elicited Errors Favor the Word Over the Stressed Syllable (p. S48)

K. N. Stevens, S. H. Blumenthal, D. M. Green, and M. Krasner, Ear-Canal Resonances and the Assessment of Hearing Thresholds at High Frequencies (p. S6)

American Speech-Language-Hearing Association Meeting, Toronto, Canada
November 18-21, 1982

E. M. Maxwell, On the Convergence of Evidence in Phonological Analysis

Large Space Antenna Systems Technology - 1982, NASA Langley Research Center
November 30 - December 3, 1982

J. H. Lang, Electrostatically-Figured Membrane Reflectors: An Overview

1982 International Conference on Lasers, New Orleans, Louisiana
December 13-17, 1982

Abstracts in Technical Digest

Papers in Proceedings

G. Bekefi, Free Electron Laser Hybrids (invited paper) (p. 4)

S. Ezekiel, Application of the Sagnac Effect in Optical Gyroscopes (invited paper) (p. 24)

J. H. Shapiro, Mysteries and Applications of Two-Photon Coherent States (invited paper) (p. 4)

48th Statistical Mechanics Meeting, Rutgers University, New Brunswick, New Jersey
December 16-17, 1982

D. Blankschtein, New Universality Class in Ferroelectrics

M. Kardar, Phase Transition in New Solvable Hamiltonians by a Central-Limit Minimization

28.2 Journal Papers Published

D. Andelman and J. S. Walker, Preserving the Free Energy in a Migdall-Kadanoff Approximation for the q-State Potts Model (Phys. Rev. B $\underline{27}$:1, 241-247 (1983))

K. Baden-Kristensen and T. F. Weiss, Supporting Cell and Extracellular Responses to Acoustic Clicks in the Free-Standing Region of the Alligator Lizard Cochlea (Hearing Res. $\underline{8}$, 295-315 (1982))

K. Baden-Kristensen and T. F. Weiss, Receptor Potentials of Lizard Hair Cells with Free-Standing Stereocilia: Responses to Acoustic Clicks (J. Physiol. $\underline{335}$, 699-721 (1983)

D. Bendedouch, S-H. Chen, and W. C. Koehler, Structure of Ionic Micelles from Small Angle Neutron Scattering (J. Chem. Phys. 87:1, 153-159 (1983))

A. Bers and K. S. Theilhaber, Three-Dimensional Theu of Waveguide-Plasma Coupling (Nucl. Fusion 23:1, 41-48 (1983))

R. J. Birgeneau, C. W. Garland, A. R. Kortan, J. D. Litster, M. Meichle, B. M. Ocko, C. Rosenblatt, L. J. Yu, and J. Goodby, The Smectic-A-Smectic-C Transition: Mean Field or Critical (Phys. Rev. A 27:2, 1251-1254 (1983))

S. Chase, P. Bugnacki, L. D. Braida, and N. I. Durlach, Intensity Perception XII. Effect of Presentation Probability on Absolute Identification (J. Acoust. Soc. Am. 73:1, 279-284 (1983))

S. L. Chuang and J. A. Kong, Wave Scattering and Guidance by Dielectric Waveguides with Periodic Surfaces (J. Opt. Soc. Am. 73:5, 669-679 (1983))

B. Coppi, Physics of Neutronless Fusion Reacting Plasmas (Phys. Scri. Vol. T2:2, 590-595 (1982))

R. C. Davidson and H. S. Uhm, Stability Properties of an Intense Relativistic Nonneutral Electron Ring in a Modified Betatron Accelerator (Phys. Fluids 25:1, 2089-2100 (1982))

M. Florentine and A. J. M. Houtsma, Tuning Curves and Pitch Matches in a Listener with a Unilateral Low-Frequency Hearing Loss (J. Acous. Soc. Am. 73:3, 961-965 (1983))

D. A. Fishman and F. R. Morgenthaler, Investigation of the Velocity of Energy Circulation of Magnetostatic Modes in Ferrites (J. Appl. Phys. 54:6, 3387-3393 (1983))

V. Fuchs, M. M. Shoucri, G. Thibaudeau, L. Harten, and A. Bers, High-Q Thermally Stable Operation of a Tokamak Reactor (IEEE Trans., Vol. PS-11, No. 1, pp. 4-18, March 1983)

W. J. Glantschnig and S-H. Chen, Light Scattering from Water Droplets in the Geometrical Optics Approximation (Appl. Opt. 20:14, 2499-2509 (1981))

T. M. Habashy, S. M. Ali, and J. A. Kong, Impedance Parameters and Radiation Pattern of Two Coupled Circular Microstrip Disk Antennas (J. Appl. Phys. 54:2, 493-506 (1983))

M. G. Hall, A.V. Oppenheim, and A. S. Willsky, Time-Varying Parametric Modeling of Speech (Signal Processing 5, 267-285 (1983))

H. A. Haus and M. N. Islam, Application of a Variational Principle to Systems with Radiation Loss (IEEE J., Vol. QE-19, No. 1, pp. 106-117, January 1983)

H. A. Haus and L. Molter-Orr, Coupled Multiple Waveguide Systems (IEEE J., Vol. QE-19, No. 5, pp. 840-844, May 1983)

C. M.Horwitz, RF Sputtering - Voltage Division Between Two Electrons (J. Vac. Sci. Technol. A1:1, 60-68 (1983))

J. Ihm and J. D. Joannopoulos, Structure of the Al-GaAs(110) Interface from an Energy-Minimization Approach (Phys. Rev. B 26:8, 4429-4435 (1982))

Y. Ito, H. S. Colburn, and C. L. Thompson, Masked Discrimination of Interaural Time Delays with Narrowband Signal (J. Acoust. Soc. Am. 72:6, 1821-1826 (1982))

T. H. Joo and J. H. McClellan, Pole-Zero Modelling and Classification of Phonocardiograms (IEEE Trans., Vol. BME-30, No. 2, pp. 110-118, February 1983)

P. A. Keating, Book Review: G. H. Yeni-Komshian, J. F. Kavanagh, and C. A. Ferguson (Eds.), Child Phonology. Vol. 1: Production; Vol. 2: Perception (Academic Press, New York, 1980), Vol. 1, pp. 304 and Vol. 2, pp. 254 (Language 58:3, 719-721 (1982))

M. Kardar, Phase Boundaries of the Isotropic Helical Potts Model on a Square Lattice (Phys. Rev. B 26:5, 2693-2699 (1982))

G. E. Kopec, A. V. Oppenheim, and R. Davis, Knowledge-Based Signal Processing (Trends Perspect. Sig. Processing 2:1, 1-6 (1982))

P. Kumar and R. S. Bondurant, Improving the Pulse Shape in Dye Laser Amplifiers: A New Technique (Appl. Opt. 22:9, 1284-1287 (1983))

S. W. Lang and J. H. McClellan, Multi-Dimensional MEM Spectral Estimation (IEEE Trans., Vol. ASSP-30, No. 6, pp. 880-887, December 1982)

S. W. Lang and J. H. McClellen, Spectral Estimation for Sensor Arrays (IEEE Trans., Vol. ASSP-31, No. 2, pp. 349-358, April 1983)

L. S. Larkey, Reiterant Speech. An Acoustic and Perceptual Validation (J. Acoust. Soc. Am. 73:4, 1337-1345 (1983))

C. R. Lawrence, C. L. Bennett, A. J. Garcia-Barreto, P. E. Greenfield, and B. F. Burke, 5 GHz Observations of Sources in the Arecibo 611 MHz Survey (Astrophys. J. (Suppl.) 51, 67-114 (1983))

J. H. McClellan, Multidimensional Spectral Estimation (IEEE Proc. Vol. 70, No. 9, pp. 1029-1039, September 1982)

J. H. McClellan and S. W. Lang, Duality for Multidimensional MEM Spectral Estimation (Proc. IEEE, Vol. 130, Pt F, No. 3, pp 230-235, April 1983)

F. S. McDermott, G. Bekefi, K. E. Hackett, J. S. Levine, and M. Porkolab, Observation of the Parametric Decay Instability During Electron Cyclotron Resonance Heating on the Versator II Tokamak (Phys. Fluids 25:9, 1488-1490 (1982))

L. Menn and S. Boyce, Fundamental Frequency and Discourse Structure (Language and Speech, Vol. 25, Part 4, pp. 341-383 (1982))

P. C. Myers and A. H. Barrett, Search for Maser Emission by Water Vapor in the v_2 Excited Vibrational State (Astrophys. J. 263, 716-717 (1982))

P. C. Myers and P. J. Benson, Dense Cores in Dark Clouds. II. NH_3 Observations and Star Formation (Astrophys. J. 266, 309-320 (1983))

F. Pegoraro and L. Sugiyama, Spatial Diffusion of Charged Energy Fusion Products by Shear-Alfvén Perturbations (Nucl. Fusion $\underline{23}$:4, 407-424 (1983))

L. R. Ram-Mohan and P. A. Wolff, Joint Density of States in Interband Transitions in Semiconductors in a Magnetic Field (Phys. Rev. B $\underline{26}$:12, 6711-6718 (1982))

C. H. Shadle, Experiments on the Acoustics of Whistling (Phys. Teacher, pp. 148-154, March 1983)

W. P. Spencer A. G. Vaidyanathan, D. Kleppner, and T. W. Ducas, Photoionization by Blackbody Radiation (Phys. Rev. A $\underline{26}$:3, 1490-1493 (1982))

D. H. Staelin and P. W. Rosenkranz, Formation of Jovian Decametric S-Bursts by Modulated Electron Streams (J. Geophys. Res. $\underline{87}$:A12, 10,401-10,406 (1982))

D. D. Stancil and F. R. Morgenthaler, Guiding Magnetostatic Surface Waves with Nonuniform In-Plane Fields (J. Appl. Phys. $\underline{54}$:3, 1613-1618 (1983))

M. Stix and E. P. Ippen, Pulse Shaping in Passively Mode-Locked Ring Dye Lasers (IEEE J., Vol. QE-19, No. 4, pp. 520-525, April 1983)

A. D. Stone, D. C. Allen, and J. D. Joannopoulos, Phase Randomness in the One-Dimensional Anderson Model (Phys. Rev. B $\underline{27}$:2, 836-843 (1983))

A. G. Vaidyanathan, W. P. Spencer, J. A. Rubbmark, H. Kuiper, C. Fabre, and D. Kleppner, Experimental Study of Non-Adiabatic Core Interactions in Rydberg States of Calcium (Phys. Rev. A $\underline{26}$:6, 3346-3350 (1982))

28.3 Journal Papers Accepted for Publication

P. J. Benson and P. C. Myers, Dense Cores in Dark Clouds. IV. HC_5N Observations (Astrophys. J.)

R. H. Berman, D. J. Tetreault, and T. H. Dupree, Observation of Self-binding Turbulent Fluctuations in Simulation Plasma and Their Relevance to Plasma Kinetic Theories (Phys. Fluids)

R. A. Close, A. Palevsky, and G. Bekefi, Radiation Measurements from an Inverted Relativistic Magnetron (J. Appl. Phys)

G. B. Crew and J. J. Ramos, Asymptotic Theory of the Internal Kink Mode in Current Carrying Toroidal Plasmas (Phys. Fluids)

S. L. Dexheimer, T. A. Brunner, and D. E. Pritchard, Angular Momentum Limitation in Vibrationally Inelastic Collisions of $I_2(B^3\Pi)$ with He and Xe (J. Chem. Phys.)

J. W. Dreher and W. J. Welch, VLA Observations of MWC 349 at 15 and 23 GHz (Astron. J.)

T. H. Dupree, Growth of Phase Space Density Holes (Phys. Fluids)

H. A. Haus and M. N. Islam, Synchroton Radiation of Wiggled Electron Beam in Rectangular Waveguide (J. Appl. Phys.)

T. Holton and T. F. Weiss, Receptor Potentials of Lizard Cochlear Hair Cells with Free-Standing Stereocilia in Response to Tones (J. Physiol.)

T. Holton and T. F. Weiss, Frequency Selectivity of Hair Cells and Nerve Fibers in the Alligator Lizard Cochlea (J. Physiol.)

B. Howland, New Test Patterns for Camera Lens Evaluation (Appl. Opt.)

Y. Q. Jin and J. A. Kong, Passive and Active Remote Sensing of Atmospheric Precipitation (Appl. Opt.)

M. Kardar, Crossover to Equivalent-Neighbor Multicritical Behavior in Arbitrary Dimensions (Phys. Rev. B)

M. Kotlarchyk and S-H. Chen, Analysis of Small Angle Neutron Scattering Spectra from Polydisperse Interacting Colloids (J. Chem. Phys.)

R. E. Meyer, G. A. Sanders, and S. Ezekiel, Observation of Spatial Variations in the Resonance Frequency of an Optical Resonator (J. Opt. Soc. Am.)

C. M. Reed, B. L. Hicks, L. D. Braida, and N. I. Durlach, Discrimination of Speech Processed by Lowpass Filtering and Pitch-Invariant Frequency Lowering (J. Acoust. Soc. Am.)

A. Sezginer and J. A. Kong, Physical Optics Approach for Scattering by Thin Helical Wires (Radio Sci.)

A. Sezginer, S. L. Chuang, and J. A. Kong, Modal Approach to Scattering of Electromagnetic Waves by a Conducting Tape Helix (IEEE Trans. (AP))

H. I. Smith, C. V. Thompson, M. W. Geis, R. A. Lemons, and M. A. Bosch, The Mechanism of Orientation in Si Graphoepitaxy by Laser or Strip-Heater Recrystallization (J. Electrochem. Soc.)

L. Tsang and J. A. Kong, Scattering of Electromagnetic Waves from a Half Space of Densely Distributed Dielectric Scatterers (Radio Sci.)

H-Z. Wang, Estimation of Snow Depth with Measured Brightness Temperatures (J. Geophys. Res.)

28.4 Letters to the Editor Published

H. A. Atwater, H. I. Smith, and M. W. Geis, Orientation Selection by Zone-Melting Silicon Films Through Planar Constrictions (Appl. Phys. Lett. 41:8, 747-749 (1982))

D. Bendedouch and S-H. Chen, Structure and Interparticle Interaction of Bovine Serum Albumin in Solution Studies by Small-Angle Neutron Scattering (J. Phys. Chem. 87.9, 1473-1477 (1983))

D. Bendedouch and S-H. Chen, Study of Intermicellar Interaction and Structure by Small Angle Neutron Scattering (J. Chem. Phys. 87:10, 1653-1658 (1983))

C. L. Bennett, C. R. Lawrence, J. A. Garcia-Barreto J. N. Hewitt, and B. F. Burke, VLA Source Counts at 6 cm Wavelength (Nature, Vol. 301, No. 5902, pp. 686-687 (1983))

R. S. Bondurant, P. Kumar, J. H. Shapiro, and M. M. Salour, Photon Counting Statistics of Pulsed Light Sources (Optics Lett. 7:11, 529-531 (1982))

C. M. Horwitz, New Dry Etch for Al and Al-Cu-Si Alloy: Reactively Masked Sputter Etching with SiF_4 (Appl. Phys. Lett. 42:10, 402-404 (1982))

K. Kash, P. A. Wolff, and W. A. Bonner, Nonlinear Optical Studies of Picosecond Relaxation Times of Electrons in n-GaAs and n-GaSb (Appl. Phys. Lett. 42:2, 173-175 (1983))

A. R. Kortan, A. Erbil, R. J. Birgeneau, and M. S. Dresselhaus, Commensurate-Incommensurate Transition in Bromine-Intercalated Graphite: A Model Stripe-Domain System (Phys. Rev. Lett. 49:19, 1427-1430 (1982))

Y. T. Li and A. L. Kurkjian, Arrival Time Estimation Using Iterative Signal Reconstruction from the Phase of the Cross Spectrum (IEEE Trans., Vol. ASSP-31, No. 2, pp. 502-504, April 1983)

J. S. Lim, J. C. Anderson, and C. L. Searle, Signal Reconstruction from Cosine Transform Magnitude (Proc. IEEE (Correspondence), Vol. 70, No. 12, pp. 1460-1462, December 1982)

J. S. Lim and F. U. Dowla, A New Algorithm for High-Resolution Two-Dimensional Spectral Estimation (Proc. IEEE (Correspondence), Vol. 71, No. 2, pp. 284-285, February 1983)

J. B. McManus, Far-Infrared Radiation from Thin-Plasmons Excited at the Difference Frequency of Two CO_2 Lasers (Appl. Phys. Lett. 41:8, 692-694 (1982))

B. W. Peuse, M. G. Prentiss, and S. Ezekiel, Elimination of Line-Shape Distortion in Laser Absorption Spectroscopy in Atomic Beams (Optics Lett. 8:3, 154-156 (1983))

C. R. Safinya, L. S. Martinez-Miranda, M. Kaplan, J. D. Litster, and R. J. Birgeneau, High-Resolution X-Ray Scattering Study of the Nematic-to-Smectic-C Transitions in 8S5-7S5 Mixtures (Phys. Rev. Lett. 50:1, 56-59 (1983))

R. E. Tench and S. Ezekiel, Precision Measurements of Hyperfine Predissociation in I_2 Vapor Using a Two-Photon Resonant Scattering Technique (Chem. Phys. Lett. 96:2, 253-258 (1983))

S. Y. Yuen, Third Order Optical Nonlinearity Induced by Effective Mass Gradient in Heterostructures (Appl. Phys. Lett. 42:4, 331-333 (1983))

S. Y. Yuen and P. Becla, Saturation of Band-Gap Resonant Optical Phase Conjugation in HgCdTe (Optics Lett. 8:7, 356-358 (1983))

M. L. Zimmerman, R. G. Hulet, and D. Kleppner, Comparisons of Approximate Bases for Hydrogen in a Magnetic Field (Phys. Rev. A (Letter) 27:5, 2731-2734 (1983))

28.5 Letters to the Editor Accepted for Publication

J. G. Fujimoto and E. P. Ippen, Transient Four-Wave Mixing and Optical Pulse Compression in the Femtosecond Regime (Optics Lett.)

P. R. Hemmer, S. Ezekiel, and C. C. Leiby, Jr. Stabilization of a Microwave Oscillator Using a Resonance Raman Transition in a Sodium Beam (Optics Lett.)

28.6 Special Publications

M. Halle and P. Kiparsky, Internal Constituent Structure and Accent in Russian Words, in E. A. Scatton, R. D. Steele, and C. E. Gribble (Eds.), Studies in Honor of Horace G. Lunt (Folia Slavica, Vol. 3, Ns. 1-2, Slavica Publishers, Inc., Columbus, Ohio, 1979), pp. 128-153

J. R. Ross, When the Be's Go, the Frost Comes, in G. Bedell, E. Kobayashi, and M. Muraki (Eds.), Explorations in Linguistics, Papers in Honor of Kazuko Inoue (Kenkyusha, Tokyo, Japan, 1980), pp. 464-470

28.7 Technical Reports Published

These and previously published Technical Reports, if available, may be obtained from the Document Room, 36-412, Research Laboratory of Electronics, Massachusetts Institute of Technology, Cambridge, Massachusetts 02139

497   Douglas Mook, The Numerical Synthesis and Inversion of Acoustic Fields Using the Hankel Transform with Application to the Estimation of the Plane Wave Reflection Coefficient of the Ocean Bottom

498   David Izraelevitz, Overspecified Normal Equations for Spectral Estimation

499   Alain C. Briançon, A 8.45 GHz GaAs FET Amplifier

29. Personnel

Jonathan Allen, Director

Professors

Allen, Jonathan	French, Anthony P.	Litster, James D.
Allis, William P.*	Frishkopf, Lawrence S.	McCune, James E.
Baygeroer, Arthur B.	Gyftopoulos, Elias P.	Morgenthaler, Frederic R.
Barrett, Alan H.	Hale, Kenneth L.	Oppenheim, Alan V.
Bekefi, George	Halle, Morris	Peake, William T.
Bers, Abraham	Harris, James W.	Penfield, Paul, Jr.
Birgeneau, Robert J.	Harvey, George G.*	Pomorska, Krystyna
Bose, Amar G.	Haus, Hermann A.	Porkolab, Miklos
Braida, Louis D.	Ippen, Erich P.	Pritchard, David E.
Bresnan, Joan W.	Jakobson, Roman*	Schreiber, William F.
Burke, Bernard F.	Kennedy, Robert S.	Searle, Campbell L.
Chen, Sow-Hsin	Keyser, Samuel J.	Siebert, William M.
Chomsky, A. Noam	King, John G.	Smith, Henry I.
Coppi, Bruno	Kiparsky, R. Paul V.	Smullin, Louis D.
Dupree, Thomas H.	Kleppner, Daniel	Staelin, David H.
Edgerton, Harold E.*	Kong, Jin Au	Stevens, Kenneth N.
Ezekiel, Shaoul	Kyhl, Robert L.	Strandberg, Malcom W.P.
Fant, Gunnar +	Lee, Francis F.	Weiss, Thomas F.
Fodor, Jerry A.	Lettvin, Jerome Y.	Wolff, Peter A.
Fonstad, Clifton G.	Lidsky, Lawrence M.	Zimmerman, Henry J.*

Associate Professors

Berker, Ahmet N.	Lim, Jae S.	Salour, Michael M.
Joannopoulos, John D.	McClellan, James H.	Shapiro, Jeffrey H.
Kastner, Marc A.	Myers, Philip C.	Troxel, Donald E.

Assistant Professors

Ceyer, Sylvia T.	Lang, Jeffrey H.	Warde, Cardinal
Dreher, John W.	McFeely, F. Read	Wyatt, John L., Jr.
Glasser, Lance A.	Musicus, Bruce R.	Zue, Victor W.
	Nelson, Keith	

*Emeritus
+ Visiting

Senior Research Scientists

Durlach, Nathaniel I.

Kamentsky, Louis A.
Klatt, Dennis H.

Rediker, Robert H.

Principal Research Scientists and Associates

Colburn, H. Steven

Melngailis, John

Perkell, Joseph S.

Postdoctoral Fellows

Bhattacharje, Gopa
Farrar, Catherine L.[1]
Furst, Miriam[2]
Jakimik, Jola A.

Keithley, Elizabeth M.[1]
Landahl, Karen L.[3]
Larkey, Leah S.[1]
MacMillan, Neil[1]

Maxwell, Edith M.[1]
Milner, Paul[1]
Price, Patti Jo[1]
Widin, Gregory P.

Research Staff

Barrett, John W.
Barrows, Francis W.
Berman, Robert H.
Bhattarcharjee, Tushar
Bilotta, Robert
Bonoli, Paul T.
Boutros-Ghali, Teymour
Cline, Richard W.
Delhorne, Lorraine A.
Englade, Ronald C.
Fitzgerald, Edward W.
Freeman, Dennis M.
Gerver, Michael
Guinan, John J., Jr.
Houtsma, Adrian J.M.
Hoyte, Lennox P.J.
Ihm, Jisoon
Irby, James H.

Jagannath, Chirravuri
Jarrell, Joseph A.
Kawasaki, Haruko
Kiang, Nelson Y.S.
Kierstead, John D.
Kortan, Ahmet R.
Krapchev, Vladimir B.
Kupferberg, Lenn C.
Lee, Dung-Hai Tom
Lo, Chi Cheung
Luckhardt, Stanley C.
Mastovsky, Ivan
McIlrath, Michael B.
Papa, D. Cosmo
Pierrehumbert, Janet M.
Plotkin, George M.
Rabinowitz, William M.

Ramos, Jesus
Reed, Charlotte M.
Rosenkranz, Philip W.
Rubbmark, Jan R.
Saenger, Katherine L.
Shao, Michael
Sharky, Nazih N.
Shefer, Ruth E.
Shipman, David W.
Spencer, William P.
Sugiyama, Linda E.
Sutton, Mark D.
Tetreault, David J.
Thompson, Carl V., II
Walker, Russell H.
Yuen, Y.C. Sunny
Zeskind, Dale A.
Zurek, Patrick M.

1. NIH Trainee
2. Bantrell Fellow
3. NSF Fellow

Visiting Scientists and Guests

Bebelaar, Dick
Bechtel, James H.
Bertin, Guiseppe
Blumstein, Sheila E.
Brown, Fielding
Buchinger, Fritz
Cerrillo, Manuel V.
Chen, Dong-Pei
Chew, Weng Cho
De Rosier, David T.
Ducas, Theodore W.
Fehrenbach, Gustav W.
Florentine, Mary S.
Fuchs, Adrian
Gabielsen, Geir W.
Geiger, Gad
Hamada, Masahiro

Hawryluk, Andrew M.
Horwitz, Christopher M.
Jacobsen, Edward H.
Jhaveii, Sonal
Kanbe, Hiroshi
Kayoun, Pierre H.
Konrad, Cristina
Kumar, Prem
Levine, Jerrold S.
Liu, Hua-Khuang
Lyrra, A. Marjatta
Mills, Allen W.
Perlman, David M.
Ram, Abhay K.
Read, Michael E.
Roberts, David H.
Rosenthal, Stanley J.

Rosowski, John J.
Scharf, Bertram
Shapira, Ruth
Shattuck-Hufnagel, Stephanie
Vaidyanathan, A. Ganesh
Wang, Hong-Ming
Wang, Hu-Zhuan
Wang, Shi-Qian
Wang, Yi-ming
Welte, Roland
Wiesner, Stephen
Wintner, Ernst
Xu, Xi Ru
Xue, Ming-Lun
Yamamoto, Yoshihisa
Yuan-Zhao, Yin
Zhong, Xubin

Research Affiliates

Barlow, John S.
Boduch, Raymond
Brown, Robert M.
Crist, Alan H.
Curby, Mark L.
Dowdy, Leonard C.
Feldman, Sharon G.
Ferrier, Linda J.
Grosjean, Francois

Hawkins, C. Sarah
Hillman, Robert E.
Holmberg, Eva Birgitta
Huggins, Allan W.F.
Jaanimagi, Paul
Larrabee, Joanne W.
Lyberg, Bertil
Makhoul, John I.
Menn, Lise
Menyuk, Paula

Miller, Joanne L.
Picard, Leonard
Pollack, Robert A.
Ram-Mohan, L. Ramdas
Schultz, Martin C.
Stefanov-Wagner, Frank J.
Steffens, David A.
Wacks, Kenneth P.
Zuniga, Michael A.

Research Assistants

Aeppli, Gabriel
Ali, Ali D.S.
Allen, Barry R.
Andelman, David
Anderson, Erik H.
Armstrong, John T.
Atwater, Harry A.
Barabell, Arthur J.
Bar-Yam, Yaneer

Bennett, Charles L.
Bogler, Phil L.
Bondurant, Roy S.
Borgeaud, Maurice
Brewer, Lawrence R.
Chen, Francine R.
Chou, Yu
Chuang, Shun-Lien
Church, Kenneth W.

Crew, Geoffrey B.
Cyphers, David S.
Dagli, Nadir
Dana, Stephane S.
DeGennaro, Steven V.
Dexheimer, Susan
Dhawan, Vivek
Dowla, Farid U.
Dreshfield, Kenneth J.

Research Assistants (continued)

Duckworth, Gregory L.	Kuznetzov, Mark	Richard, Michael D.
Ezzeddine, Amin K.	Kwasnick, Robert F.	Rohatgi, Rajeev R.
Fisher, Alan S.	Lamb, Richard H.	Rohlicek, Robin J.
Francis, Gregory E.	Lamel, Lori F.	Rose, Christopher
Fujimoto, James G.	Larson, Brent D.	Sanders, Glen A.
Gabriel, Kaigham J.	Lattes, Ana Luisa	Sara, Jason
Gamble, Edward B., Jr.	Lau, Sun Tong	Schadler, Edward H.
Garber, Edward M.	Lawrence, Charles R.	Schloss, Robert P.
Garcia-Barreto, J. Anthony	Lee, Jay Kyoon	Schott, Jean-Pierre
Garnavitch, Peter M.	Leong, Robert S.	Scott, Thomas P.
Garner, Richard C.	Leung, Hong Chung	Seiler, Larry D.
Ghavamishahidi, Ghavam	Lin, Sching Lih	Seneff, Stephanie
Goldhor, Richard S.	Livingston, Jay N.	Sezginer, Abdurrahman
Gould, Philip L.	Magill, Peter D.	Shadle, Christine H.
Griffin, Daniel W.	Mahoney, James H.	Shih, Shih-Ming
Habashi, Tarek M.	Malik, Naveed A.	Skarda, Gregory M.
Hackett, Kirk E.	Mayberry, Matthew J.	Smith, Neil
Hakimi, Farhad	McDerott, F. Scott	Specht, Eliot D.
Harrison, William A.	McManus, John B.	Stathis, James H.
Harten, Leo P.	Medina, Antonio	Stautner, John P.
Heiney, Paul A.	Mesite, Paula L.	Stein, Josephine A.
Hemmer, Philip R.	Meyer, Raymond E.	Stewart, Brian A.
Hewitt, Jacqueline N.	Migdall, Allan L.	Stix, Michael
Hinshelwood, David	Milios, Evangelos E.	Stone, Alfred D.
Horowitz, David M.	Mizumoto, Chris T.	Sulecki, Joan M.
Hulet, Randall G.	Mochrie, Simon G.J.	Tench, Robert E.
Humphreys, David A.	Molter-Orr, Lynne	Truong, Toan Vinh
Huttenlocher, Daniel	Moskowitz, Philip E.	Uchanski, Rosalie M.
Isaacs, Eric D.	Moskowitz, Warren P.	Walkup, Robert E.
Islam, Mohammed N.	Murphy, David C.	Warnock, James D.
Izraelevitz, David	Nathan, Krishna S.	Warren, Alan C.
Jackson, James M.	Nawab, Syed H.	Welch, George R.
Jacobs, Kenneth D.	Nguyen, Trung Tien	Wengrovitz, Michael S.
Kash, Kathleen	Pan, Davis Yen	Whitaker, Norman A., Jr.
Kash, Michael M.	Papurt, David M.	White, Frederic M.
Keavney, Christopher J.	Park, Dongwook W.	White, Lawrence W.
Khan, Malik M.A.	Peterson, Patrick M.	Williams, Brian C.
Kim, Sei-Hee	Puese, Bruce W.	Wong, Albert K-S
Kirkpatrick, Douglas A.	Poh, Soon Yun	Wong, Stephen B.
Kissel, Steven E.	Prentise, Mara G.	Yam Young
Knowlton, Stephen F.	Putnam, Roger S.	Yorsz, Jeffrey
Krause, Edward A.	Rappaport, Carey M.	Youngdale, Eric R.
Krystal, Andrew D.		Zayhowski, John J.

Teaching Assistants

Armstrong, Robert C.
Arrott, Anthony P.
Chambers, William N.
Colavita, M. Mark
Damon, Richard S.
Delatizky, Jonathan
Engelke, Charles W.
Esmersoy, Cengiz
Espy, Carol Yvonne
Garcia, Armando

Hoang, Phuong-Quan
Huntzinger, Mark E.
Ito, Yoshiko
Joo, Tae-Hong
Karl, William C.
Komichak, Michael J.
Lee, Chong U.
McLeod, Kenneth J.
Mizumoto, Chris T.
Ocko, Benjamin M.

Pachtman, Arnold
Pappas, Thrasyvoulos
Song, William S.
Szabo, Bernard I.
Timp, Gregory L.
Vallese, Francesco J.
Wagner, Stuart S.
White, Jeffrey R.
Wroclawski, John T.
Zubowski, Charles A.

Graduate Students

Allard, Terry T.
Anderson, James C.
Benson, Priscilla J.
Bergano, Neal S.[1]
Berger, Elliot N.
Bezdjian, Krikor A.
Bickley, Corine A.[2]
Boebinger, Gregory S.[3]
Bordley, Thomas E.
Briancon, Alain C.
Bristol, Jr., Norman[1]
Bustamante, Diane K.[2]
Cantarutti, Paolo
Carley, David W.[4]
Chan, Philip[5]
Chao, Yao-Ming
Chiang, Wei-Chung
Chike-Obi, Balogun[6]
Curtis, Susan R.[1]
DiFilippo, David[7]

Dove, Webster P.
Evans, William H.[8]
Fajans, Joel[3]
Fiorentini, Henry G.
Fratamico, John J.[3]
Fujimura, Akira
Gabriel, M. Christina[1]
Gentile, Thomas R.
Gifford, Margaret L.[2]
Glaser, Michelle J.[9]
Glass, James P.[7]
Hamilton, Greg D.[1]
Hamza, Abdelhaq M.[10]
Harton, Sara M.A.[11]
Heron, Courtney D.[12]
Howland, Bradford
Hsu, Stephen C.[8]
Hu, Robert Sueh-Chien
Hu, Weiming[13]
Hughey, Barbara J.[14]

Jin, Jiang-Sheng[15]
Jin, Yaqiu[15]
Joshi, Kiran Raj
Kobota, Ichiro
Kunoff, Estelle M.[16]
Kurkjian, Andrew L.[17]
LaRow, Michael R.[9]
Lezec, Henri J.
Maeda, Mari
Magnus, Margaret H.
Malvar, Henrique S.[18]
Marroquin, Jose Luis[19]
Martinelli, Julio J.[19]
Martínez-Miranda, Luz J.[8]
Matson, Mark D.
Mauel, Michael E.
McCormick, Steven P.[1]
McCue, Michael P.[2]
Mesa, Osvaldo S.[1]
Messac, Achille, Jr.

1. *Bell Laboratories Fellow*
2. *NIH Trainee*
3. *Hertz Fellow*
4. *HST Fellow*
5. *Singapore Government Fellow*
6. *Nigerian Government Loan*
7. *Canadian Government Fellow*
8. *NSF Fellow*
9. *Hughes Aircraft Fellow*
10. *Algerian Scholarship*

11. *Lincoln Labs Fellow*
12. *GEM Fellow*
13. *Honeywell Scholarship*
14. *M.I.T. Karl T. Compton Fellow*
15. *Chinese Government Fellow*
16. *IBM Fellow*
17. *Schlumberger Fellow*
18. *Brazilian Government Scholarship*
19. *Mexican Government Fellow*

Graduate Students (continued)

Miller, Glen W.[1]	Ressler, Andrew L.	Urbaniak, Walter A.
Mook, Douglas R.	Robinson, Andrew L.[8]	Vachon, Guy
Moser, James R.[2]	Saxberg, Bror V.H.[9]	Van Hove, Patrick L.[13]
Myers, Cory[3]	Schulert, Andrew J.[2]	Velez, Richardo E.[14]
Ocenasek, Josef[4]	Schulz, Brian L.[10]	Vlannes, Nickolas P.
O'Rourke, John	Sekiguchi, Hiroshi[11]	Voldman, Steven H.
Paulik, Mark J.[1]	Shapiro, Philip D.	Waissman, Roberto S.[15]
Paulos, John J.[5]	Shin, Robert T.I.	Wang, David L.[6]
Pettit, Steven L.[6]	Shinn, Neal D.	Weiner, Andrew M.
Pineda, Juan	Sundaram, Ramikrishnan[12]	Williams, Douglas D.
Ponikvar, Donald R.[7]	Teich, Jonathan M.[7]	Williams, Gregory E.[16]
Prince, Jerry L.	Towe, Elias D.	Yorker, Jeffrey G.
Randolph, Mark[4]	Ueki, Gordon	Zhang, Lixia[17]

Undergraduate Students

Ahern, Lance J.	Chase, Scott I.	Foss, Kristin K.
Ames, Michael	Chavez-Pirson, Arturo	Furuno, David S.
An, Chae H.	Chen, David A.	Ghosh, Biswa R.
Ataki, Patrick	Chiang, Carol J.	Giambalvo, Corrado
Atlas, Susan	Corcoran, Christopher	Gleckman, Philip L.
Aune, Timothy J.	Cotter, Vincent J.	Gorodishcher, Ilya
Babalitis, Panagiotis A.	Della Fera, Anthony	Guy, Donald
Bade, Edward R.	Denton, Denise	Hagemeister, Mark
Ball, Kevin D.	Derozairo, Andrew M.	Hakkarainen, J. Mikko
Baltus, Donald G.	Detlefs, William F.	Hamburger, Robert O.
Barsony, Mary	Dixon, Stephen K.	Harrahy, David P.
Bavly, Eric M.	Doyle, John M.	Hawes, David J.
Bonney, Laura A.	Drogaris, Anthony N.	Hildebrant, Eric M.
Bounds, Jeffrey K.	Duffey, Thomas P.	Hill, Brian A.
Burgess, George H.	Duncan, Ronald B.	Hodgkinson, Alan E.
Canning, John M.	Elias, Eric	Hong,
Carney, Laurel H.	Epstein, Michael A.	Hosein, Patrick A.
Cataltepe, Tanju	Ericson, Daniel W.	Isnardi, Michael
Chambers, William N.	Felshin, Susan L.	Jain, Sudhanshu K.

1. General Motors Fellow
2. NSF Fellow
3. Schlumberger Fellow
4. Bell Laboratories Fellow
5. IBM Fellow
6. Hughes Aircraft Fellow
7. Hertz Fellow
8. Digital Equipment Corporation Fellow
9. M.I.T. Fellow

10. American Bell, Inc. Fellow
11. Toshiba Fellow
12. Winton Hayes Fellow
13. Belgian American Education Foundation
14. Mexican Government Fellow
15. National Research Council of Brazil
16. Lincoln Labs Fellow
17. People's Republic of China

Undergraduate Students (continued)

Jones, Linda
Kalogny, Howard
Kaplan, Mark S.
Kardan, Kaveh
Kay, James M.
Kellam, Jeffrey A.
Kesler, Morris P.
Kidd, Robert C.
Kim, Micheal W.
Kim, Richard Y.
Kochanski, Gregory
Kositsky, Joel
Lambert, Katherine H.
Laves, Alan L.
Levine, Eric C.
Liebeler, Eric C.
Liu, Shih-Chii
Loughridge, Michael F.
Luna, Joel J.
Luthiger, Walter E.
Maloney, John P.
Mars, Mark E.
Matter, Michael C.
McCrae, Jack E., Jr.
Mok, Chee Kong
Moore, Barbara K.

Mutz, Andrew
Nevins, Bryan D.
Nulan, Craig A.
Nykolak, Gerald
O'Donnell, Shawn R.
Opalsky, David*
Paczuski, Maya
Passman, Judith
Pearsall, C. Robert, II
Pemberton, Joseph C.
Persichetti, Arthur M.
Pinsker, Robert I.
Rains, William A.
Ralston, John D.
Raman, Shankar
Record, Rush H.
Rode, Christian S.
Rotman, Ruth R.
Sachdev, Subir
Sadri-Azarbayesani, Babak
Schaefer, Robert J.
Schenck, Jeffrey L.
Scherdin, Steven M.
Schnitzler, Raymond A.
Schutkeker, John
Schwinn, Daniel J.
Secker-Walker, Hugh

Shapiro, Jerome
Sherloch, Thomas
Sidikman, Kenneth L.
Song, Sammy M.
Spellman, Roger
Stanzel, Robert P.
Steinbeck, John W.
Suggs, Bradley N.
Teachy, Robert D.
Thayer, Jeffrey S.
Tien, Ben Tze
Tsai, John C-H
Tsang, Grace P-Y
Wan, Poang-Liang
Washington, Emanuel E.
Weidelman, John R.
Winkelman, John R.
Wise, Ben P.
Wong, Geoffrey E.
Wong, Gerald G.
Wong, Raymond W.
Xanthos, James A.
Yates, Beverly A.
Yeh, Huoy-Ming
Yi, Ki Hyong
Zabor, William C.

Administrative Staff

Bella, Charles J.
Duffy, Donald F.

Maguire, Lawrence E.
McCarthy, Barbara L.
Moore, Janet E.

Keyes, Richard V., Jr.
Peck, John

Support Personnel

Aalerud, Robert W.
Aufiero, Elaine E.
Bella, Rose Carol
Bendiner, Nancy H.

Budd, Holly N.
Burrill, Lisa J.
Cabral, Manuel, Jr.
Carter, James M.

Chambers, Virginia N.
Clements, Donald A.
Cook, John F.
Donnelly, Marie

*Boston University Student

Support Personnel (continued)

Doucette, Wilfred F.	Kaloyanides, Venetia	North, Donald K.
Dove, Monica Edelman	Kopf, Cynthia Y.	O'Keefe, Patrick M.
Duffy, Cheryl A.	Lauricella, Deborah A.	Poynor, ; A.
Eccles, Miriam R.	Lauricella, Virginia R.	Rettmar .th F.
Evans, Thomas M.	Lavalle, Edward R.	Robinson, Aɪn
Foster, Stella J.	Leach, George H.	Scalleri, Mary
Fownes, Marilyn R.	Ledgister, Enid L.	Sincuk, Joseph, Jr.
Gale, Donna L.	Lewis, Ionia D.	Smith, Clare F.
Garalis, Thalia	Lorusso, Catherine	Southwick, Marie L.
Gelinas, Andrea L.	Lydon, Catharine A.	Stubbs, Frederick A.H.
Grande, Esther D.	McCue, Kathleen M.	Taylor, David M.
Griswold, Marsden P.	McDonnell, Russell A.	Taylor, Vicky-Lynn
Hall, Kyra M.	McKinnon, Rita C.	Vine. Brent H.
Holcomb, A. Linnea	Mitchell, Joseph E.	Williams, Arbella P.C.
Hughes, Martin O.	Nelson, Sylvia A.	Worner, Pamela S.
	Nickerson, John C.	

30. Research Support Index

National Aeronautics and Space Administration
    Contract NAGW 373   74
    Contract NAG3-215   59
    Contract NAG5-141   82
    Contract NAG5-270   83
    Contract NAG5-22929   77
    Contract NAS5-26861   82
    Contract S-10665-C   74
    Grant NAG5-10   76

National Bureau of Standards
    Grant NB-8-NAHA-3017   9

National Institutes of Health
    Grant AM-31546   3
    Grant GM-21189   190
    Grant 1 P01 CA31303-01   66
    Grant 1 R01 NS1691701A1   187
    Grant 5 P01 NS13126-07   179
    Grant 5 R01 NS04332-20   151
    Grant 5 R01 NS11080-06   190
    Grant 5 R01 NS1284606   182
    Grant 5 R01 NS14092-04   186
    Grant 5 T32 NS07040-08   151
    Grant 5 T32 NS07099   182, 187
    Training Grant 2 T32 NS07047-06   179
    Training Grant 5 T32 NS07047-05   179

National Oceanic and Atmospheric Administration
    Grant 04-8-M01-1   75

National Science Foundation
    Grant AST79-19553   75
    Grant AST80-22864   70
    Grant AST81-21416   69
    Grant BNS77-16861   181
    Grant BNS77-21751   186
    Grant CHE79-02967-A04   14, 15
    Grant DAR80-08752   31
    Grant ECS79-19475   32
    Grant ECS80-07102   137, 138, 139, 141, 142, 143, 144, 145, 146, 147, 148, 149, 150
    Grant ECS80-20639   37, 38, 39
    Grant ECS81-18160   175
    Grant ECS81-20637   127
    Grant ECS82-00646   101, 107
    Grant ECS82-03390   81
    Grant ECS82-05701   92, 94, 97
    Grant ECS82-11650   40

National Science Foundation (continued)
Grant ENG78-23145	81
Grant ENG79-07047	107
Grant MCS-8112899	151
Grant PCM81-11534	89
Grant PHY79-09739	44, 45, 46
Grant PHY79-09743	7, 9
Grant PHY82-10486	10
Grant 1ST80-17599	151
Grant 8008628-DAR	64, 65

Providence Gravure, Inc. (Grant)   168

Sandia National Laboratory
Contract 31-5606   101

Schlumberger-Doll Research Center   82

Schlumberger-Doll Research Fellowship   146

Systems Development Foundation   151

Toshiba Company Fellowship   149

U.S. Air Force
Contract F49620-81-C-0054   171, 176

U.S. Air Force Geophysics Laboratory (AFSC)
Contract F19628-79-C-0082   46, 48

U.S. Air Force – Office of Scientific Research
Contract AFOSR-81-0067	15, 18
Contract AFOSR-82-0053	101
Contract F49620-79-C-0071	55, 56
Contract F49620-80-C-0008	53
Contract F49620-83-C-0008	101

U.S. Air Force – Rome Air Development Center
Contract F19628-80-C-0077   43, 47

U.S. Army Research Office
Contract DAAG29-81-K-0126   63, 64, 65

U.S. Army Research Office – Durham
Contract DAAG29-80-K-0022   128

Index